NASA CR-72565
TWR - 3293

FINAL REPORT

DEVELOPMENT OF A FILAMENT WOUND CASE DESIGN FOR SOLID PROPELLANT ROCKET MOTORS IN THE 260-INCH DIAMETER CLASS

by

C.W. Vogt

THIOKOL CHEMICAL CORPORATION
WASATCH DIVISION
Brigham City, Utah

prepared for

NATIONAL AERONAUTICS AND SPACE ADMINISTRATION

March 1969

CONTRACT NAS 3-10287

NASA Lewis Research Center
J. J. Notardonato, Project Manager

Publications No. 0369-22650

NASA CR-72565
TWR - 3293

FINAL REPORT

DEVELOPMENT OF A FILAMENT WOUND CASE DESIGN FOR SOLID PROPELLANT ROCKET MOTORS IN THE 260-INCH DIAMETER CLASS

by

C. W. Vogt

THIOKOL CHEMICAL CORPORATION
WASATCH DIVISION
Brigham City, Utah

prepared for

NATIONAL AERONAUTICS AND SPACE ADMINISTRATION

March 1969

CONTRACT NAS-10287

NASA Lewis Research Center
J. J. Notardonato, Project Manager

Publications No. 0369-22650

Page Intentionally Left Blank

FOREWORD

This final report covers the work performance by the Wasatch Division of Thiokol Chemical Corporation under Contract NAS3-10287 from 1 Jul 1967 through 28 Feb 1969. This work was initiated by the Chemical and Nuclear Rocket Processing Section (Project 16083), under the administration of Mr. J. J. Notardonato of Lewis Research Center, National Aeronautics and Space Administration, Cleveland, Ohio 44135.

The program was conducted under the direction of Mr. T. Walker, Program Management, with Mr. C. W. Vogt, Structural Design, performing the design tasks and technical coordination. The following personnel were principal contributors to the program:

Mr. C. S. Wright and D. C. Youngkeit, Filament Winding

Mr. R. E. Warner, Tool and Facilities

Mr. E. H. Dunn, Test

Page Intentionally Left Blank

ABSTRACT

During the period between July 1967 to March 1969, a program to develop technology for the design and fabrication of a 260-in. (6.6 m) diameter fiberglass motor case was successfully completed. During the course of the program, technology specifically in the areas of skirt attachment and aft dome designs was investigated. Skirt loads up to 17,900 lb/in. (approximately 3.06 meganewtons/meter, MN/m) and domes with port openings up to 70 percent of chamber diameter were successfully demonstrated.

The program consisted of two primary tasks: (1) the design and fabrication of ten 18-in. (0.457 m) diameter subscale vessels, and (2) the design and fabrication of one 54-in. (1.372 m) diameter vessel with a 70 percent aft port opening and a 15,000 lb/in. (2.6 MN/m) minimum skirt load. All vessels were filament wound with epoxy impregnated S-994 glass roving. Both helical and planar winding patterns were evaluated. In conjunction with the polar winding pattern, aft domes with tape reinforcements and cut openings were evaluated.

The test results from the 18-in. diameter subscales correlated, in general, with theoretical predictions, indicating the feasibility of a 54-in. diameter vessel design having a planar winding pattern with a cut dome opening. The 54-in. vessel was fabricated and tested, successfully demonstrating a skirt loading of 17,900 lb/in. (3.06 MN/m) at a pressure of 5,860 psig (40.4 MN/m^2g).

Page Intentionally Left Blank

TABLE OF CONTENTS

LIST OF ILLUSTRATIONS

LIST OF ILLUSTRATIONS (Cont)

LIST OF ILLUSTRATIONS (Cont)

LIST OF ILLUSTRATIONS (Cont)

LIST OF ILLUSTRATIONS (Cont)

LIST OF TABLES

DEVELOPMENT OF A FILAMENT-WOUND CASE DESIGN FOR SOLID PROPELLANT ROCKET MOTORS IN THE 260-INCH DIAMETER CLASS

By C. W. Vogt
Thiokol Chemical Corporation
Wasatch Division

SUMMARY

This report constitutes the final report for NASA Contract No. NAS 3-10287 "Development of Filament-Wound Case for Solid Propellant Rocket Motor." The task of this program was to develop technology applicable to the design and fabrication of a 260-in. (6.6 m) diameter filament wound rocket motor case. The program was conducted from July 1967 to March 1969 and included the design and fabrication of ten 18-in. (0.457 m) diameter vessels and a 54-in. (1.372 m) diameter subscale motor case with a potential 260-in. configuration.

The 18-in. diameter vessels consisted of three helical and eight planar wound designs with L/D ratios of 3 and 5. A maximum skirt loading of 13,500 lb per circumferential in. (2.36 MN/m) at an internal pressure of 6,150 psig (42.4 MN/m^2g) was obtained from a planar wrapped vessel with an aft dome having a 70 percent port opening and tape reinforcements around the opening. A helical vessel with no aft dome reinforcements obtained a skirt loading of 12,400 lb/in. (2.17 MN/m) at an internal pressure of 5,620 psig (38.7 MN/m^2g). Five vessels failed prematurely: three due to skirt rupture, one in the aft dome, and one due to excessive bladder leakage.

During the 18-in. diameter test effort, it was demonstrated that the planar wound vessels with the reinforced aft dome were the most efficient and the simplest type to wind. Therefore, it was selected for the 54-in. diameter vessel design. The 54-in. diameter vessel was designed to an L/D ratio of 3, with a 70 percent aft port opening and a skirt load of 15,000 lb/in. (2.6 MN/m) at an internal pressure of 5,000 psig (34.5 MN/m^2g).

The actual 54-in. diameter vessel had a length of 160 in. (4.064 m) and an outside diameter of 55.1 in. (1.40 m). The aft polar boss had a port opening of 37.1 in. (0.942 m) and included threaded holes for the hydrotest closure attachment. The vessel successfully went through a 3-min proof cycle held at 4,000 psig (27.6 MN/m^2g) prior to burst, which occurred at 5,860 psig (40.4 MN/m^2g). Failure occurred in the aft dome, in which the hoop wrap at midcylinder had a filament stress of 375,000 psi (2.59 GN/m^2). The total thrust load just prior to burst was 3.0×10^6 lb (1.36×10^6 kg), which subjected the skirt to a compressive load of 17,900 lb/in. (3.06 MN/m).

The design configuration for a 260-in. diameter case, as demonstrated by the 54-in. diameter subscale case, was based on state-of-the-art design techniques and materials. A 260-in. diameter design with an L/D ratio of 5 and the same geometric configurations as the 54-in. vessel would have an estimated minimum performance factor of 0.50×10^6 in.-lb/lb (0.13 MN m/kg), which is far superior to the performance of an equivalent all steel vessel. The only foreseeable restrictions to a fiberglass design as applied to a 260-in. diameter motor are the time and money required to develop the necessary fabrication, and handling techniques to install the glass roving material with the necessary control to obtain the high performance composite structure.

INTRODUCTION

Fiberglass has proven to be an efficient structural material for solid fuel rocket motor cases. It has been used on motor cases up to 156 in. (approximately 4 m) in diameter, both segmented and monolithic, with both types successfully fired and demonstrated as being state-of-the-art designs. Currently both the Minuteman and Poseidon missile systems employ fiberglass motor case components, which is further evidence that fiberglass should be considered as candidate material for motors in the 260-in. (6.6 m) diameter class, especially where greater reliability with a reduction of weight is desired.

The objective of this program was to develop design and fabrication technology for a 260-in. (6.6 m) diameter fiberglass rocket motor case with an aft port opening varying from 50 to 70 percent of the chamber diameter and a forward skirt capable of carrying an axial compressive load of 15,000 lb per circumferential inch (2.6 MN/m).

The test media for this program consisted of ten 18-in. (0.457 m) diameter pressure vessels and one 54-in. (1.372 m) diameter subscale motor case, all of which were designed to an ultimate internal pressure of 5,000 psig (34.5 MN/m^2g). The 18-in. vessels were used to evaluate winding patterns and structural configurations in order to generate data for the design and configuration of the 54-in. demonstration motor case - the candidate subscale case design for a 260-in. diameter motor.

18-INCH DIAMETER VESSELS

Design

The designs of the 18-in. (0.457 m) diameter vessels were based on the evaluation of large aft port openings and high forward skirt thrust loadings for filament wound motor cases. Of particular interest was the skirt attachment area and the dome shell structure around the large port openings.

The three basic case designs were (1) helical-hoop wrap, (2) planar-hoop wrap, and (3) planar-hoop wrap with a tape reinforced aft dome and a cut dome opening. The three basic aft port openings were 50, 60 and 70 percent of the case chamber diameter with aft dome thrust relief to give the respective skirt loads of 5,700, 8,000, and 11,000 lb per circumferential in. (1.0, 1.4, and 1.9 MN/m) at an internal pressure of 5,000 psig (34.5 MN/m^2g). The vessel geometries and loadings that were evaluated are tabulated in Table I, and the 18-in. vessel designs are shown in Appendix A. The respective drawing numbers for each of the vessels are as follows:

Vessel 1	9U41359
Vessel 2	9U41361
Vessel 3	9U41363
Vessel 4	9U41364
Vessel 5	9U41365
Vessel 6	9U41366
Vessel 7	9U41367
Vessel 9	9U41369

Vessel 8 was identical to Vessel 5 except for an increase in the skirt wall thickness and additional tape reinforcements in the aft dome. IR & D No. 4 was not in the original program plan and was included at the latter part of Task I to obtain more data on the planar wrap design with a cut aft dome opening.

Each of the 18-in. diameter vessels had its own primary design considerations, and the type of analysis as applied to these areas is shown in the following sections, using the various vessels as illustrative examples.

TABLE I

DESIGN SPECIFICATION FOR 18-IN. DIAMETER VESSEL

Vessel	Type[a]	Length (in.)	Length (mm)	Aft Boss Bore Dia (in.)	Aft Boss Bore Dia (mm)	Forward Boss Bore Dia (in.)	Forward Boss Bore Dia (mm)	Forward Skirt Compressive Load[b] (lb/in.)	Forward Skirt Compressive Load[b] (MN/m)
1	(1)	36	(914)	9.0	(229)	8.2	(208)	5, 700	(0.998)
2	(1)	36	(914)	12.5	(318)	12.0	(305)	11, 000	(1.926)
3	(3)	90	(2, 286)	9.0	(229)	3.6	(91)	5, 700	(0.998)
4	(3)	36	(914)	10.5	(267)	3.6	(91)	8, 000	(1.401)
5	(3)	36	(914)	12.5	(318)	3.6	(91)	11, 000	(1.926)
6	(3)	36	(914)	12.5	(318)	3.6	(91)	Capped Ports (w/o skirts)	
7	(2)	36	(914)	9.0	(229)	3.6	(91)	5, 700	(0.998)
8	(3)	36	(914)	12.5	(318)	3.6	(91)	11, 000	(1.926)
9	(1)	90	(2, 286)	12.5	(318)	8.2	(208)	11, 000	(1.926)
IR & D No. 4	(3)	36	(914)	10.5	(267)	3.6	(91)	8, 000	(1.401)

[a]Type of fabrication
(1) Helical-hoop wrap.
(2) Planar-hoop wrap.
(3) Planar-hoop wrap with tape reinforced aft dome and cut dome opening.

[b]Thrust load at 5, 000 psig (34.5 MN/m^2g).

Case cylindrical section. - The vessels were wound with S-994-HTS continuous glass roving preimpregnated with medium temperature cured epoxy resin. The longitudinal wrap was either applied in a planar (polar) or a helical type winding pattern with the hoop wrap either interspersed or segregated, depending on design requirements. Based on past performance data, a glass tensile strength of 360,000 psi (2.48 GN/m^2) was selected for the ultimate filament strength. Figure 1 depicts actual hoop burst test data as a function of the hoop glass thickness and mean hoop wrap radius. The design ultimate for the polar and helical wrap was also established at 360,000 psi.

The two methods of analysis that were employed for the cylindrical section were: (1) the "netting" approach*, and (2) the treatment of the structure as a composite elastic orthotropic shell. For low angles of longitudinal wrap (greater than 0 deg and less than 20 deg, 0-0.35 rad) and a balance** load pattern, the "netting" analysis has proven to be very adequate. However, as the angle of the longitudinal wrap increases and the magnitudes of the hoop and longitudinal strains differ, the Poisson's effects, which are a function of the resin matrix, become influential and must be taken into consideration. The equations used in these two approaches are as follows:

"Netting" Analysis

$$\sigma_{g\alpha} = \frac{N_\varphi}{t_{\alpha g} \cos^2 \alpha} \tag{1}$$

$$\sigma_{g\theta} = \frac{N_\theta}{t_{\theta g} + t_{\alpha g} \sin^2 \alpha} \tag{2}$$

Elastic Orthotropic Analysis

$$\sigma_{g\alpha} = E_g \left(\epsilon_\varphi \cos^2 \alpha + \epsilon_\theta \sin^2 \alpha \right) \tag{3}$$

$$\sigma_{g\theta} = E_g \, \epsilon_\theta \tag{4}$$

$$\epsilon_\varphi = \frac{1}{t_\alpha} \left[\frac{N_\varphi}{E_\varphi} - \mu^{\alpha}_{\theta\varphi} \frac{N_\theta}{E_\theta} \left(\frac{t_\alpha}{t_\theta} \right) \right] \tag{5}***$$

*Only the filaments are assumed to carry the membrane loading.

**Equal longitudinal and hoop strain.

***Equation (5) is based on the assumption that negligible longitudinal load is carried by the hoop wrap due to crazing.

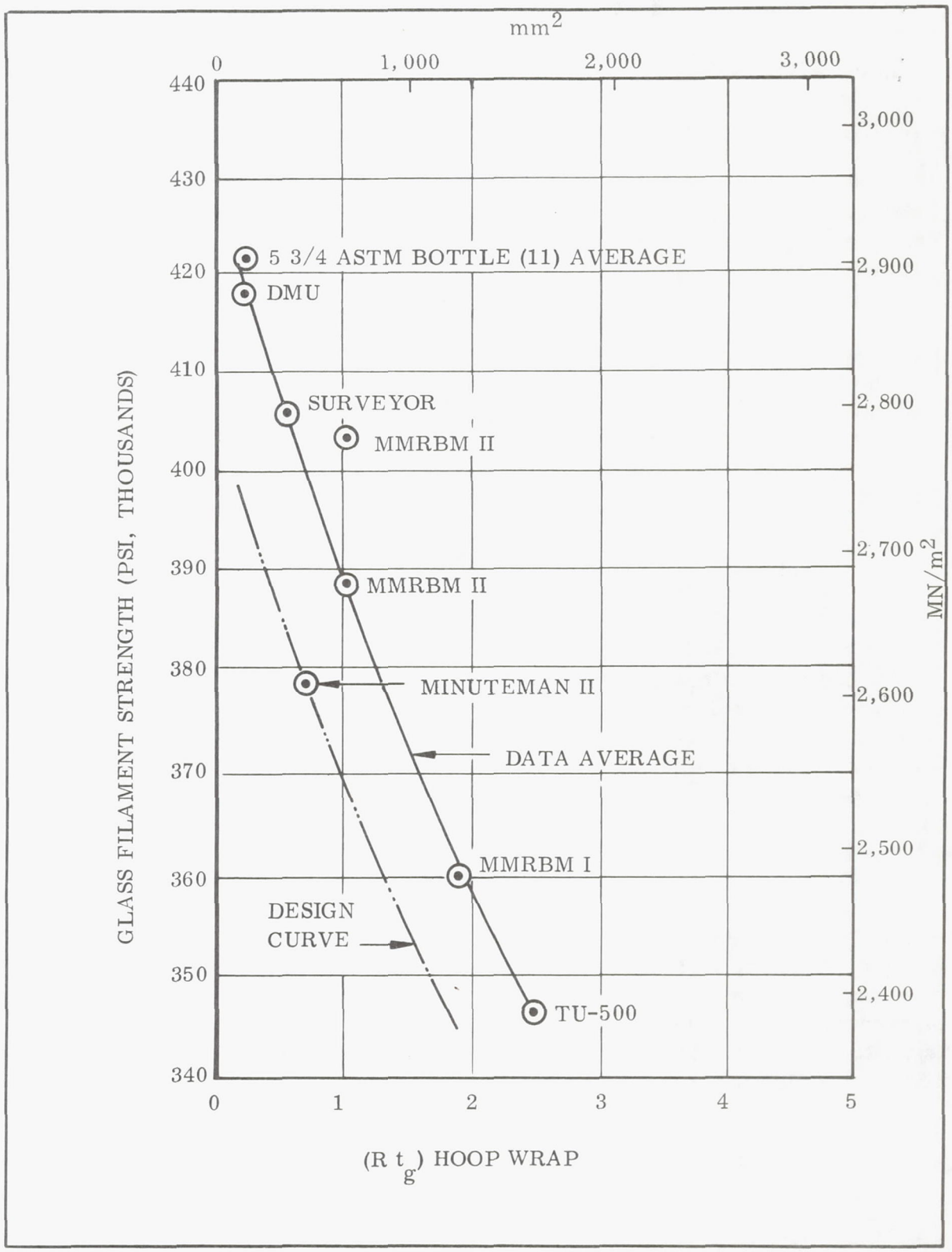

Figure 1. - Hoop Burst Test Data for S-994 HTS Filament Strength

$$\epsilon_\theta = \frac{1}{t_c}\left(\frac{N_\theta}{E_\theta} - \mu_{\varphi\theta}\frac{N_\varphi}{E_\varphi}\right) \tag{6}$$

$$\frac{E_\theta}{E_\varphi} = \frac{\mu_{\theta\varphi}}{\mu_{\varphi\theta}} \tag{7}$$

$$E_\theta = \frac{1}{t_c}\sum_{i=1}^{n}\left(E_\theta t\right)_n \tag{8}$$

$$E_\varphi = \frac{1}{t_c}\sum_{i=1}^{n}\left(E_\varphi t\right)_n \tag{9}$$

$$\mu_{\varphi\theta} = \frac{\sum_{i=1}^{n}\left(E_\theta t \mu_{\varphi\theta}\right)_n}{\sum_{i=1}^{n}\left(E_\theta t\right)_n} \tag{10}$$

The filament orientation of the longitudinal wrap is a function of the dome openings and vessel lengths. For helical designs the cylindrical wrap angle (α) is established from the dome geodesic requirements at the cylinder-dome tangent plane which is defined as:

$$\alpha_o = \sin^{-1}\frac{R_E}{R_{cyl}} \tag{11}$$

where R_E is the radius of the dome opening and R_{cyl} is the radius of the cylindrical section. The wrap angle (α) may either equal α_o where α_o is identical for the two domes or may be an average value where the α_o is different for each dome. The planar wrap angle ($\bar{\alpha}$) for the polar wrap designs is a function of the two dome openings (R_{EA}, R_{EF}) and the total dome-to-dome chamber length (L_{TOT}) is as defined below:

$$\bar{\alpha} = \tan^{-1}\frac{R_{EA} + R_{EF}}{L_{TOT}} \tag{12}$$

The elastic properties (E_θ, E_φ, $\mu_{\varphi\theta}$) for a balanced S-994 glass epoxy resin laminate are a function of filament orientation and are shown plotted relative to the filament orientation in Figures 2 and 3 with the effects of crazing included. The equations used to determine these properties are depicted in References 1 and 2 and have been programed at Thiokol Wasatch Division on a high speed digital computer.

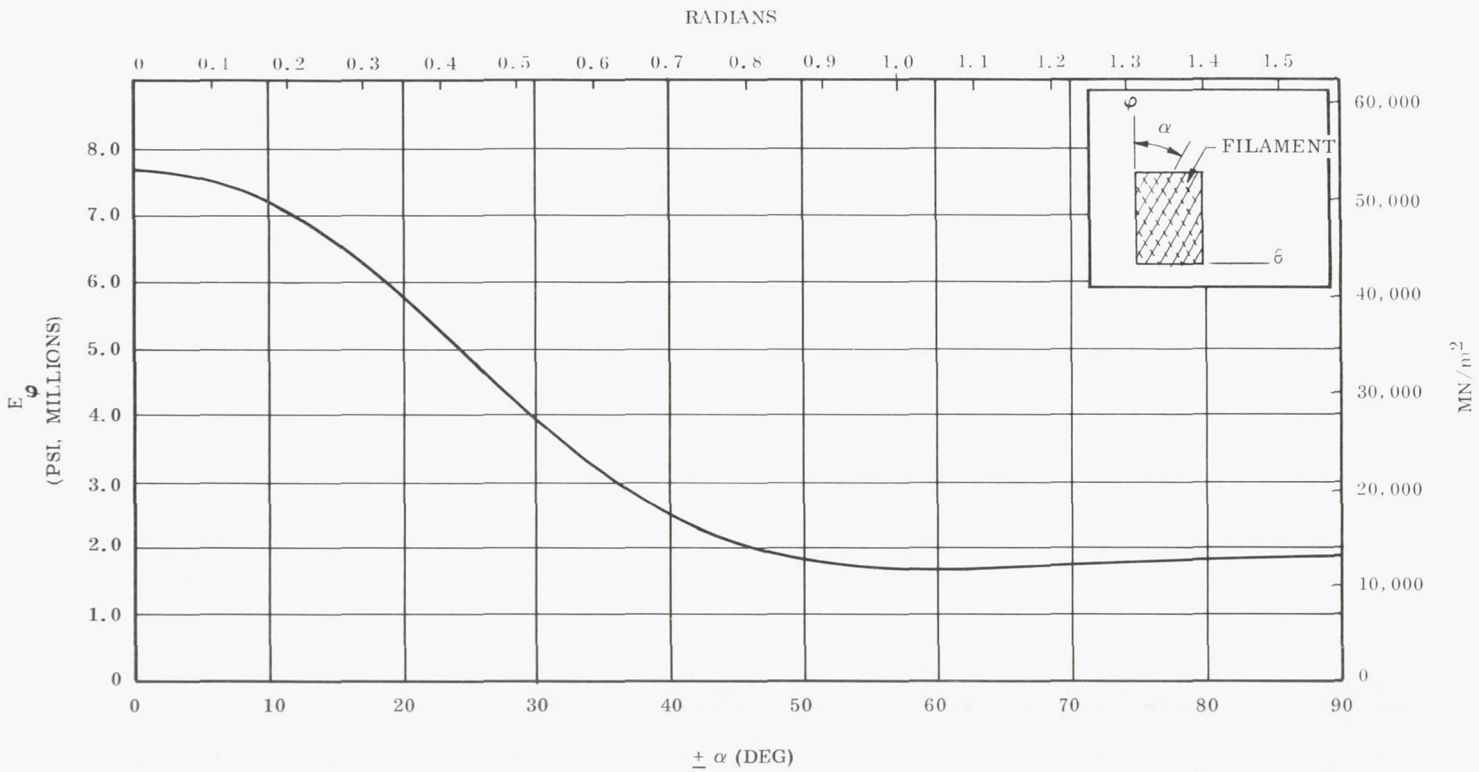

Figure 2. - Extensional Composite Elastic Modulus, S-994 Glass Filament, Epoxy Resin 20 Percent (Weight)

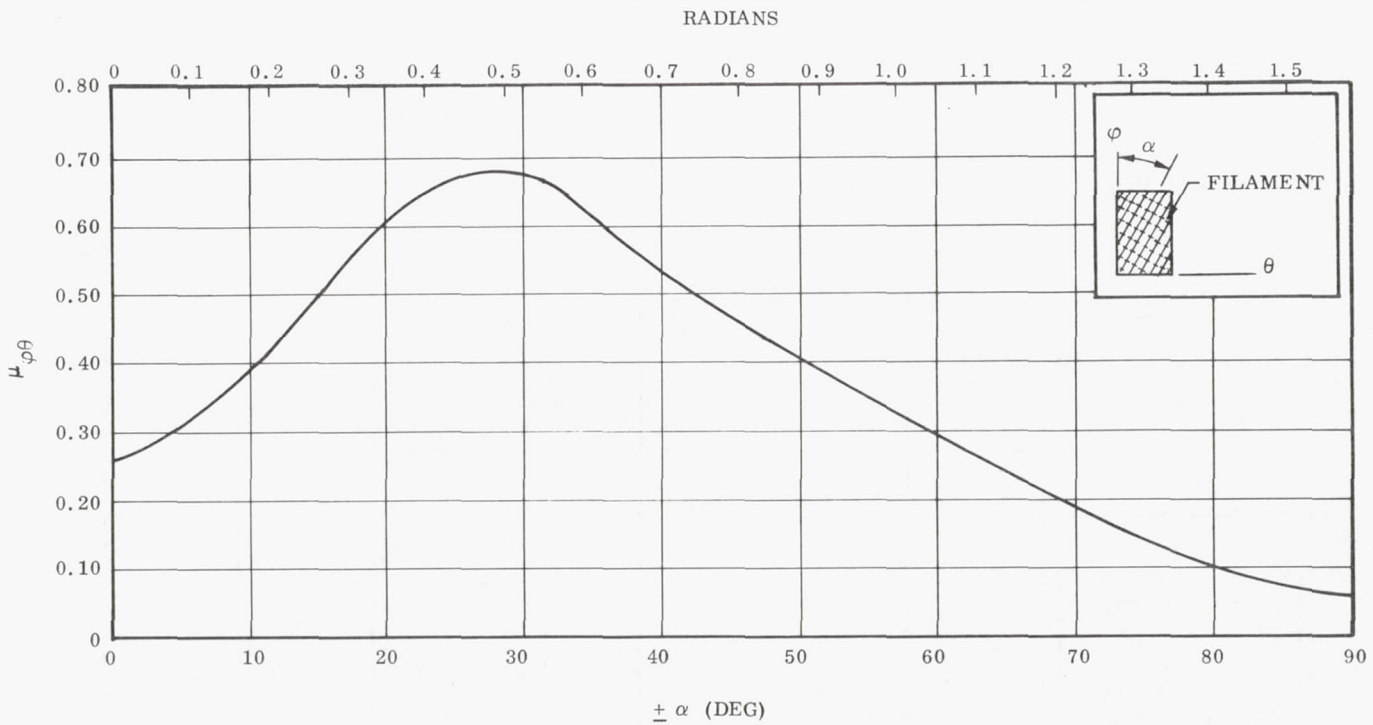

$\mu_{\varphi\theta}$ = RATIO OF STRAIN IN θ DIRECTION TO STRAIN IN φ DIRECTION, AS CAUSED BY AN EXTENSIONAL STRESS IN φ DIRECTION.

Figure 3. - Composite Elastic Poisson's Ratio, S-994 Glass Filament, Epoxy Resin 20 Percent (Weight)

The wrap configurations and the method of analysis employed in the cylindrical section are shown in Table II for all the 18-in. diameter vessels. The two extreme wrap configurations were Vessel 2, with a 50-deg (0.87 rad) helical wrap pattern, and Vessel 3 with a 3.5-deg (0.06 rad) planar pattern.

Forward dome structure. - The forward dome contours were generated by the "netting" analysis, using a high speed digital computer. The dome shape is a function of the longitudinal wrap geometry in that the principal load vector is essentially maintained coincidental with the filament orientation. For the helical wrap designs the basic objective was to keep the dome shape as close to geodesic as possible in order to prevent filament slippage during fabrication and to maintain uniform filament stresses throughout the dome. The domes for the planar wrap designs, which were inherently nongeodesic, were shaped to keep the principal load vectors as close to the filament orientation as possible while keeping the hoop strains in the area of the tangent plane as small as possible.

Helical wrap design: Vessels 1, 2, and 9 had helical winding patterns with the aft domes of Vessels 1 and 2 being true geodesics. The geodesic shape is a function of the filament orientation (α_i) which is defined as:

$$\alpha_i = \sin^{-1} \frac{R_{\alpha i}}{R_{cyl}} \tag{13}$$

where $R_{\alpha i}$ is the radius of any point on the shell and R_{cyl} is the radius of the cylindrical section. This geodesic requirement is maintained from the tangent plane to the inflection point, or to where the filament orientation becomes $\pm$ 54 deg 45 min (0.958 rad) relative to the meridian. The advantage of the helical goedesic design is that there is essentially no winding slippage and that the vessel designs are not length limited. The greatest disadvantage to a true geodesic configuration is that the two dome openings must be identical. For a helical wrap design a general disadvantage is that the crossover areas inherent to the multicircuit pattern degrade the strength of the composite.

The forward and aft domes of Vessel 1 were geodesic and had equal forward and aft dome openings. Vessel 2 also had geodesic domes, in that the forward dome had a geodesic filament pattern at the forward tangent line and a forward glass opening equal to that of the aft dome. However, due to the severe loading imposed by the forward boss on the dome shell, the basic dome shape was modified and the quantity of glass roving was increased. The forward and aft domes of Vessel 9 were not wound in a geodesic pattern in order to minimize the size of the forward opening. The limiting factor was slippage during winding, and past experience has shown that a deviation from the geodesic angle at the tangent plane could be as high as 8.0 deg (0.14 rad) without inducing slippage during winding. The geodesic angle (α_{oA}) for the aft dome

TABLE II

CYLINDRICAL SECTION WRAP CONFIGURATION AND FILAMENT STRESSES FOR 18-IN. DIAMETER VESSEL

Vessel	No. of Hoop Plies[a]	No. of Longitudinal Layers[b]	Longitudinal Filament Orientation (deg)	Longitudinal Filament Orientation (rad)	[p = 5,000 psig (34.5 MN/m^{2}g)] Hoop Filament Stress at Midcylinder (psi)	Hoop Filament Stress at Midcylinder (GN/m^2)	Longitudinal Filament Stress at Tangent Plane (psi)	Longitudinal Filament Stress at Tangent Plane (GN/m^2)	Longitudinal Filament Stress at Midcylinder (psi)	Longitudinal Filament Stress at Midcylinder (GN/m^2)	Wrap Sequencing
1	24	14	±34.5	(0.602)	343,000 (1)[c]	(2.36)	320,000 (2)	(2.21)	250,000 (2)	(1.72)	Hoop overwrap
2	10	22	±50	(0.873)	359,000 (2)[d]	(2.48)	294,000 (1)	(2.03)	190,000 (2)	(1.31)	Hoop overwrap
3	34	9	±3	(0.052)	333,000 (1)	(2.30)	296,000 (1)	(2.04)	238,000 (1)	(1.64)	Hoop overwrap
4	34	9	±9	(0.157)	329,000 (1)	(2.27)	302,000 (1)	(2.08)	203,000 (1)	(1.40)	Interspersed
5	34	9	±9	(0.157)	329,000 (1)	(2.27)	272,000 (1)	(1.87)	160,000 (1)	(1.10)	Interspersed
6	34	10	±9	(0.157)	328,000 (1)	(2.26)	287,000 (1)	(1.98)	287,000 (1)	(1.98)	Interspersed
7	34	9	±13	(0.227)	324,000 (1)	(2.23)	311,000 (1)	(2.14)	250,000 (1)	(1.72)	Hoop overwrap
8	35	10	±9	(0.157)	320,000 (1)	(2.21)	245,000 (1)	(1.69)	144,000 (1)	(0.99)	Interspersed
9	22	16	±42	(0.733)	335,000 (2)	(2.31)	310,000 (2)	(2.14)	220,000 (2)	(1.52)	Hoop overwrap
IR & D No. 4	34	10	±9	(0.157)	328,000 (1)	(2.26)	272,000 (1)	(1.88)	183,000 (1)	(1.26)	Interspersed

[a] A hoop ply has 200 ends/in./ply (7,874/m).
[b] A longitudinal layer has 406 ends/in./layer (15,984/m).
[c] (1) denotes "netting" analysis.
[d] (2) denotes orthotropic composite analysis.

opening of Vessel 9 as calculated from equation (11) is as follows:

$$\alpha_{oA} = \sin^{-1}\left(\frac{R_{EA}}{R_{cyl}}\right)_{aft} = \sin^{-1}\frac{7.00}{9.15} = 50 \text{ deg } 00 \text{ (0.87 rad) min}$$

A helical winding angle of 42 deg, 0.73 rad (8 deg, 0.14 rad, off geodesic) was selected to allow the diameter of the forward dome opening to be compatible with a 34-deg (0.60 rad) geodesic angle. From equation (11) the radius of the forward opening is:

$$\left(R_{EF}\right)_{fwd} = R_{cyl} \sin 34 \text{ deg} = 7.0 \text{ in. (178 mm)}$$

Further reduction in the size of the forward opening would tend to compromise the design efficiency of the vessel. Additional helical wrap or tape reinforcements would be required in the resulting high stressed area around the forward boss, and the resulting dome shape would not be ideal for length-to-volume motor requirements.

Polar wrap design: The remaining 18-in. diameter vessels were all wound in a polar pattern,and all essentially had identical forward dome profiles. The polar or in-plane wrapping pattern is very attractive due to the simplicity of winding and due to the fact that there are usually no multi-loop filament crossover points. The greatest disadvantage to this type of pattern is roving slippage during winding, which limits the total length of the vessel and the diameter of the polar openings.

The planar wrapped vessels all had 30 percent dome (glass) openings. The contour of the dome was a function of the planar wrap angle ($\bar{\alpha}$) with the dome shape established by a modified version of the "netting" analysis. Due to dome distortions during pressurization and the low tensile strength of the shell structure in the hoop direction near the tangent plane, the "netting" analysis has been modified to establish contours that will give a slightly negative hoop load bias at low pressures. The shell deforms as a function of increasing pressure and the initial negative hoop strain becomes slightly positive. Strain gage data reveals that for shell structure with a filament orientation of less than 30 deg (0.52 rad) relative to the meridian, crazing will initiate at a hoop strain of around 1 percent. The limitation on the extent of the dome contour modification is the magnitude of the initial negative hoop load bias which could cause possible crippling of the structure, or the resulting high meridional tensile loads in the area of the polar bosses which could cause filament rupture.

Skirt attachment. - The forward skirt attachment design was identical for all vessels with only the length and thicknesses varied relative to the thrust loading. The thrust load in the skirt is transferred into the case through two elastomeric shear plies as shown in Figure 4. The percentage of the load taken out of the skirt by each shear ply is a function of the extensional stiffnesses of the case, skirt and overwrap structure, and the shear stiffness of each shear ply. The two primary modes of deflection are a result of the axial membrane strain in the longitudinal wrap and the axial movement of the skirt.

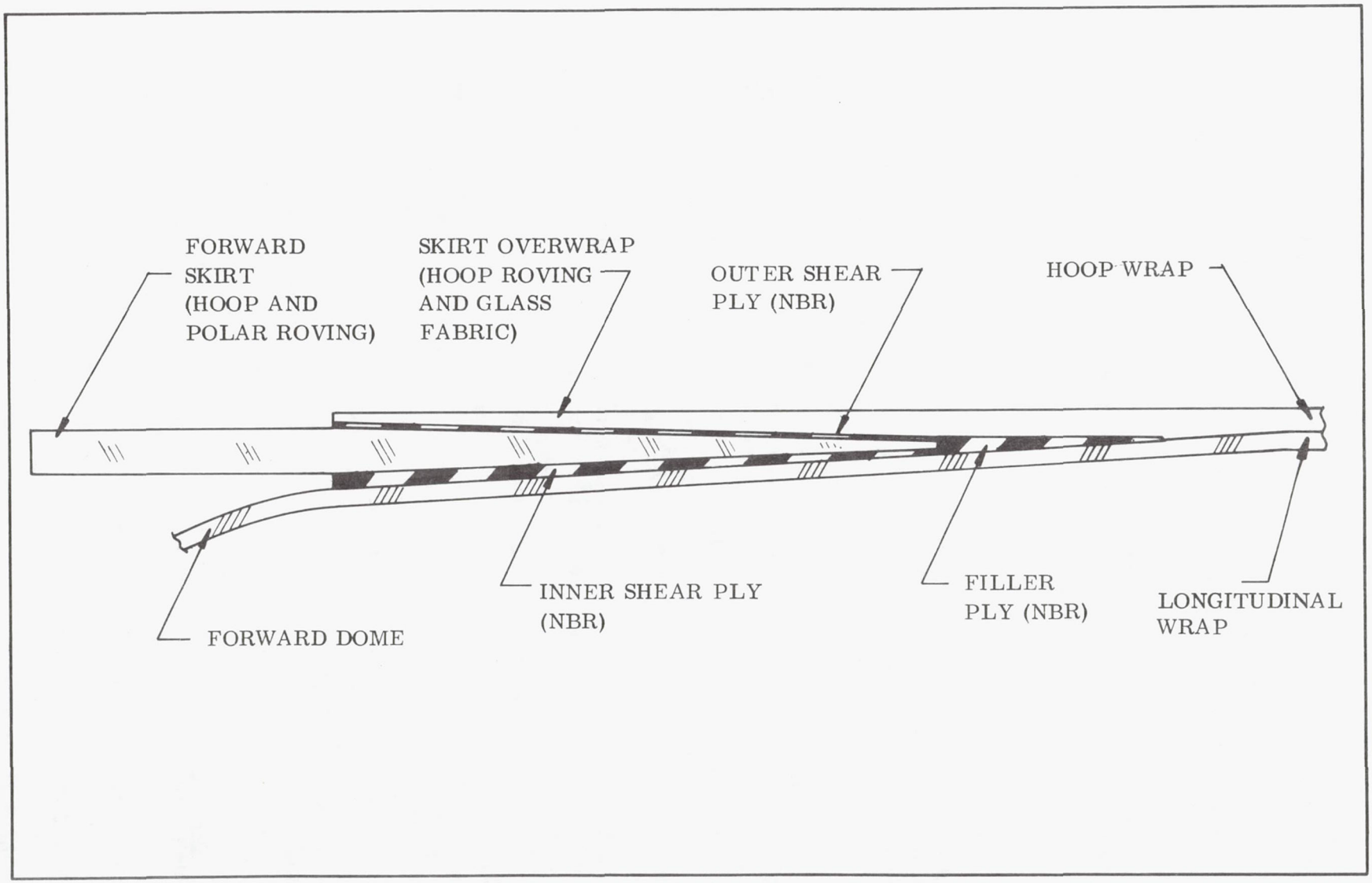

Figure 4. - Skirt Attachment Configuration

The analysis used to obtain the basic equilibrium equations employs the shear lag principle where the elastomeric shear ply is considered the shear web; and the case, skirt and overwrap structure are considered axial stringers. The basic differential equations as presented in Reference 3 are as follows:

$$\frac{d\tau_R}{dx} = \left(\frac{\sigma_A}{E_A} - \frac{\sigma_B}{E_B}\right)\left(\frac{G}{t_{oR} + \alpha_x}\right) \tag{14}$$

$$\frac{d\sigma_B}{dx} = -\left(\tau_R + \beta\sigma_s\right)\left(\frac{1}{t_{oB} + \beta_x}\right) \tag{15}$$

$$\frac{d\sigma_A}{dx} = \frac{\tau_R}{t_A} \tag{16}$$

where the thickness of the shear ply ($t_{oR} + \alpha_x$) and the thickness of one of the stringers ($t_{oB} + \beta_x$) is a linear variable relative to distance (x) along the attachment area. These basic differential equations (14), (15), and (16) are programed on the digital computer and solved to determine the stress profiles along the attachment area.

During case expansion a portion of the thrust load (N_{s1}) and a portion of the load in the overwrap (P_{o1}) are transferred into the case longitudinal wrap as a function of axial shear distortion in the shear ply. The skirt is treated as being fixed at the thin end, allowing compressive deformation of the skirt structure. The remainder of the thrust load (N_{s2}) is transmitted from the skirt through the inner and outer shear ply as a function of the axial movement of the skirt relative to both the overwrap and longitudinal wrap structure. Figure 5 depicts the analytical models as applied to the two types of deformation. The axial and shear stresses along the length of the joint are calculated by the digital computer.

The design and analysis of the Vessel 8 skirt attachment area is typical to that of all vessels. The elastic properties and structural geometry data for Vessel 8 that were entered into the digital computer are as follows:

Skirt

t_1 = 0.05 in. (1.3 mm)

t_2 = 0.54 in. (13.7 mm)

E_φ = 4.1×10^6 psi (28.3 GN/m^2)

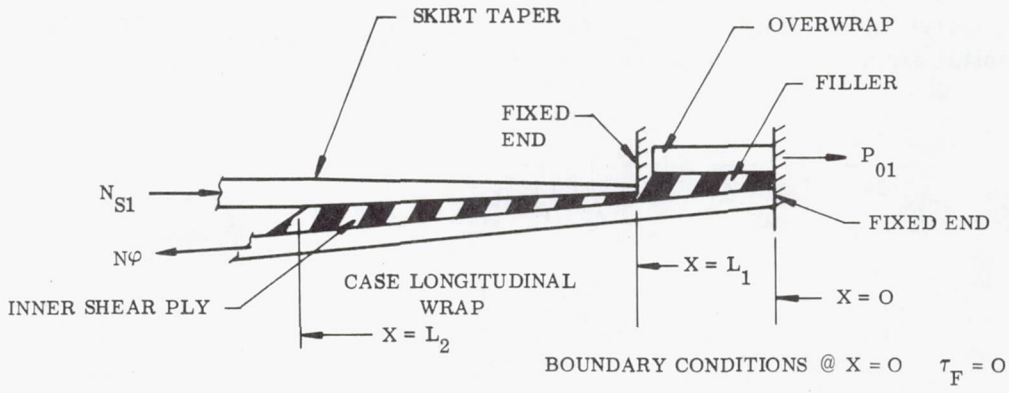

CASE EXPANSION

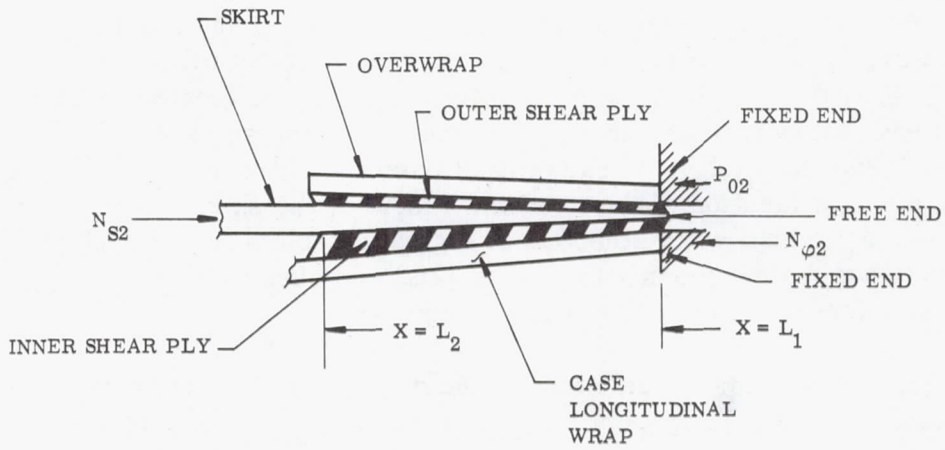

SKIRT MOVEMENT

Figure 5. - Skirt Attachment Analytical Models

Overwrap

$t = 0.24$ in. (6.1 mm)

$E_{\varphi} = 3.0 \times 10^6$ psi (20.7 GN/m^2)

Longitudinal wrap

$t_{\alpha} = 0.14$ in. (3.6 mm)

$E_{\alpha\varphi} = 6.6 \times 10^6$ psi (45.5 GN/m^2)

Axial strain

$x = L_2 = 0.024$ in./in. (4.2 N/m)

$x = L_1 = 0.019$ in./in. (3.3 N/m)

$x = 0 = 0.013$ in./in. (2.3 N/m)

Outer shear ply

$t = 0.06$ in.

$G = 300$ psi (2.1 MN/m^2)

Inner shear ply

$t_1 = 0.03$ in. (10.8 mm)

$t_2 = 0.27$ in. (6.9 mm)

$G = 300$ psi (2.1 MN/m^2)

Filler ply

$t_o = 0.03$ (0.8 mm)

$t_1 = 0.14$ (3.6 mm)

$G = 300$ psi (2.1 MN/m^2)

Joint length

$L_1 = 3.0$ in. (76 mm)

$L_2 = 15.0$ in. (381 mm)

The axial strain in the longitudinal wrap is a result of an iterative process where the transfer of the thrust load is first approximated and then corrected by several runs on the computer.

The final results from this analysis are summarized below, where the loads are as defined in Figure 5.

The loads transmitted by the inner shear ply and filler as a result of case expansion between the distances:

$x = 0$ and $x = L_1$ $\quad N_{s1} = 1,150$ lb/in. (0.201 MN/m) and
$P_{01} = 370$ lb/in. (0.065 MN/m),

$x = L_1$ and $x = L_2$ $\quad N_{s1} = 4,680$ lb/in. (0.819 MN/m),

thus giving a total load of $\quad N_{s1} = 5,830$ lb/in. (1.02 MN/m) and
$P_{01} = 370$ lb/in. (0.065 MN/m).

The relative load transfer through the inner and outer shear ply is:

$$P_{02} = 0.72\, N_{s2}$$

$$N_{\varphi 2} = 0.28\, N_{s2}$$

The net resulting loads at 5,000 psig (34.5 $MN/m^2 g$) as a result of superimposing the two loading conditions are as follows:

$N_s = 11,000$ lb/in. (1.9 MN/m)

$N_{s2} = 5,170$ lb/in. (0.905 MN/m)

$P_{02} = 3,720$ lb/in. (0.651 MN/m)

$P_o = 3,350$ lb/in. (0.586 MN/m)

$N_{\varphi 2} = 1,450$ lb/in. (0.253 MN/m)

The shear stress profile in the two shear ply is shown plotted in Figure 6 as a function of the axial distance along the joint. The discontinuity bending and shear loads have negligible effects on the shear stresses in the shear ply.

The critical area in the skirt attachment area is at the leading edge of the inner shear ply. As shown in Figure 6, the shear stresses in the NBR peak out in this area to a stress of 800 psi (5.5 MN/m^2). Test data on NBR-epoxy/glass lap shear bonds with at least a 1,000 psi (6.9 MN/m^2) lateral compressive load bias has demonstrated an ultimate lap shear joint strength of 1,000 psi, a value

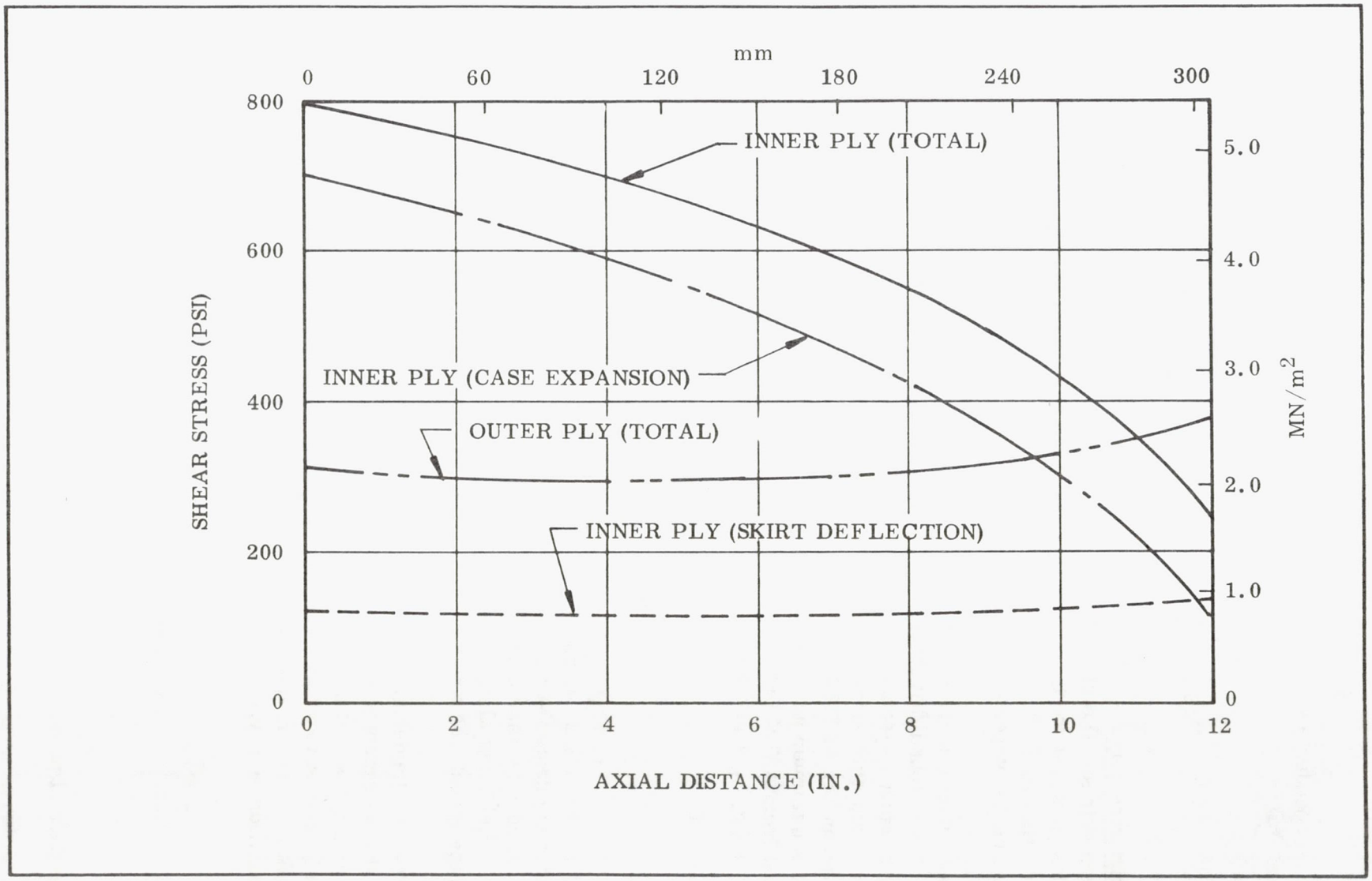

Figure 6. - Vessel 8 Skirt Shear Ply, Shear Stress Distribution

relatively independent of lap length. Therefore, the theroretical margin of safety for the joint was:

$$MS = \frac{F_{su}}{\tau} - 1 = \frac{1,000}{800} - 1 = +0.25$$

Skirt structure. - All 18-in. diameter vessels (with the exception of Vessel 6) had forward skirts. The skirt designs fell into three basic categories in accordance with the design thrust loads. These basic loads were 5,700, 8,000, and 11,000 lb/circumferential in. (1.0, 1.4, and 1.9 MN/m) which, along with the discontinuity bending moments, governed the skirt thickness requirements.

Each skirt was evaluated with respect to both buckling and material fracture criteria. It was found that the latter was more critical as a result of the high discontinuity bending moments in the skirt in the area adjacent to the case. The skirt compressive fracture strengths in the axial direction were first determined from test specimens per ASTM D695, neglecting the effects of hoop crazing. On Vessels 2, 4, and 5 the minimum axial compressive strength (70,000 psi or 483 MN/m^2) as determined from ASTM D695 was used as the material ultimate for the maximum axial stress ($\sigma_{\varphi max}$) in the skirt:

$$\sigma_{\varphi max} = \frac{N_s}{t_s} \pm \frac{6M}{t_s^2}$$

However, on Vessels 2, 4, and 5 it was vividly demonstrated by premature skirt failures that the design strength criteria must also include the effects of the hoop strain as induced by case expansion. The tensile hoop stress not only adds to the total stress field, but also causes some crazing in the longitudinal layers which degrades the structural strength in the axial direction.

Prior to the design of Vessels 8 and 9, a new material fracture criterion based on the maximum work theory was applied to the skirt structure. This approach for determining the material strength criteria is presented in Reference 4 and has been widely used in recent years, specifically on boron-epoxy and boron-glass-epoxy composites for aircraft application. The maximum work theory as applied to a plane stress condition in a typical ply of longitudinal wrap is as follows:

$$\left(\frac{\sigma_x}{F_x}\right)^2 - \left(\frac{1}{F_x^2} + \frac{1}{F_y^2} - \frac{1}{F_z^2}\right) \sigma_x \sigma_y + \left(\frac{\sigma_y}{F_y}\right)^2 + \left(\frac{\tau_{xy}}{F_s}\right)^2 = 1 \qquad (17)$$

where the field of plane stress in the longitudinal ply is shown on the following page.

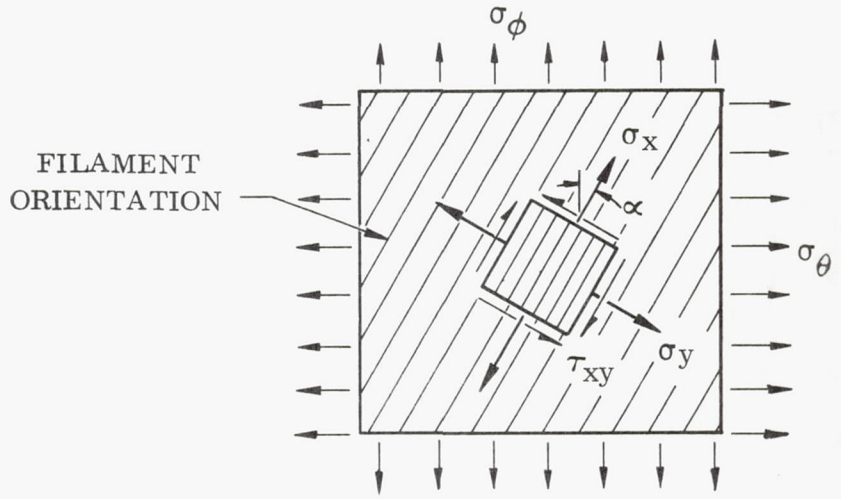

Since the material ply strength in the y and z plane is essentially the same, equation (17) reduces to the following failure criteria where a total value exceeding unity denotes failure:

$$\left(\frac{\sigma_x}{F_x}\right)^2 - \left(\frac{1}{F_x^2}\right) \sigma_x \sigma_y + \left(\frac{\sigma_y}{F_y}\right)^2 + \left(\frac{\tau_{xy}}{F_s}\right)^2 \leq 1 \tag{18}$$

The stresses in the x and y planes are obtained from the standard transformation equations

$$\sigma_x = \sigma_\varphi \cos^2 \alpha + \sigma_\theta \sin^2 \alpha \tag{19}$$

$$\sigma_y = \sigma_\varphi \sin^2 \alpha + \sigma_\theta \cos^2 \alpha \tag{20}$$

$$\tau_{xy} = -\left(\sigma_\varphi - \sigma_\theta\right) \sin \alpha \cos \alpha \tag{21}$$

The analysis performed on Vessel 8 is typical to that performed on vessels subsequent to Vessel 5. The approach used to determine the moments and shears in the case and skirt structure was based on a shell discontinuity analysis. This analysis was performed with the aid of the digital computer, which was used to compute the elastic material properties and free body influence coefficients. The resulting equations for the radial deflections and rotations were equated and solved for the internal bending moments and transverse shears.

The breakdown of the Vessel 8 structure into the basic free bodies and the tabulation of the elastic properties for each are shown in Figure 7. These properties and body geometries were put into the digital computer from which the theoretical deflections and loads were obtained as shown plotted in Figure 8.

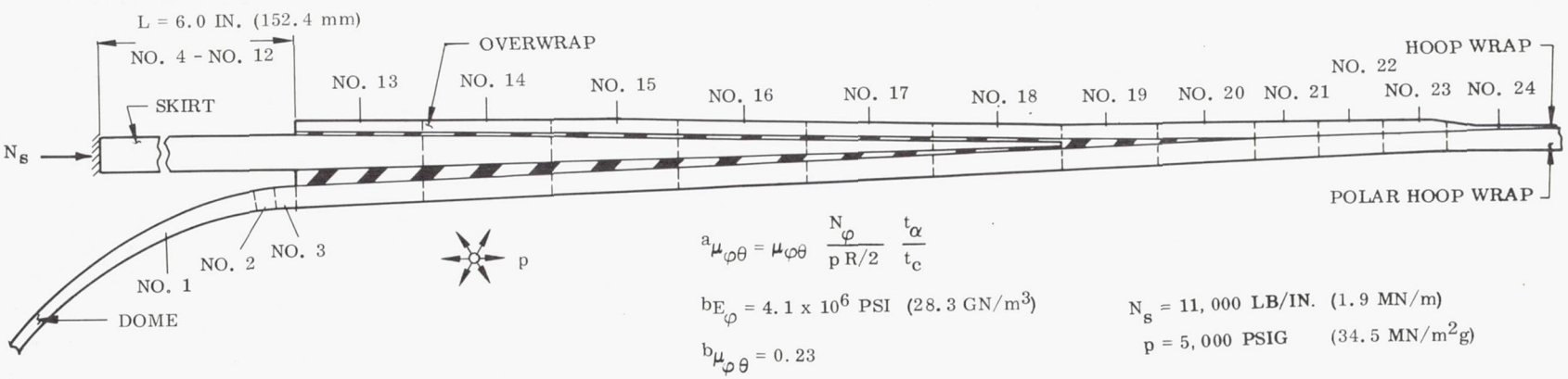

FREE BODY NO.	COMPOSITE THICKNESS (t_c, IN.)	(mm)	COMPOSITE HOOP MODULUS (E_θ, PSI)	(GN/m^2)	COMPOSITE LONG. BEND. STIFFNESS (D_φ, LB-IN.^{3})	(MN m^3)	AVERAGE RADIUS (R, IN.)	(mm)	LENGTH OF FREE BODY (L, IN.)	(mm)	POISSON'S[a] EFFECT DUE TO LONG. STRESS $E_\varphi = E_{\alpha\varphi}$
1	0.15	(3.8)	1.6×10^6	(11.0)	2.5×10^3	(187)	8.30	(210.8)	--	--	0.65
2	0.15	(3.8)	1.6	(11.0)	2.5	(187)	8.35	(212.1)	0.20	(5.1)	0.65
3	0.15	(3.8)	1.6	(11.0)	2.5	(187)	8.37	(212.6)	0.20	(5.1)	0.65
4 - 12[b]	0.54	(13.7)	4.4	(30.3)	57	(4,270)	9.15	(232.4)	0.667 (ea)	(16.9)	--
13	0.87	(22.1)	4.8	(33.1)	50	(3,742)	9.20	(233.7)	2.00	(50.8)	0.066
14	0.83	(21.1)	5.1	(35.2)	28	(2,096)					0.066
15	0.90	(22.9)	4.9	(33.8)	25	(1,871)					0.058
16	0.82	(20.8)	4.9	(33.8)	15	(1,123)					0.061
17	0.72	(18.3)	5.0	(34.5)	10	(748)					0.065
18	0.64	(16.3)	5.0	(34.5)	9	(671)			2.00	(50.8)	0.010
19	0.56	(14.2)	5.1	(35.2)	8	(599)			1.50	(38.1)	0.078
20	0.56	(14.2)	5.1	(35.2)	8	(599)			1.50	(38.1)	0.078
21	0.53	(13.5)	5.1	(35.2)	15	(1,123)			1.00	(25.4)	0.069
22	0.47	(11.9)	5.2	(35.9)	12	(898)			1.00	(25.4)	0.064
23	0.41	(10.4)	5.3	(36.5)	10	(748)			1.00	(25.4)	0.073
24	0.37	(9.4)	5.4×10^6	(37.2)	5×10^3	(374)	9.20	(233.7)	--	--	0.081

Figure 7. - Vessel 8 Forward Skirt-Case Junction Area

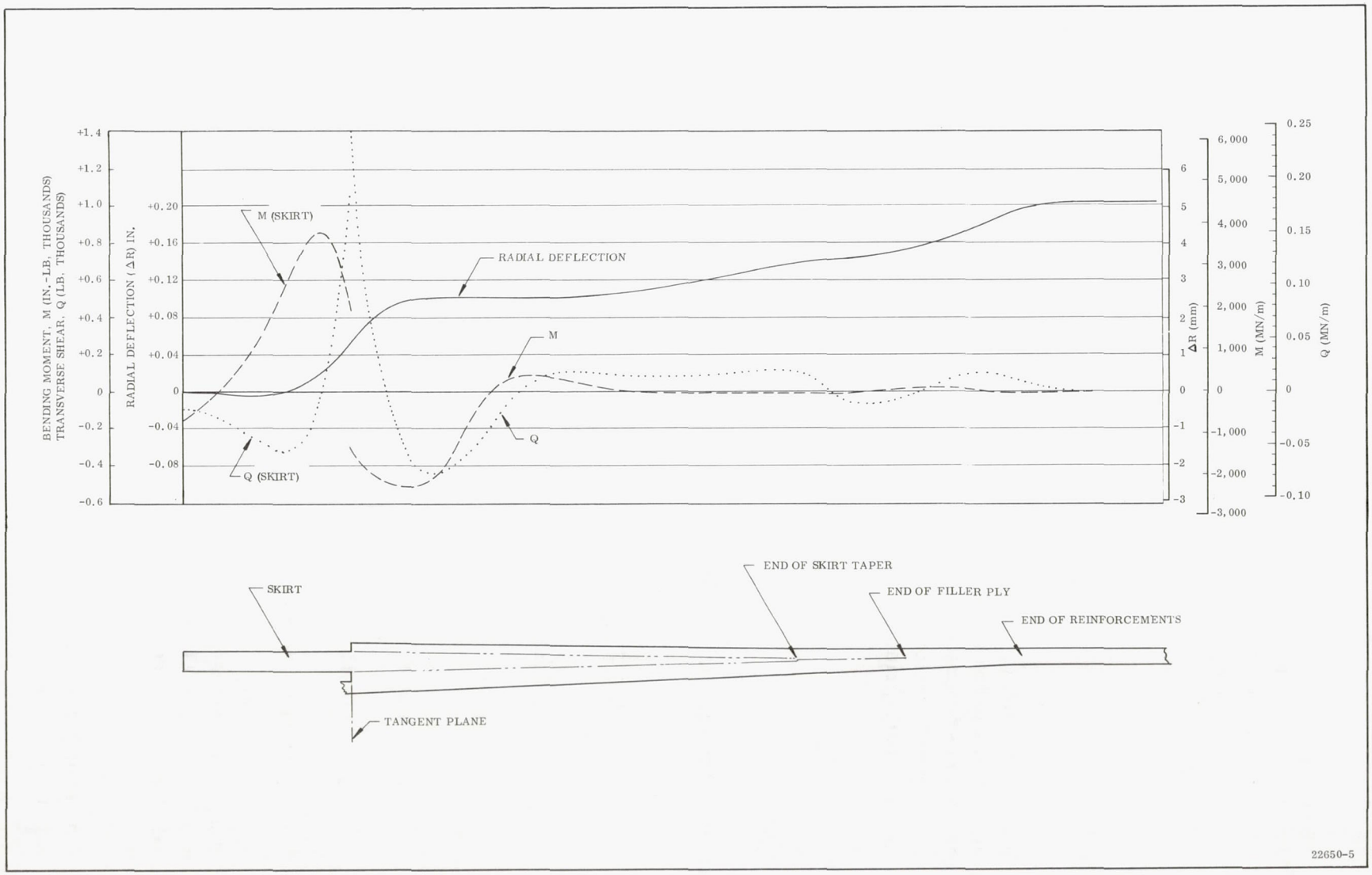

Figure 8. Vessel 8 Skirt Junction Discontinuity Loads and Deflections $\left[p = 5,000 \text{ psig } (34.5 \text{ MN/m}^2\text{g})\right]$

The critical area is in the skirt structure between free bodies No. 5 and 6 where the compressive stress is maximum in the outside layer of the longitudinal wrap. The stresses in this layer are obtained from equations (22) and (23).

$$\sigma_{\varphi} = \frac{E_{\varphi\alpha}}{(E_{\varphi}t)_c} \left(N_s + \frac{6\,M}{t_c} \right) \tag{22}$$

$$\sigma_{\theta} = \frac{\Delta R}{R} E_{\theta\alpha} \tag{23}$$

where $(E_{\varphi}t)_c$ is the total composite stiffness and $E_{\alpha\varphi}$ and $E_{\alpha\theta}$ are the moduli of the longitudinal layers in the axial and hoop directions respectively. The skirt structure was made up of interspersed hoop and polar wrap with 50 percent of each by volume. The polar wrap orientation (α) was $\pm$ 10 deg (0.17 rad), and the elastic modulus of a polar layer in each principal direction is as follows:

$$E_{\alpha\varphi} = 7.2 \times 10^6 \text{ psi}$$

$$E_{\alpha\theta} = 1.6 \times 10^6 \text{ psi}$$

The principal stresses in the longitudinal wrap at 5,000 psig (34.5 MN/m^2g) are:

$$\sigma_{\varphi} = \frac{7.2}{4.1\,(0.54)} \left[11{,}000 + \frac{6\,(830)}{0.54} \right] = -66{,}000 \text{ psi } (455 \text{ MN/m}^2)$$

$$\sigma_{\theta} = \frac{0.013}{9.15} \quad (1.6 \times 10^6) \quad = 2{,}300 \text{ psi } (15.8 \text{ MN/m}^2)$$

The stresses in the x-y plane as calculated from equations (19), (20), and (21) are:

$$\sigma_x = -66{,}000 \cos^2 10 \text{ deg} + 2{,}300 \sin^2 10 \text{ deg} = -64{,}100 \text{ psi } (442 \text{ MN/m}^2)$$

$$\sigma_y = -66{,}000 \sin^2 10 \text{ deg} + 2{,}300 \cos^2 10 \text{ deg} = 250 \text{ psi } (1.7 \text{ MN/m}^2)$$

$$\tau_{xy} = -(-66{,}000-2{,}300) \sin 10 \text{ deg} \cos 10 \text{ deg} = 11{,}700 \text{ psi } (80.7 \text{ MN/m}^2)$$

Substituting these stresses into the maximum work failure criteria equation (18), the theoretical margin of safety, equation (24), is based on material strengths as estimated from the Vessel 4 and 5 skirt failures by applying equation (14) to the failures.

The strengths of the longitudinal ply as estimated from the Vessels 2, 4, and 5 skirt failures are:

F_x = 72,000 psi (496 MN/m^2) (compressive)

F_y = 5,000 psi (34.5 MN/m^2) (tensile/compressive)

F_s = 25,000 psi (172 MN/m^2) (in-plane shear)

The margin of safety for the skirt structure with respect to the material fracture strengths can be obtained from equation (18) as rewritten in the form of equation (24):

$$MS = \left[\frac{1}{\left(\frac{\sigma_x}{F_x}\right)^2 - \left(\frac{\sigma_x\sigma_y}{F_x^2}\right) + \left(\frac{\sigma_y}{F_y}\right)^2 + \left(\frac{\tau_{xy}}{F_s}\right)^2}\right]^{1/2} - 1 \qquad (24)$$

$$= \left[\frac{1}{\left(\frac{64,100}{72,000}\right)^2 - \frac{64,100\ (250)}{(72,000)^2} + \left(\frac{250}{5,000}\right)^2 + \left(\frac{16,700}{25,000}\right)^2}\right]^{1/2} - 1$$

$$= [1.001]^{1/2} - 1 = 0.0$$

The margin of safety with respect to axial compressive buckling was based on the data presented in Reference 5. The buckling data was adapted to the skirt by using the orthotropic form of the classical buckling equation:

$$\sigma_{CR} = \frac{C\ [E_\theta E_\varphi]^{1/2}}{R/t} \qquad (25)$$

where the coefficient of buckling (C) was obtained from Reference 5 and is shown in Figure 9 as a function of the skirt R/t ratio.

Vessel 8

$R/t = 16.9$

$C = 0.48$

$$\sigma_{CR} = 0.48\ \frac{[4.4\ (4.1)]^{1/2}}{16.9} = 120,000 \text{ psi } (827\ MN/m^2)$$

The indicated critical buckling stress (σ_{CR}) of the skirt is higher than the fracture strength of the material; therefore, the buckling strength of the skirts on Vessel 8 and on the other 18-in. vessels was not considered critical.

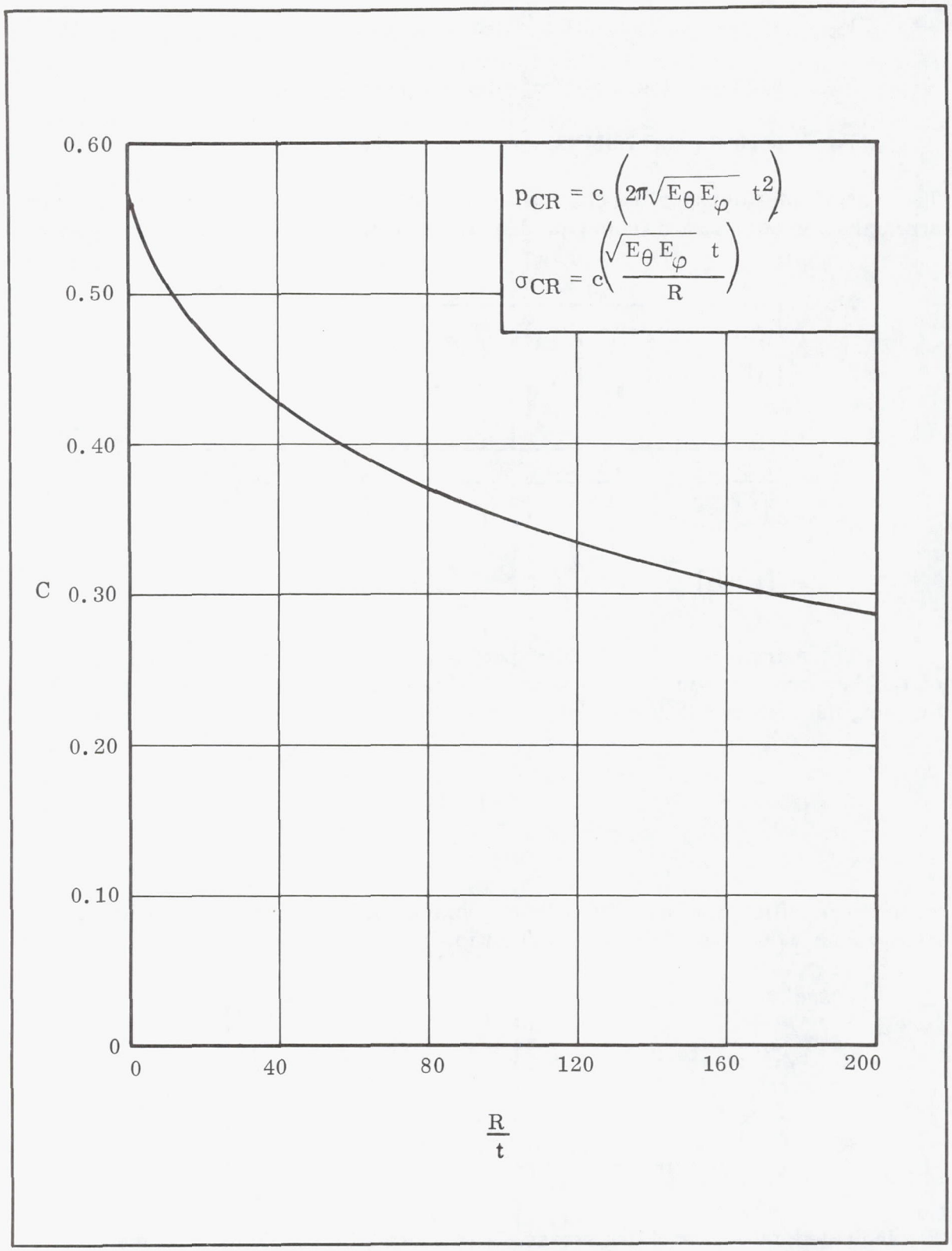

Figure 9. - Design Buckling Coefficient Curve for "Long" Cylinders

Polar boss. - The forward polar boss on all vessels and the aft boss on Vessel 6 were all capped off, thus transmitting the full blowoff load into the glass shell. The aft boss of all vessels (with the exception of Vessel 6) were thrust relieved by a piston/closure fixture which virtually eliminates the blowoff load between the dome shell and the boss ring.

The polar boss is critical in ring torsional stiffness and in flange bending strength. The boundary loading on the boss is a function of the closure attachment joint and the hoop foundation stiffness of the glass buildup over the boss flange. The internal loads of the ring were determined by a discontinuity type of analysis in which the free body radial deflections and rotations were equated to determine the internal bending and shear loads.

A representative design is the Vessel 1 and 9 forward boss and closure assembly shown in Figure 10. Both components were fabricated of AISI 4340 steel and had threaded joint connections. The total blowout load (P_T) at 5,000 psig (34.5 MN/m^2g) on the boss with respect to the glass dome shell is obtained from the following equation:

$$P_T = p\pi R_o^2 \tag{26}$$

$$= 5,000\,\pi\,(6.4)^2$$

$$= 643,000 \text{ lb } (2.86 \text{ GN})$$

The slope (ψ) of the dome-boss interface relative to the case centerline was 45 degrees (0.79 rad). The pressure distribution between the glass buildup and the boss is a function of the composite hoop stiffness of the glass where the distortion of the boss tapered section is neglected. The radial deflection (ω_o) of the glass buildup relative to the boss is as follows:

$$\omega_o = \frac{P_T}{2\pi\,(\text{INC})\sin\psi \sum_{i=1}^{N} \left[\frac{E_\alpha \theta^t_\alpha R_I}{R^2_{EL}}\right]} \tag{27}$$

where:

(INC) = Width of element (see Figure 8)

ψ = Slope of dome boss interface

R_I = Average interface radius of element

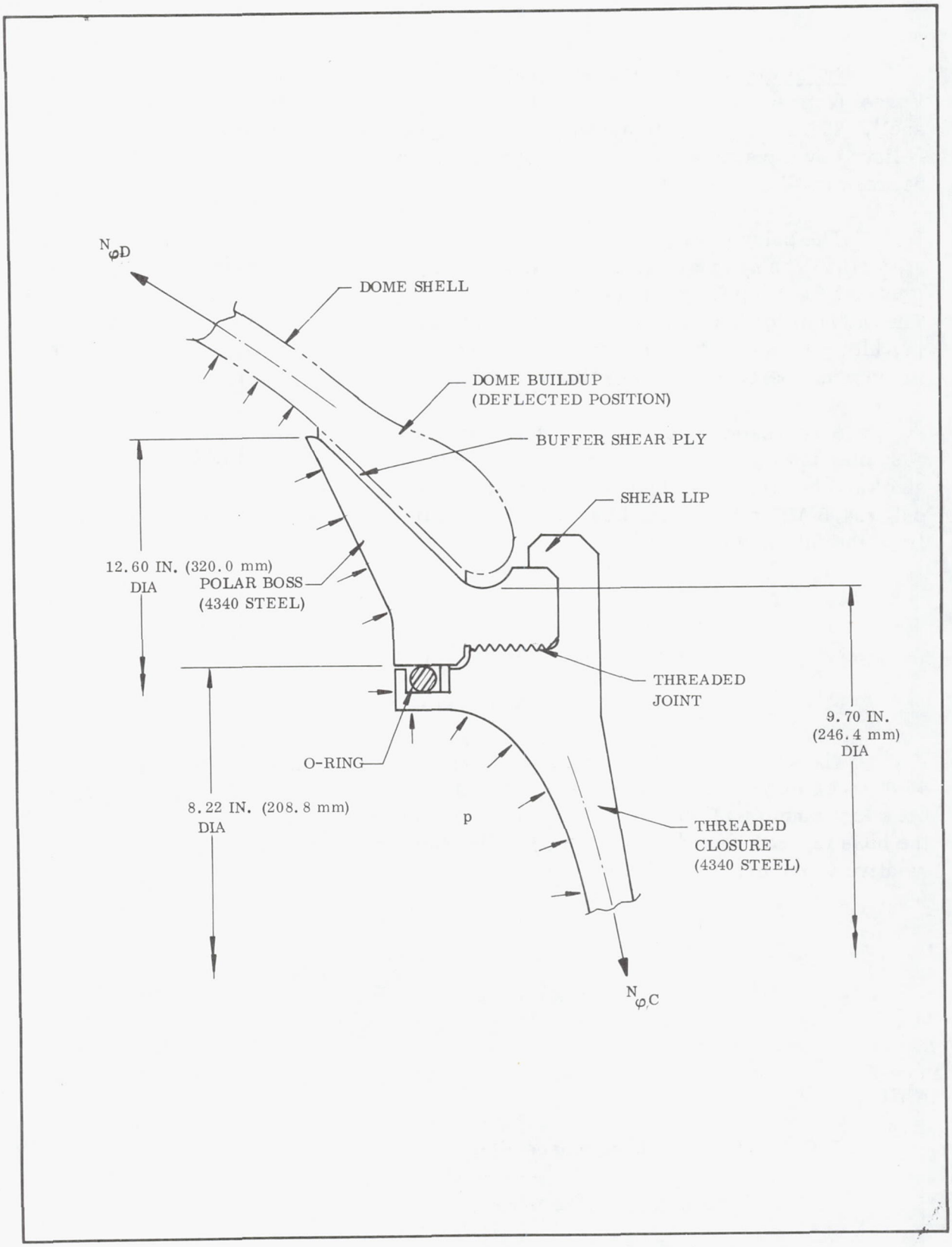

Figure 10.-Vessels 1 and 9 Forward Polar Boss and Closure

R_{EL} = Radius of element centroid

$$\omega_o = \frac{643,000}{2\pi\ (0.20)\ \sin 45\ \text{deg}\ (5.49 \times 10^6)}$$

$$= 0.132 \text{ in. (outward) } (3.35 \text{ mm})$$

The center of pressure at the glass buildup interface ($\bar{R}_I$) in the unpressurized position is:

$$\bar{R}_I = \frac{\sum_{i=1}^{N=11} \left(\frac{E_{\alpha\theta} t_\alpha R_I}{R_{EL}^2} \right)}{\sum_{i=1}^{N=11} \left(\frac{E_{\alpha\theta} t_\alpha}{R_{EL}^2} \right)} \tag{28}$$

$$= \frac{5.49}{1.009} = 5.44 \text{ in. } (138.2 \text{ mm})$$

The reaction load (N_R) between the boss and dome in the pressurized position is:

$$N_R = \frac{P_T}{2\pi\ (\bar{R}_I + \omega_o)\ \cos\psi} \tag{29}$$

$$= \frac{643,000}{2\pi\ (5.44 + 0.132)\ \cos 45\ \text{deg}}$$

$$= 26,000 \text{ lb/in. at } (\bar{R}_I + \omega_o) = 5.57 \text{ in. } (141.5 \text{ mm})$$

The deflection of the NBR buffer ply between the boss and the dome shell will also induce a surface shear loading on the boss, but its magnitude relative to that of the reaction loading is small. This loading (Q_R) may be approximated by considering the glass deflection (ω_o), the rubber shear modulus (G) and thickness (t_R):

$$Q_R = \frac{\omega_o\ G\ (R_o^2 - R_I^2)}{2 \sin\psi\ \ t_R\ R_I} \tag{30}$$

$$= \frac{0.132\ (300)\ (6.3^2 - 4.9^2)}{2 \sin 45\ \text{deg}\ (0.09)\ (5.44)} \quad (0.16 \text{ MN/m})$$

$$= 900 \text{ lb/in. } (0.16 \text{ MN/m})$$

The two reaction loads, N_R and Q_R, as obtained from equation (29) and (30) and the relative dome deflection, ω_o, as obtained from equation (27) were used in the discontinuity analysis along with the relation that the rotation of the glass build-up is equal to that of the boss. Figure 11 depicts the free body breakdown and a summary of the loads and deflections of Vessel 1 and 9 forward boss and closure.

The critical stress areas in a typical polar boss-closure design are:

1. Bending in the boss tapered section.

2. Shear across the flange shear lip.

3. Shear in the joint threads/or tension in the bolts.

4. Bending in the closure shell.

The theoretical stresses in the Vessel 1 and 9 polar boss and closure and those in the other 18-in. diameter vessels are summarized in Table III. The basic design configurations are shown in Figures 12 thru 14. All vessels, with the exception of Vessel 2, had a threaded type joint connection between the boss and closure. Vessel 2 had a bolted type joint because of the nature of the bending moments present in this area. The magnitude and direction of these moments would have opened up a threaded connection and caused failure in the threads.

Cut-port aft domes. - An efficient way to fabricate a filament wound vessel with a large dome opening is to add reinforcements to the dome structure and cut the opening after vessel cure. This type of dome structure was evaluated on Vessels 3, 4, 5, 6, 8 and IR & D No. 4. The reinforcements were made up of unidirectional tapes, laid tangent to the opening diameter, and interspersed between the polar layers.

The loads associated with a dome with a large polar opening are a combination of the pressure membrane loads and the discontinuity load generated at the polar boss and at the cylinder-dome tangent plane. Because of the relatively short free span area of the dome, there is considerable influence of the polar boss and cylindrical section on the shell behavior. Therefore, the dome shell must be treated as a composite orthotropic structure and analyzed by a discontinuity type of analysis. The two basic variables are the dome contour, which affects the membrane loads, and the composite elastic properties, as influenced by the addition of reinforcements. The critical area is the shell buildup over the polar boss. The hoop load in this area is induced primarily by the polar boss, while the meridional loading is a function of the meridional slope of the shell. The tapes are used to carry the hoop loading and thus the quantity of reinforcement may be estimated accordingly. The actual hoop stresses in this area can be determined from the results of the discontinuity analysis. The polar wrap carries the meridional

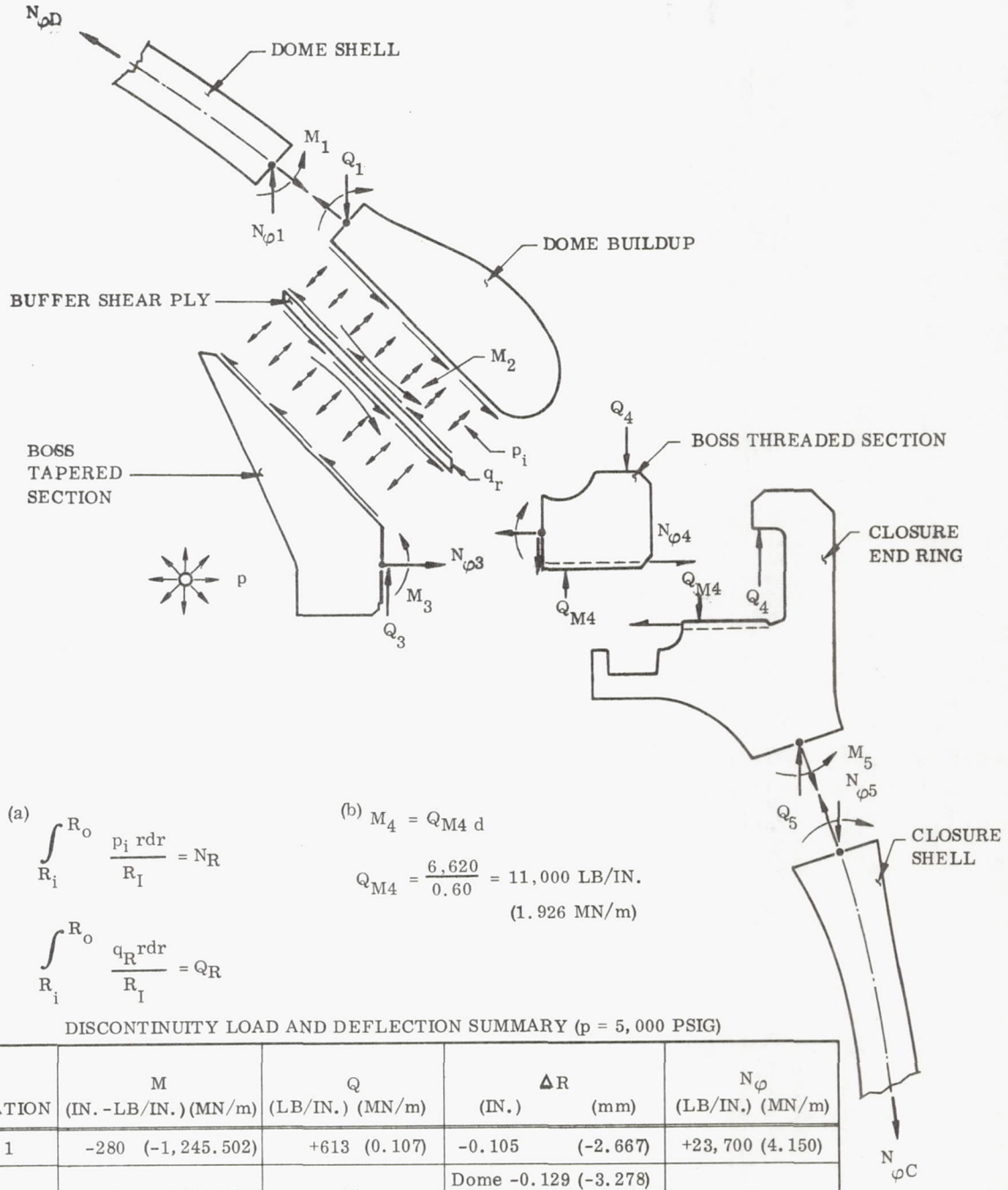

(a)

$$\int_{R_i}^{R_o} \frac{p_i \, r dr}{R_I} = N_R$$

$$\int_{R_i}^{R_o} \frac{q_R r dr}{R_I} = Q_R$$

(b) $M_4 = Q_{M4} \, d$

$$Q_{M4} = \frac{6,620}{0.60} = 11,000 \text{ LB/IN.}$$

(1.926 MN/m)

DISCONTINUITY LOAD AND DEFLECTION SUMMARY (p = 5,000 PSIG)

STATION	M (IN.-LB/IN.) (MN/m)	Q (LB/IN.) (MN/m)	ΔR (IN.) (mm)	N_φ (LB/IN.) (MN/m)
1	-280 (-1,245.502)	+613 (0.107)	-0.105 (-2.667)	+23,700 (4.150)
2	-64 (-284.686)	(a)	Dome -0.129 (-3.278) Boss -0.005 (-0.127)	--
3	-6,630 (-29,491.699)	-2,570 (-0.450)	+0.0062 (-0.158)	+9,270 (1.623)
4	(b)	+15,900 (2.784)	+0.0013 (-0.033)	+9,270 (1.623)
5	+1,180 (5,248.900)	+8,020 (1.404)	-0.00108 (-0.207)	+27,200 (4.763)

Figure 11. - Vessel 1 Forward Polar Boss and Closure Load and Deflection Summary

TABLE III

POLAR BOSS AND CLOSURE STRESS SUMMARY FOR 18-IN. DIAMETER VESSEL

Polar Boss	Bending (tapered section) (psi)	Bending (tapered section) (MN/m^2)	Shear (shear lip) (psi)	Shear (shear lip) (MN/m^2)	Joint Stress (psi)	Joint Stress (MN/m^2)	Bending (closure shell) (psi)	Bending (closure shell) (MN/m^2)	Boss/Closure Material
Vessels 1 and 9 (Forward)	140,000	(965.0)	24,000	(166.0)	33,000-Thread shear	(228.0)	130,000	(896.0)	4340 Steel
Vessel 2 (Forward)	134,000	(924.0)	14,000	(96.5)	110,000-Bolt tension	(758.0)	113,000	(779.0)	4340 Steel
Vessels 3, 4, 5, 6, 7, 8, and IR & D No. 4 (Forward)	37,200	(257.0)	27,000	(186.0)	5,700-Thread shear	(39.0)	(a)		2014-T6 Aluminum alloy
Vessel 6 (Aft)	(a)		80,600	(556.0)	50,000-Thread shear	(345.0)	82,500	(569.0)	4340 Steel

[a]Stresses insignificant.

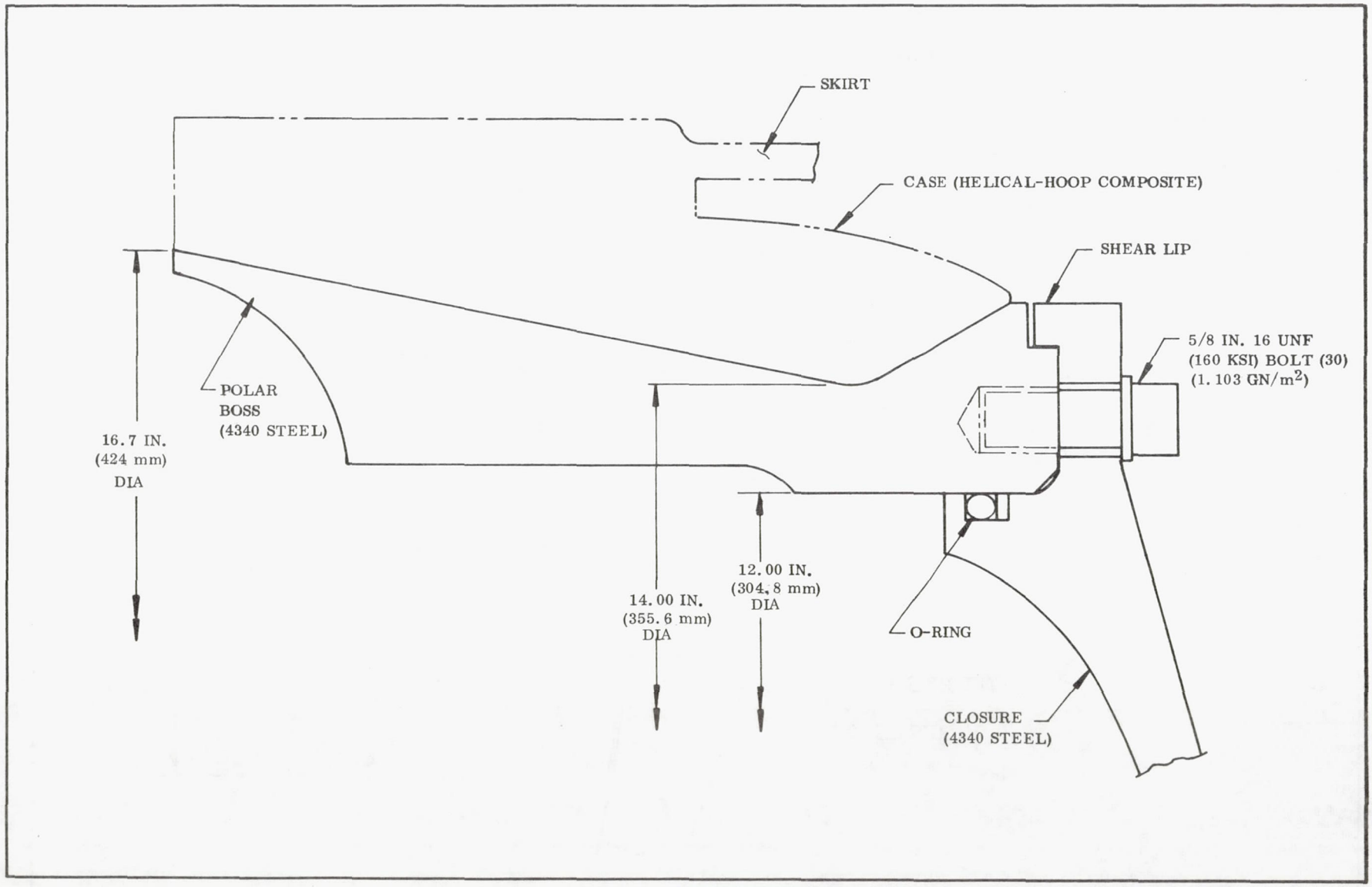

Figure 12. - Vessel 2 Forward Polar Boss and Closure

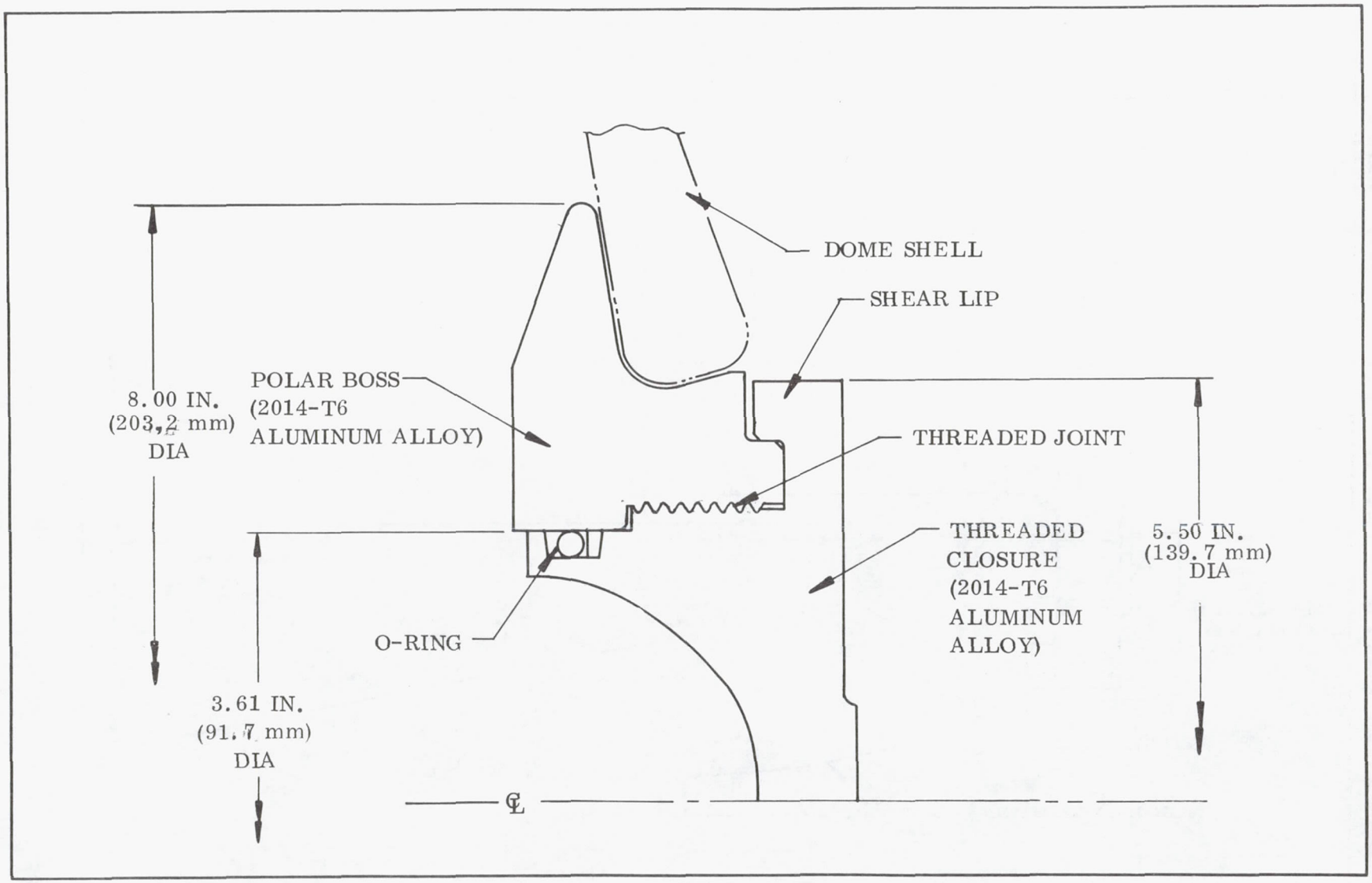

Figure 13. - Vessels 3 thru 8 and IR & D No. 4 Forward Polar Boss and Closure

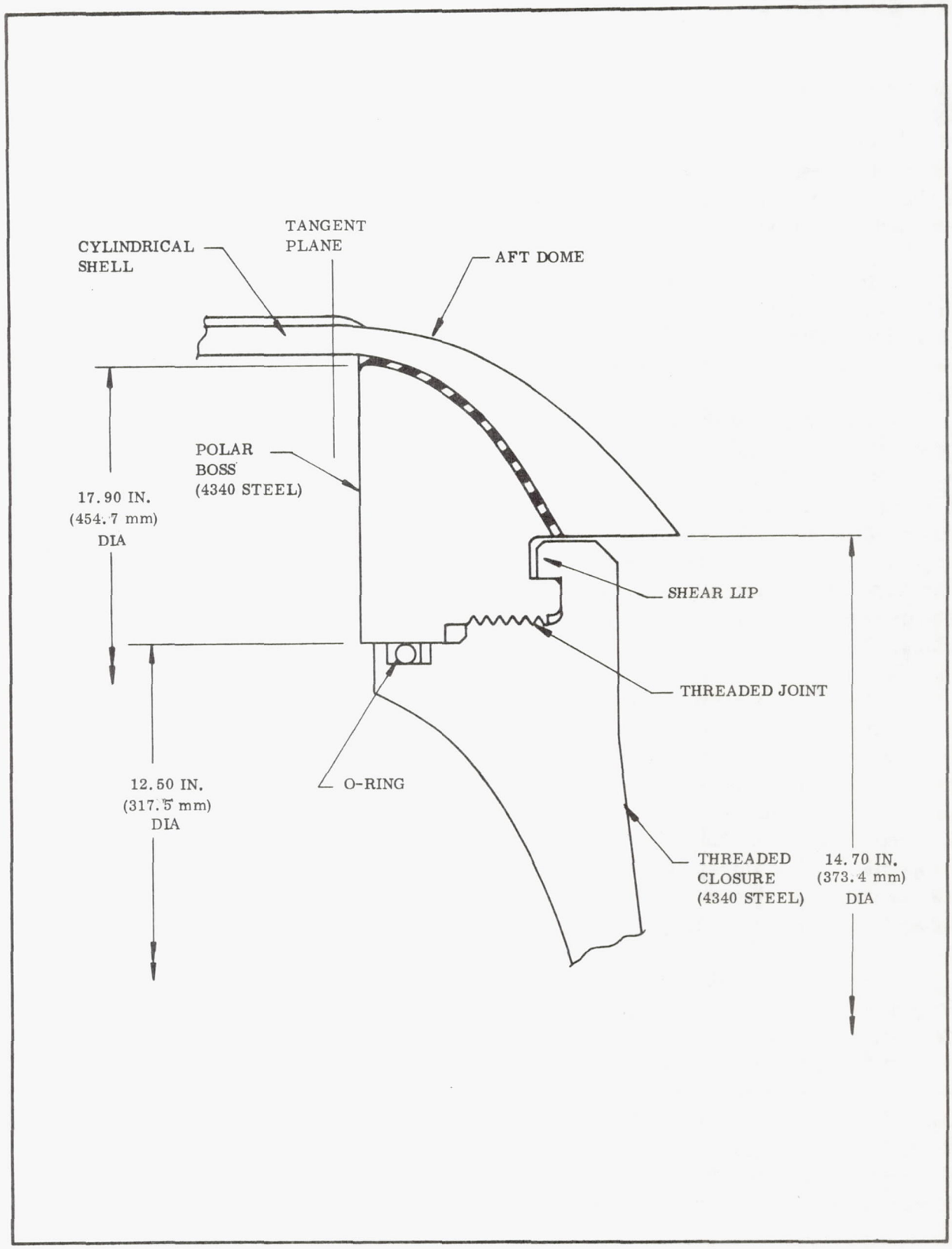

Figure 14. - Vessel 6 Aft Polar Boss and Closure

membrane load and also reacts the discontinuity bending moments. As indicated, the design is iterative in nature in that a progressive change in contour and quantity of reinforcement will yield an optimum design where the hoop, meridional, and interlaminar shear stresses are within design limits. The basic tradeoff is between a shallow dome with high discontinuities and meridional membrane loadings, and a long conical shaped dome with high hoop loading.

IR & D No. 4, a modified version of Vessel 4, was a symmetrically wrapped polar wound vessel with a 60 percent aft port opening and thrust relieved by a 10.8 in. (274 mm) piston. The aft dome was reinforced with unidirectional tapes and is a good representative example of a vessel with a cut-dome opening.

The design of the aft dome structure was based on the tapes carrying the hoop load and the polar wrap carrying the meridional load with a shear load interaction between the two. Since the dome was highly thrust compensated, the hoop loading was predominant and the dome contour was primarily based on the tape filament orientation. The "netting" type of analysis was used to generate the dome contour as a function of the biaxial loading and tape filament orientation. Several contours were generated and evaluated with respect to the additional bending and shear loading imposed by the discontinuities around the polar boss and at the tangent plane.

The elastic properties of the shell composite were derived from the two basic constituents, S-994 glass filament and E717 epoxy resin, and translated into the hoop and meridional directions as a function of the local filament orientations of both the polar wrap and tape reinforcement. The composite extensional and bending stiffnesses were based on the rule of mixtures as applied to a multilayered composite. The digital computer was used to determine the elastic properties and stiffness coefficients as required by the discontinuity analysis. A 10 percent reduction in elastic properties associated with resin crazing was also taken into consideration.

Figure 15 depicts the dome profile as broken into six free bodies. The length of a free body usually varies from two to four times the composite thickness, depending upon the change in hoop loading and elastic properties. The shell section over the polar boss is treated as a ring which is allowed to deflect radially but is assumed to rotate with the polar boss. The aft boss on this vessel was essentially fixed due to the extreme rigidity of the hydrotest fixture. However, since the dome shell has negligible effect on the boss-closure discontinuity, the rotation of the boss could have been obtained prior to the final shell discontinuity analysis if it was of significant magnitude.

Table IV depicts the tape and polar thicknesses and wrap angles, including the membrane loads along the periphery of the shell. Table V shows the average composite elastic properties and free body geometry data which was put into the

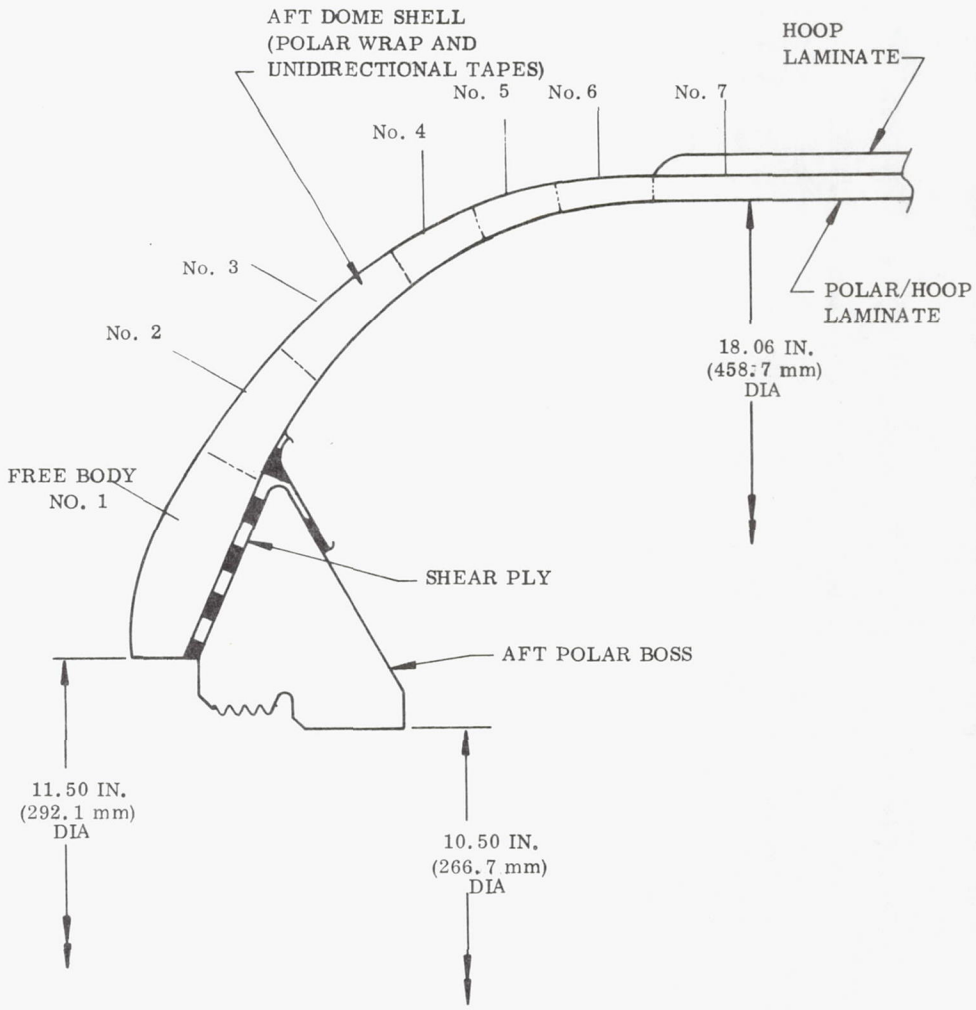

Figure 15. - IR & D Vessel No. 4 Aft Dome Profile

TABLE IV

AFT DOME CONSTITUENT PROPERTIES FOR IR & D VESSEL NO. 4

[p = 5,000 psig (34.5 MN/m^2g)]

Radius		Slope		Polar Wrap[a]				Tape Layers[b]				Membrane Loads			
				Thickness		Wrap Angle		Thickness		Wrap Angle		Meridional		Hoop	
(in.)	(mm)	(deg)	(rad)	(in.)	(mm)	(deg)	(rad)	(in.)	(mm)	(deg)	(rad)	(lb/in.)	(MN/m)	(lb/in.)	(MN/m)
9.02	(229.1)	13	(0.227)	0.144	(3.657)	12.5	(0.218)	0.059	(1.499)	43	(0.75)	14,700	(2.574)	1,610	(0.282)
8.95	(227.3)	17	(0.267)	0.147	(3.734)	14.0	(0.244)	0.075	(1.905)	44	(0.77)	14,800	(2.592)	2,100	(0.368)
8.75	(222.3)	24	(0.419)	0.151	(3.835)	16.0	(0.279)	0.094	(2.388)	45	(0.79)	15,000	(2.627)	3,000	(0.525)
8.46	(214.9)	35	(0.611)	0.159	(4.039)	18.5	(0.323)	0.117	(2.972)	47	(0.82)	15,400	(2.697)	5,000	(0.876)
8.14	(206.8)	45	(0.785)	0.168	(4.267)	20.0	(0.349)	0.147	(3.734)	50	(0.87)	15,800	(2.767)	8,900	(1.558)
7.77	(197.4)	52	(0.908)	0.178	(4.521)	22.0	(0.384)	0.185	(4.699)	53	(0.93)	16,000	(2.802)	14,000	(2.451)
7.20	(182.9)	60	(1.047)	0.196	(4.978)	25.0	(0.436)	0.235	(5.969)	60	(1.05)	16,000	(2.802)	29,000	(5.078)
0.80	(20.32)	65	(1.135)	0.209	(5.309)	26.0	(0.454)	0.303	(7.696)	67	(1.17)	16,000	(2.802)	65,000	(11.382)
6.56	(166.6)	66	(1.152)	0.221	(5.613)	27.0	(0.471)	0.384	(9.754)	70	(1.22)				
6.30	(160.0)	66	(1.152)	0.231	(5.867)	28.5	(0.497)	0.238	(6.045)	78	(1.36)				
6.00	(152.4)	66	(1.152)	0.248	(6.299)	29.5	(0.515)	0.205	(5.207)	90	(1.57)				
5.80	(147.3)	66	(1.152)	0.258	(6.553)	30.0	(0.524)	0.175	(4.445)	90	(1.57)				

Polar Boss Interface

[a]Planar wrap pattern.
[b]Geodesic wrap pattern.

TABLE V

IR & D VESSEL NO. 4
AFT DOME FREE BODY GEOMETRY AND ELASTIC PROPERTIES

Free Body No.	Average Thickness, t (in.)	(mm)	Average Radius, $\bar{R}$ (in.)	(mm)	Average Slope, ψ (deg)	(rad)	Meridional Extensional Modulus[a] $E_\varphi \times 10^{-6}$ (psi)	(MN/m^2)	Hoop Extensional Modulus $E_\theta \times 10^{-6}$ (psi)	(MN/m^2)	Poisson's Ratio[b] $\mu_{\varphi\theta}$	Length, L (in.)	(mm)	Type of Free Body
1	0.50	(12.7)	6.5	(165)	66	(1.51)	2.6	(0.0179)	4.0	(0.0276)	0.40	1.50	(38.1)	Ring
2	0.46	(11.7)	7.5	(191)	58	(1.01)	3.1	(0.0214)	2.4	(0.0165)	0.44	0.88	(22.4)	Curved Shell Segment
3	0.32	(8.1)	8.3	(211)	44	(0.77)	3.6	(0.0248)	1.8	(0.0124)	0.54	1.20	(30.5)	
4	0.26	(6.6)	8.7	(221)	30	(0.52)	4.2	(0.290)	1.7	(0.0117)	0.55	0.61	(15.5)	
5	0.23	(5.8)	9.0	(229)	19	(0.33)	4.7	(0.0324)	1.6	(0.0110)	0.53	0.62	(15.8)	
6	0.21	(5.3)	9.1	(231)	10	(0.18)	5.1	(0.0352)	1.6	(0.0110)	0.49	0.72	(18.3)	
Cyl	0.37	(9.4)	9.2	(234)	0	(0)	3.5	(0.0241)	5.1	(0.0352)	0.29	Semi-infinite		Cylinder

[a] Meridional bending stiffness $(D_\varphi) = \dfrac{E_\varphi t^3}{12\,(1 - \mu_{\varphi\theta}\mu_{\theta\varphi})}$

[b] $\mu_{\varphi\theta}$ is the ratio of the hoop strain to the meridional strain as induced by the meridional stress, $\mu_{\theta\varphi} = \mu_{\varphi\theta}\dfrac{E_\theta}{E_\varphi}$

digital computer. The final results of the discontinuity analysis are shown in Table VI.

The critical area for a reinforced dome is around the polar boss. The glass stress in the tapes over the polar boss, where the tapes are oriented normal to the meridian (α_T = 90 deg, 1.575 rad), is obtained from the following equation:

$$\sigma_{Tg} = \frac{\Delta R}{\bar{R}} E_g \tag{31}$$

$$= \frac{0.15}{6.50} (12.4 \times 10^6)$$

$$= 280,000 \text{ psi } (1.93 \text{ GN/m}^2)$$

The margin of safety (MS) is based on a glass filament strength for the tapes that is identical to that selected for the hoop and longitudinal wrap.

$$MS = \frac{F_{tg}}{\sigma_{Tg}} - 1$$

$$= \frac{360,000}{286,000} - 1$$

$$= 0.26$$

The glass stress in the polar wrap and tapes at the outside diameter of the polar boss is a function of the meridional and hoop loading.

The composite meridional stress (σ_φ) on the outside surface of the shell at a radius of 7.0 in. (178 mm) and a slope (ψ) of 62 deg (1.09 rad) is:

$$\sigma_\varphi = \left[\frac{6M}{t^2} + \frac{N_\varphi}{t} + \frac{Q \sin \psi}{t}\right] \tag{32}$$

$$= \frac{6\ (1,350)}{(0.45)^2} + \frac{16,000}{0.45} - \frac{2,020 \sin 62 \text{ deg}}{0.45}$$

$$= 40,000 + 35,600 - 4,000$$

$$= 71,600 \text{ psi } (494 \text{ MN/m}^2)$$

TABLE VI

DISCONTINUITY ANALYSIS RESULTS FOR IR & D VESSEL NO. 4

[p = 5,000 psig (34.5 MN/m^2g)]

Station Between Free Body No.	Station Between Free Body No.	Moment (M) (in. lb/in.)	Moment (M) (MN/m)	Shear (Q) (lb/in.)	Shear (Q) (MN/mm)	Rotation ($\Delta\theta$) (deg)	Rotation ($\Delta\theta$) (rad)	Radial Displacement (ΔR) (in.)	Radial Displacement (ΔR) (mm)
1	2	-1,350	(-6,005)	-2,020	(-0.354)	0 (input)	(0)	-0.15	(-3.81)
2	3	-570	(-2,535)	-1,290	(-0.226)	+0.94	(0.016)	-0.14	(-3.56)
3	4	+160	(711.7)	-430	(-0.075)	+1.8	(0.031)	-0.12	(-3.05)
4	5	+290	(1,289.9)	-80	(-0.014)	+0.50	(0.009)	-0.11	(-2.79)
5	6	+240	(1,067.5)	+260	(0.046)	-1.5	(-0.026)	-0.11	(-2.79)
6	7	-80	(-355.8)	+660	(0.116)	+2.5	(0.044)	-0.14	(-3.56)

SIGN CONVENTION

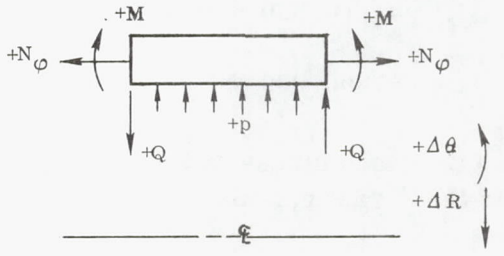

At the same location the composite hoop stress (σ_θ) is:

$$\sigma_\theta = \frac{\Delta R}{\bar{R}} E_\theta \tag{33}$$

$$= \frac{0.14}{7.0} (3.5 \times 10^6)$$

$$= 70,000 \text{ psi } (483 \text{ MN/m}^2)$$

Based on the two principal stresses obtained from equations (32) and (33), the resulting polar glass stress at the local polar filament orientation of $\pm$ 25 deg (0.44 rad) is:

$$\sigma_{\alpha g} = \left[\frac{\sigma_\varphi \cos^2 \alpha_P}{E_\varphi} + \frac{\sigma_\theta \sin^2 \alpha_P}{E_\theta}\right] E_g \tag{34}$$

$$= \left[\frac{71,600 \cos^2 25 \text{ deg}}{2.9 \times 10^6} + \frac{70,000 \sin^2 25 \text{ deg}}{3.5 \times 10^6}\right] 12.4 \times 10^6$$

$$= \left[0.020 + 0.004\right] 12.4 \times 10^6$$

$$= 300,000 \text{ psi } (2.07 \text{ GN/m}^2)$$

and the tape glass stress at this location where the tape filament orientation is $\pm$63 deg (1.10 rad) can also be obtained from equation (34).

$$\sigma_{Tg} = \left[\frac{\sigma_\varphi \cos^2 \alpha_T}{E_\varphi} + \frac{\sigma_\theta \sin^2 \alpha_T}{E_\theta}\right] E_g$$

$$= \left[\frac{71,600 \cos^2 63 \text{ deg}}{2.9 \times 10^6} + \frac{70,000 \sin^2 63 \text{ deg}}{3.5 \times 10^6}\right] 12.4 \times 10^6$$

$$= \left[0.005 + 0.016\right] 12.4 \times 10^6$$

$$= 260,000 \text{ psi } (1.79 \text{ GN/m}^2)$$

The resulting margins of safety are:

Polar Wrap

$$MS = \frac{F_{tug}}{\sigma_{\alpha g}} - 1$$

$$= \frac{360,000}{300,000} - 1$$

$$= 0.20$$

Tape

$$MS = \frac{F_{tug}}{\sigma_{Tg}} - 1$$

$$MS = \frac{360,000}{260,000} - 1$$

$$= 0.38$$

The average meridional load ($N_{\alpha\varphi}$) in the polar wrap is maximum at the outside diameter of the polar boss. Since the polar wrap terminates at the dome opening, the load ($N_{\alpha\varphi}$) must be transferred into the tapes in double lap shear as a function of the constituent stiffnesses. The total load that must be transferred is determined as follows:

$$N_{\alpha\varphi} = N_{\varphi} \frac{E_{\alpha\varphi}\, t_{\alpha}}{E_{\varphi}\, t} \tag{35}$$

$$= 16,000 \frac{(4.5 \times 10^6)\ (0.20)}{(2.9 \times 10^6)\ (0.46)}$$

$$= 10,800 \text{ lb/in. } (1.89 \text{ MN/m})$$

There were nine polar wrap layers in the dome, therefore each polar layer transmitted a meridional loading of 1,200 lb/in. (0.21 MN/m) into the adjacent tapes over the polar boss.

The meridional load transfer from the tapes into the polar wrap is maximum at the dome cylinder tangent line where the final three tape layers terminate. This load is a function of the component stiffnesses and is as follows:

$$N_{\alpha T} = N_{\varphi} \frac{E_{T\varphi}\, t_T}{E_{\varphi}\, t}$$

$$= 14{,}700 \frac{(1.9 \times 10^6)\ (0.059)}{(3.5 \times 10^6)\ (0.20)}$$

$$= 2{,}400 \text{ lb/in. } (0.42 \text{ MN/m})$$

and with three tapes in double lap shear, each tape must transmit a loading of 800 lb/in. (0.14 MN/m) into the polar wrap.

A glass/epoxy composite is capable of safely transmitting at least 2,000 lb/in. (0.35 MN/m) in single lap shear; therefore, loads as obtained from equation (35) are safe.

Fabrication

The 18-in. diameter vessels were filament wound on sand polyvinyl alcohol (PVA) mandrels molded over a center steel shaft. The sand type mandrel was selected because of its concrete-like hardness, simplicity of fabrication, and low cost. The skirt structure was prefabricated and installed on the case during case winding, while the rubber bladder was installed "green" prior to case winding. The skirt bond and the vulcanization of the bladder were all achieved during case cure. The details on the tooling configuration and vessel fabrication are discussed in the following subsections.

Mandrel tooling.- The sand mandrel castings were made up of fine mesh silica sand with a PVA resin binder. The mixture formulation is as follows:

Sand	100 parts
PVA	25 parts
Water	3.5 parts
Methanol	1.75 parts

The resin was first dissolved into the water methanol solution and then added to the sand. The two ingredients were thoroughly mixed in a commercial type mechanical mixer prior to molding.

The molds for the case consisted of both fiberglass and steel shells. The exact dome contours for each vessel were obtained by sweeping a thin layer of plaster inside the fiberglass shell as shown in Figure 16. The cylindrical section of the case was directly cast without the use of plaster. Both fiberglass and steel cylindrical molds were used during the course of the program, the latter being the recommended type.

The sand was hand packed into the respective molds (all of which included center shafts) and each was oven dried for approximately 24 hr at 250° F (394°K) to drive off the water and alcohol solvents. After drying, the mold shells were unbolted and split as shown in Figure 17 and the center shaft segments removed. The sand castings were then slipped onto a common center shaft. Figure 18 shows two dome segments installed. On longer vessels, such as Vessels 3 and 9, center cylindrical segments were installed between the dome segments. The segments were bonded together with a filled, ambient cured epoxy resin, and all defects in the sand casting were cleaned up with plaster. The complete sand surface was then covered with Teflon tape.

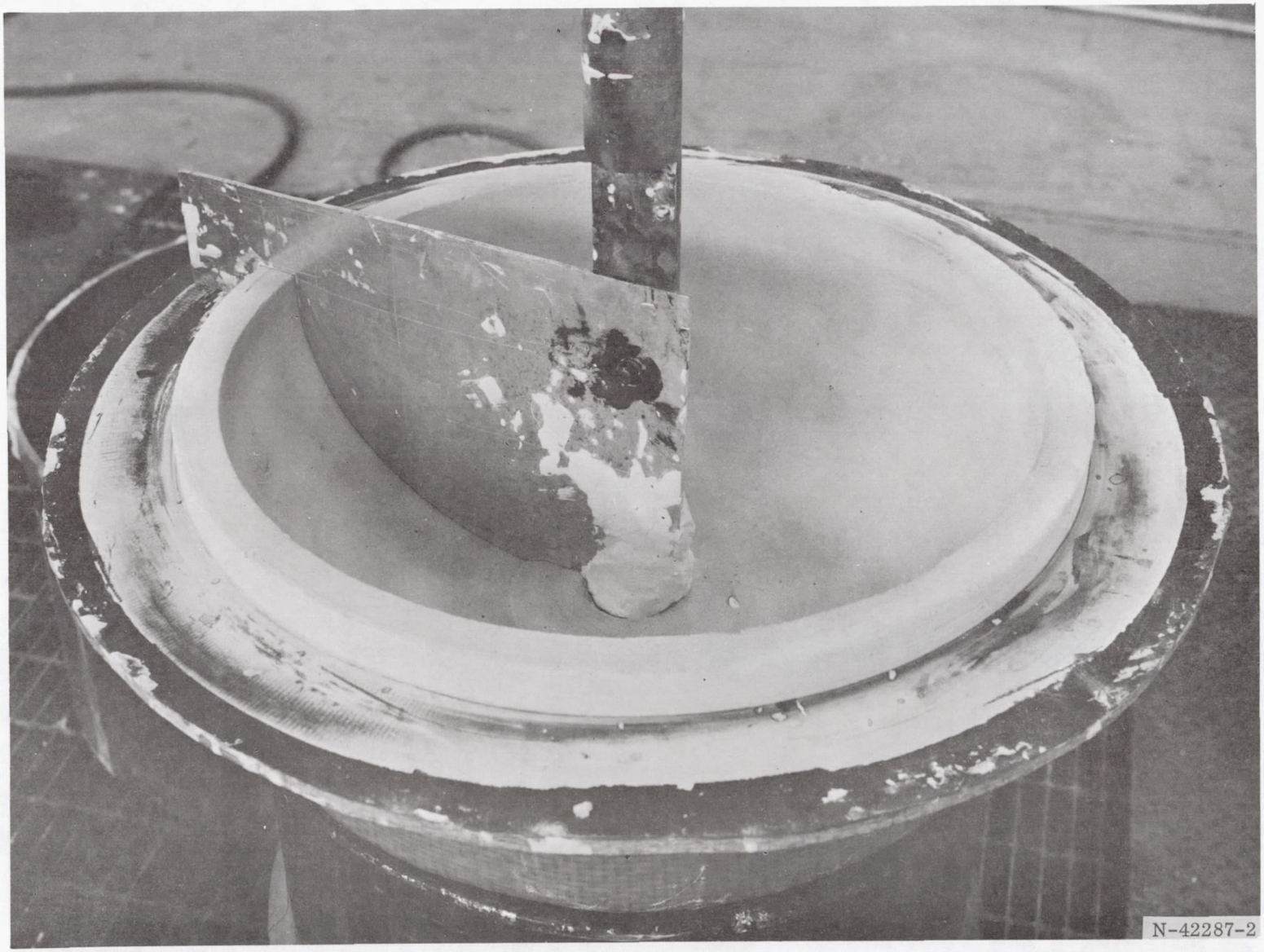

Figure 16. Plaster-Glass Mold with Sweep Template in Place

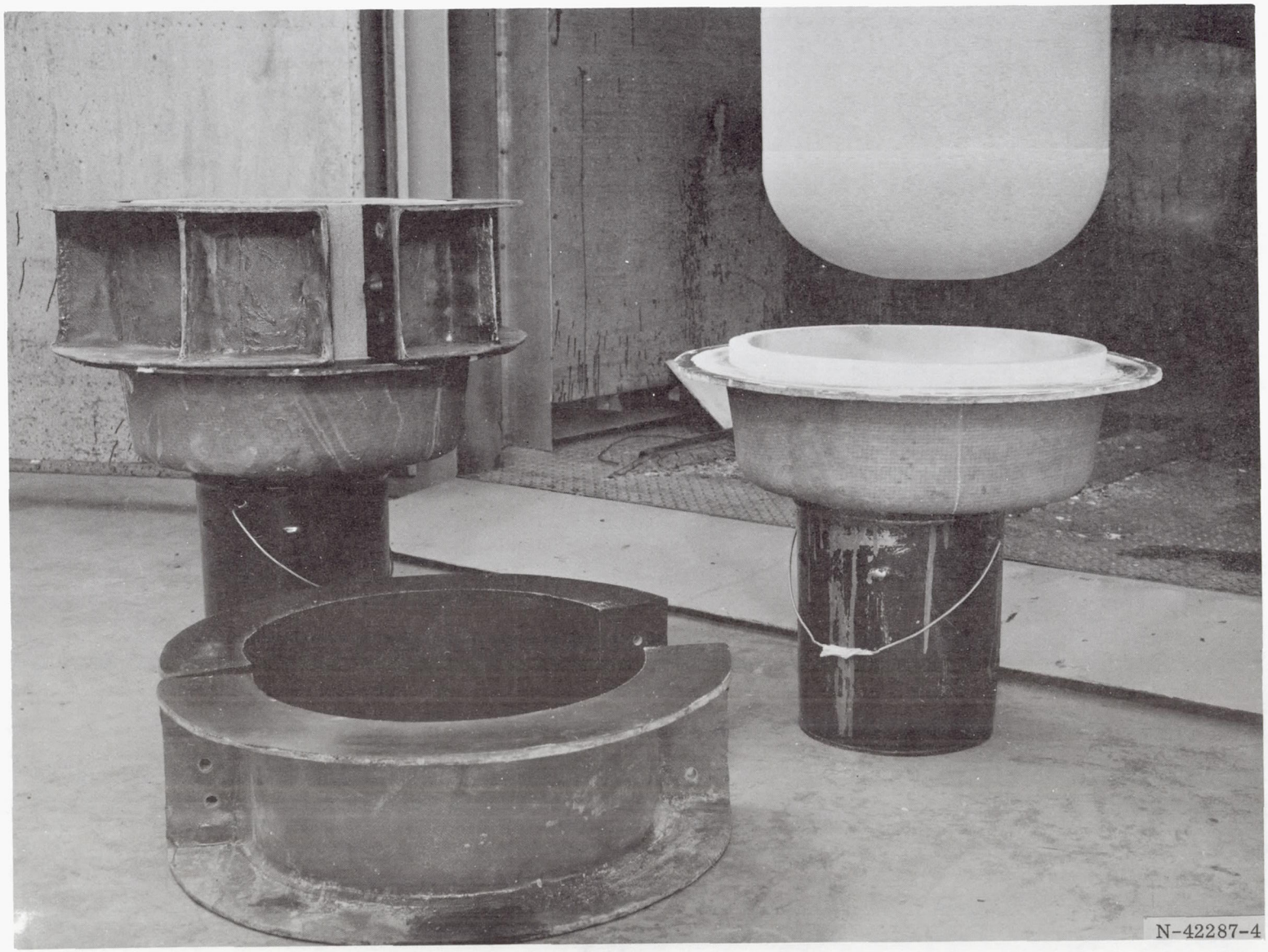

Figure 17. Cured Sand Mandrel Being Removed from Molds

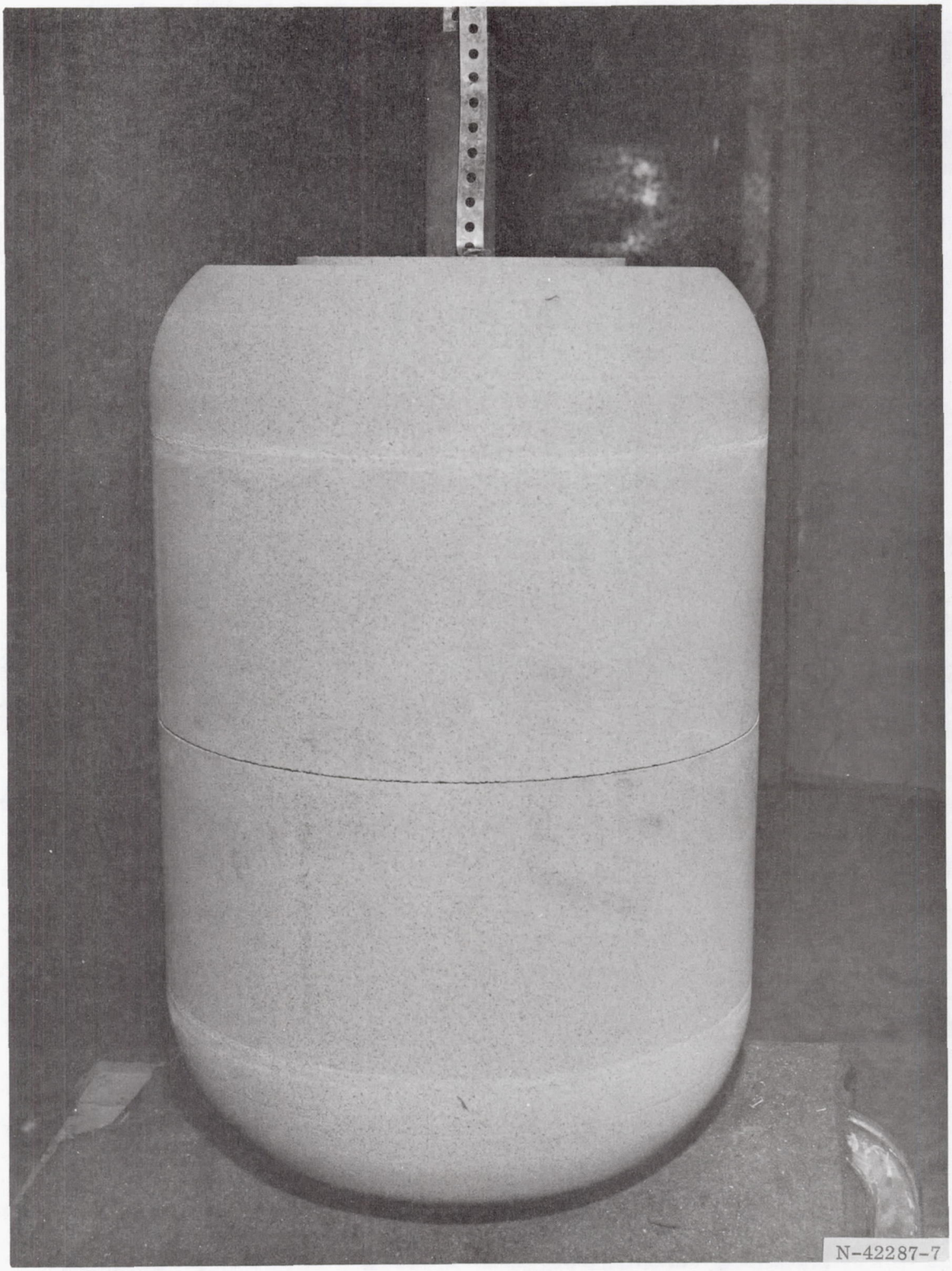

Figure 18. Sand Mandrel Halves Being Joined

The skirt mandrel consisted of a collapsible steel shell with end bulkheads and a center shaft. A thin shell of plaster was swept over the steel to a cylindrical contour having a local conical cutout for the shear ply. Teflon tape was used as the release agent between the skirt and the plaster.

Case fabrication.- The 18-in. diameter subscale vessels were all filament wound with 20 end S-994 glass roving preimpregnated with epoxy resin. The roving (No. XF-7030) was procured from US Polymeric Inc where the Owens-Corning glass roving was impregnated with the medium temperature cure epoxy resin, E-717. All cases and skirts were wound at a tension of 10 lb (44.5 N) per roving and were cured at a glass-resin composite temperature of 300 $\pm$ 10° F (422 $\pm$ 5.5°K) for a duration of 6 hours.

The skirt structure for all vessels was made up of equal amounts of interspersed hoop and polar wrap with the polar wrap wound at a planar wind angle of $\pm$ 10 degrees (0.16 rad). The filament end density for the hoop and polar wrap was 200 to 205 ends/in./ply (7874 to 8071 ends/m/ply). The inner skirt shear ply, made of Gen Gard V-45 rubber, was installed in the cutout area of the mandrel in the "green" condition prior to winding. The resin and V-45 were cured together, and the skirt structure was machined to the final configuration prior to mandrel removal. Figure 19 shows the cross section of the skirt composite on the mandrel with the machining cuts indicated. The mandrel was removed by disassembling the bulkhead, collapsing the steel shell, and breaking away the plaster from the skirt.

The case mandrel was covered with a 0.03 in. (0.8 mm) thickness of "green" V-45 rubber. The original program plan called for a polyisoprene rubber bladder, which was actually installed on Vessels 1, 2, and 3. Test results indicated that the polyisoprene to fiberglass bond was poor and resulted in leakage in each of these vessels. On Vessel 4 and subsequent vessels the bladder material was changed to V-45 which worked perfectly. The polar boss and skirt shear ply material for all vessels was also V-45 rubber. The polar bosses were installed over the bladder material and attached to the shaft. "Green" V-45 was installed in the shear ply area of the boss, and the complete rubber surface was wiped down with methyl ethyl ketone (MEK). The polar bosses were also thoroughly cleaned with MEK and brushed with one coat of Chemlok-220 adhesive in the bladder and shear ply bonding areas prior to boss installation. Vulcanization of the bladder and shear ply to the bosses occurred during case cure.

The unidirectional tapes used to reinforce the aft domes of the vessel with cut-dome openings were made on a flat flip-flop steel mandrel. The steel plate was covered with Teflon film and a single ply of roving was wound over the plate to an end density of 240 ends/in./ply (9449 ends/m/ply). Adhesive-backed paper was applied at the two trim edges of the mandrel prior to cutting off the reinforcements. The paper backing prevented the rovings from separating after removal from the mandrel.

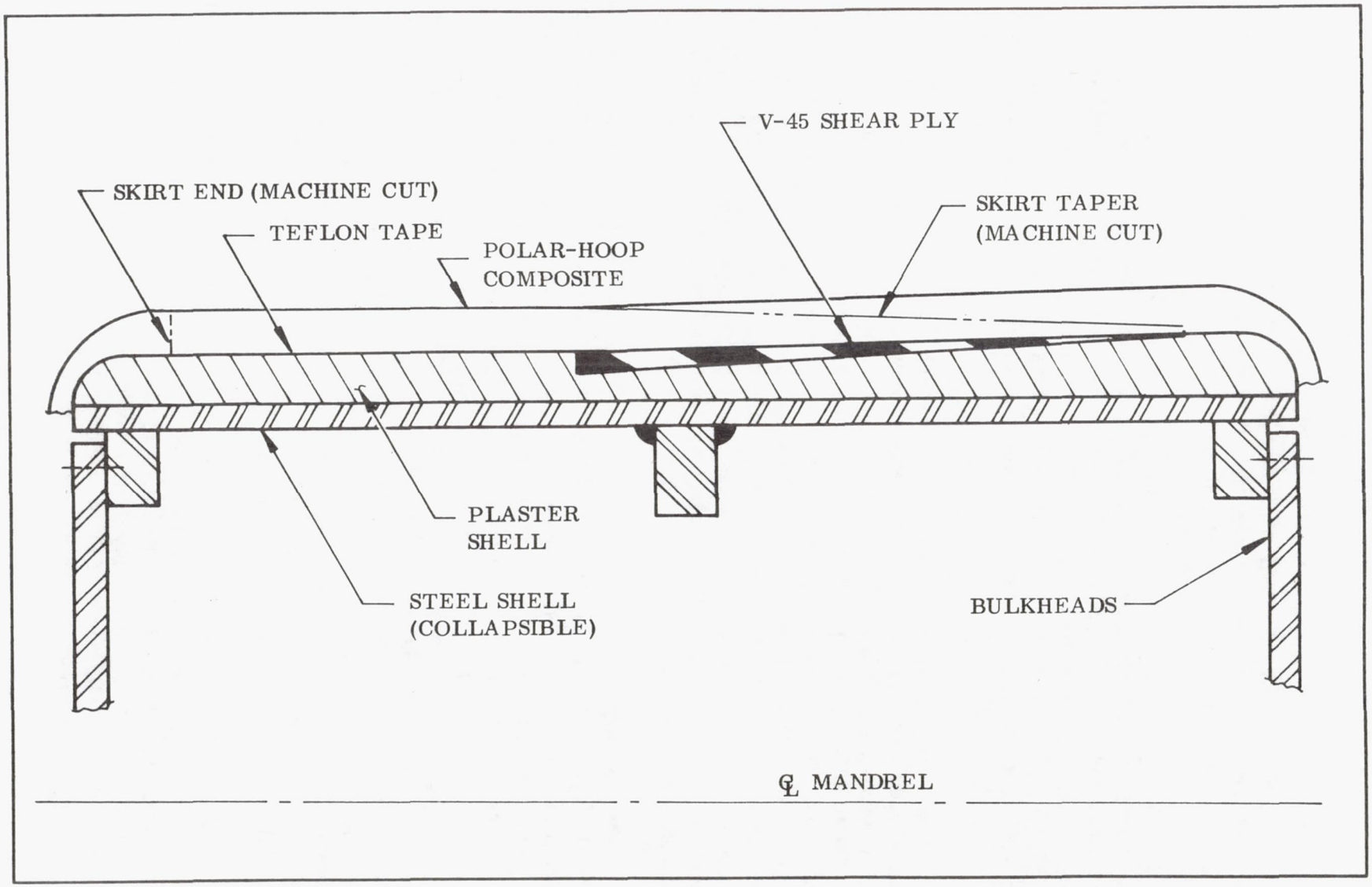

Figure 19. - Skirt Structure on Mandrel

Vessels 1, 2, and 9 were helically wound on a small McClean-Anderson constant-angle helical winding machine in the horizontal position. A two circuit pattern was used on these three vessels,which was based on the L/D ratio of the case cylinder tangent-line to tangent-line length. The roving was dwelled at the polar bosses to made the circuitry on the domes compatible to that in the cylinder.

The remaining seven 18-in. vessels were polar wound on an Accurate planar winding machine. The vessels were wound in the vertical position, aft end up, to facilitate the installation of the aft dome reinforcement. The vessels which required reinforcements had the aft polar bosses submerged into the mandrel to allow the polar winding pattern to cross over the aft dome and close at the same tangential radius as that of the forward dome. The tape reinforcements were laid up tangent to the diameter of the desired cut opening and were hand pressed into place along a geodesic path on the dome. The tape layers were trimmed with the aid of a template at the specified true length location along the contour from the tangent plane. Figure 20 shows the basic tape reinforcement layup configuration over the polar wrap during fabrication.

The hoop wrap was interspersed with the polar wrap on all vessels having the tape reinforcements with the exception of Vessel 3. The number of hoop plies per layer was established by the tape layer thicknesses at and near the aft tangent plane. By making the hoop and tape layers thicknesses equal, the contour of the polar layers was maintained smooth and continuous. In addition, the interspersement of the hoop wrap strengthened the polar wrap laminate in the hoop direction making it less critical with respect to crazing along the plane of the filaments due to the hoop strain. This crazing in the polar wrap, along with the poor polyisoprene bladder, created a premature failure in Vessel 3. Severe leakage occurred at the forward tangent line due to water entering the large crazed areas in the region of the skirt attachment.

Upon completion of winding of the longitudinal wrap (polar or helical), the prefabricated skirt structure was installed. Locally aft of the forward tangent the cases have a conical section to mate up with the skirt. The contact surface of the inner shear ply, which is vulcanized to the skirt structure, was thoroughly cleaned with a high speed emery abrasive wheel and wiped with MEK. Liquid epoxy resin (Union Carbide ERL-2774), which is compatible with the U.S.P. E-717, was applied to this surface of shear ply prior to skirt installation in order to reduce sliding friction and to thoroughly wet both bonding surfaces. An axial load sufficient to cause full contact of the bonding surfaces was applied to the skirt during installation. Upon completion of winding the case, the preload of the skirt fixture was relaxed so that the skirt would not move during cure.

After installation of the skirt, the outer shear ply and filler ply, (V-45 rubber), were laid up "green" in the prescribed area, and a layer of S-994 fabric, style S/34-901, was placed over the rubber with the "fill" yarn oriented parallel

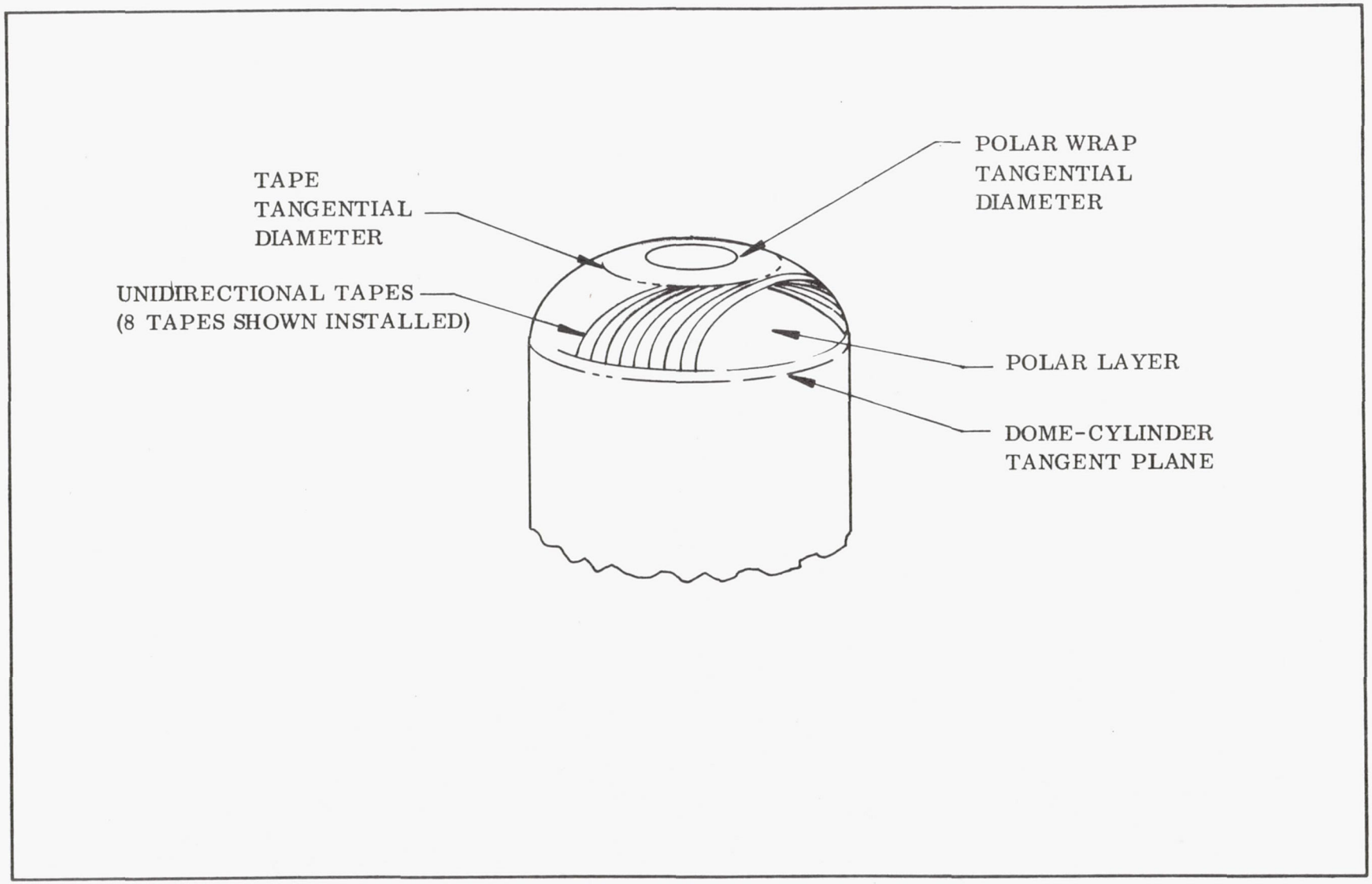

Figure 20. - Installation of Tape Reinforcements

to the case axis. The overwrap structure consisted of hoop roving and S/34-901 glass fabric, 50 percent of each by volume. The fabric in the overwrap was terminated in the area just aft of the filler ply, while the layers of hoop wrap were terminated along the cylinder anywhere from the filler ply to the aft tangent plane, depending on design requirements. The cases were then placed in the oven for cure in the vertical position, aft end up. No vacuum bagging or debulking wrap was required because the compaction of the polar wrap was sufficient to debulk the aft dome tapes, and the hoop wrap was sufficient to debulk the overwrap and polar layers.

After cure, the case-mandrel assembly was put into a lathe where the skirt face and aft dome opening (Vessels 3 thru 5, 8, and IR & D No. 4) were machined. The mandrel was taken out of the case by disassembling the polar boss and skirt fixtures, removing the center shaft, and injecting water onto the sand-PVA casting.

Testing

The 18-in. (0.457 m) diameter vessels were hydrostatically tested using water as the pressurizing media, with a positive displacement pump supplying the pressure head. All vessels were tested in the enclosed Wasatch Division hydrotest facility, and all vessels with the exception of Vessel 6 were fixtured, forward skirt down, in the thrust simulation fixture. The vessels were mounted to the existing hydrotest fixture with an adapter base structure. The simulated thrust load in the skirt was induced by a piston/cylinder arrangement attached to the aft boss of the vessel. The thrust load was transmitted from the piston into the bearing plate and through the columns to the skirt. Figure 21 shows Vessel 9 set up for testing with all fixtures installed.

During the tests the positive displacement pump was run at maximum capacity. The test plan called for a minimum pressurization rate of 550 psig (3.792 MN/m^2g) per minute, which was essentially met for all vessels with the two major exceptions being Vessels 3 and 9. These two vessels were 90 in. (2.286 m) in length, and the flow requirement for the makeup water limited the average maximum pressurization rate to 268 psig (1.848 MN/m^2g) per minute. Eleven tests were performed and six tests included the full proof cycle with a pressure hold of 3 min at 4,000 psig (27.57 MN/m^2g). The actual pressurization rates are summarized in Table VII for both the proof and burst cycles. As indicated in Table VII, Vessel 2 was tested twice as a result of a repair made to the damage which was incurred during the first test.

The instrumentation on each 18-in. diameter vessel consisted of 10 strain gages and three extensometers, with the locations established by the critical design features on the vessel. The primary areas of interest were:

1. Hoop and meridional strain in the forward dome.
2. Hoop and axial strain in the skirt.
3. Hoop and meridional strain in the aft dome.
4. Axial strain in the overwrap.
5. Hoop and axial strain in the cylindrical section.

High elongation strain gages with a special Thiokol acetate backing were used successfully to measure strain in all parts of the vessel. The only area where strain gages have proven useless is in the measurement of the axial strain in the case cylindrical section. A strain gage installed in the axial direction on the hoop overwrap is subject to erroneous pickups due to the crazing. This crazing, which occurs in the direction of the hoop filament, tends to rupture the gages; therefore, the axial strain was measured with extensometers only. These extensometers were also used

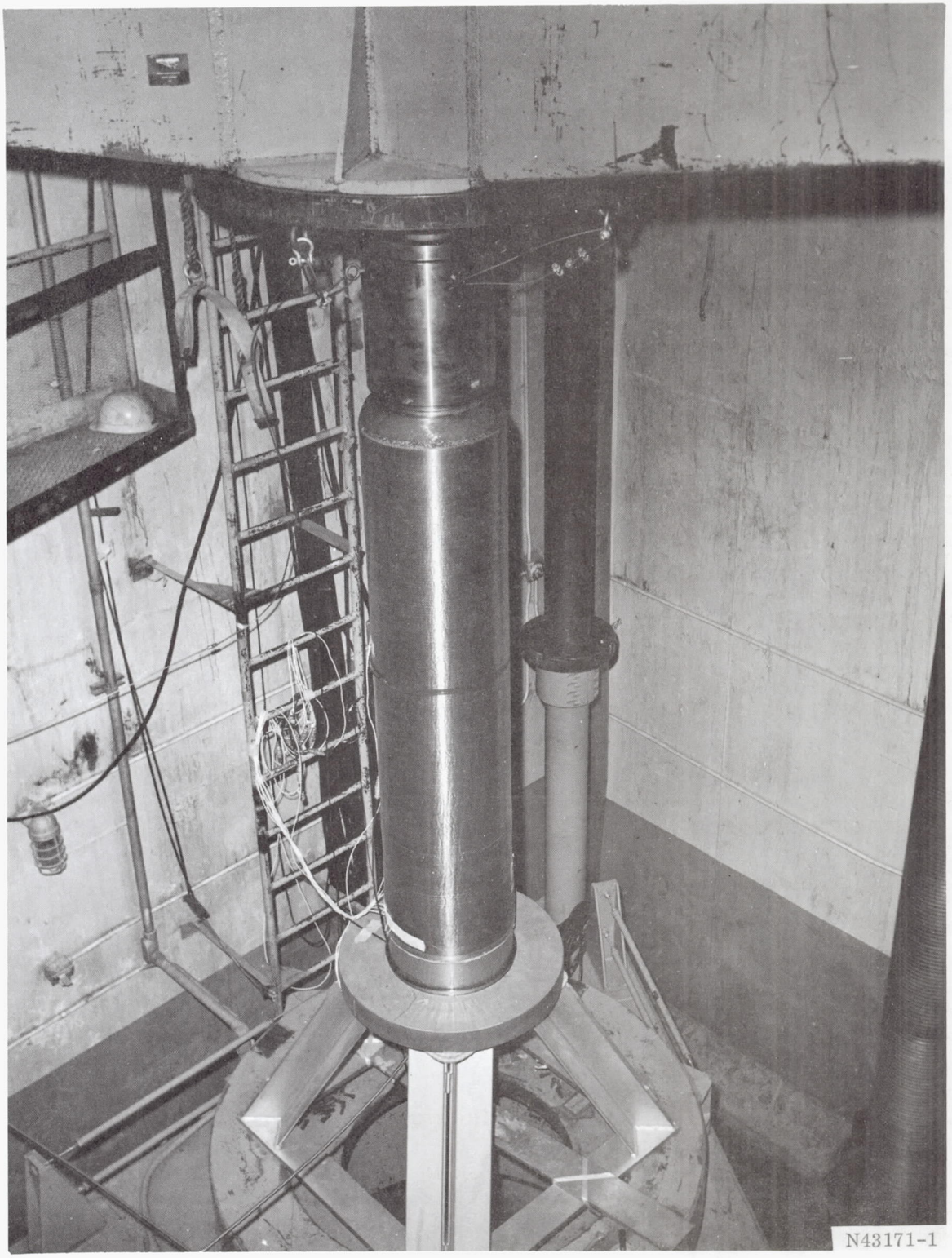

Figure 21. Vessel 9 Installed in Hydrotest Bay

TABLE VII

18-IN. DIAMETER VESSEL HYDROSTATIC TEST
PRESSURIZATION RATES

Vessel	Proof Cycle (psig/min)	Proof Cycle ($MN/m^2g/s$)	Burst Cycle (psig/min)	Burst Cycle ($MN/m^2g/s$)
1	750	(0.0862)	750	(0.0862)
2 (Test No. 1)	790	(0.0907)	--	--
2 (Test No. 2)	760	(0.0873)	985	(0.1131)
3	267	(0.0307)	--	--
4	506	(0.0582)	--	--
5	606	(0.0696)	--	--
6	583	(0.0670)	--	--
7	750	(0.0862)	760	(0.0873)
8	690	(0.0793)	816	(0.0938)
9	270	(0.0310)	268	(0.0308)
IR & D No. 4	638	(0.0733)	606	(0.0696)

to measure the circumferential case growth and the axial movement of the forward polar boss relative to the leading edge of the skirt.

In order to minimize damage to the extensometers, they were removed after the proof cycle prior to burst. The strain gages were retained during the burst cycle, and it was found that the destruction of the gages going through the two pressurization cycles was surprisingly small. The only exceptions were the hoop gages at midcylinder, which tended to fracture at the higher strain levels due to the crazing of the hoop overwrap.

Vessel Design Evaluation

Of the 11 tests that were conducted, six entailed both a proof and burst cycle. From the vessels that did not make it through the proof cycle, two inadequate design areas were discovered. Two vessels demonstrated a critical skirt design, and another vessel demonstrated an inadequate bladder material. However, both problems occurred early in the task, which allowed time to correct these marginal areas. By the completion of this task, sufficient data had been generated to design a 54-in. (1.372 m) diameter subscale version of a 260-in. (6.6 m) diameter motor case.

Table VIII shows a summary of the actual vessel configurations that were tested. The data shown in this table also include actual thicknesses, densities, and resin contents that were measured after hydrotest. A summary of the actual test results is shown in Table IX with stresses and performance parameters calculated as a function of the pressure at failure.

The important data obtained from each of the vessels are summarized in the following subsections.

Vessel 1. - Vessel 1 was helically wound with equal geodesic dome contours and equal openings that were about 54 percent the size of the chamber diameter. The three primary areas of interest in the Vessel 1 test were: (1) the skirt attachment design, (2) the strain behavior of the helical wrap in both the cylindrical section and forward dome, and (3) the strength of the hoop overwrap in the cylinder.

Vessel 1 failed during the burst cycle at a pressure of 5,595 psig (38.58 MN/m^2g). Failure occurred in the hoop wrap as shown in Figure 22, with all other areas structurally intact except for the aft polar boss. As a result of failure, the thrust simulation piston slammed down against the housing and fractured the boss. This test was the first evaluation of the skirt attachment design, and a post-test inspection of this area revealed no potential problem areas.

The behavior of the helical wrap was predicted by both the "netting" and orthotropic composite analytical techniques. It was found that the strain behavior of the forward dome, midway between the tangent plane and outside diameter of the

TABLE VIII

SUMMARY OF THE 18-IN. DIAMETER VESSEL CONFIGURATIONS

	Vessel 1	Vessel 2	Vessel 2 Rework	Vessel 3	Vessel 4	Vessel 5	Vessel 6	Vessel 7	Vessel 8	Vessel 9	Vessel IR & D No. 4 (#4 Mod)
Case OD (Basic Cyl) (in.)	18.71	18.81	19.02	18.71	18.72	18.69	18.74	18.72	18.76	18.77	18.74
(mm)	(475.2)	(477.8)	(483.1)	(475.2)	(475.5)	(474.7)	(476.0)	(475.5)	(476.5)	(476.8)	(476.0)
Case Length (Face to Face of Bosses) (in.)	35.89	35.98	35.98	89.88	35.98	35.99	35.99	35.94	36.0	91.61	35.98
(mm)	(911.6)	(913.9)	(913.9)	(2,283.0)	(913.9)	(914.2)	(914.2)	(912.9)	(914.4)	(2,326.9)	(913.9)
Case Weight (Incl Forward Closure) (lb)	107.0	287.5	308.2	156.5	91.0	99.0	169.0[a]	76.5	110.0	234.0	87.0
(Kg)	(48.5)	(130.4)	(139.8)	(71.0)	(41.3)	(44.9)	(76.7)	(34.7)	(49.9)	(106.1)	(39.5)
Closure Cap (lb)	20.0	55.5	55.5	2.5	2.5	2.5	2.5	2.5	2.5	20.0	2.5
(Kg)	(9.1)	(25.2) (Incl Bolts)	(25.2) (Incl Bolts)	(1.1)	(1.1)	(1.1)	(1.1)	(1.1)	(1.1)	(9.1)	(1.1)
Forward Boss (lb)	16.4	103.6	103.6	3.4	3.4	3.4	3.4	3.4	3.4	16.4	3.4
(Kg)	(7.4)	(47.0)	(47.0)	(1.5)	(1.5)	(1.5)	(1.5)	(1.5)	(1.5)	(7.4)	(1.5)
Aft Boss (lb)	2.65	6.1	6.1	4.3	5.7	6.7	50.0	2.6	6.8	6.1	5.3
(Kg)	(1.2)	(2.8)	(2.8)	(2.0)	(2.6)	(3.0)	(22.7)	(1.2)	(3.1)	(2.8)	(2.4)
Case Volume (cu in.)	7,740	7,820	7,820	21,500	7,860	7,790	8,110	7,810	7,900	21,600	7,900
(m^3)	(0.127)	(0.128)	(0.128)	(0.352)	(0.129)	(0.128)	(0.133)	(0.128)	(0.129)	(0.354)	(0.129)
Case Wall Thickness (Basic Cyl) (in.)	0.357	0.365	0.511	0.326	0.344	0.334	0.346	0.330	0.355	0.349	0.350
(mm)	(9.07)	(9.27)	(12.98)	(8.28)	(8.74)	(8.48)	(8.79)	(8.38)	(9.02)	(8.87)	(8.89)
Hoop Wrap Thickness (in.)	0.154	0.073	0.219	0.211	0.225	0.227	0.227	0.210	0.230	0.148	0.225
(mm)	(3.91)	(1.85)	(5.56)	(5.36)	(5.72)	(5.77)	(5.77)	(5.33)	(5.84)	(3.76)	(5.72)
Long. Wrap Thickness (in.)	0.203	0.292	0.292	0.115	0.119	0.107	0.119	0.120	0.125	0.201	0.125
(mm)	(5.16)	(7.42)	(7.42)	(2.92)	(3.02)	(2.72)	(3.02)	(3.05)	(3.18)	(5.11)	(3.18)
Long. Wrap Angle (deg)	34.5	50.0	50.0	3.5	9.0	9.0	9.0	13.0	9.0	42.0	9.0
(rad)	(0.602) Helical	(0.873) Helical	(0.873) Helical	(0.061) Polar	(0.157) Polar	(0.157) Polar	(0.157) Polar	(0.227) Polar	(0.157) Polar	(0.733) Helical	(0.157) Polar
Total Composite Density (lb/cu in.)	0.0728	0.0728	0.0728	0.0734	0.0716	0.0743	0.0721	0.0730	0.0720	0.0718	0.0720
(Kg/m^3)	(2,015.1)	(2,015.1)	(2,015.1)	(2,040.0)	(1,981.9)	(2,056.6)	(1,995.7)	(2,020.6)	(1,993.0)	(2,161.8)	(1,993.0)
Total Composite Resin Content (% Wt)	20.2	19.7	19.7	19.6	19.6	19.8	20.0	19.6	20.0	21.2	20.0
Domes											
Forward Type	Geodesic	Geodesic	Geodesic	Planar	Planar	Planar	Planar	Planar	Planar	Planar	Planar
Forward Density (lb/cu in.)	0.0700	0.0730	0.0730	0.0707	0.0679	0.0684	0.0608	0.0651	0.0680	0.0692	0.0680
(Kg/m^3)	(1,937.6)	(2,020.6)	(2,020.6)	(1,956.9)	(1,879.5)	(1,893.3)	(1,682.9)	(1,801.9)	(1,882.2)	(1,915.5)	(1,882.2)
Forward Resin Content (% Wt)	22.9	19.7	19.7	23.3	23.7	23.5	23.0	23.8	23.5	22.6	23.5
Aft Type	Geodesic	Geodesic	Geodesic	Tape Reinf	Tape Reinf	Tape Reinf	Tape Reinf	Planar	Tape Reinf	Planar	Tape Reinf
Aft Density (lb/cu in.)	0.0700	0.0709	0.0709	0.0686	0.0662	0.0670	0.0650	0.0529	0.0670	0.0706	0.0670
(Kg/m^3)	(1,937.6)	(1,962.5)	(1,962.5)	(1,898.8)	(1,832.4)	(1,854.6)	(1,799.2)	(1,464.3)	(1,854.6)	(1,954.2)	(1,854.6)
Aft Resin Content (% Wt)	22.9	20.2	20.2	25.7	24.2	24.0	23.8	24.4	24.0	21.4	24.0
Skirt											
Length (in.)	4.32	4.36	4.50	4.65	4.50	4.50	--	4.40	5.77	6.30	4.34
(mm)	(109.7)	(110.7)	(114.3)	(118.1)	(114.3)	(114.3)	--	(111.8)	(146.6)	(160.0)	(110.2)
Thickness (in.)	0.253	0.310	0.310	0.201	0.246	0.308	--	0.208	0.569	0.545	0.438
(mm)	(6.43)	(7.87)	(7.87)	(5.11)	(6.25)	(7.82)	--	(5.28)	(14.45)	(13.84)	(11.13)

[a] Includes aft closure cap.

TABLE IX

SUMMARY OF THE 18-IN. DIAMETER VESSEL TEST RESULTS

	Vessel 1	Vessel 2	Vessel 2 Rework	Vessel 3	Vessel 4	Vessel 5	Vessel 6	Vessel 7	Vessel 8	Vessel 9	Vessel IR & D No. 4
Pressurization Rate (psig/min) ($MN/m^2g/s$)	750 (0.0862)	770 (0.0885)	740 (0.0850)	275 (0.0316)	490 (0.0563)	600 (0.0690)	600 (0.0690)	680 (0.0781)	816 (0.0938)	270 (0.0310)	606 (0.0696)
Failure Pressure (psig) (MN/m^2g)	5,595 (38.58)	4,000 (27.58) (Hold)	4,700 (32.41)	3,600 (24.82)	3,500 (24.13)	3,150 (21.72)	3,850 (26.54)	5,960 (41.09)	6,150[a] (42.40)	5,620 (38.75)	5,800 (39.99)
Area of Failure	Hoop Fil at Midcylinder	Skirt Attach Bond	Skirt Rupture	Forward Dome Leakage	Skirt Rupture	Skirt Rupture	Aft Dome	Hoop Fil at Midcylinder	Aft Dome[a] Crazed	Hoop Fil at Aft Cyl	Hoop Fil at Aft Cyl
Values at Failure											
Hoop Filament Stress (psi) (GN/m^2)	385,000 (2.655)	250,000 (1.724)	100,000 (0.690)	240,000 (1.655)	230,000 (1.586)	210,000 (1.448)	250,000 (1.724)	380,000 (2.620)	385,000 (2.655)	360,000 (2.482)	380,000 (2.620)
Hoop Composite Stress (psi) (GN/m^2)	150,000 (1.034)	99,000 (0.683)	84,000 (0.579)	100,000 (0.690)	90,000 (0.621)	86,000 (0.593)	100,000 (0.690)	170,000 (1.172)	160,000 (1.103)	150,000 (1.034)	150,000 (1.034)
Hoop Composite Density, ρ (lb/cu in.) (Kg/m^3)	1,976 (0.0714)	1,957 (0.0707)	2,115 (0.0764)	1,976 (0.0714)	1,993 (0.0720)	1,985 (0.0717)	1,976 (0.0714)	2,046 (0.0739)	2,012 (0.0727)	1,976 (0.0714)	1,976 (0.0714)
Hoop Composite, σ/ρ (in.) (MNm/Kg)	$2.1 \times 10^{+6}$ (0.523)	$1.4 \times 10^{+6}$ (0.349)	$1.1 \times 10^{+6}$ (0.274)	$1.4 \times 10^{+6}$ (0.349)	$1.25 \times 10^{+6}$ (0.312)	$1.2 \times 10^{+6}$ (0.299)	$1.4 \times 10^{+6}$ (0.349)	$2.3 \times 10^{+6}$ (0.573)	$2.2 \times 10^{+6}$ (0.548)	$2.1 \times 10^{+6}$ (0.523)	$2.1 \times 10^{+6}$ (0.523)
Long. Filament Stress (psi)[b] (GN/m^2)	273,000 (1.882)	230,000 (1.586)	270,000 (1.862)	213,000 (1.469)	210,000 (1.448)	190,000 (1.310)	220,000 (1.517)	370,000 (2.551)	330,000 (2.275)	325,000 (2.241)	310,000 (2.137)
Long. Composite Stress (psi)[b] (GN/m^2)	*113,000* (0.779)	*60,000* (0.414)	*70,000* (0.483)	*125,000* (0.862)	*120,000* (0.827)	*110,000* (0.758)	*164,000* (1.131)	*170,000* (1.172)	*190,000* (1.310)	*105,000* (0.724)	*177,000* (1.220)
Long. Composite Density, ρ (lb/cu in.) (Kg/m^3)	1,954 (0.0706)	2,026 (0.0732)	2,046 (0.0739)	1,921 (0.0694)	1,899 (0.0686)	1,904 (0.0688)	1,680 (0.0607)	1,810 (0.0654)	1,929 (0.0679)	1,938 (0.0700)	1,886 (0.0681)
Long. Composite, σ/ρ (in.)[b] (MNm/Kg)	$1.6 \times 10^{+6}$ (0.399)	$0.82 \times 10^{+6}$ (0.204)	$0.96 \times 10^{+6}$ (0.236)	$1.8 \times 10^{+6}$ (0.449)	$1.75 \times 10^{+6}$ (0.435)	$1.6 \times 10^{+6}$ (0.398)	$2.7 \times 10^{+6}$ (0.673)	$2.6 \times 10^{+6}$ (0.648)	$2.8 \times 10^{+6}$ (0.679)	$1.5 \times 10^{+6}$ (0.374)	$2.6 \times 10^{+6}$ (0.647)
PV/W (in.) (MNm/Kg)	$0.405 \times 10^{+6}$ (0.101)	$0.11 \times 10^{+6}$ (0.0271)	$0.12 \times 10^{+6}$ (0.0297)	$0.50 \times 10^{+6}$ (0.123)	$0.30 \times 10^{+6}$ (0.0754)	$0.25 \times 10^{+6}$ (0.0619)	$0.26 \times 10^{+6}$[c] (0.0464)	$0.61 \times 10^{+6}$ (0.152)	$0.43 \times 10^{+6}$ (0.110)	$0.52 \times 10^{+6}$ (0.129)	$0.52 \times 10^{+6}$ (0.131)
Maximum Stress in Skirt (psi) (MN/m^2)	-41,900 (-288.9)	-36,200 (-249.6)	-42,500 (-293.0)	-29,300 (-202.0)	-46,400 (-319.9)	-41,000 (-283.7)	-- --	-48,500 (-334.4)	-46,000 (-317.2)	-34,000 (-234.4)	-39,000 (-268.9)
Skirt Load (lb/in.) (MN/m)	-6,400 (-1.121)	-8,800 (-1.541)	-10,350 (-1.812)	-4,100 (-0.718)	-5,600 (-0.981)	-7,200 (-1.261)	-- --	-6,800 (-1.191)	-13,500 (-2.364)	-12,400 (-2.171)	-9,300 (-1.628)

[a] Pressure shut down with no burst.
[b] In the forward dome at the tangent plane.
[c] Excludes aft closure cap weight.

Figure 22. Vessel 1 After Hydrotest

polar boss, was best predicted by the composite orthotropic approach. Figures 23 and 24 show the actual and predicted strains in the meridional and hoop direction as a function of pressure.

In the cylindrical section, the composite analytical technique also gave the best predictions. Figures 25 and 26 show the actual and theoretical strains in the hoop and axial directions as a function of pressure as obtained from reduced extensometer data during the proof cycle. Strain gages were not used to record axial strains in the cylinder, and the hoop strain gage failed to operate. The calculated stress in the hoop filaments at failure was 385,000 psi (2.655 GN/m^2), which was in agreement with the data shown in Figure 1.

The results of this initial test indicated:

1. The skirt attachment design would be compatible with the higher load requirements of the subsequent vessels.

2. The strain behavior in the helical wrap with a filament orientation greater than 30 deg (0.523 rad) was best predicted by the composite analytical approach.

Vessel 2. - The geodesic design of Vessel 2 required that both the forward and aft dome openings be identical in size. The inside diameter of these openings was approximately 78 percent of the case chamber diameter, which meant that the retention of the forward polar boss was a critical design requirement. Vessel 2 was also the first vessel to be tested with a skirt loading requirement of 11,000 lb (1.926 MN/m) per circumferential inch, which was the largest of the three loading categories.

Vessel 2 underwent two tests. During the first test, failure occurred in the skirt attachment area during the 4,000 psig (27.58 MN/m^2g) pressure hold of the proof cycle. Failure was a result of a poor bond between the inner shear ply and the case. When the bond failed, the thrust load was transferred entirely through the outer shear ply, which caused the overwrap to fail locally in axial compression in the area of the filler ply as shown in Figure 27. The remaining structure was undamaged, and it was decided to replace the skirt and retest the vessel. The poor bond between the shear ply and case was a result of a fabrication discrepancy where the inner shear ply surface was not mechanically cleaned with a high speed emery wheel prior to skirt installation.

Vessel 2, with the new skirt, went through the proof cycle but failed in the skirt structure as shown in Figure 28 during the burst cycle. Failure occurred at a pressure of 4,700 psig (32.41 MN/m^2g) and a skirt load of 10,350 lb/in. (1.812 MN/m). The aft polar boss and dome were fractured as a result of failure.

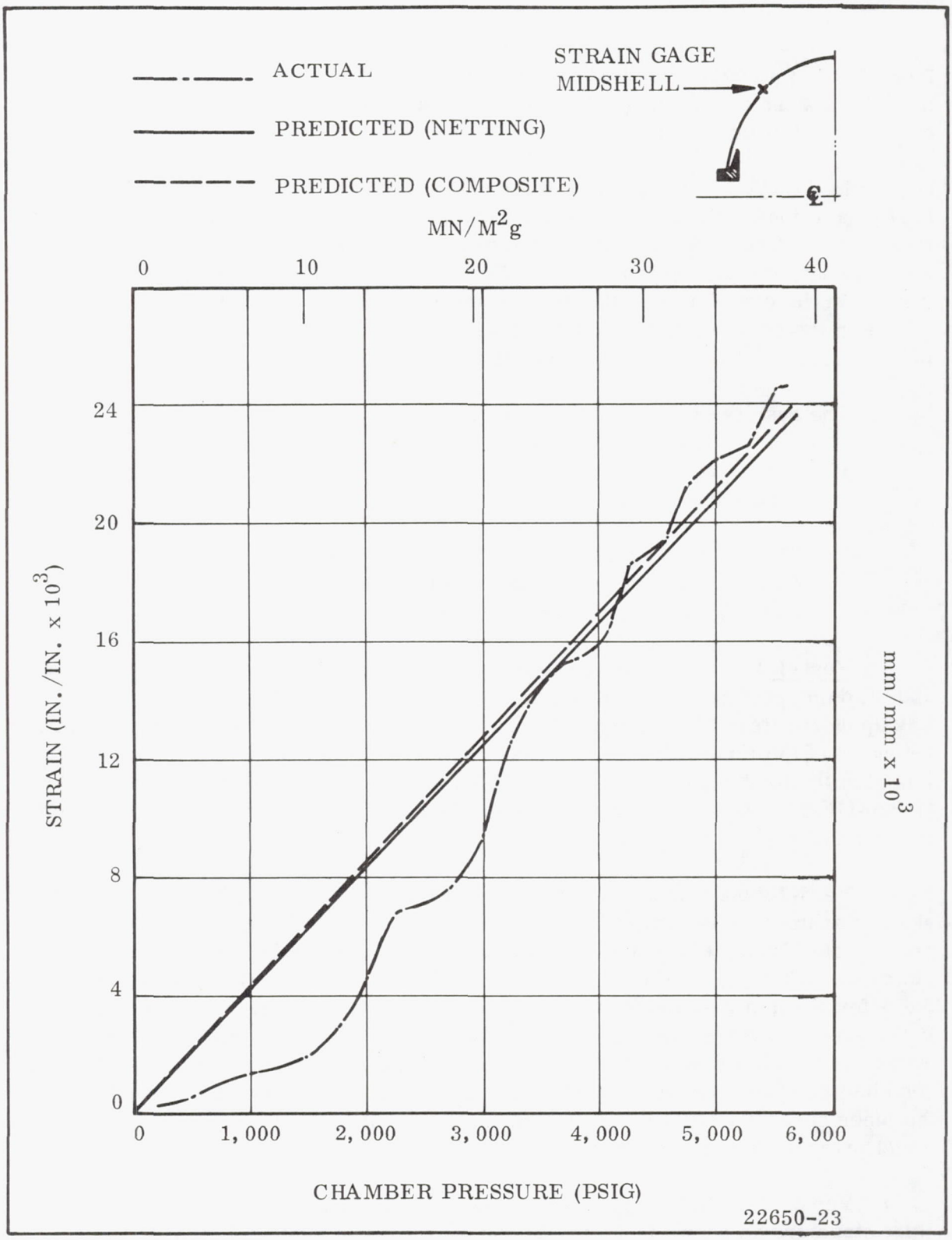

Figure 23. Vessel 1 Meridional Strain in Forward Dome (Burst Cycle)

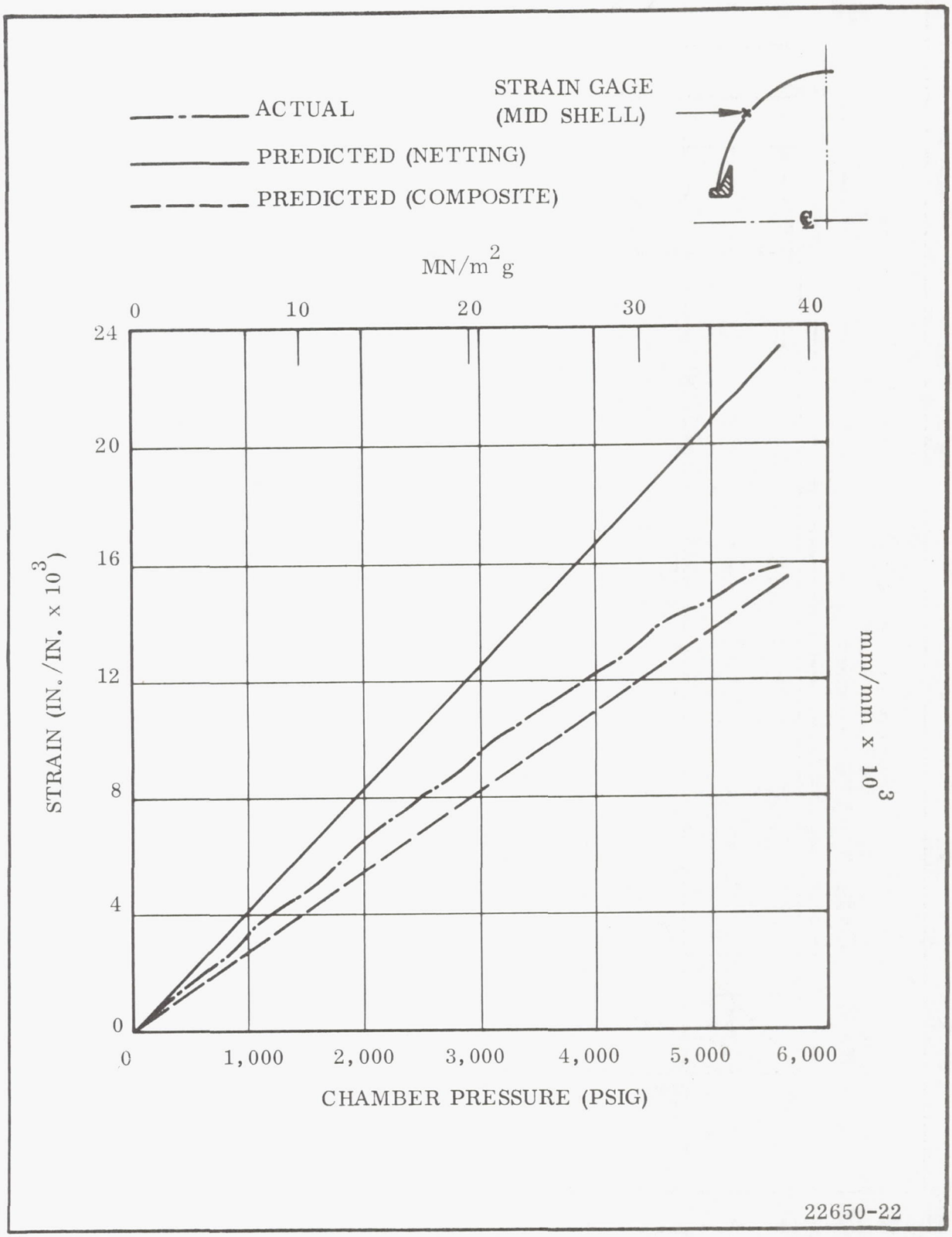

Figure 24. Vessel 1 Hoop Strain in Forward Dome (Burst Cycle)

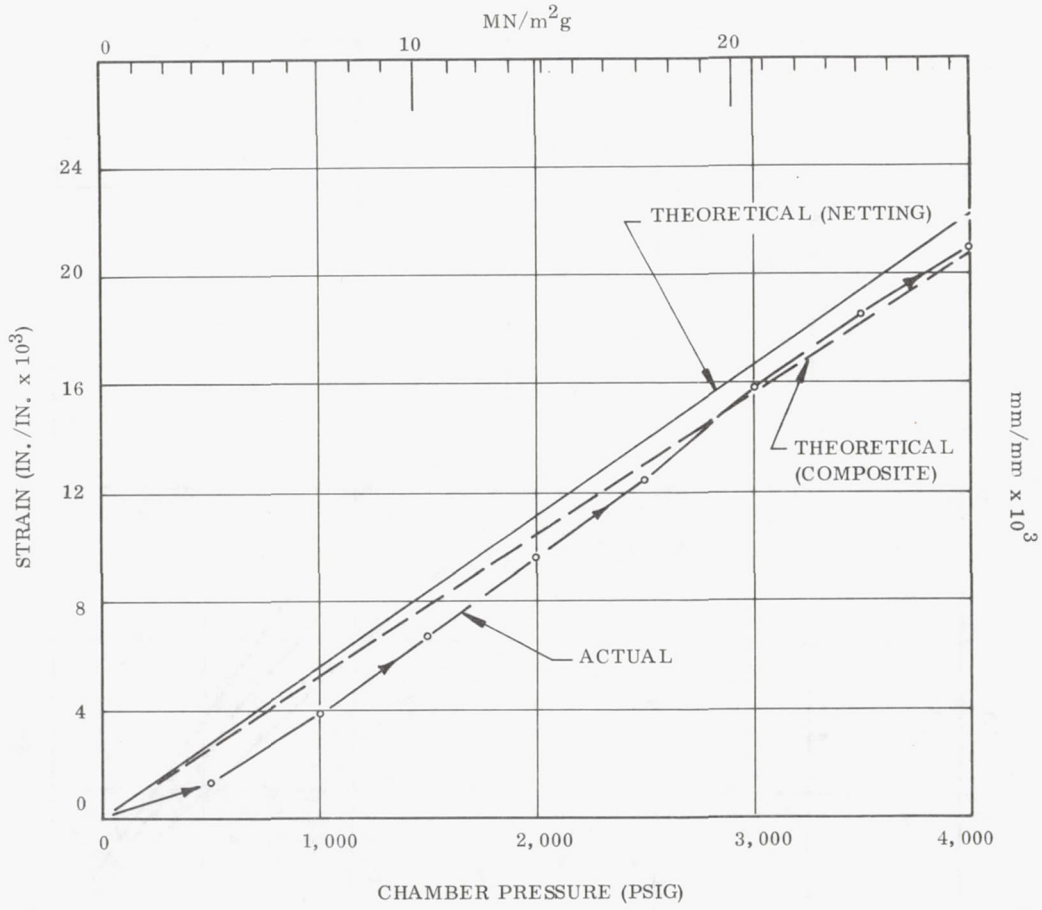

Figure 25. Vessel 1 Hoop Strain in Cylindrical Section at Midcylinder (Proof Cycle)

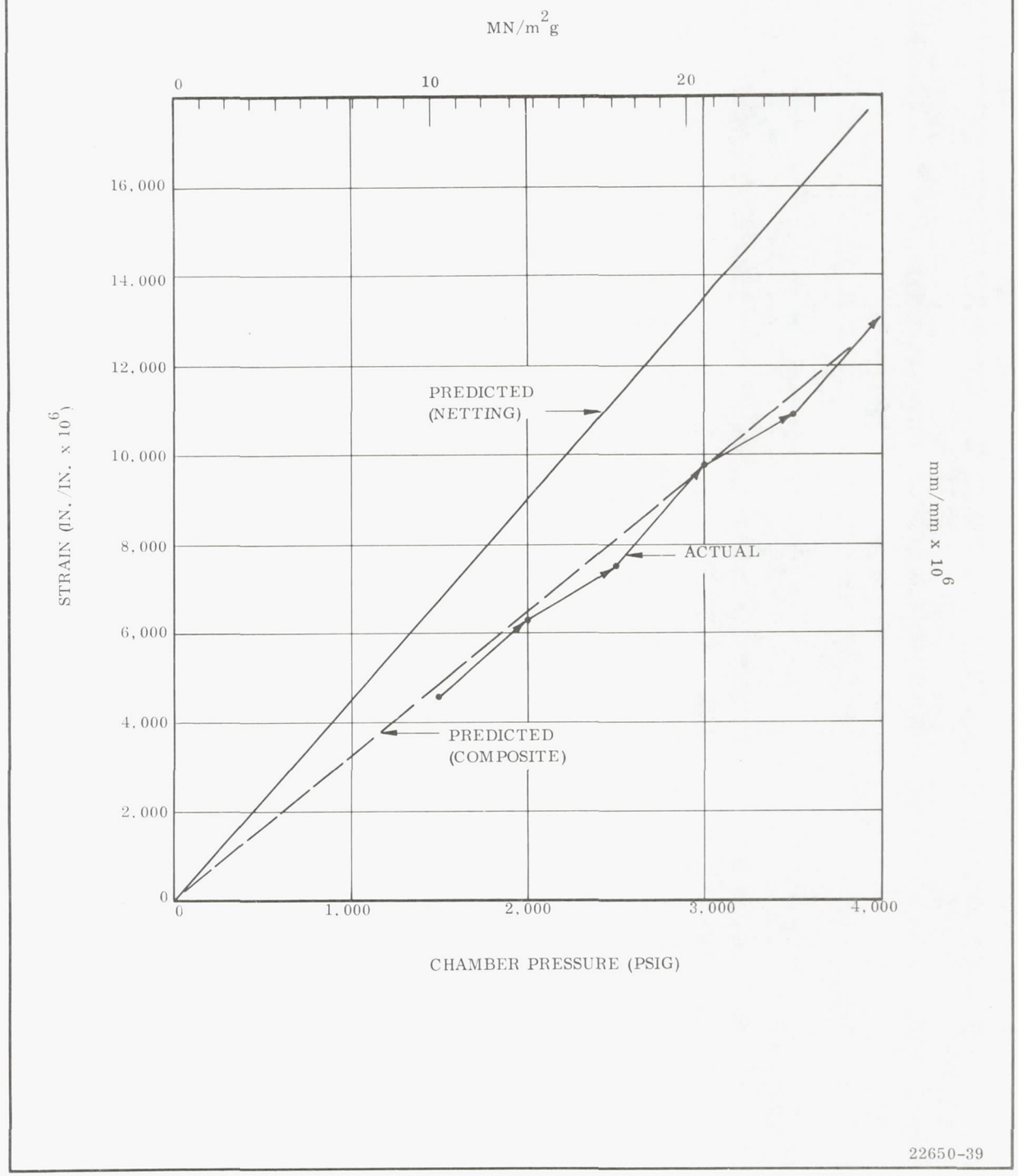

Figure 26. Vessel 1 Axial Strain in Cylindrical Section (Proof Cycle)

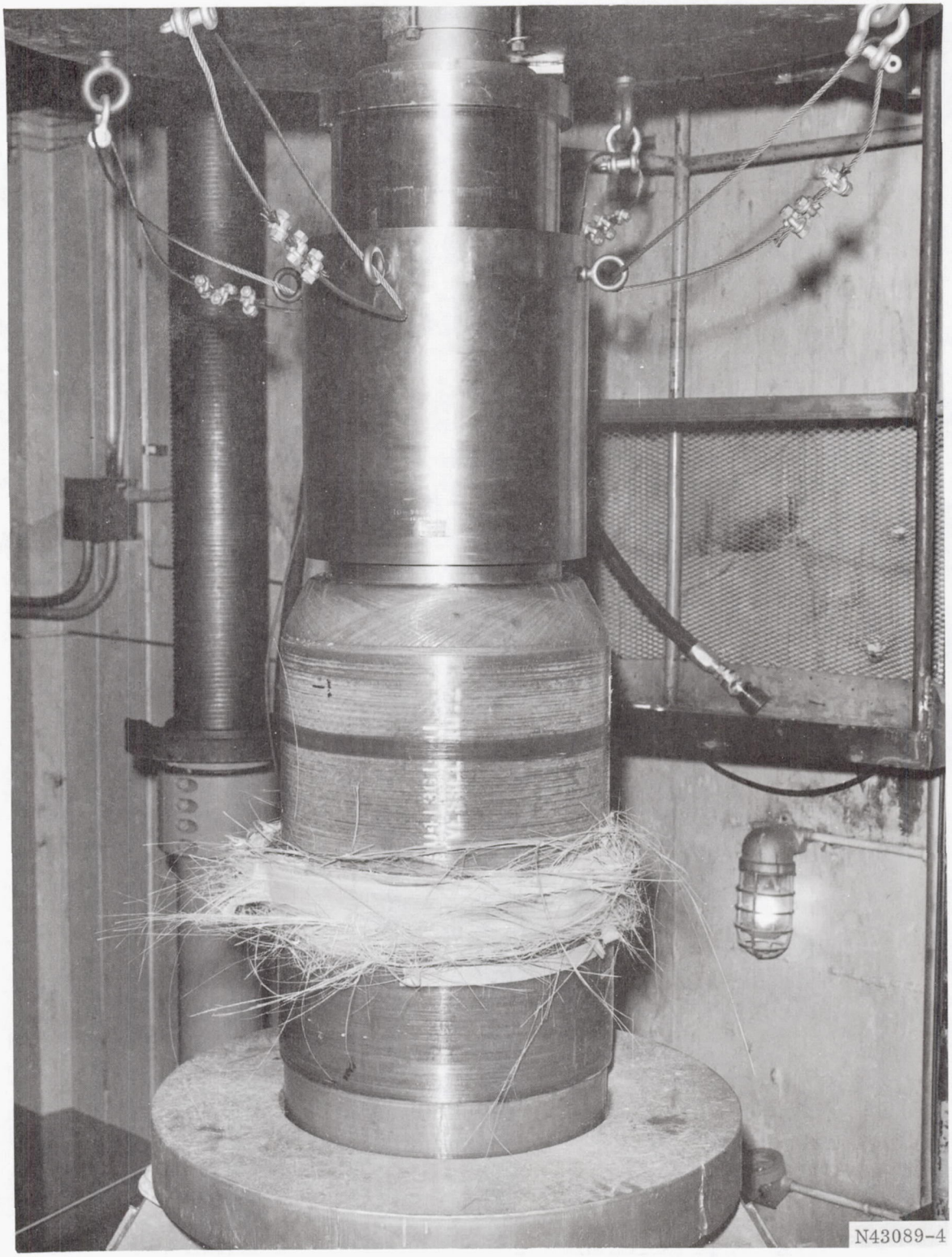

Figure 27. Vessel 2 After Hydrotest 1

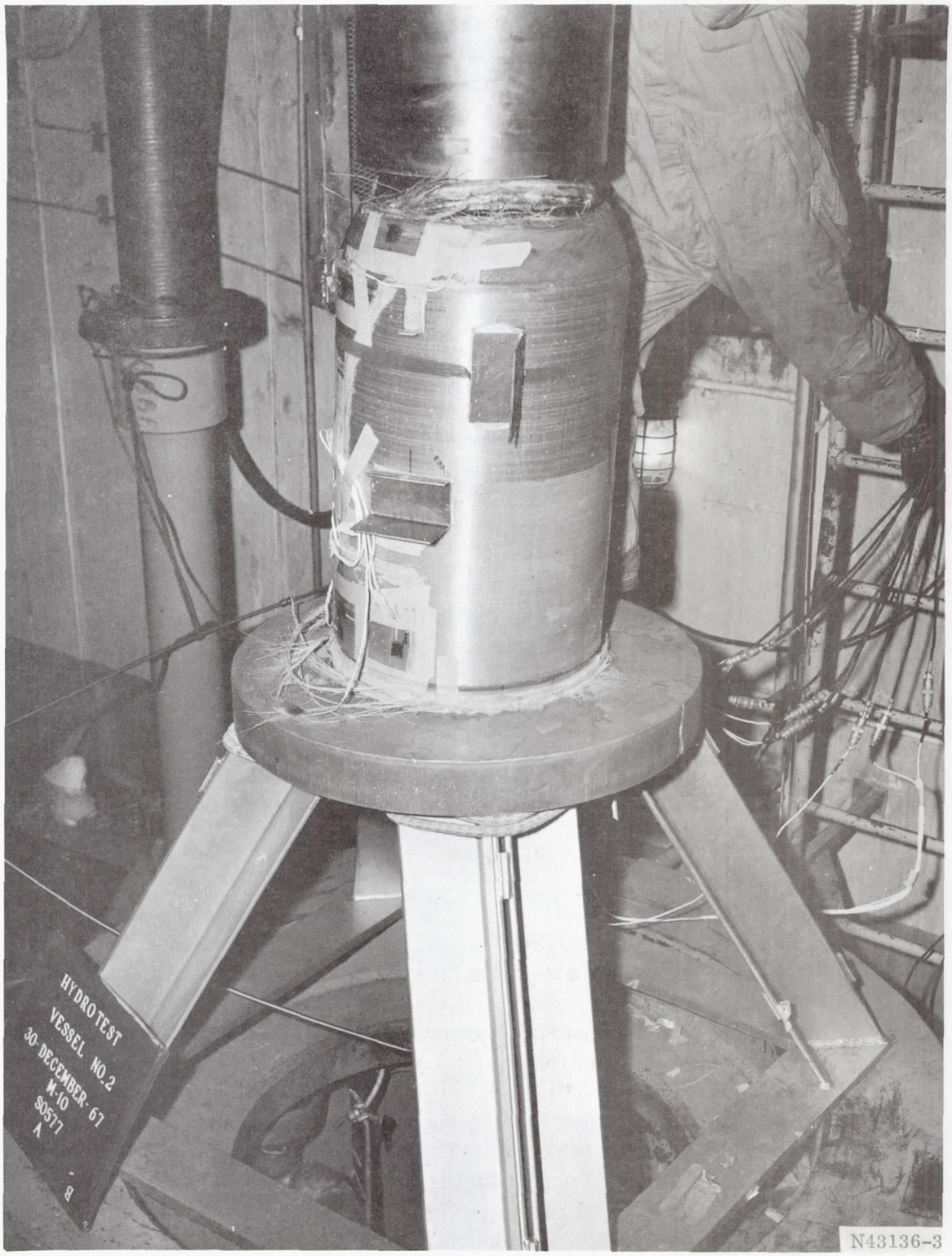

Figure 28. Vessel 2 After Hydrotest 2

For this second test the overwrap structure was made thicker (0.27 vs 0.13 in., 6.86 vs 3.30 mm) and the outer shear ply thinner (0.06 vs 0.15 in., 1.52 vs 3.81 mm) in order to reduce the shear stresses in the inner shear ply. The longitudinal strain in the overwrap in the area of the filler ply as recorded during both tests is shown plotted as a function of pressure in Figure 29. This figure shows that the axial compressive stress in the overwrap in the area of the filler ply decreased with increasing pressure. This decreased stress is a result of changes in the filler ply shear modulus due to the rubber distortion and the increased bending in the wall due to crazing.

The skirt failure during the second test was caused by axial and bending stresses in the skirt. No axial strain gages were located in this area, and thus the composite stress at failure had to be estimated from the discontinuity analysis. The calculated composite stress at failure was approximately -42,000 psi (-289.58 MN/m^2) at the outside surface of the skirt, just forward of the leading edge of the overwrap. The indicated fracture strength of the skirt was lower than anticipated; thus failure was considered to be influenced by the tensile hoop and in-plane shear stresses in this area. Figure 30 shows both the actual and predicted hoop strains in this area as a function of pressure.

The forward polar boss and dome behaved as predicted, with the boss being retained entirely by the hoop restraint of the helical and hoop wrap in the forward dome. At skirt rupture during the second test, the axial blowout load on the boss (and reacted by the dome) was 720,000 lb (3.203 MN). The hoop strain in the dome structure was close to that predicted by the discontinuity analysis as shown in Figure 30.

The results of the Vessel 2 test indicated:

1. The skirt attachment design appeared adequate for all vessels.

2. A polar boss and dome design for vessels with extremely large port openings was demonstrated.

3. The need for a new material fracture criterion for the skirt structure was indicated.

Vessel 3. - Vessel 3 was the first in the series of in-plane wrap designs with a reinforced and cut opening aft dome. The areas of interest were: the fabrication problems associated with slippage during winding, and the strain behavior of the forward and aft domes. The case was tested three times because of bladder leakage problems. Instrumentation was operational during the first two tests. The recorded data from the second test was used to evaluate the structural behavior of the vessel.

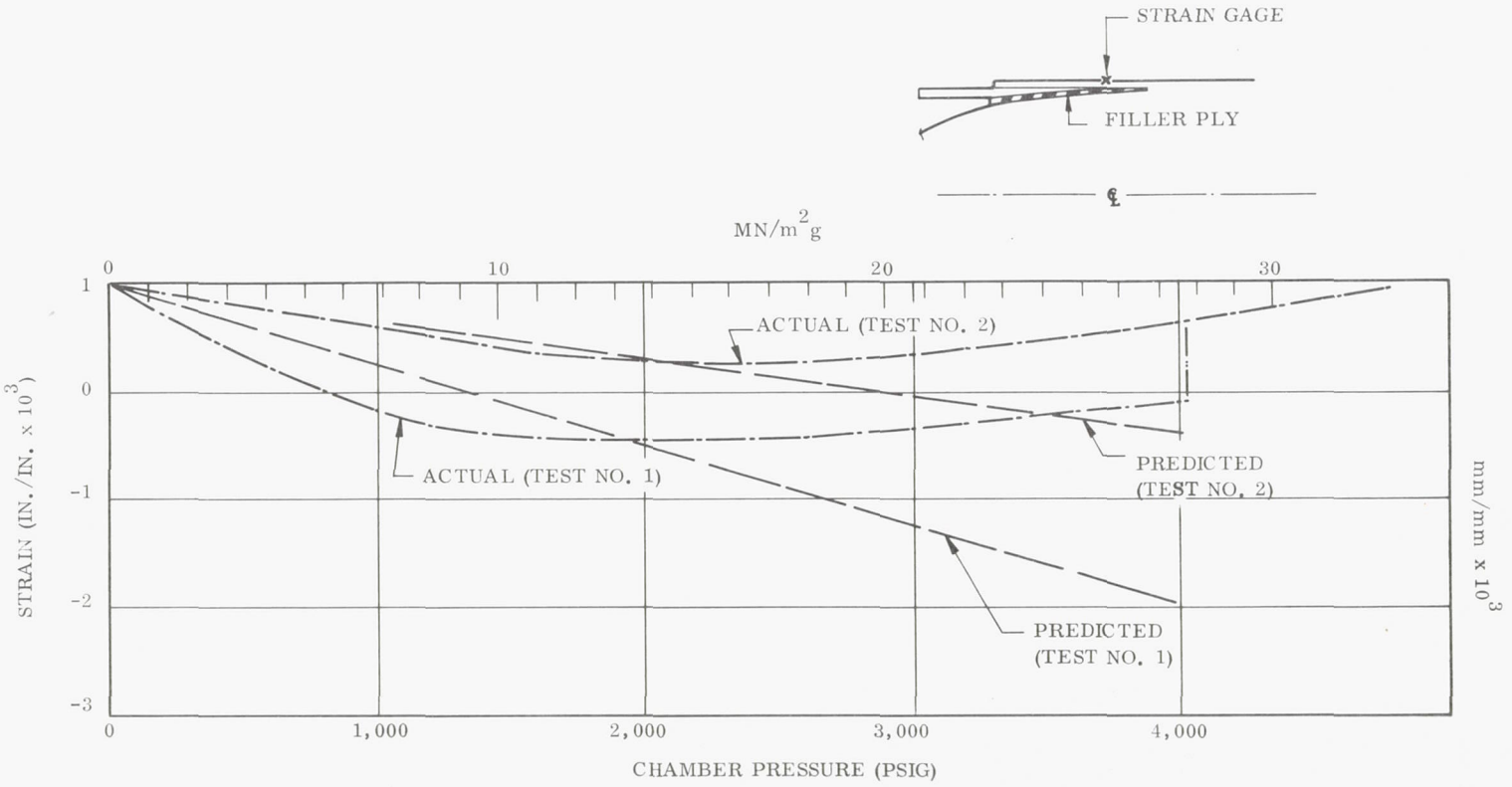

Figure 29. Vessel 2 Axial Strain in Overwrap Above Filler Ply (Tests 1 and 2)

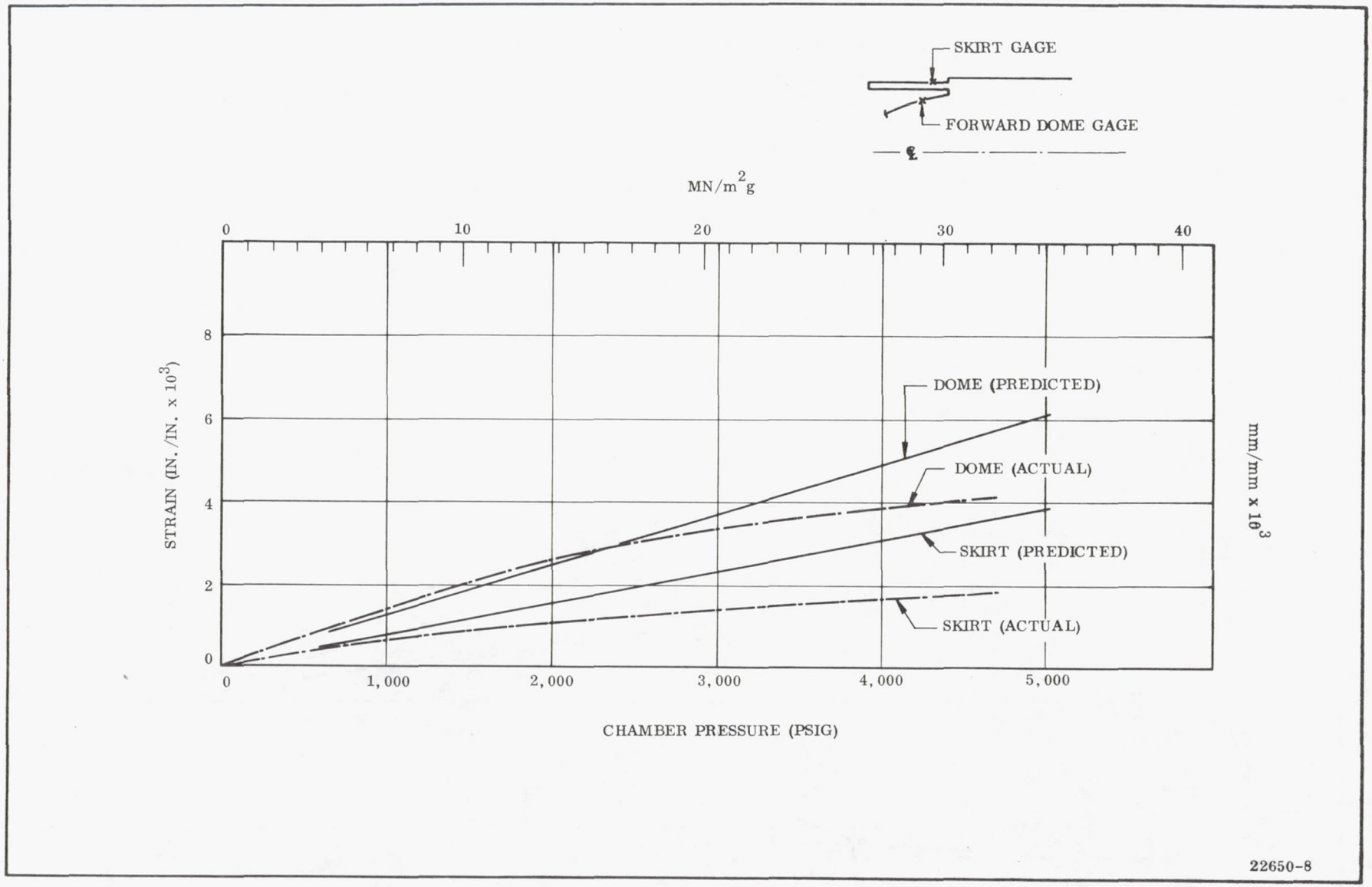

Figure 30. Vessel 2 Hoop Strain in Forward Dome and Skirt (Test 2, Burst Cycle)

The polar (in-plane) pattern had a planar wrap angle of 3.5 deg (0.0613 rad) as established by the two equal polar wrap openings ($D_E/D_{cyl} = 0.30$) and the total length of the vessel ($L/D_{cyl} = 5.0$), and was prone to some slippage during fabrication. The final polar layer moved away from the forward boss about 1 in. (25 mm) during vessel cure, the prior layers slipping progressively less.

Vessel 3, shown in Figure 31 installed in the bay, was tested three times prior to failure. The polyisoprene bladder was not only of poor quality, but did not appear to adhere to the glass/epoxy composite very well; thus severe leakage was responsible for stopping two test attempts. Prior to the third test, the interior of the vessel was completely coated with liquid urethane in an attempt to seal all porous areas. At 3,600 psig (24.82 MN/m^2g) during the final attempt, the polar wrap ruptured locally at the leading edge of the inner shear ply as shown in Figure 32, causing a severe leak and final termination of testing. A post-test inspection revealed that the polar wrap in the cylindrical section had severe axial craze lines running from tangent plane to tangent plane as a result of the hoop strain. The magnitude of the radial pressure was apparently enough to force the water through a weak area in the bladder and into an opened craze line in an area around the skirt attachment.

The strain behavior of the forward dome was typical to that of a shallow shell having a small polar opening. The shell contour was designed to have an initial negative membrane hoop stress bias near the tangent plane in order to prevent crazing as a result of contour changes during pressurization. The design was based on a contour that would give a free body a compressive membrane stress component of 1,000 psi (6.89 MN/m^2) at the tangent plane at an internal pressure of 660 psig (4.5 MN/m^2g). This design criterion was developed during a study program[a] conducted at the Wasatch Division on the strain behavior of shallow planar wrapped domes with small polar openings. Figure 33 shows the actual hoop strain behavior near the tangent plane and at the mid-point of the shell.

The aft dome behaved fairly close to prediction in the critical area around the polar boss. Figure 34 shows the hoop strain at the center of the shell and in the area over the boss, along with the predicted hoop strain at the boss as obtained from a discontinuity analysis.

The results from the Vessel 3 tests indicated:

1. The need was indicated for a new bladder material and interspersement of hoops in the polar laminate to prevent leakage at high pressures.

2. The methods of analysis used to predict the strain behavior in the forward and aft domes were demonstrated to be very adequate.

[a]IR & D Dome Crazing Study Program, January 1967.

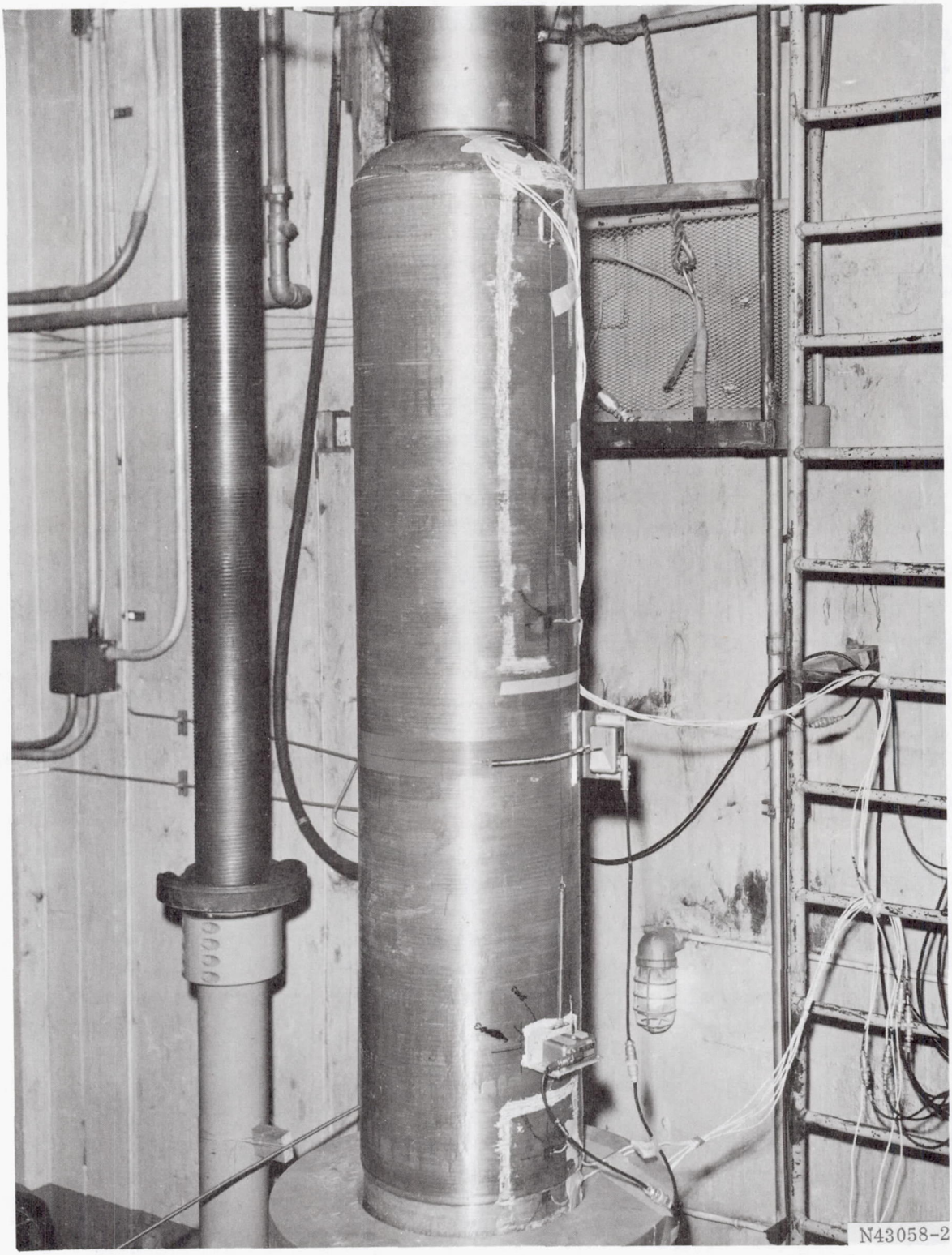

Figure 31. Vessel 3 Installed in Test Bay

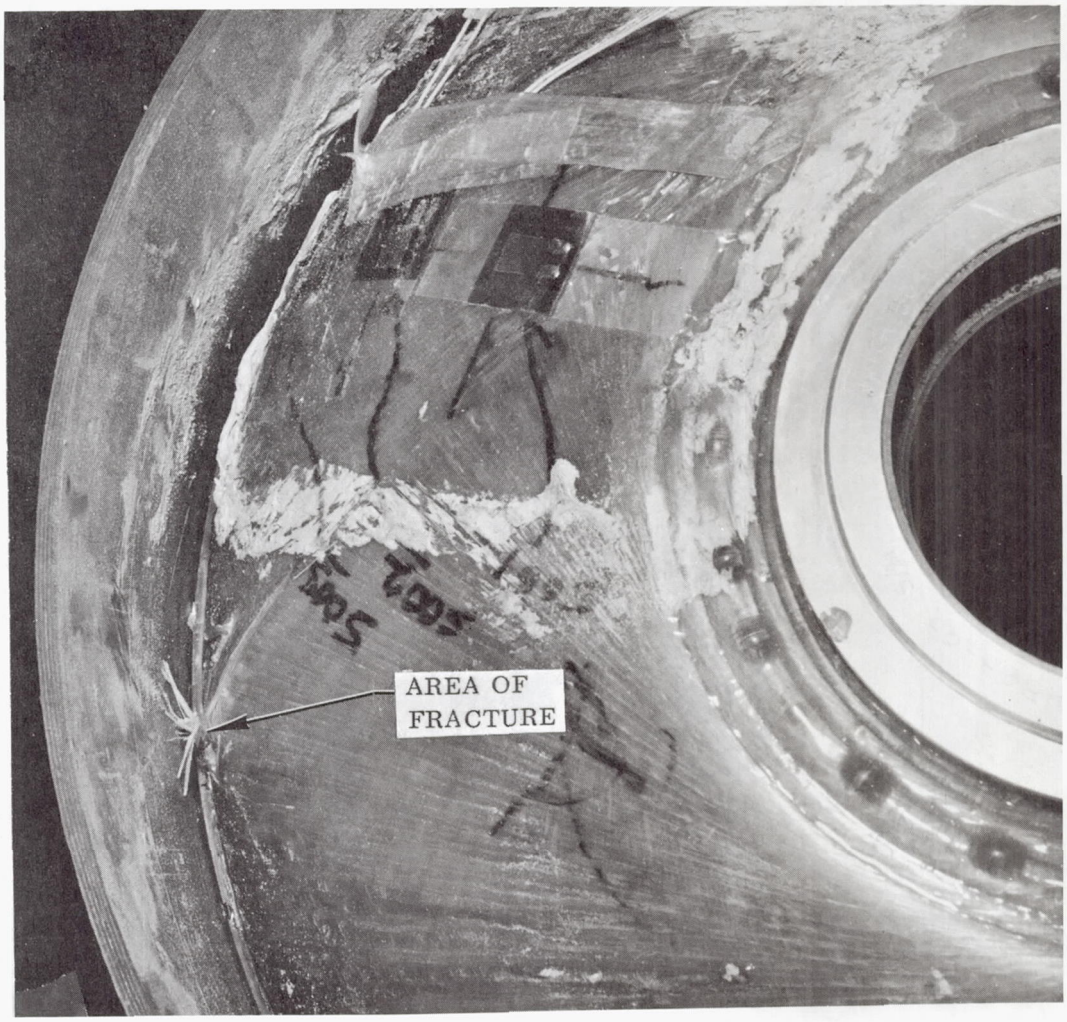

Figure 32. Vessel 3 Failure Location in Forward Dome

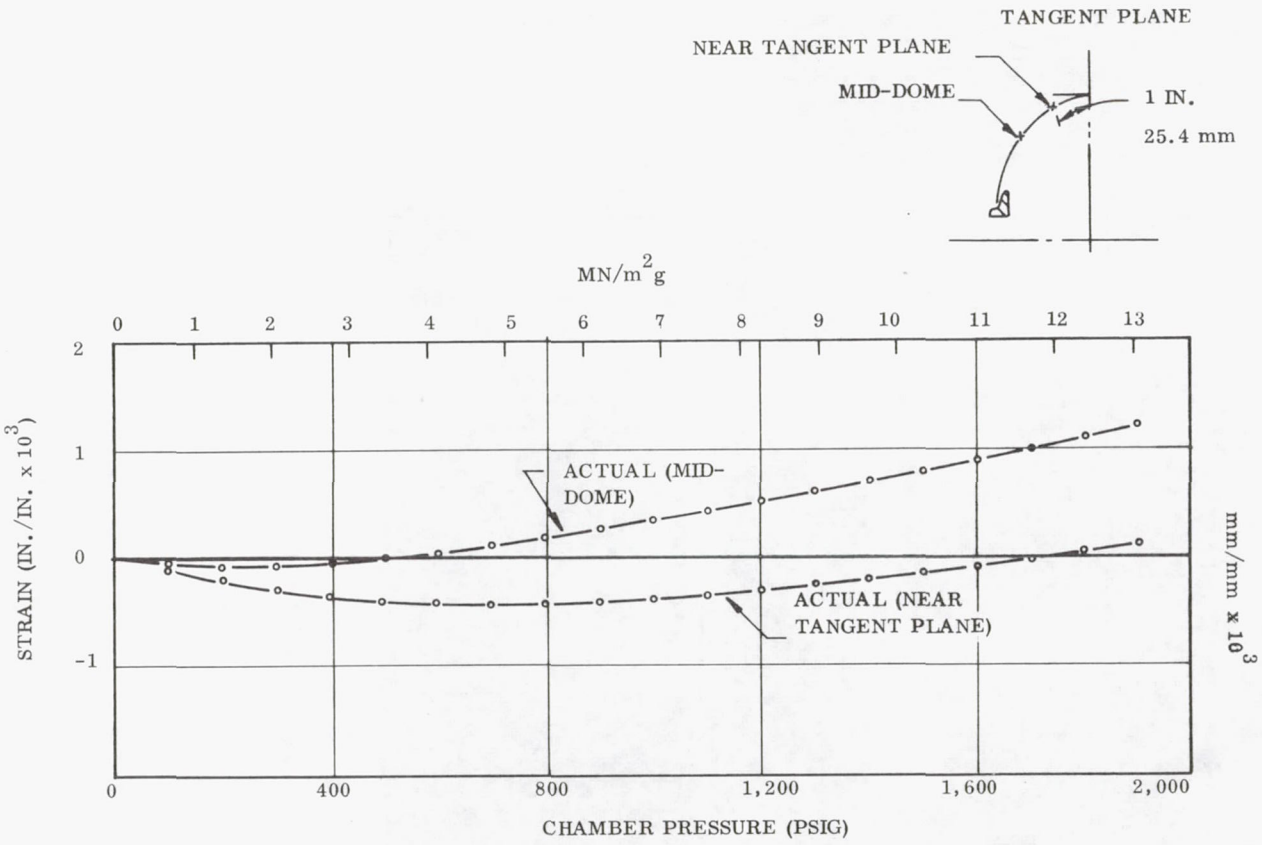

Figure 33. Vessel 3 Hoop Strain in Forward Dome

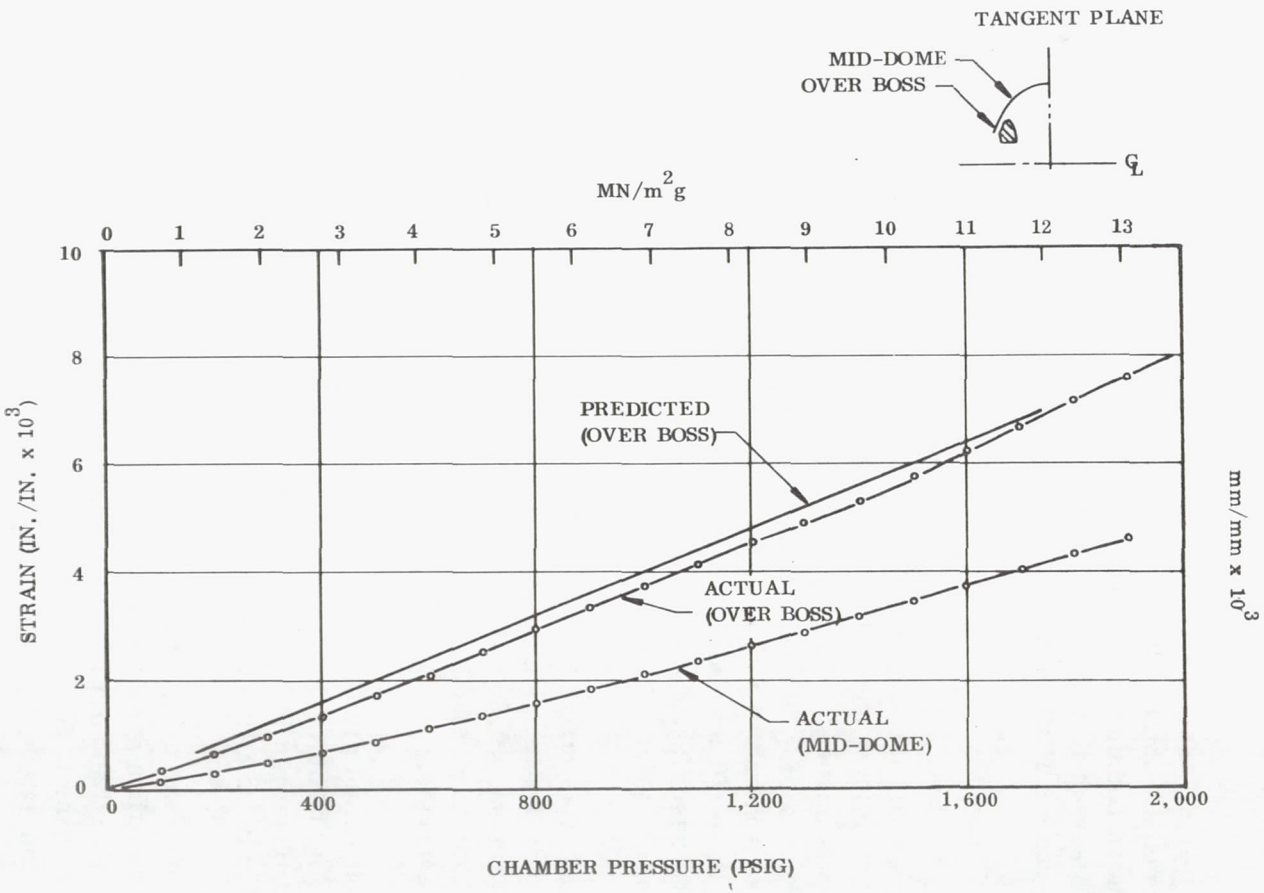

Figure 34. Vessel 3 Hoop Strain in Aft Dome

3. During fabrication it was evident from the amount of slippage that occurred during winding and cure that the L/D ratio of 5 and the 30 percent polar openings were at a maximum for a planar wrap design.

Vessel 4. - Vessel 4 was the second in the series of polar wound vessels with a reinforced aft dome. The basic design differed from Vessel 3 in that it had a larger aft dome opening, a larger skirt loading, and an L/D ratio of 2. From a fabrication standpoint it was the first vessel to reflect the bladder material change from polyisoprene to NBR, and it was also the first to have hoops interspersed in the polar wrap.

During the test the three primary areas of interest were: (1) the skirt structure, which failed during the Vessel 2 test; (2) the strain behavior of the cylindrical section with interspersed wrap; and (3) the strain behavior in the aft dome with a 60 percent opening. The vessel failed in the skirt structure during the proof cycle at a pressure of 3,500 psig (24.13 MN/m^2g). The failure, which is shown in Figure 35, was a result of material fracture or buckling that occurred at an axial load of 5,600 lb/in. (0.981 MN/m) and was similar to that experienced during the second test of Vessel 2. The only other damaged area was in the forward dome and was a result of the skirt failure.

The skirt was instrumented in the area of the maximum theoretical bending moment with only a strain gage oriented in the hoop direction. At failure, the indicated hoop strain was +0.0010 in./in. with a theoretical combined axial membrane and bending moment stress of -46,000 psi (-317.16 MN/m^2) as estimated from the discontinuity analysis.

The actual and predicted axial and hoop strains in the cylindrical section are shown in Figure 36. The apparent crazing in the polar wrap was not as locally severe as that observed in Vessel 3, but was uniformly distributed in the polar wrap and identified only by a lightening of the amber color of the resin.

At failure, the hoop stress in the aft dome over the polar boss was around 7 percent greater than predicted by the discontinuity analysis. Figure 37 shows the plot of the predicted and actual hoop strain as a function of pressure. The dome apparently lost some of its hoop stiffness as a result of crazing with the increasing pressure, but the extent of this loss in stiffness could not be determined because of the premature skirt failure.

The pertinent information obtained from the Vessel 4 test was:

1. The test backed up the need for a new fracture criterion for the skirt structure as was indicated by the Vessel 2 test.

Figure 35. Vessel 4 Skirt After Failure

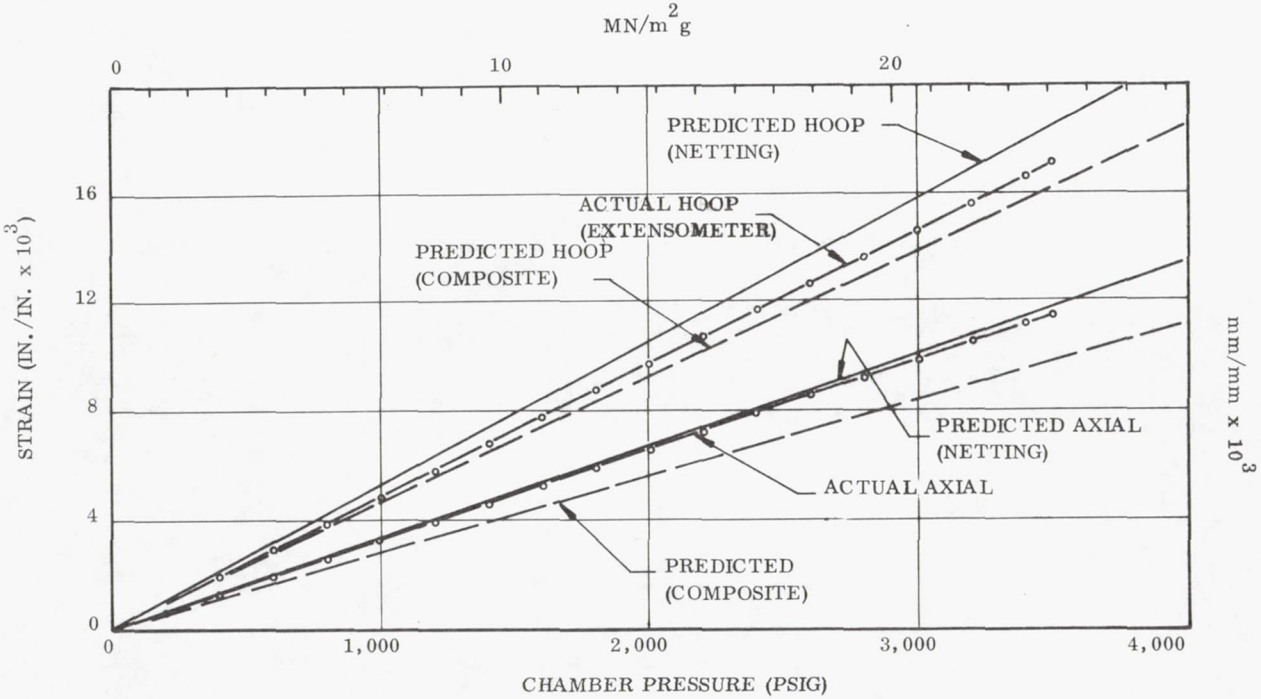

Figure 36. Vessel 4 Hoop and Axial Strain in Cylindrical Section at Midcylinder

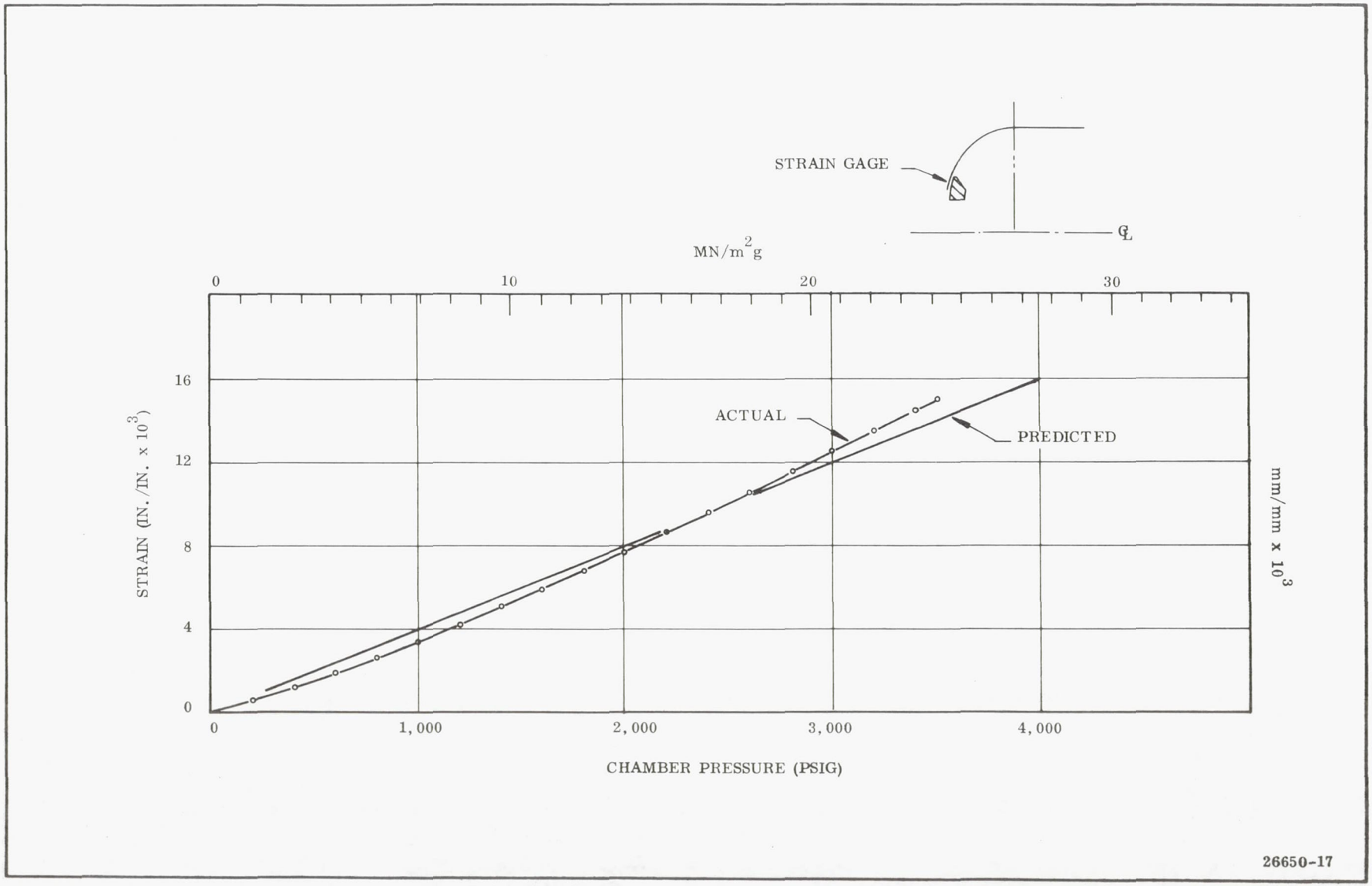

Figure 37. Vessel 4 Hoop Strain in Aft Dome

2. The strain data from the case cylindrical section showed that the "netting" analysis was slightly conservative, yet very adequate, with respect to a longitudinal wrap with a small angular filament orientation.

3. The strain data obtained from the aft dome indicated that the influence of crazing on the material properties was greater than had been anticipated, and that its effects would have to be compensated for on subsequent designs.

4. The new NBR (Gen Gard V-45) bladder and interspersement of hoops in the polar laminate proved to be essential in preventing leakage at high pressures. All remaining vessels would require the NBR bladder, and remaining cut dome designs would require interspersed wrap.

Vessel 5. - Vessel 5 was third in the series of cut dome designs. The design was identical to that of Vessel 4 except for the larger aft dome opening (70 percent) and the higher skirt loading. The critical areas were again the skirt structure and the reinforcements in the aft dome. Vessel 5 was fabricated along with Vessel 4, and thus the design could not be modified in accordance with the Vessel 4 test data.

During the proof cycle, Vessel 5 failed in the skirt structure at a pressure of 3,150 psig (21.72 MN/m^2g) and with a skirt load of 6,800 lb/in. (1.19 MN/m). The nature of the failure, which is shown in Figure 38, was identical in appearance to that of Vessel 4. The measured hoop strain in the area of the maximum bending stress was 0.0012 in./in. at failure. The maximum axial stress in this area as obtained from the discontinuity analysis, was 41,000 psi (283 MN/m) which, along with the indicated hoop stress, subjected the longitudinal wrap to a plane stress pattern that was almost identical to that in the skirt of Vessel 4 and similar to that in the skirt of Vessel 2.

The strain behavior in the aft dome was also similar to that experienced during the Vessel 4 test. At failure, the strain was approximately 7 percent greater than predicted as shown in Figure 39, which shows plots of both the actual and predicted hoop strains in the critical area over the polar boss as functions of pressure.

The results from the Vessel 5 test supplemented the skirt fracture data from the test of Vessels 2 and 4, and supported the validity of the discontinuity analysis as applied to a tape reinforced dome. Utilization of this data in support of the subsequent designs is as follows:

1. The data pertaining to the skirt fracture were extremely important with respect to the establishment of the material fracture strengths

Figure 38. Vessel 5 Skirt After Failure

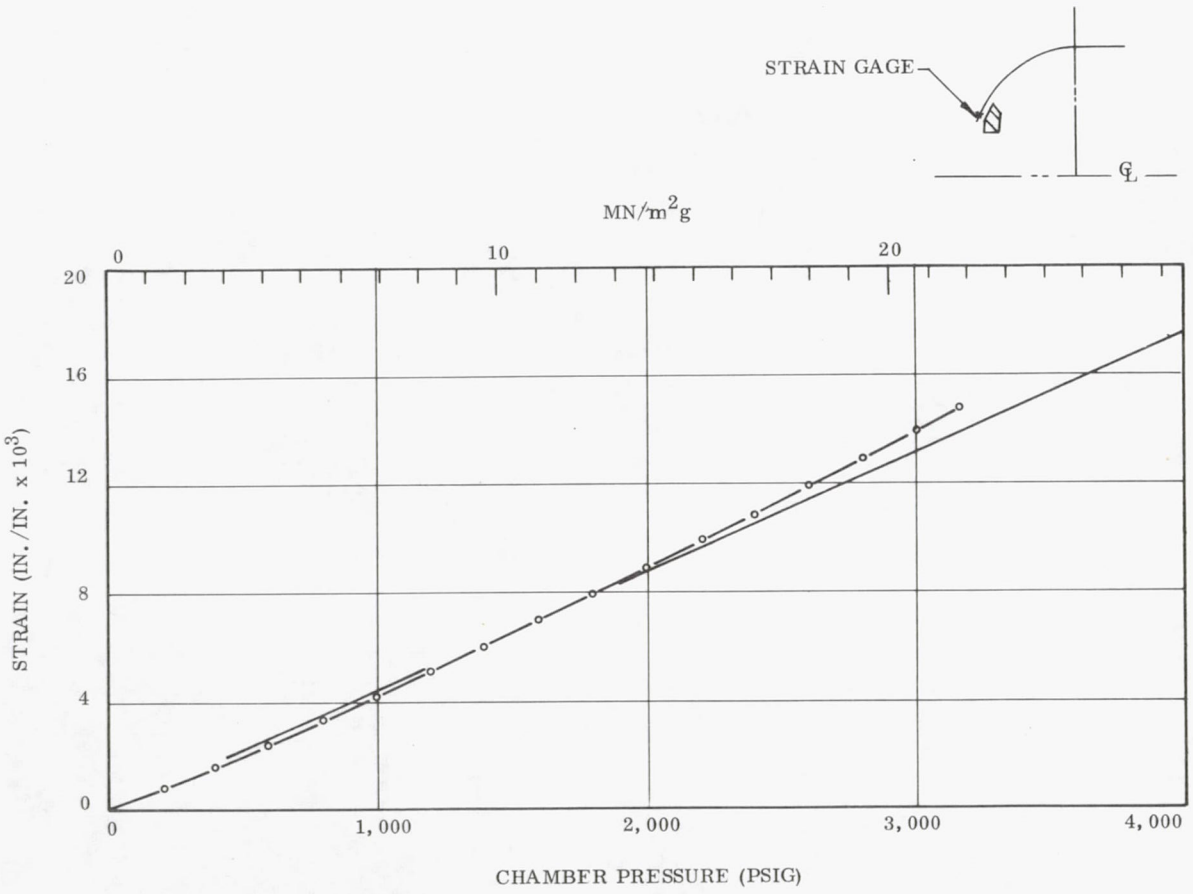

Figure 39. Vessel 5 Hoop Strain in Aft Dome

which were used in conjunction with the failure criterion presented in the 18-Inch Diameter Vessel Design Section. The maximum stresses in the plane of the filament of the longitudinal layer in the skirts of Vessels 2, 4, and 5 at failure are given in Table X as calculated from equations (19), (20), and (21). The strengths for the longitudinal layer in the direction of the ply filament were estimated from data presented in Reference 6 and modified to reflect the failure conditions in all three skirts. The resulting strengths that were established for use in equation (18) are:

$$F_x = 75,000 \text{ psi } (517 \text{ MN/m}^2) \text{ (compression)}$$

$$F_y = 5,000 \text{ psi } (34.5 \text{ MN/m}^2) \text{ (tensile-compression)}$$

$$\tau_{xy} = 25,000 \text{ psi } (172 \text{ MN/m}^2) \text{ (in-plane shear)}$$

The resulting fracture indicators as obtained from the summation of terms in equation (18) for the Vessel 2, 4, and 5 skirts at failure are as follows:

Vessel	Term Summation Equation (18)
2	+1.1
4	+1.3
5	+1.0

Equation (18) and the three established material strength values will be applied to subsequent vessels based on the results of the discontinuity analysis.

2. The strain data from the Vessel 4 and 5 tests indicated that additional tape reinforcements were required in the aft dome to compensate for the loss in hoop stiffness as a function of increasing pressure. Extrapolating the data, it appears that a 10 percent increase in the dome shell composite hoop stiffness (Et) around the polar boss would be required on subsequent designs to insure the structural integrity of the aft dome at pressures up to 5,000 psig (34.5 MN/m^{2}g). To achieve this condition, the theoretical elastic properties of the glass-epoxy composite would be reduced accordingly.

TABLE X

MAXIMUM STRESSES IN THE SKIRT LONGITUDINAL WRAP
IN THE PLANE OF THE FILAMENT

	σ_x		σ_y		τ_{xy}	
Vessel	(psi)	(MN/m^2)	(psi)	(MN/m^2)	(psi)	(MN/m^2)
2	-66, 000	(-455)	+1, 100	(7.58)	+12, 200	(84.12)
4	-72, 000	(-495)	-670	(-4.62)	+12, 900	(88.95)
5	-64, 000	(-441)	-140	(-0.965)	+11, 600	(79.98)

Vessel 6. - The configuration of Vessel 6 was similar to that of Vessel 5 in that it had the same port sizes and L/D ratio. However, Vessel 6 had both ports capped off and had no skirt. The primary area of interest was the reinforced aft dome that had an 82 percent dome opening. In order to accommodate the quantity of tapes required to react the hoop loading, Vessel 6 had an additional layer of polar wrap so that there would be sufficient shear area to transfer the meridional loads between the polar and tape layers.

Vessel 6 was supported in chocks and tested in the horizontal position. Failure occurred during the proof cycle at a pressure of 3,850 psig (26.54 MN/m^2g) as a result of a polar wrap failure near the aft tangent plane as shown in Figure 40. The polar boss and closure were completely expelled from the case.

The hoop and meridional strains in the aft dome are shown in Figures 41 and 42, respectively. The strain data indicated that there was a large discontinuity in the area of failure. The resulting high bending moments overstressed the inner layers of the polar wrap, causing the premature failure. The termination of the tape layers and the local bearing pressure of the polar boss probably influenced the failure in this area. Failure in the tape reinforcements in the hoop direction was a result of the aft boss and closure being expelled from the vessel.

The results from the Vessel 6 test indicated that the rate of change in the meridional slope of the dome was too severe, as indicated by the low hoop strains and high discontinuity bending moments.

Vessel 7. - Vessel 7 was the only polar wound vessel with standard winding in forward and aft polar bosses. The vessel had an L/D ratio of 2 with a forward dome contour and a skirt attachment configuration identical to that of Vessel 3. The two areas of interest were the integrity of the skirt structure and the potential roving slippage problems which might occur during the application of the polar wrap. Since the NBR bladder was working so well, the $\pm$ 13 deg (0.2269 rad) polar laminate was wound without any hoop interspersement.

Winding the polar wrap around 30 and 56 percent polar openings of a vessel with an L/D ratio of 2 presented no roving slippage problems during winding or cure.

The vessel went through proof and failed at a pressure of 5,960 psig (41.093 MN/m^2g) during the burst cycle. Failure was due to a clean burst in the hoop overwrap at the center of the cylindrical section of the vessel as shown in Figure 43. The aft boss and a local section of the skirt were fractured as a result of failure. However, the skirt appeared uniformly crazed as if failure might have been pending. The cylindrical ring of fiberglass shown in Figure 43 around the piston housing was a section of the hoop overwrap that was expelled during burst.

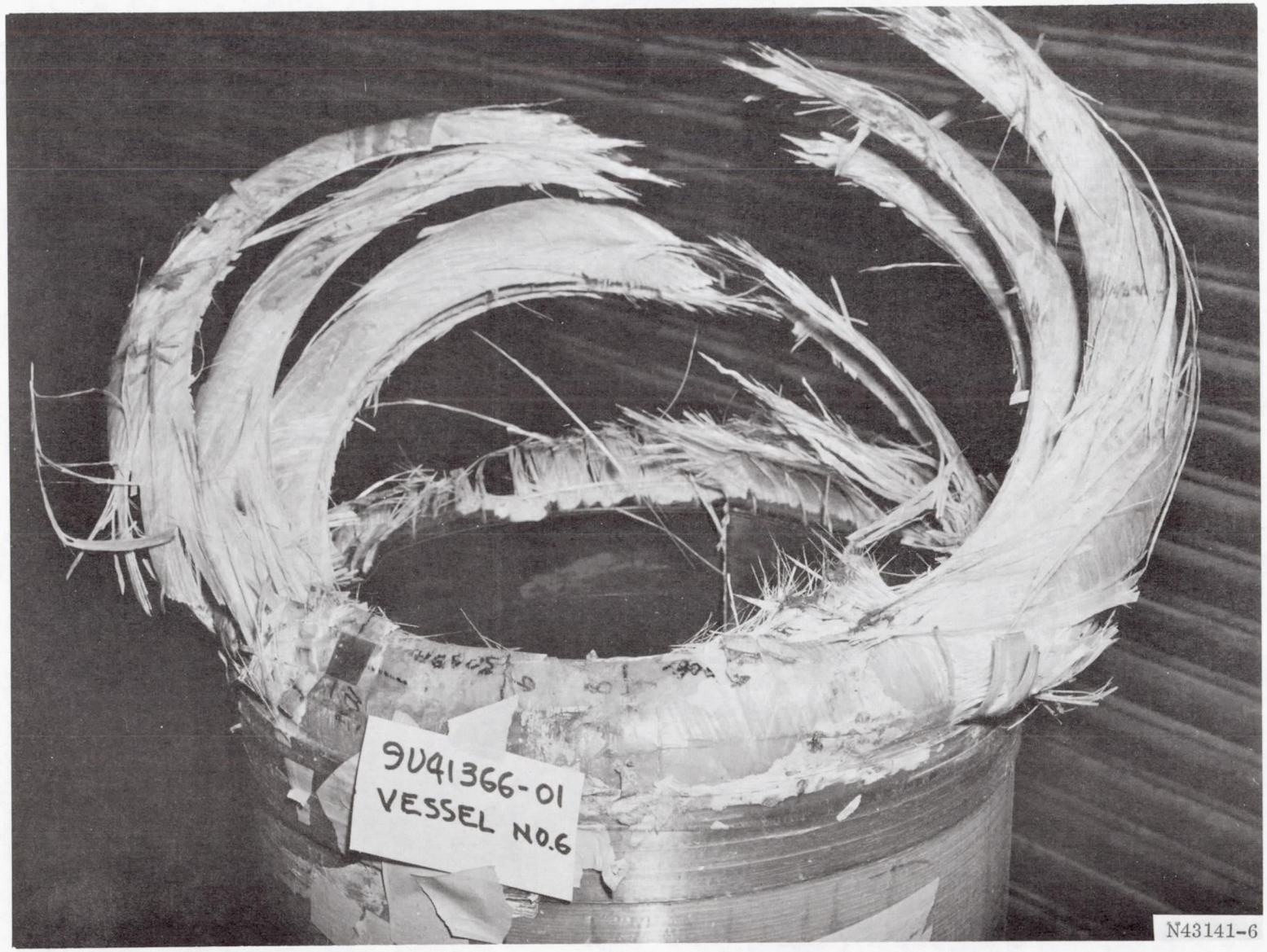

Figure 40. Vessel 6 Aft Dome After Failure

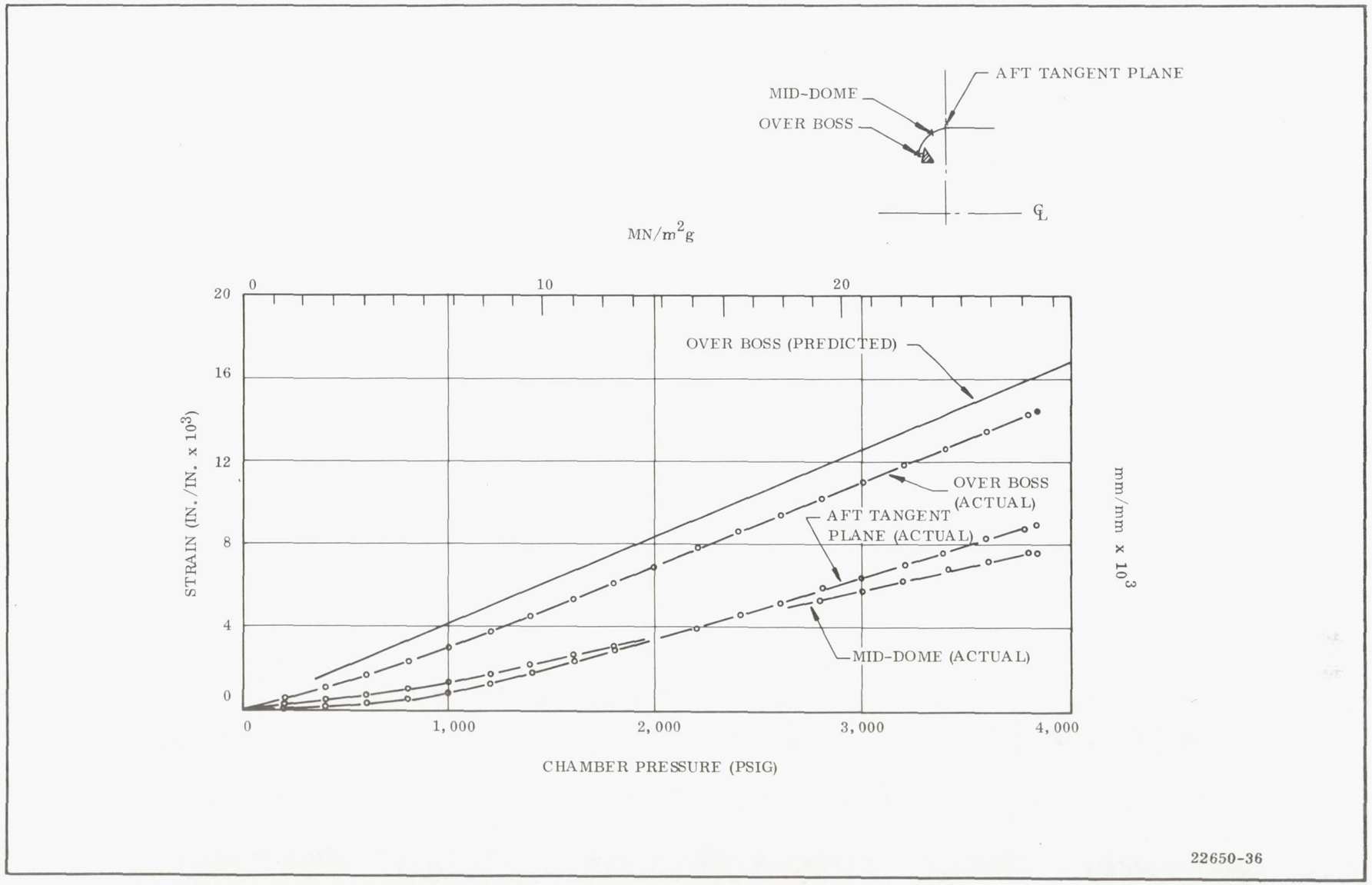

Figure 41. Vessel 6 Hoop Strain in Aft Dome

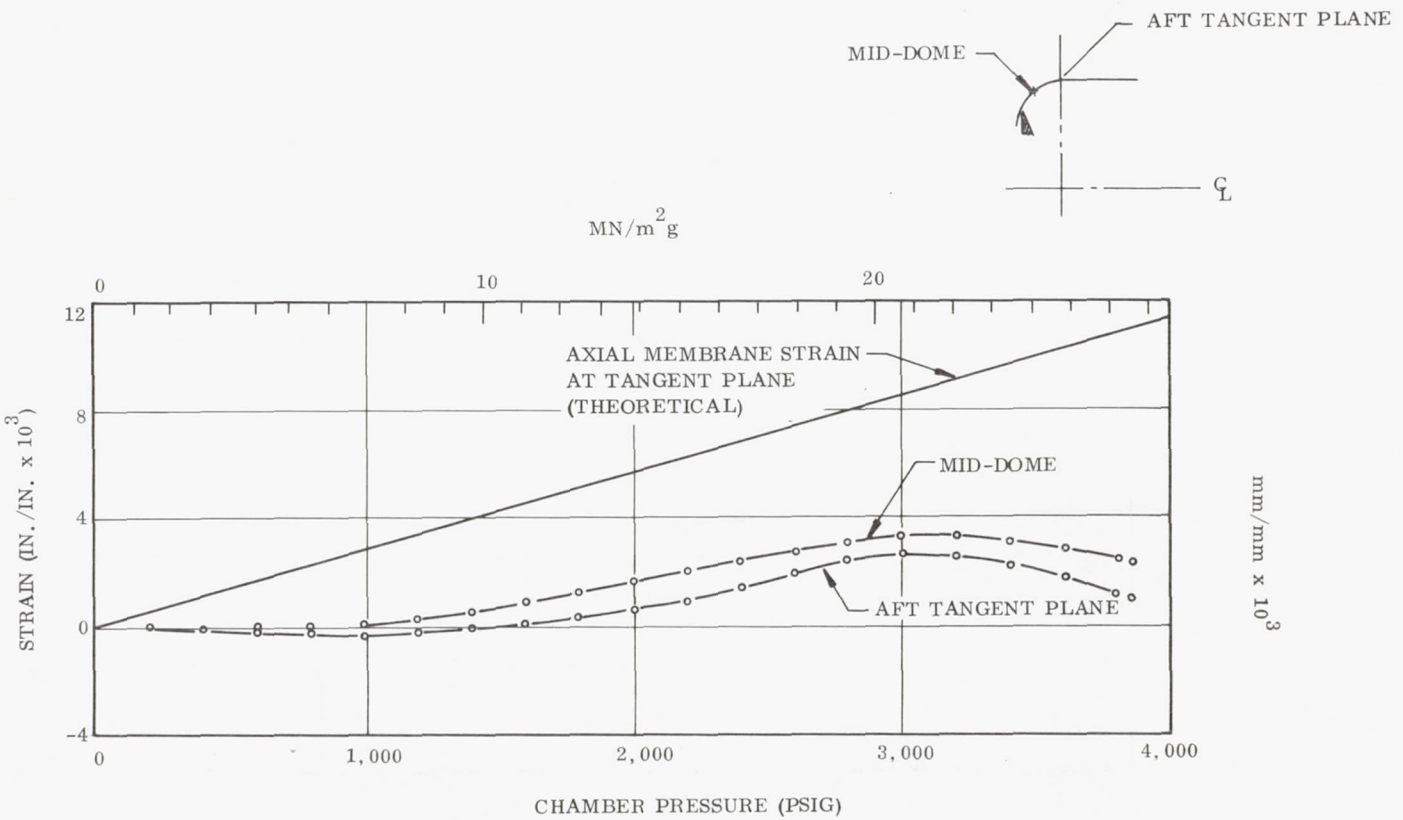

Figure 42. Vessel 6 Meridional Strain in Aft Dome

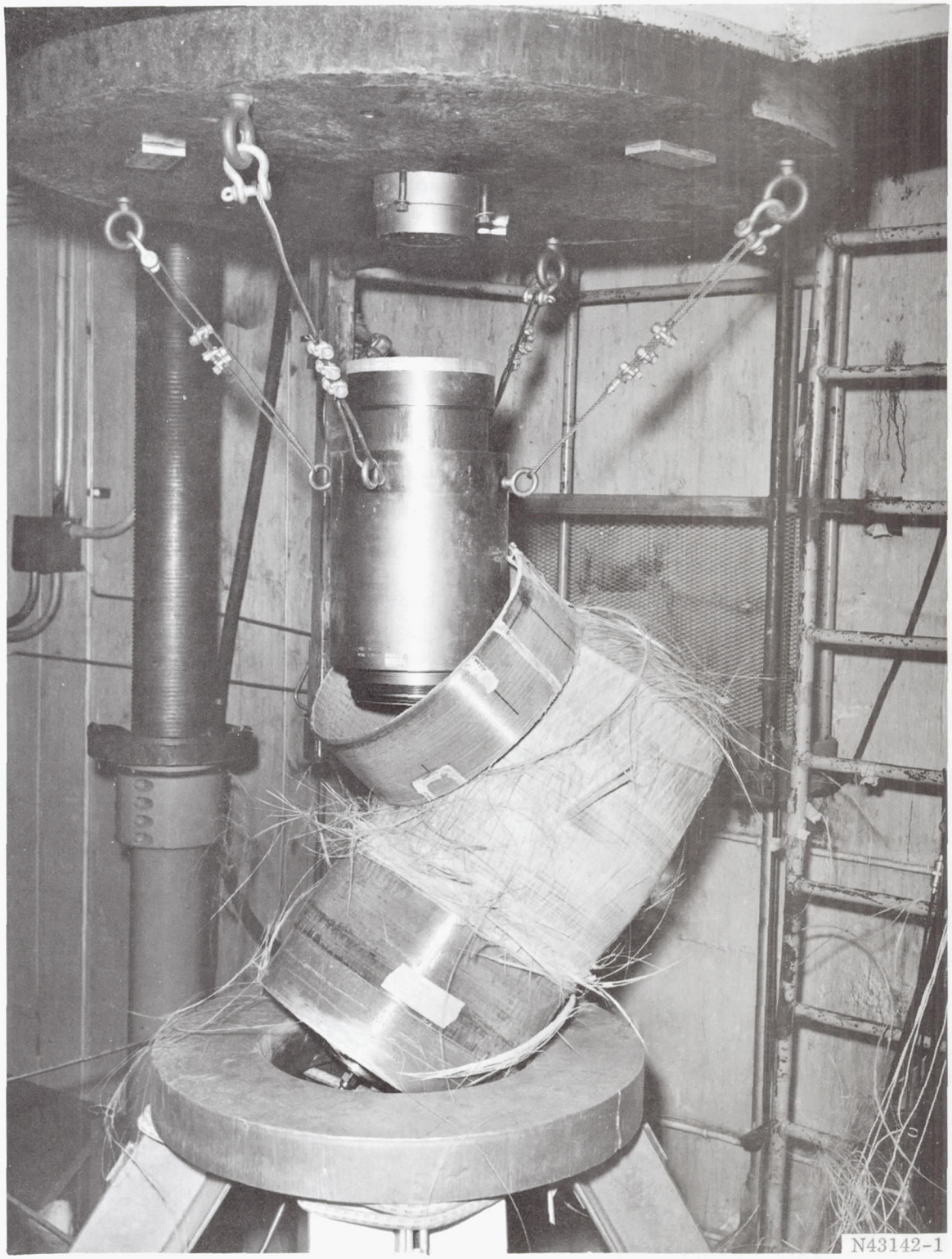

Figure 43. Vessel 7 After Hydrotest

The actual and predicted hoop strain data in the area of failure are shown in Figure 44. The data are shown from the proof cycle only because of a strain gage failure and the absence of the extensometer during the burst cycle. At failure, the calculated filament stress in the hoop wrap was 380, 000 psi (2.62 GN/m^2).

The theoretical axial and hoop stress in the skirt at burst gave a fracture indication value of 1.1 as obtained from equation (18). The appearance of the skirt after failure indicated pending failure.

The results from the Vessel 7 test indicated:

1. The hoop filament strength was in accordance with previous test data as shown in Figure 1.

2. The NBR bladder continued to work extremely well.

3. The skirt behavior indicated that the material fracture criteria as established by equation (18) is conservative, yet very adequate for design purposes.

Vessel 8. - During the course of the program, the design of Vessel 8 was revised to duplicate the configuration of Vessel 5 with the skirt redesigned to the new fracture criterion of equation (18). The theoretical thickness of the skirt was increased from 0.31 in. (7.9 mm) to 0.54 in. (13.7 mm), which was a little conservative, but demonstration of the skirt attachment area at the higher loadings was considered mandatory. The winding sequence for the skirt structure was also revised to give a greater concentration of longitudinal layers at the inner and outer surfaces of the skirt. However, the total quantity of each was still maintained at 50 percent by volume. The objective was to increase the axial bending stiffness and strength without degrading the hoop extensional stiffness. The aft dome structure was also strengthened, in accordance with the test data from Vessel 5, by the addition of another tape and polar layer. With the exception of the skirt and aft dome areas, Vessel 8 was identical to Vessel 5 as shown in Figure 45.

Vessel 8 was taken through a complete proof cycle and then pressurized to 6, 150 psig (42.40 MN/m^2g). At this pressure the test was terminated due to safety requirements on the pumping system. An inspection immediately after the test revealed only minor crazing in the aft dome. However, an axial cut through the vessel, shown in Figure 46, revealed that the interface between the hoop and polar wraps aft of the filler ply was fractured, thus indicating that the filler ply transferred all of the load from the overwrap into the polar-hoop laminate.

The axial strain data in the skirt overwrap 10 in. (254 mm) aft of the leading edge of the overwrap and at the center of the filler ply is shown in Figure 47. The data show that there was no abrupt change in strain behavior as a result of the fracture at the interface.

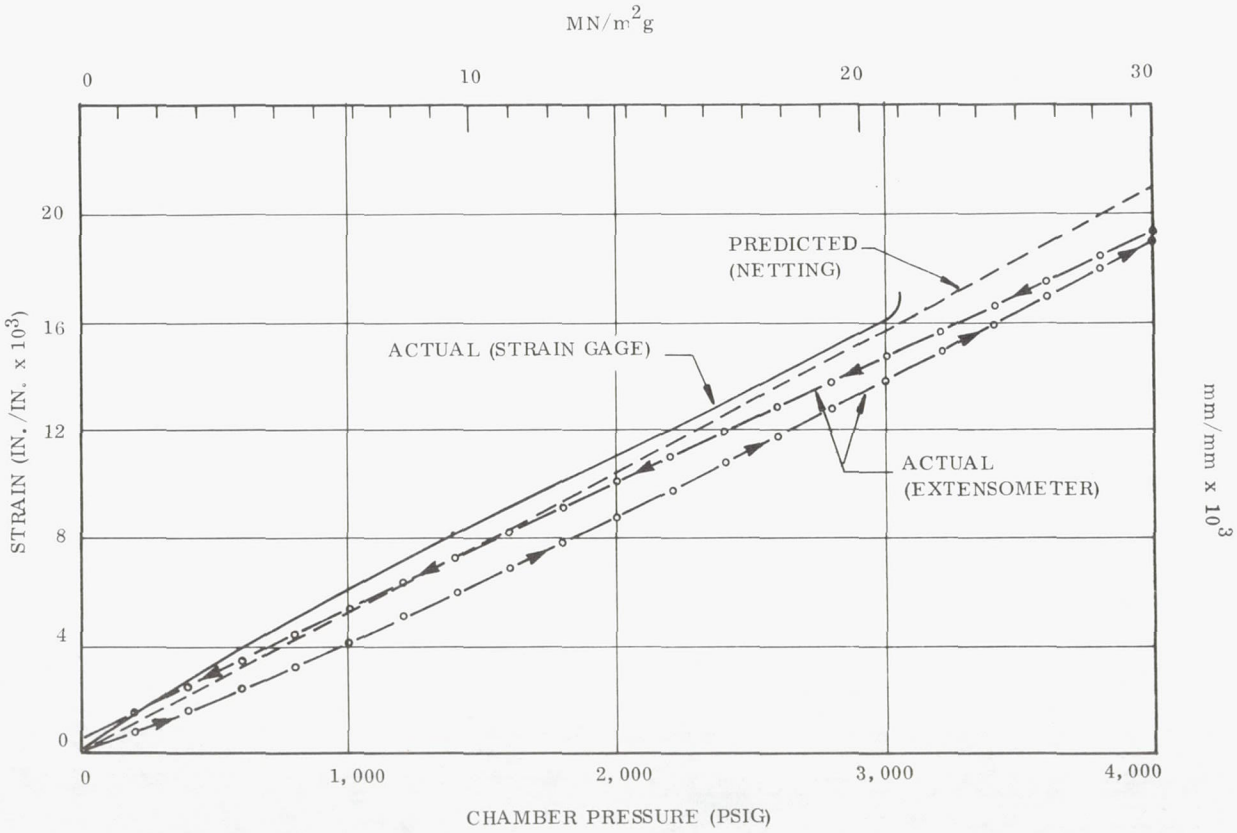

Figure 44. Vessel 7 Hoop Strain at Midcylinder (Proof Cycle)

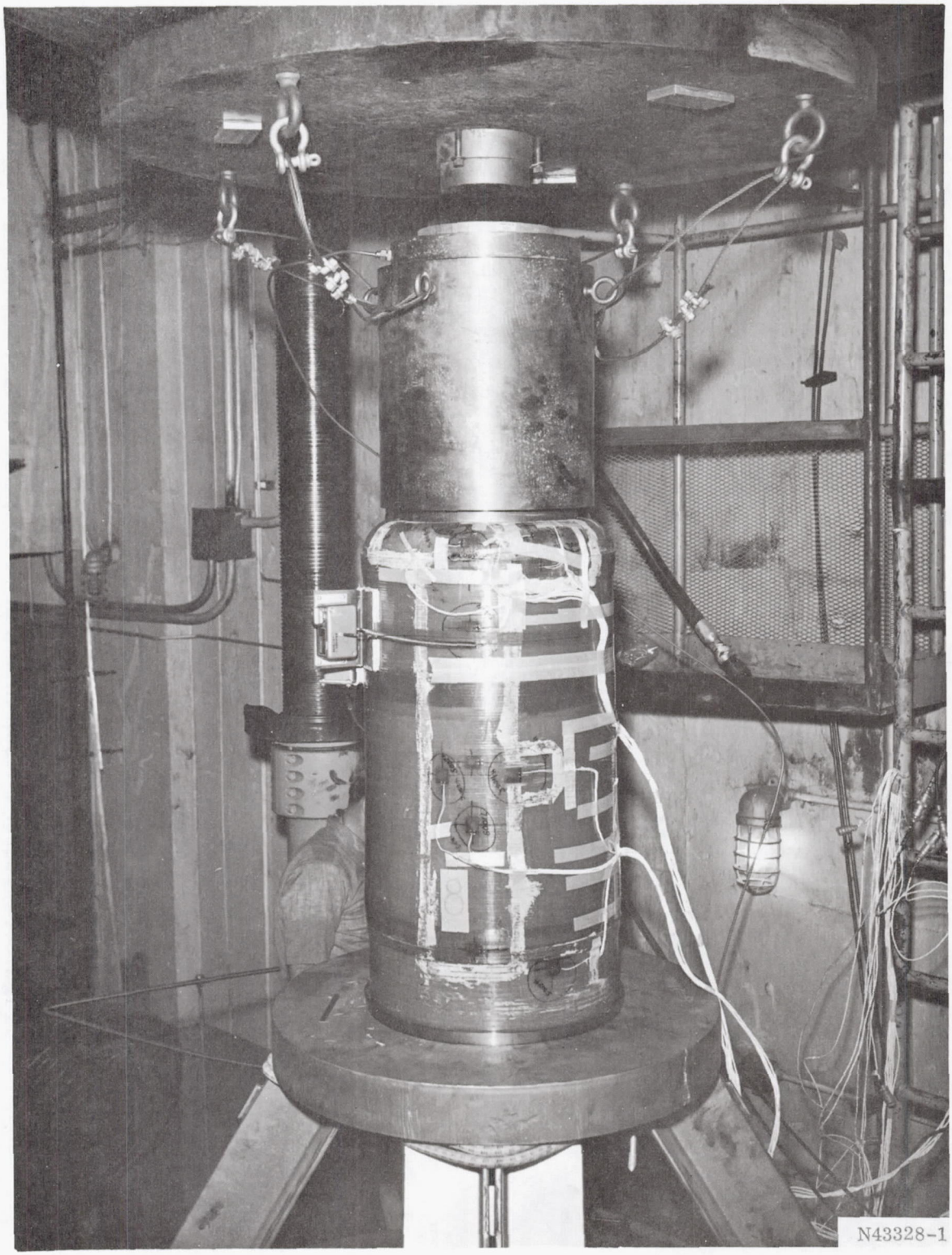

Figure 45. Vessel 8 Installed in Test Bay Prior to Hydrotest

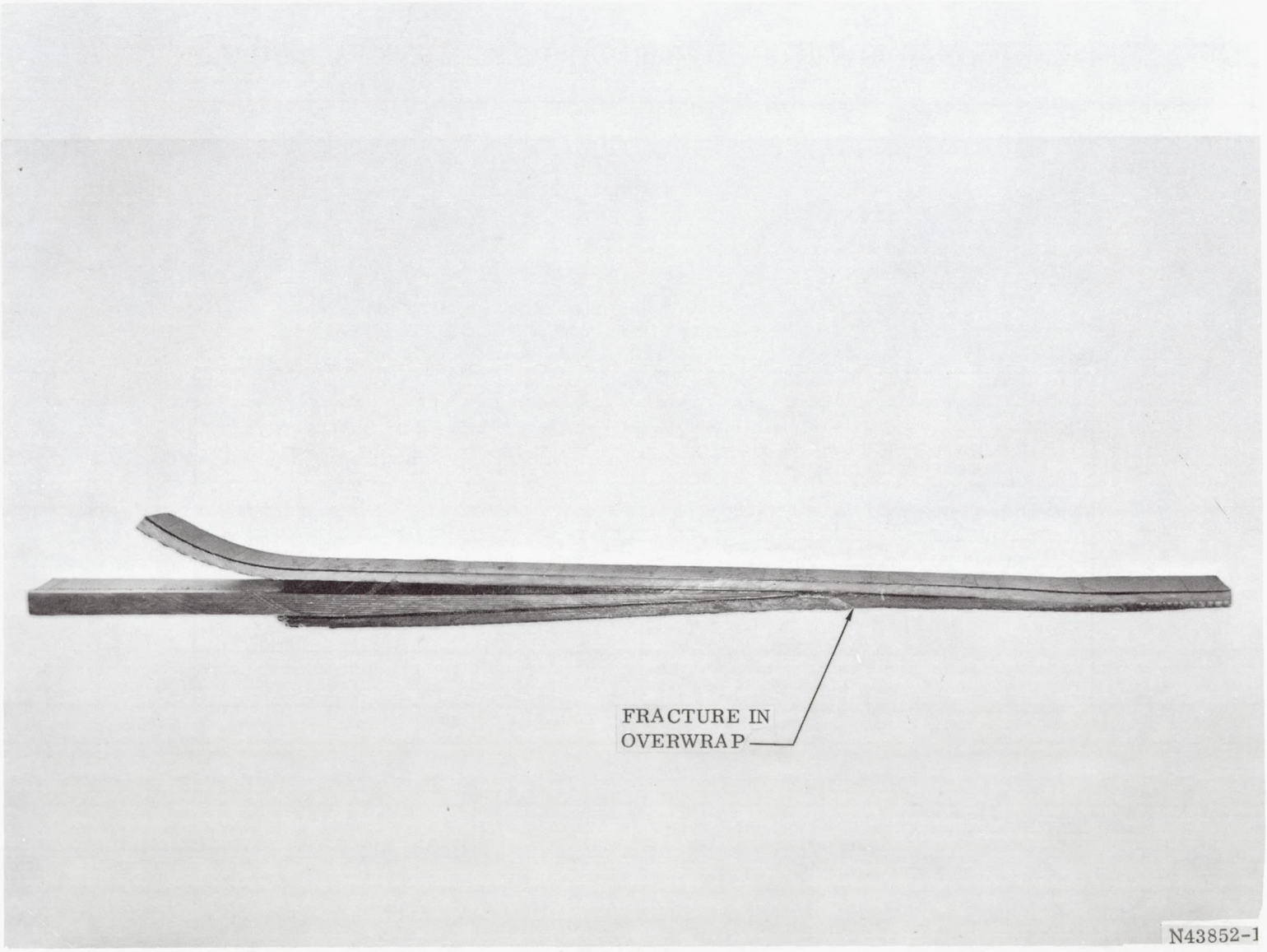

Figure 46. Axial Cross Section of Vessel 8 Wall

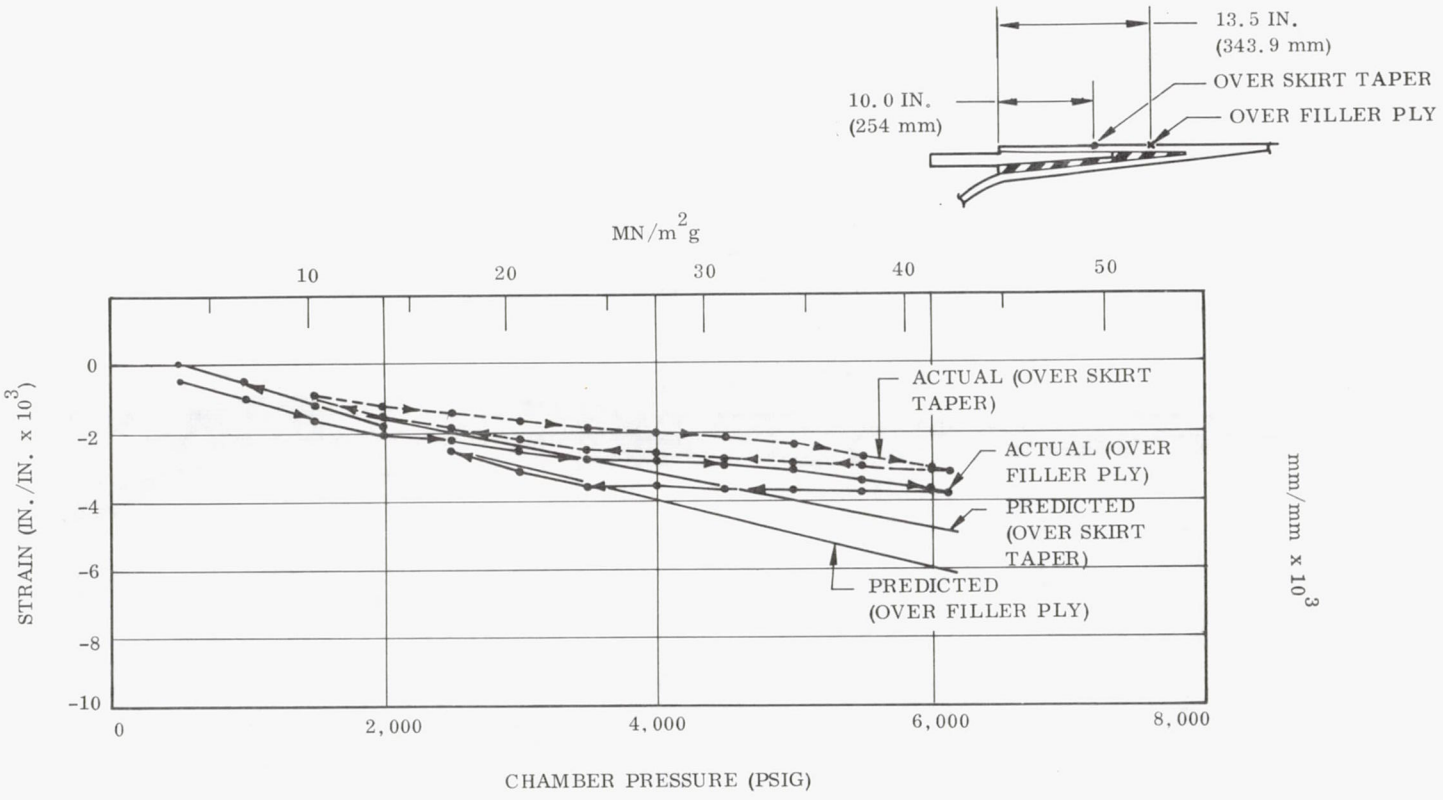

Figure 47. Vessel 8 Axial Strain in Skirt Overwrap Structure (Burst Cycle)

The hoop and axial strains in the aft dome are shown in Figures 48 and 49, respectively. The axial strain data indicates that the bending moment in the shell appeared to be relieved to some extent by crazing in the dome structure. The hoop gage at the dome opening also reflected the crazing which appeared to start at a pressure of approximately 4, 300 psig (30 MN/m^2g).

At 6, 150 psig (42.40 MN/m^2g) the theoretical fracture indicator, as obtained from equation (18) was +3.0. The revised winding sequence was apparently responsible for increasing the fracture strength of the skirt and the margin of safety based on the strength estimations made after the Vessel 5 test.

The results from the Vessel 8 test were:

1. The skirt structure and skirt attachment area were still operational at a loading of 13, 500 lb/in. (2.36 MN/m).

2. The aft dome design was adequate, but the contour could have had a more gradual change in the meridional slope to minimize the meridional discontinuities and crazing.

Vessel 9. - Vessel 9 was helically wound with unequal dome openings and nongeodesic contours. The areas of interest were the slippage behavior of the roving during the application of the helical wrap, and the performance of the skirt structure under the maximum load condition. The skirt and skirt attachment designs were essentially identical to those of Vessel 8, with only the stiffness characteristics of the helical wrap being different.

During fabrication it was evident that there were no problems involved with winding over the nongeodesic domes. In fact the forward dome opening apparently could have been reduced another 20 percent without experiencing slippage problems. The rovings crossing the aft dome were not as stable as those on the forward dome and, therefore, it was estimated that the maximum safe deviation, 8 deg (0.14 rad) from geodesic, had been established.

The vessel successfully went through the proof cycle and was then burst at a pressure of 5, 620 psig (38.75 MN/m^2g). The failure occurred in the hoop wrap locally near the aft tangent plane as shown in Figure 50. The actual and theoretical hoop strains at midcylinder, shown plotted in Figure 51, indicate a hoop filament stress of 360, 000 psi (2.482 GN/m^2) at failure.

A post-test inspection of the vessel revealed a fracture in the skirt overwrap structure, 13 in. (330 mm) aft of the forward edge of the overwrap and running completely around the vessel. However, in spite of the fracture, the inner shear continued to carry the thrust load until burst occurred. The loading at burst was 12, 400 lb/in. (2.171 MN/m), which theoretically subjected the inner shear ply to a maximum shear stress of 1, 300 psi (8.96 MN/m^2) at the thin end.

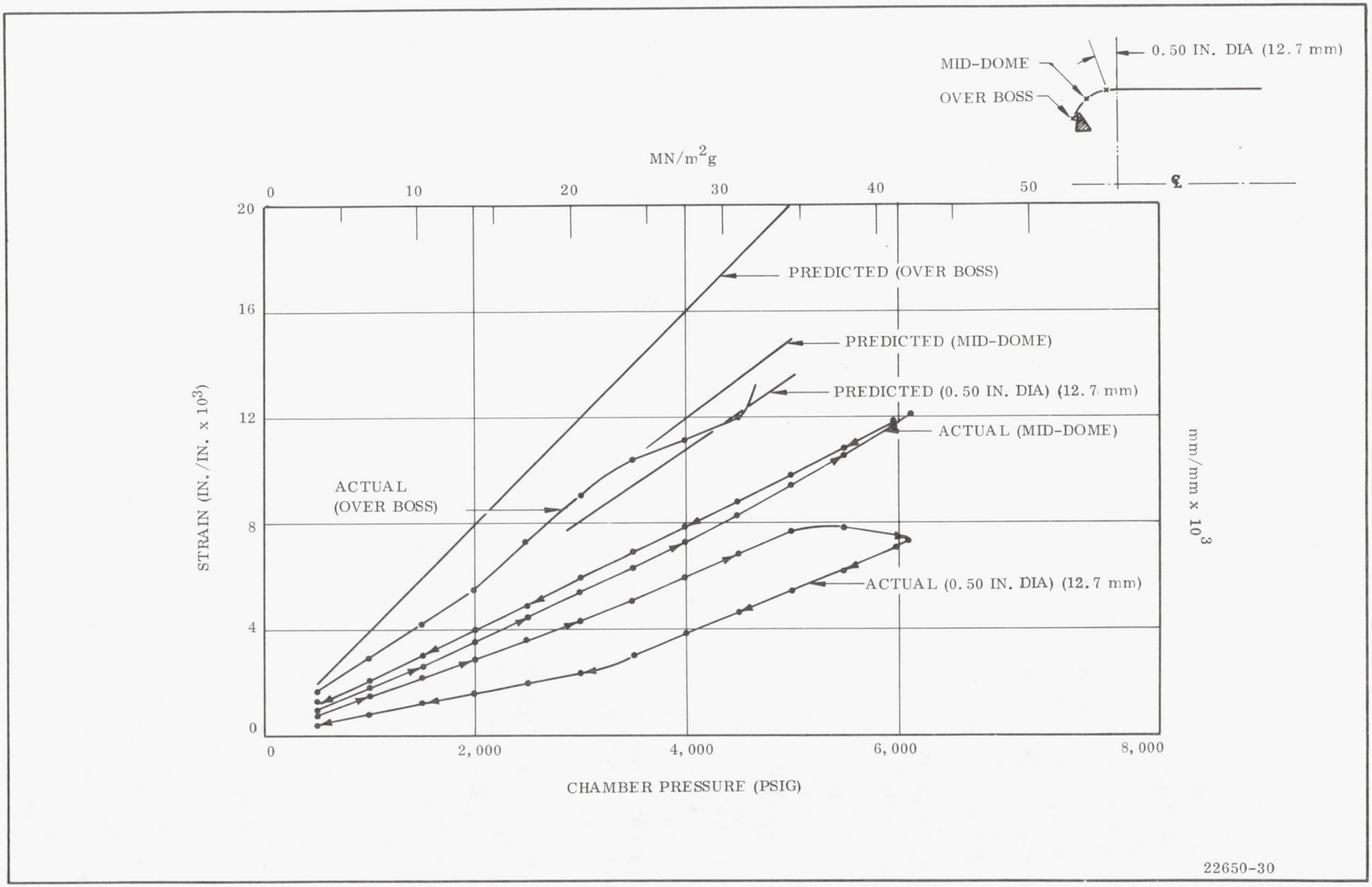

Figure 48. Vessel 8 Hoop Strain in Aft Dome (Burst Cycle)

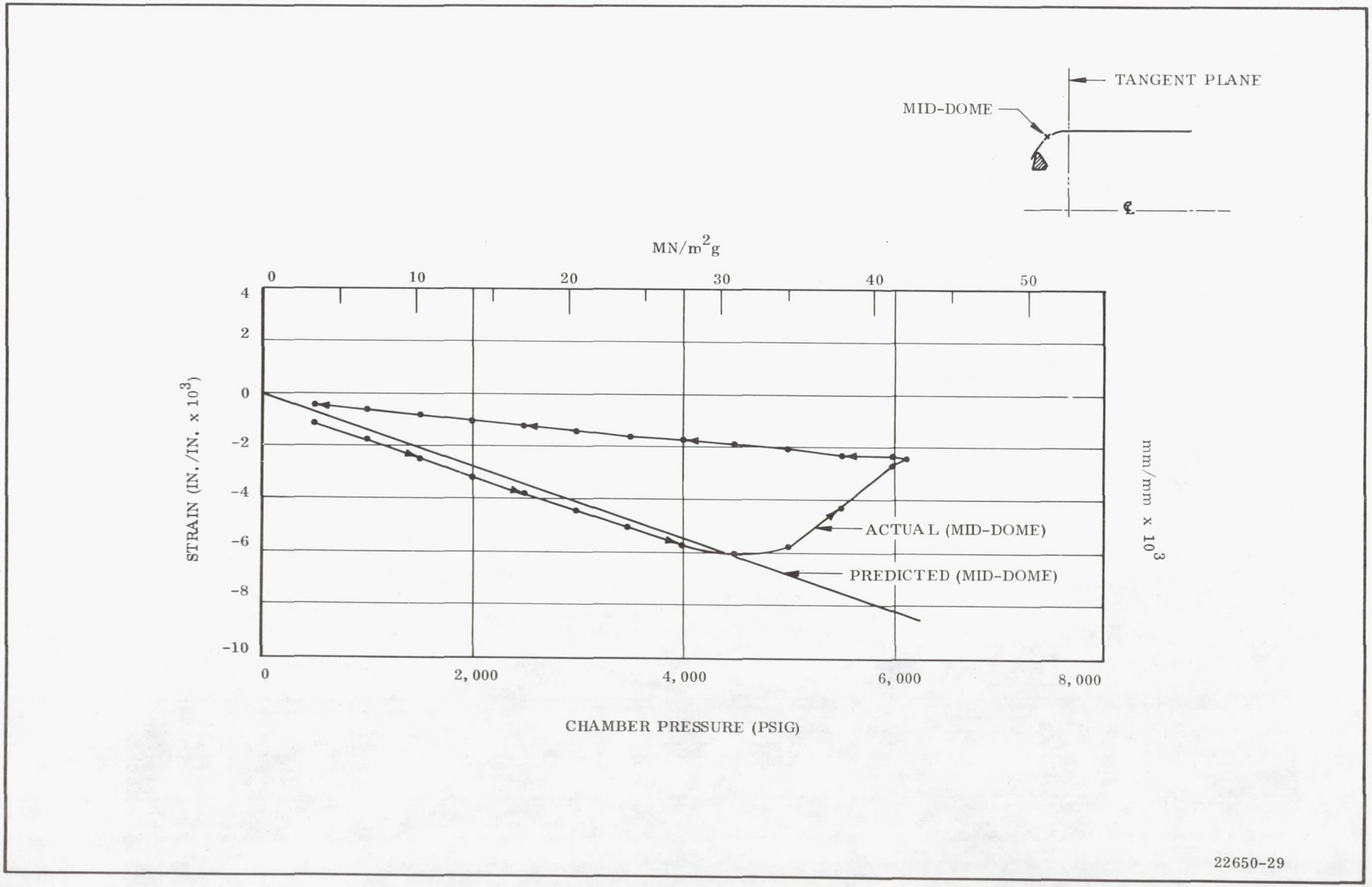

Figure 49. Vessel 8 Meridional Strain in Aft Dome (Burst Cycle)

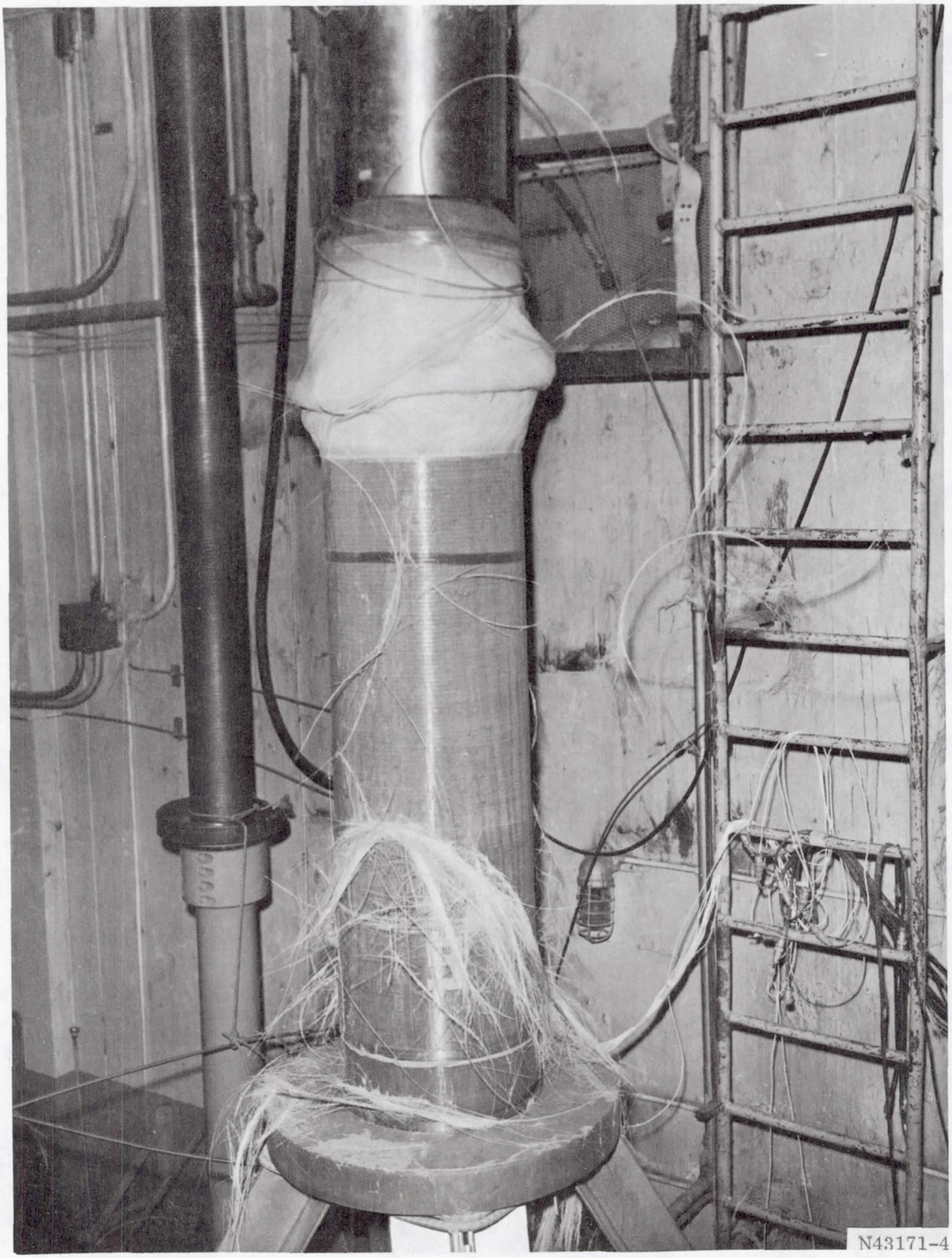

Figure 50. Vessel 9 After Hydrotest

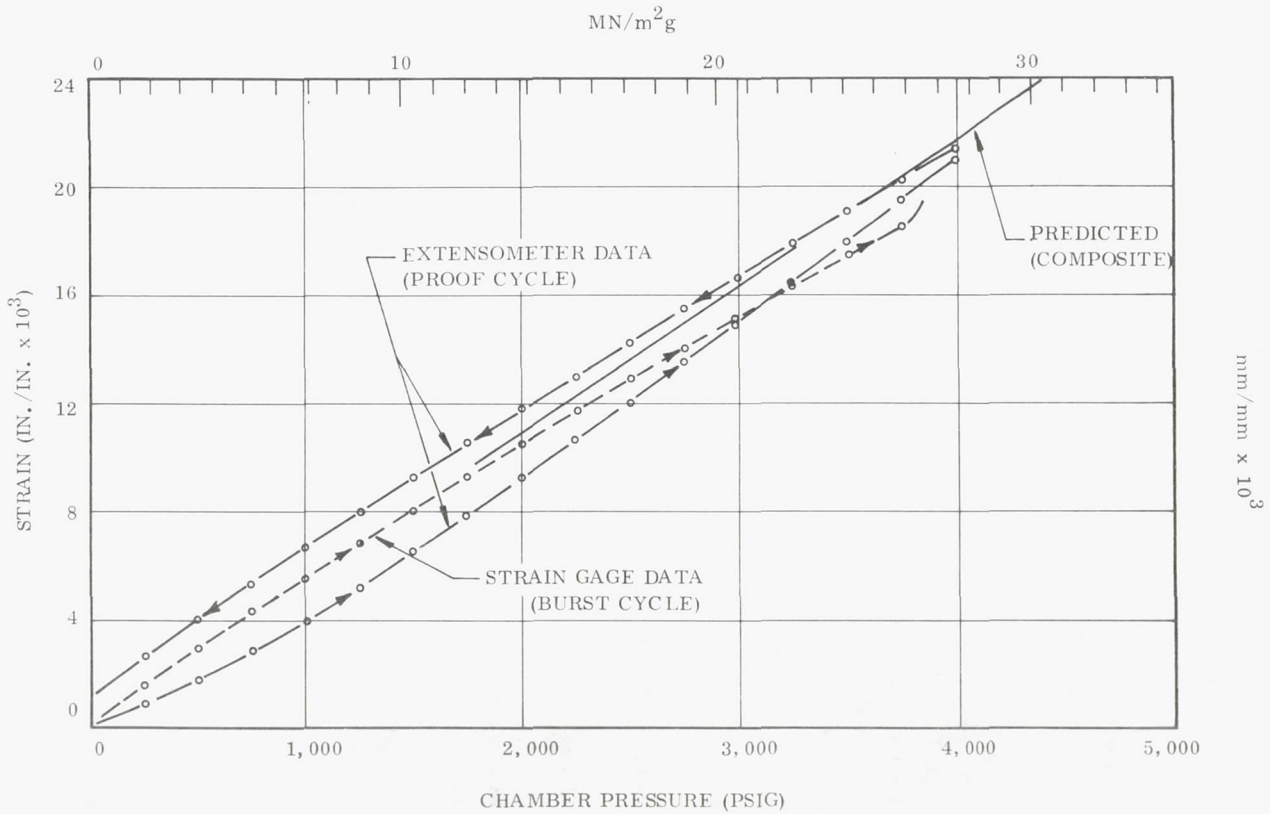

22650-40

Figure 51. Vessel 9 Hoop Strain at Midcylinder

The strain data shown plotted in Figure 52 indicated that the skirt overwrap fracture occurred during the burst cycle at approximately 4,750 psig (32.75 MN/m^2g) with the stress in the overwrap approximately 12,000 psi (82.7 MN/m^2). A cut through the cross section of this area, which is shown in Figure 53, revealed that the fabric in the laminate was severely wrinkled, and that it thus greatly degraded the axial compressive strength of the structure. The wrinkles were created as a result of the skirt slipping axially during the final stages of winding or during cure.

In order to evaluate the discontinuity analysis and the theoretical bending moments in the skirt, six hoop strain gages were placed in the immediate skirt-case junction area. The recorded and predicted displacements at burst in this area are shown in Figure 54. The predicted radial displacement values are greater than the actuals, but the change in the slope of the two deflection profiles were essentially the same. The rate of change in the slope governs the magnitude of the bending moments, and thus the data does indicate that bending loads from the discontinuity analysis are fairly valid. The theoretical fracture indicator as determined from equation (17) at failure was +1.02, which again indicates a margin of safety for the revised skirt design.

The fabrication and test of Vessel 9 demonstrated:

1. The feasibility of winding helical pattern nongeodesic dome contours and with a forward dome opening 30 percent smaller than the aft.

2. The necessity for rigid and secure fixturing to hold the skirt in place during final winding and cure.

3. The discontinuity analysis is adequate for determining the displacements and bending loads in the vessel shell structure.

4. The skirt design criteria is conservative, but will be used for all subsequent vessels to insure a full evaluation of other areas.

IR & D Vessel No. 4. - Near the conclusion of the design effort for the 18-in. vessels, the decision was made to terminate this task with an additional test supported strictly by Wasatch Division fundings. This additional effort was directed at a redesign of Vessel 4 to obtain more data pertaining to both the skirt and the cut dome designs.

IR & D No. 4 differed from Vessel 4 in that it had a skirt designed and wrapped in accordance with that established by Vessels 8 and 9 and an aft dome with additional tape reinforcements as indicated from the Vessel 4 and 5 tests.

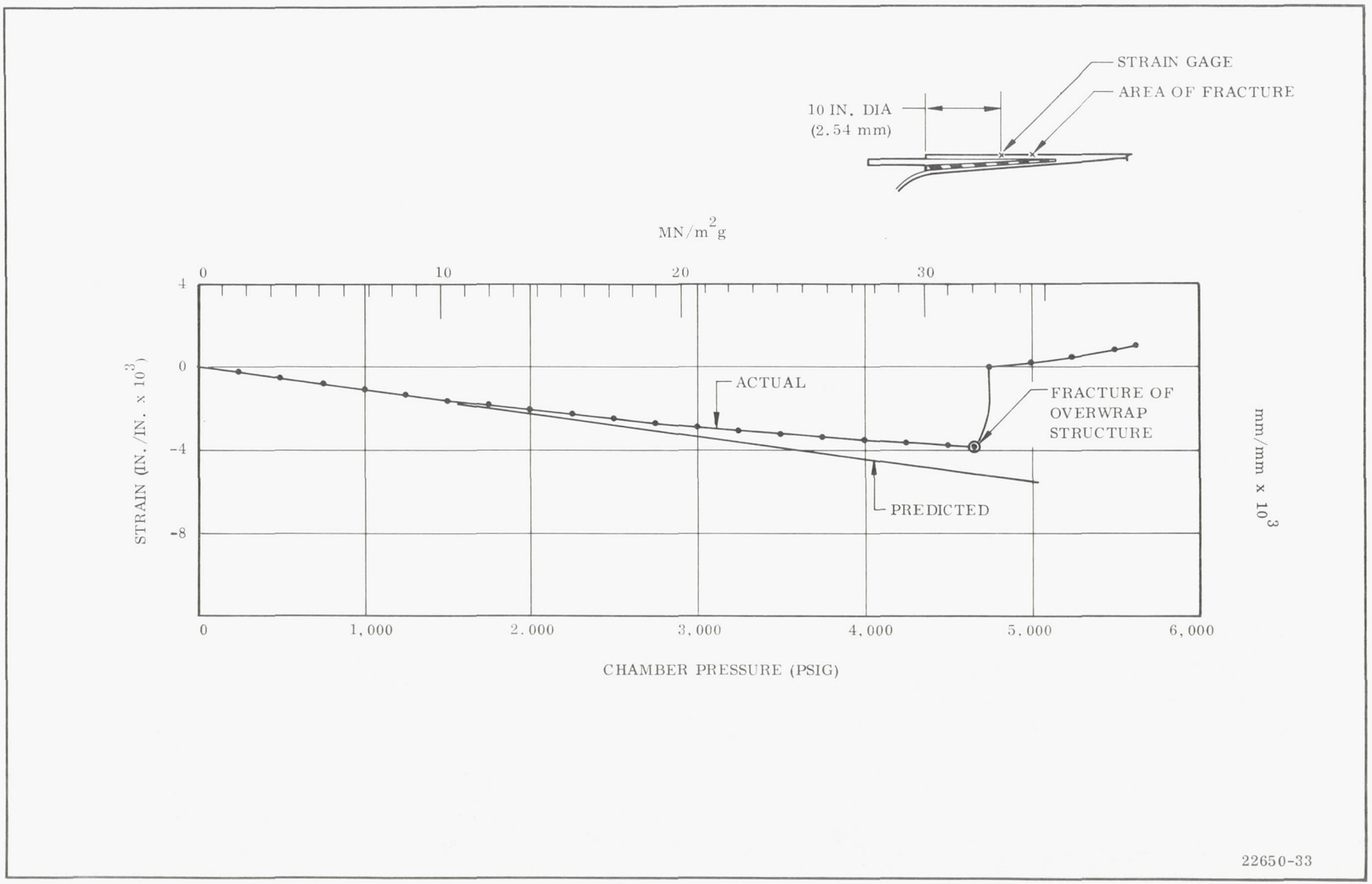

Figure 52. Vessel 9 Axial Strain in Skirt Overwrap

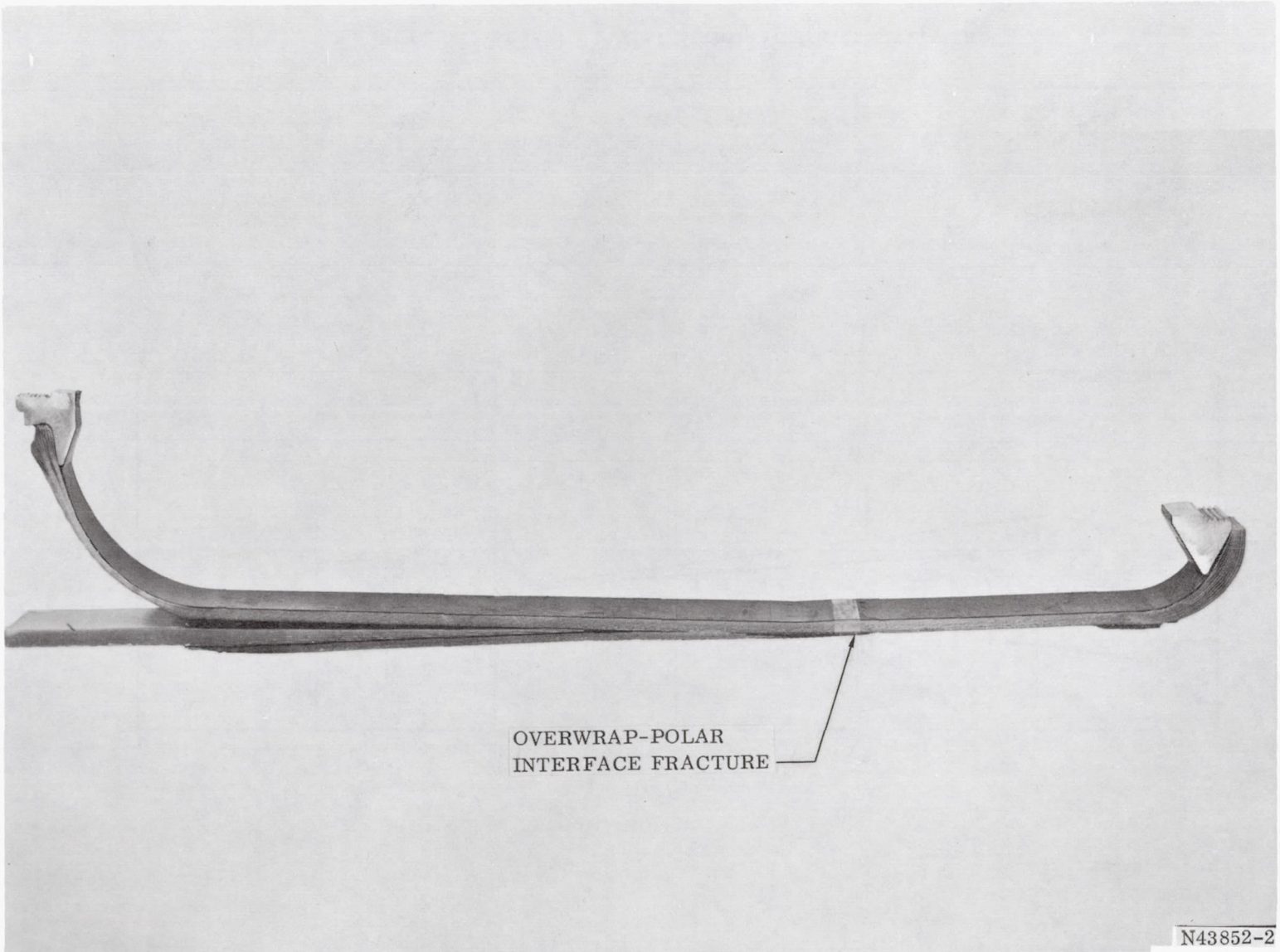

Figure 53. Cross Sectional Cut Through Skirt Attachment Area of Vessel 9

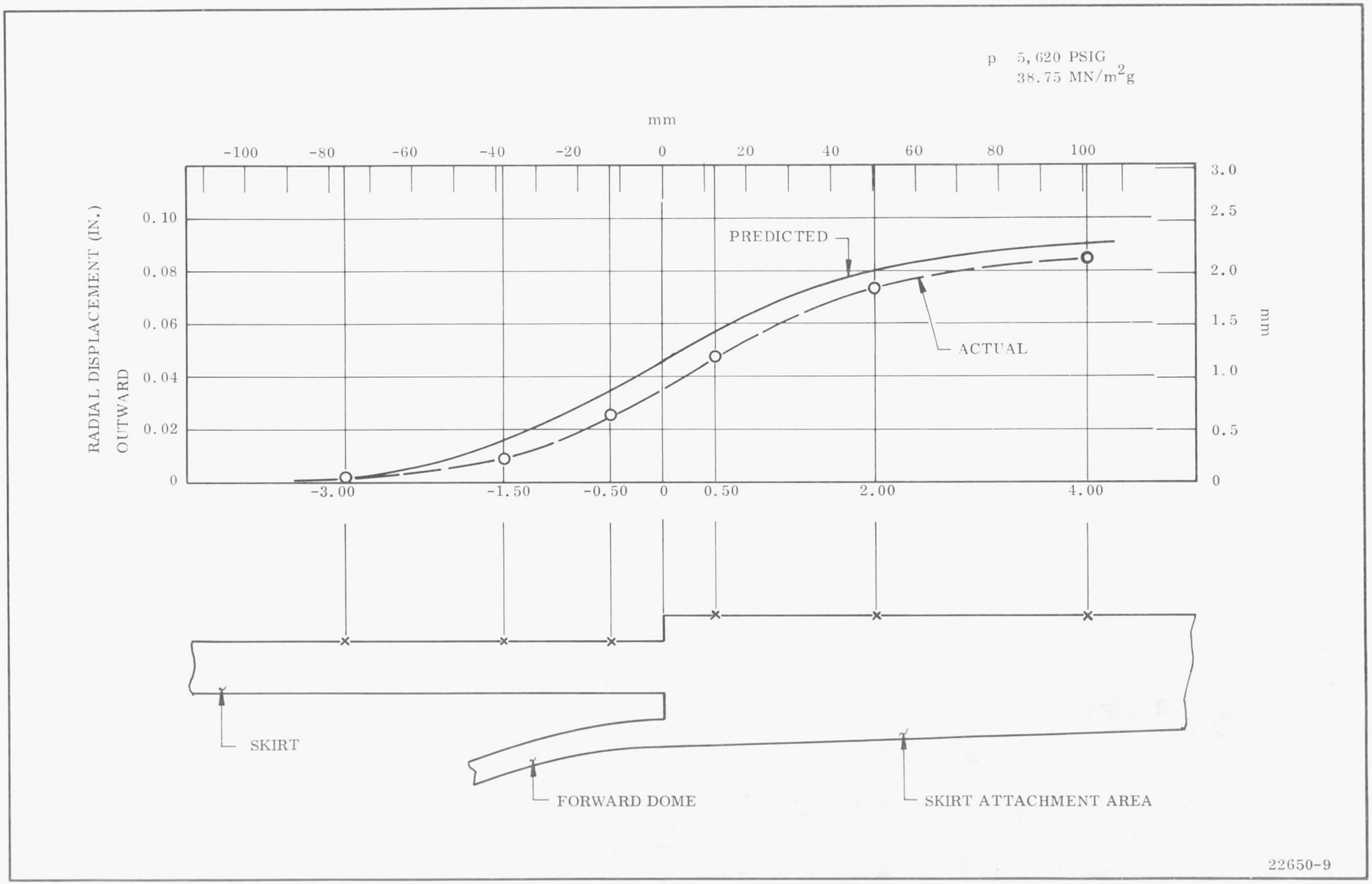

Figure 54. Vessel 9 Radial Deflections in Skirt Juncture Area

IR & D No. 4 successfully went through the proof test with no indications of structural problems. During the burst cycle this vessel went to 5,800 psig (39.99 NM/m^2g), where failure occurred in the hoop wrap at an apparent hoop filament stress of 380,000 psi (2.62 GN/m^2). The hoop laminate burst locally near the aft tangent plane as shown in Figure 55, with the aft dome and polar boss fracturing as a result of the burst. The skirt and forward dome area showed no sign of fracture or severe crazing.

The predicted and actual hoop strains in the cylindrical section near the aft tangent plane in the aft dome are shown in Figures 56 and 57 for both the proof and burst cycles. The material properties used for the glass-resin composite were adjusted to include the additional effects of crazing as indicated during the Vessel 4 and 5 tests. The change resulted in a predicted strain value of approximately 20 percent greater than actual in the area over the polar boss. However, this conservatism in the aft dome design was not considered detrimental to the efficiency of the vessel and should be included to compensate for potential fabrication discrepancies.

The theoretical fracture indicator for the skirt structure, as obtained from equation (17), was +1.2 at failure, which corresponds approximately to the values indicated for Vessels 8 and 9.

The results from the IR & D No. 4 test, along with those from Vessels 8 and 9, fully demonstrated the cut aft dome and high performance skirt designs. As a result of this test and the Vessel 8 test, the decision was made to propose the cut aft dome opening configuration in conjunction with the tape reinforcements and the in-plane wrapping pattern for the 260-in. case design.

Figure 55. IR & D Vessel No. 4 After Hydrotest

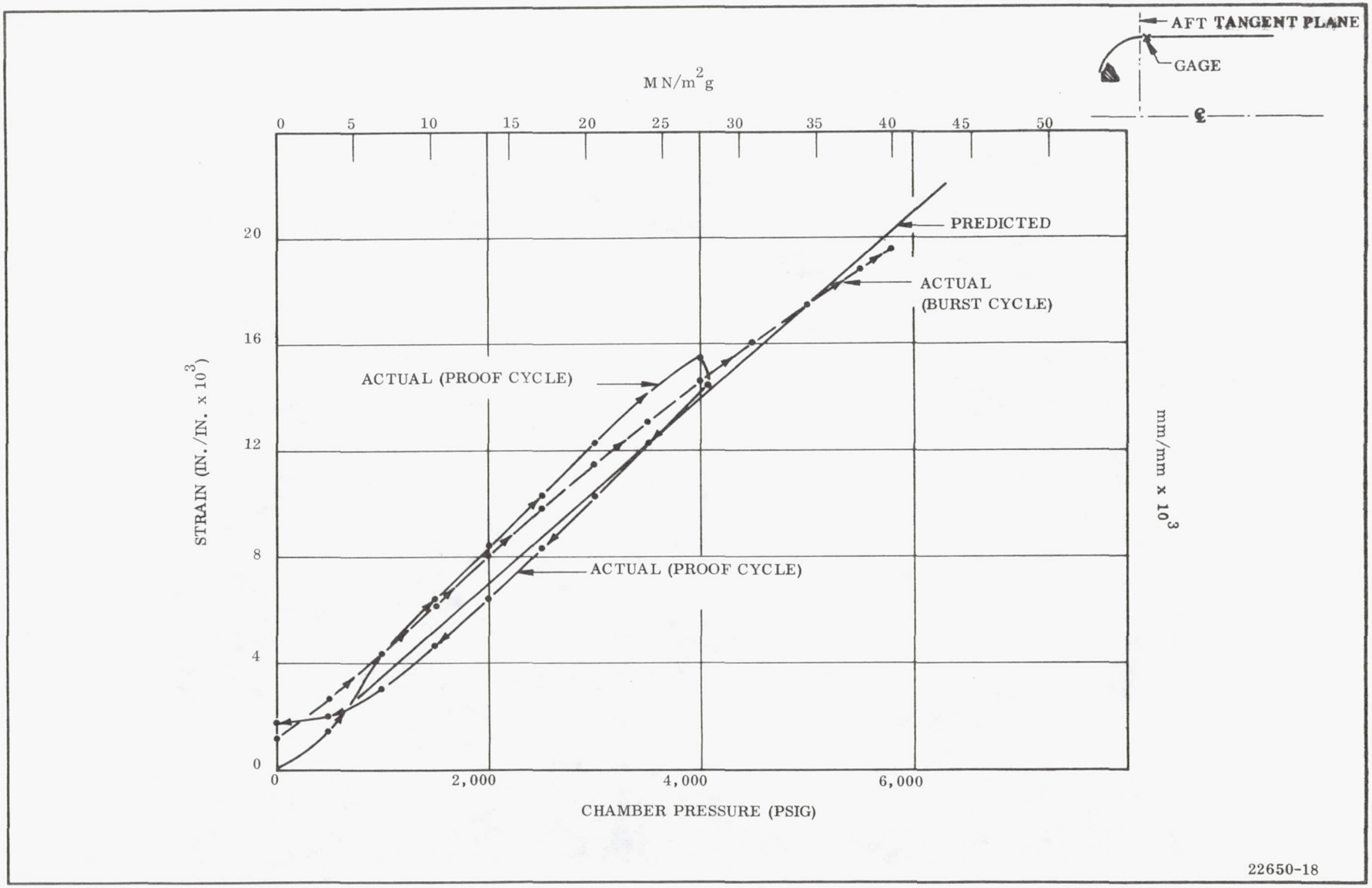

Figure 56. IR & D Vessel No. 4 Hoop Strain in Cylindrical Section at Aft Tangent Plane

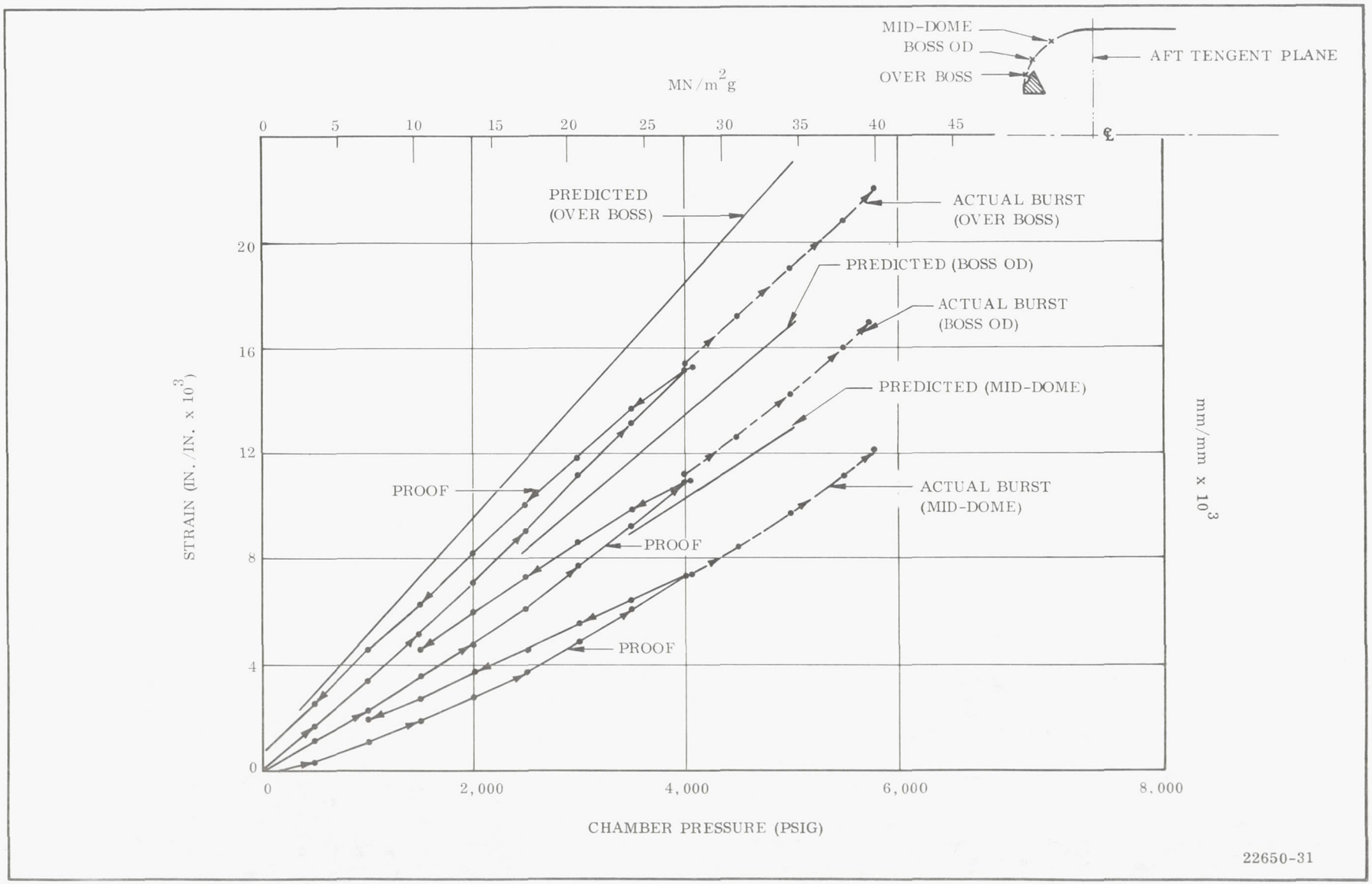

Figure 57. IR & D Vessel No.4 Hoop Strain in the Aft Dome

54-INCH DIAMETER VESSEL

From the results of the 18-in. (0.457 m) diameter vessel tests, it was evident that the polar wrap vessels with the reinforced aft domes were the most efficient designs with respect to volume, length, and weight. The efficiency of the helical vessels was limited by the size of the forward openings and by quantity of helical wrap as established by loads in the forward dome. Fabrication time of the polar wrapped vessels was a little more lengthy due to the handling of the reinforcement tapes, but this extra processing time did not outweigh the inherent advantages of the planar pattern.

Since it was evident that neither type had a distinct cost advantage, the polar wrap/tape reinforcement design was selected for the 260-in. (6.6 m) motor case because of its structural efficiency. The 54-in. (1.372 m) diameter subscale of the 260-in. motor case was designed to meet the following requirements:

1. The port in the aft boss would be 70 percent of the basic case cylindrical section.

2. The total vessel length would be three times the cylindrical diameter.

3. The forward skirt compressive load would be 15,000 pounds per inch of circumference (2.6 MN/m) at an internal pressure of 5,000 psig (34.5 MN/m^2g).

The overall vessel design parameters would be based on the data obtained from the 18-in. diameter vessels.

The 54-in. diameter subscale had an outside diameter of 55.1 in. (1,400 mm) and a boss face to face length of 160 in. (4.064 m). The forward and aft polar boss ports were 12.0 and 37.1 in. (305 and 942 mm), respectively. The forward boss was designed to be completely closured off while the aft was to be adapted to a hydrotest thrust simulation fixture with a 25.6-in. (650 mm) diameter piston. In the same manner as the 18-in. vessels, the 54-in. subscale had only a forward skirt. The final design configuration (Drawing 7U42115) is shown in Appendix A and the details of the design approach, the method of fabrication, and the test results are covered in the following sections.

Design

The 54-in. diameter vessel was of an interspersed polar hoop wrap design with a symmetrical polar pattern and a tape reinforced aft dome. The polar wrap

had a ±6 deg (0.10 rad) planar angle and consisted of 27 layers (54 ply) with each ply having 203 ends per in. (7,992 ends/m). The hoop wrap consisted of 105 plies with 200 ends per in. (7,874 ends/m) in each interspersed between the polar layers. The forward polar boss was wound in place, while the aft was submerged below the dome contour to be compatible with the symmetrical polar pattern. The aft dome structure consisted of 26 laminates of tangential tape layers and the 27 layers of polar wrap. The polar layers were tangent to a diameter 28 percent of that of the basic cylinder, while the tapes were tangent to a 76 percent diameter. The skirt, which was prefabricated and then installed during case winding, consisted of 34 layers of polar wrap oriented ±11 deg (0.19 rad) and 74 plies of hoop wrap interspersed between the polar layers in a sequence established after the testing of Vessels 8 and 9. The skirt was connected to the case by an inner and outer NBR shear ply. The inner ply was fabricated integrally with the skirt structure, while the outer ply was installed "green" after skirt installation and cured with the case.

All of these basic areas on the 54-in. subscale were evaluated during the 18-in. diameter vessel effort including the establishment of the respective methods of analysis and the design criteria. The structural analysis, as applied to the various areas of this vessel, is based on an ultimate design pressure of 5,000 psig (34.5 MN/m^2g).

Cylindrical section. - The structure of the cylindrical section was made up of interspersed polar and hoop wrap where the polar wrap was critical at the two tangent planes and the hoop wrap at midcylinder. The design filament strength level was established at 330,000 psi (2.28 GN/m^2) which was estimated from the data shown in Figure 1 and from the hydrostatic burst of the 156-in. (3.96 m) diameter AF 156-7 motor case.[a] The AF 156-7 case burst at a hoop filament stress of 330,000 psi (2.28 GN/m^2), but the burst data were not entered on Figure 1 because of possible structural degradation due to the effects of local heating after the static firing. However, this value was still used despite possible size effects.

The inplane wrap angle was established from the two polar wrap openings on each dome and the total length of the vessel. The resulting wrap angle ($\bar{\alpha}$) as obtained from equation (12) was:

$$\bar{\alpha} = \tan^{-1}\left[\frac{R_{EA}+R_{EF}}{L_{ToT}}\right] \tag{12}$$

$$= \tan^{-1}\left[\frac{8.0+8.0}{160}\right]$$

$$= 5 \text{ deg } 43 \text{ min}, \ 0.0995 \text{ rad } (6 \text{ deg } 00 \text{ min}, \ 0.105 \text{ rad, machine setting})$$

[a] Air Force Contract AF 04(695)-773

The stresses in the hoop and polar filaments in the cylindrical structure were determined from the "netting" approach which proved to be adequate for filament orientations of less than 20 deg (1.43 rad) relative to either of the two principal axes. The predicted membrane filament stresses at the forward tangent plane and at midcylinder, as obtained from equation (1), are tabulated below based on the parameters shown.

	N_φ		$t_{\alpha g}$		α		$\sigma_{g\alpha}$	
Location	(lb/in.)	(MN/m)	(in.)	(mm)	(deg)	(rad)	(psi)	(MN/m^2)
Forward Tangent Plane	66,200	11.6	0.239	6.07	7	0.123	277,000	1,910
Midcylinder	54,400	9.5	0.228	5.79	6	0.105	242,000	1,670

The maximum stress in the polar wrap at the forward and aft tangent planes must also include the effects of the discontinuity bending moments which are shown in the following sections pertaining to the forward and aft domes.

The maximum stress in the hoop wrap will be at center of the cylindrical section away from the end restraints of the two domes. Again, the "netting" technique was found to be sufficient and the maximum hoop filament stress as obtained from equation (2) is as follows:

	N_θ		$t_{\theta g}$		$\sigma_{g\theta}$	
Location	(lb/in.)	(MN/m)	(in.)	(mm)	(psi)	(MN/m^2)
Midcylinder	138,400	18.17	0.436	11.07	320,000	2,200

Based on the filament design strength of 330,000 psi (2.28 GN/m^2) the predicted margin of safety at 5,000 psig (34.5 MN/m^2g) was:

$$MS = \frac{330,000}{320,000} - 1 = +0.03$$

Skirt attachment. - The design of the skirt attachment area was based on the configuration established by testing of Vessel 8 and 9. The method of analysis involving equations (13), (14), and (15) was demonstrated to be adequate and thus was again used to determine the shear stress profile along each shear ply. The geometry and elastic properties of the structure that were entered into the digital computer were as follows:

Skirt

t_1 = 0.06 in. (1.5 mm)
t_2 = 0.89 in. (22.6 mm)
} Linear Taper

$E_\varphi = 4.60 \times 10^6$ psi (31.7 GN/m^2)

Overwrap

$t = 0.40$ in. (10.2 mm)

$E_\varphi = 3.8 \times 10^6$ psi (26 GN/m^2)

Case Structure (under the inner shear ply)

$t = 0.97$ in. (24.6 mm)

$E_{\alpha\varphi} = 3.1 \times 10^6$ psi (21 GN/m^2)

Axial Strain

at $X = L_2$, $\epsilon_\varphi = 0.023$ in./in. (4.0 N/m)

at $X = L_1$, $\epsilon_\varphi = 0.019$ in./in. (3.3 N/m)

at $X = 0$, $\epsilon_\varphi = 0.018$ in./in. (3.2 N/m)

Outer Shear Ply

$t = 0.06$ in. (1.5 mm)

$G = 300$ psi (2.1 MN/m^2)

Inner Shear Ply

$t_1 = 0.03$ in. (0.8 mm)

$t_2 = 0.30$ in. (7.6 mm)

} Linear Taper

$G = 380$ psi (2.6 MN/m^2)

Filler Ply

$t_o = 0.03$ in. (0.8 mm)

$t_1 = 0.15$ in. (3.8 mm)

$G = 300$ psi (2.1 MN/m^2)

Joint Lengths

$L_1 = 4.0$ in. (102 mm)

$L_2 = 19.0$ in. (483 mm)

Figure 5 defines the basic geometry of the joint as broken into the two analytical models from which the results of each were superimposed to give the final stress profile. The loads transmitted as a result of case expansion (based on the shown boundary conditions) are:

CASE EXPANSION

BOUNDARY CONDITIONS: AT X = 0 $\tau_R = 0$

AT X = L_1 SKIRT TAPER FIXED

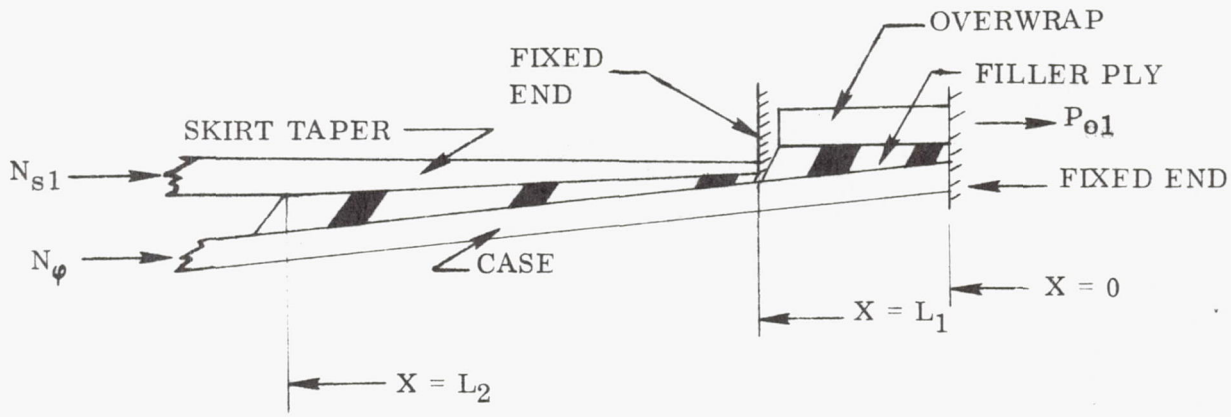

Loads Transferred by Shear Ply and Filler Ply

Case Expansion Between	N_{s1} (lb/in.)	N_{s1} (MN/m)	P_{o1} (lb/in.)	P_{o1} (MN/m)
X = O and X = L_1	2,000	0.35	450	0.079
X = L_1 and X = L_2	7,700	1.3	--	--
Total Load	9,700	1.7	450	0.079

and the load transfer relationships as a result of the skirt deflection are:

SKIRT DEFLECTION

BOUNDARY CONDITION: AT X = L_1 ENDS OF DOME AND OVERWRAP ARE FIXED. SKIRT END IS FREE TO DEFLECT AND ITS DEFLECTION RELATIVE TO THE DOME AND OVERWRAP IS EQUAL.

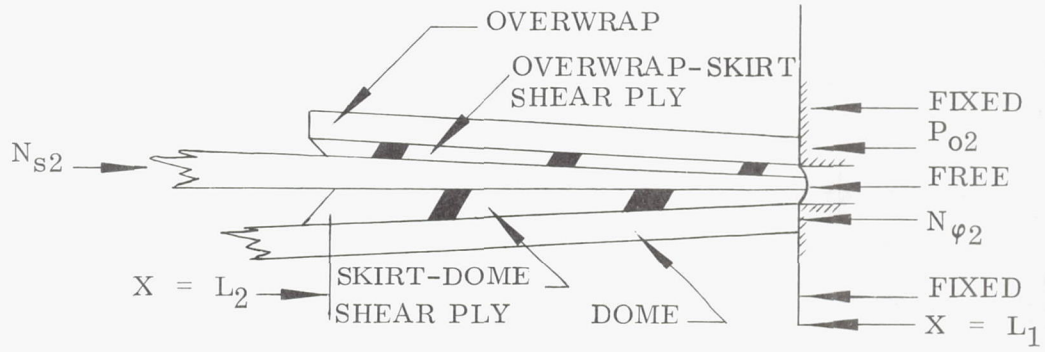

RELATIVE LOAD TRANSFER THROUGH THE SHEAR PLIES

$P_{o2} = 0.73\ N_{s2}$ $\qquad$ $N_{\varphi 2} = 0.27\ N_{s2}$

The total loading at 5,000 psig (34.5 MN/m^2g) as obtained by superimposing the two loading conditions is as follows:

N_s = 15,000 lb/in. (2.6 MN/m)

N_{s2} = 5,300 lb/in. (0.93 MN/m)

P_{o2} = 3,900 lb/in. (0.68 MN/m)

P_o = 3,450 lb/in. (0.604 MN/m)

$N_{\varphi 2}$ = 1,400 lb/in. (0.25 MN/m)

The resulting stresses in the two shear ply are shown in Figure 58. The peak stress is at the leading edge of the inner shear ply where the predicted shear stress is 1,000 psi (6.9 MN/m^2) and the indicated margin of safety at 5,000 psig (34.5MN/m^2g) is zero. The length of filler ply was designed sufficiently long enough to safely transfer the total P_{o2} loading from the overwrap into the case structure if fracture at the interface did occur as was experienced during the Vessel 8 test.

Skirt structure. - A major effort during the evaluation of the 18-in. diameter vessel designs was the establishment of a fracture criterion for the skirt structure. It was found that the structure was fracture critical with respect to the combined effects of the axial thrust load and discontinuity bending moments. The fracture criterion, as defined by equation (18), was used in conjunction with revised strength levels to size the skirt structure. The original strength values as estimated from the Vessel 2, 4, and 5 tests were increased about 10 percent as a result of the skirt behaviors during the Vessel 8, 9, and IR & D No. 4 tests. The strengths of the skirt structure on these three latter vessels were improved by a better sequencing of the polar-hoop layers and a more careful control in processing.

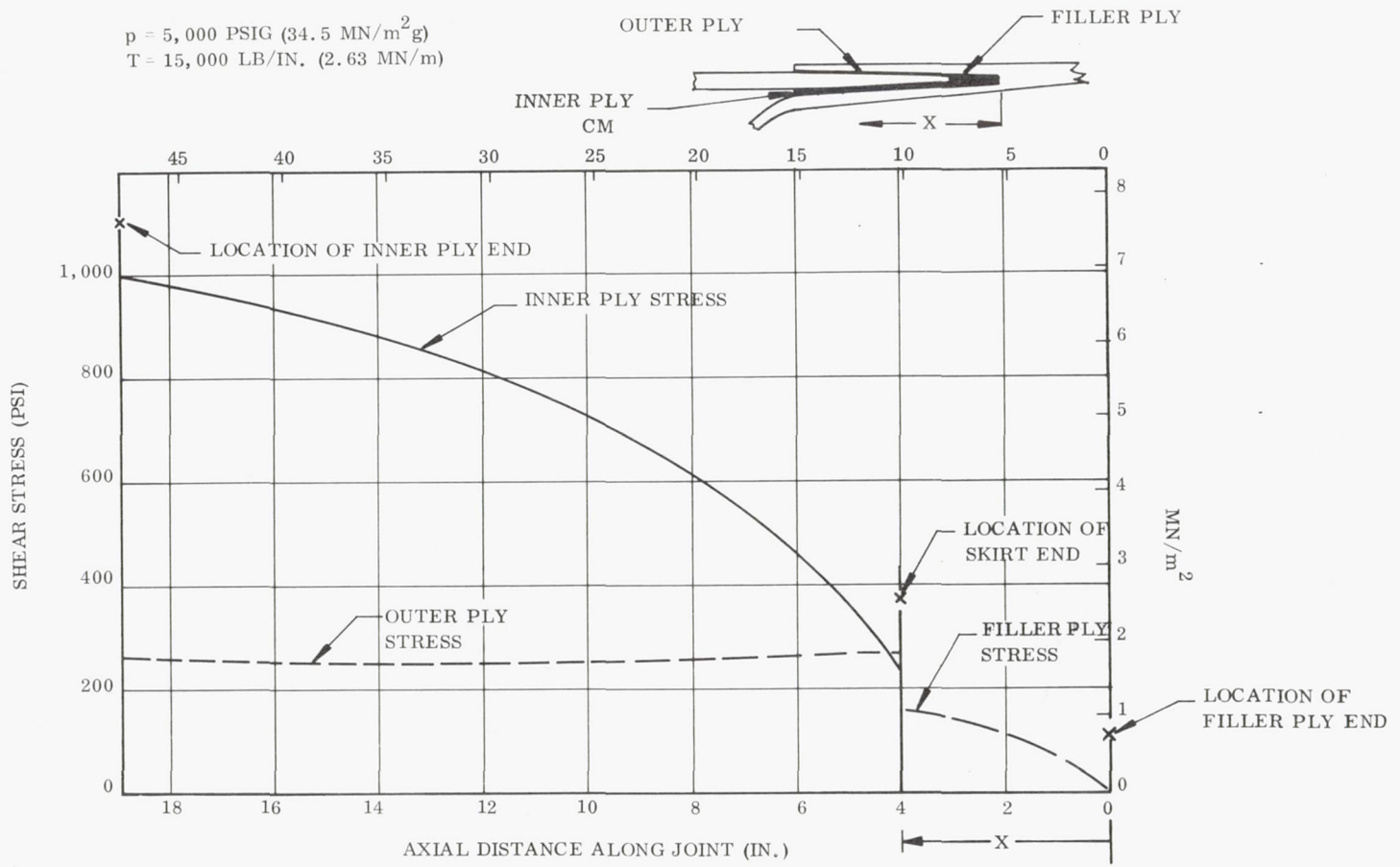

Figure 58. 54-In. Subscale Skirt Shear and Filler Ply Predicted Stress Distribution

The discontinuity analysis used to determine the deflections and loads in the skirt-case junction area was identical to that used on the 18-in. vessels. Again a digital computer was employed to generate the elastic properties and to influence coefficients for the structure (shown in Figure 59 as broken down into 24 free bodies). Also included in Figure 59 is a tabular summary of the pertinent parameters and elastic properties used in the discontinuity analysis. The resulting bending moments, transverse shear loads, and the radial displacement profile is shown in Figure 60 for the entire skirt attachment area.

The critical area in the skirt structure was 2 in. (50.8 mm) forward of the tangent plane where:

$$M = 3,500 \text{ in. lb/in. } (16,000 \text{ Nm/m})$$

$$N_S = 15,000 \text{ lb/in. } (2.6 \text{ MN/m})$$

$$\Delta R = 0.085 \text{ in. (outward) } (2.16 \text{ mm})$$

The maximum principal stresses in the longitudinal layers occurred at the outer surface of the skirt and were obtained from equations (22) and (23).

$$\sigma_\varphi = \frac{E_{\alpha\varphi}}{(E_\varphi t)_c}\left[N_S + \frac{6M}{t_c}\right]$$

$$= \frac{7.2}{4.6\ (0.89)}\left[15,000 + \frac{6\ (3,500)}{0.89}\right]$$

$$= 68,000 \text{ psi } (470 \text{ MN/m}^2)$$

$$\sigma_\theta = \frac{\Delta R}{R} E_{\alpha\theta}$$

$$= \frac{0.085}{27.0}\ (1.6 \times 10^6)$$

$$= 5,000 \text{ psi } (34.5 \text{ MN/m}^2)$$

The resulting stresses translated into the direction of a longitudinal ply, $\pm$11 deg (0.19 rad) from the (φ) direction, are calculated from equations (19), (20) and (21):

$$\sigma_x = -65,100 \text{ psi } (-449 \text{ MN/m}^2)$$

$$\sigma_y = +2,200 \text{ psi } (15.2 \text{ MN/m}^2)$$

$$\tau_{xy} = 12,200 \text{ psi } (84.1 \text{ MN/m}^2)$$

At 5,000 psig (34.5 MN/m^{2}g) the predicted fracture indicator, as obtained from equation (18), and the following revised strength levels:

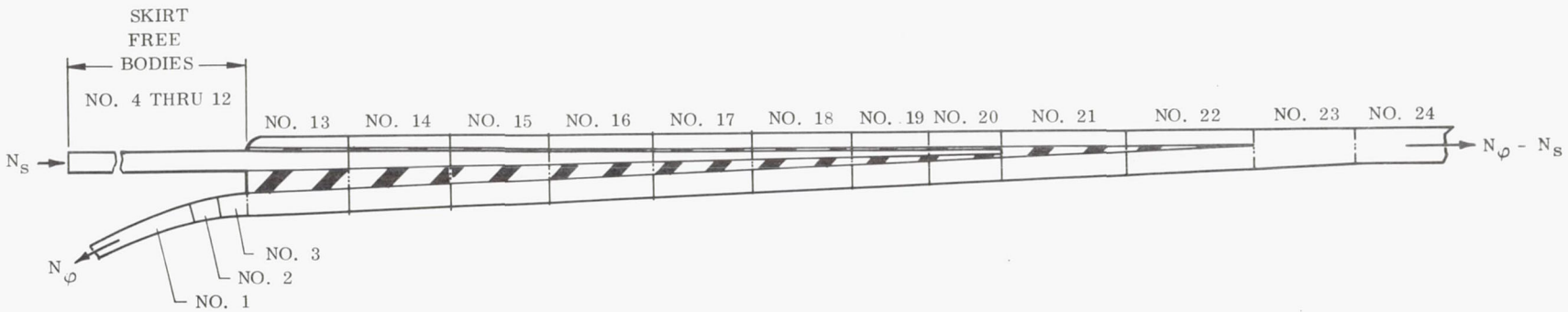

FREE BODY NO.	MEMBRANE POLAR WRAP STRAIN, ϵ_φ (IN./IN.)	COMPOSITE THICKNESS, t_c (IN.)	(mm)	COMPOSITE HOOP MODULUS, E_θ (PSI)	(GN/m^3)	COMPOSITE LONGITUDINAL BENDING STIFFNESS, D_φ (IN.^{3})	(MN/m^3)	AVERAGE RADIUS, $\bar{R}$ (IN.)	(mm)	LENGTH OF FREE BODY, L (IN.)	(mm)	POISSON'S* EFFECT DUE TO LONGITUDINAL STRESS IN POLAR WRAP
1	0.023	0.43	(10.9)	$1.3 \times 10^{+6}$	(9.0)	$0.032 \times 10^{+6}$	(2,395)	25.76	(654.3)	--		0.400
2	0.023	0.80	(20.3)	3.9	(26.9)	0.120	(8,981)	25.40	(645.2)	1.0	(25.4)	0.180
3	0.023	0.95	(24.1)	4.4	(30.3)	0.180	(1,347)	26.00	(660.4)	1.0	(25.4)	0.180
4 THRU 12	--	0.89	(22.6)	4.6	(31.7)	0.281	(2,103)	26.80	(680.7)	1.1(EA)	(28.2)	--
13	0.023	1.99	(50.6)	4.7	(32.4)	0.370	(2,769)	26.40	(670.6)	2.0	(50.8)	0.023
14	0.023	1.98	(50.3)	4.7	(32.4)	0.320	(2,395)	26.45	(671.8)	2.0	(50.8)	0.023
15	0.022	1.86	(47.2)	4.7	(32.4)	0.280	(2,096)	26.50	(673.1)	2.0	(50.8)	0.023
16	0.021	1.80	(45.7)	4.7	(32.4)	0.250	(1,871)	26.60	(675.6)	2.0	(50.8)	0.024
17	0.020	1.72	(43.7)	4.7	(32.4)	0.240	(1,796)	26.65	(676.9)	2.0	(50.8)	0.024
18	0.019	1.65	(41.9)	4.7	(32.4)	0.240	(1,796)	26.70	(678.2)	2.0	(50.8)	0.024
19	0.019	1.54	(39.1)	4.7	(32.4)	0.230	(1,723)	26.75	(679.5)	1.5	(38.1)	0.024
20	0.019	1.47	(37.3)	4.7	(32.4)	0.230	(1,723)	26.78	(680.2)	1.5	(38.1)	0.024
21	0.018	1.37	(34.8)	4.7	(32.4)	0.220	(1,646)	26.80	(680.7)	2.0	(50.8)	0.026
22	0.018	1.32	(33.5)	4.7	(32.4)	0.220	(1,646)	26.90	(683.3)	3.5	(88.9)	0.026
23	0.018	1.17	(29.7)	4.7	(32.4)	0.210	(1,572)	27.00	(685.8)	3.5	(88.9)	0.030
24	0.018	1.06	(26.9)	$4.9 \times 10^{+6}$	(33.8)	$0.210 \times 10^{+6}$	(1,572)	27.10	(688.3)	--		0.030

$$*\mu_{\varphi\theta} = \overset{\alpha}{\mu}_{\varphi\theta}\left(\frac{2N_\varphi}{pR_2}\right)\frac{E_{\alpha\theta}\, t_\alpha}{E_\theta\, t_c}$$

Figure 59. 54-In. Subscale Forward Skirt/Case Junction Area

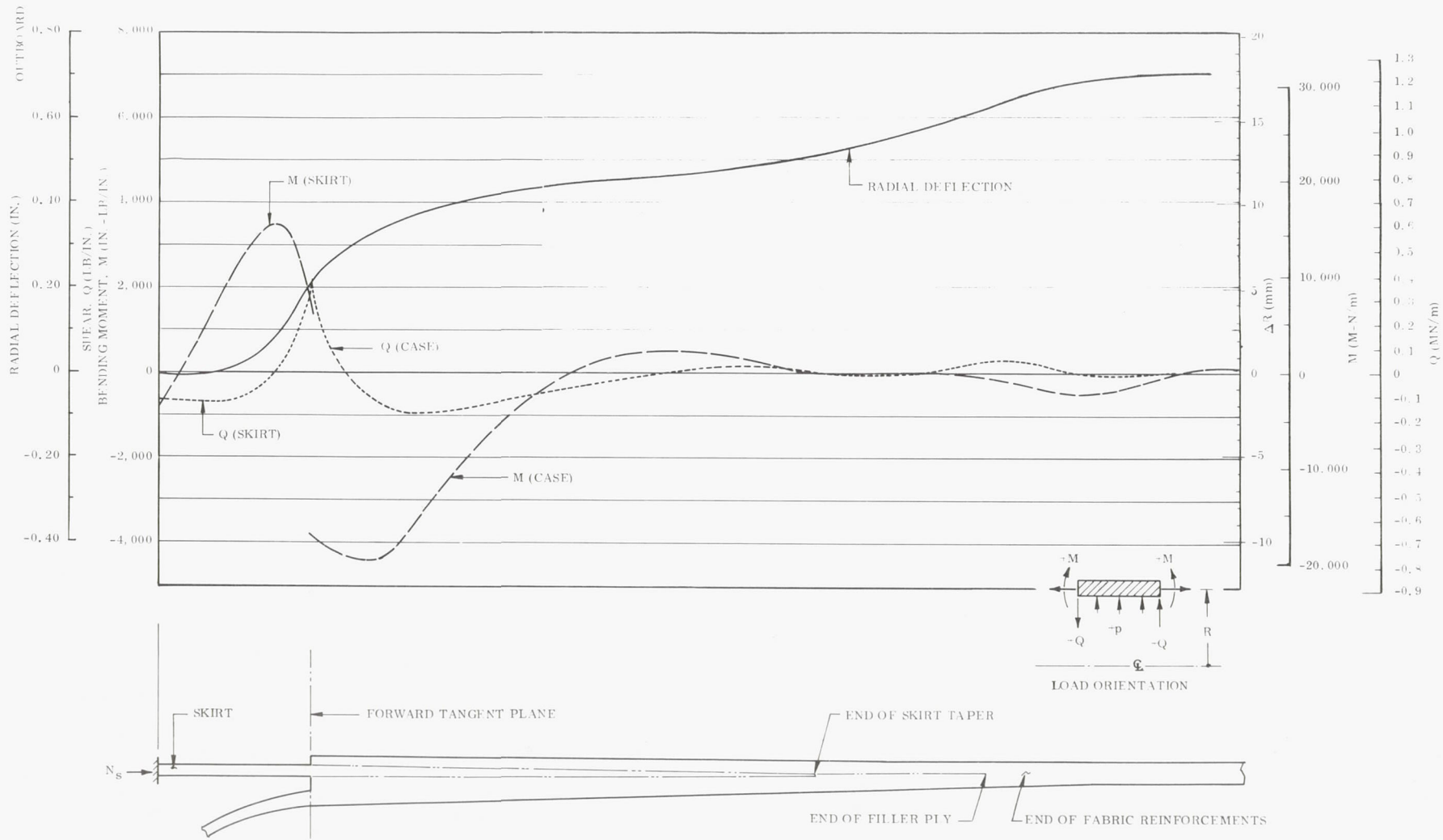

Figure 60. 54-In. Subscale Predicted Discontinuity Loads and Deflections in Skirt/Case Junction Area

$$F_x = 80,000 \text{ psi } (552 \text{ MN/m}^2) \text{ (compression)}$$

$$F_y = 6,000 \text{ psi } (41.4 \text{ MN/m}^2) \text{ (tension)}$$

$$F_s = 30,000 \text{ psi } (207 \text{ MN/m}^2) \text{ (inplane shear)}$$

is calculated as shown:

$$\left(\frac{\sigma_x}{F_x}\right)^2 - \frac{\sigma_x \sigma_y}{F_x^2} + \left(\frac{\sigma_y}{F_y}\right)^2 + \left(\frac{\tau_{xy}}{F_s}\right)^2 = A$$

$$\left(\frac{65,100}{80,000}\right)^2 + \frac{65,000\ (2,200)}{(80,000)^2} + \left(\frac{2,200}{6,000}\right)^2 + \left(\frac{12,200}{30,000}\right)^2 = A$$

$$A = 0.98$$

where A is less than unity, therefore indicating a safe structure at 5,000 psig (34.5 MN/m^2g). The resulting margin of safety, as obtained from equation (24), is:

$$MS = \left[\frac{1}{A}\right]^{1/2} - 1$$

$$= [1.10] - 1 = +0.01$$

The margin of safety with respect to axial compressive buckling was based on the data presented in Reference 5 which is shown plotted in Figure 9 . The critical axial stress (σ_{cr}) was obtained from equation (25) and is based on the material properties and geometry shown:

$$\sigma_{cr} = \frac{C[E_\theta E_\varphi]^{1/2}}{R/t_s}$$

where

$E_\theta = 4.66 \times 10^6$ psi (32.1 GN/m^2)

$E_\varphi = 4.64 \times 10^6$ psi (32.0 GN/m^2)

$R = 27.0$ in. (686 mm)

$t_s = 0.89$ in. (22.6 mm)

$C = 0.45$ (reference Figure 9)

$$\sigma_{cr} = \frac{0.45[(4.66)(4.64)]10^6}{27.0/0.89}$$

$$= 69,000 \text{ psi } (476 \text{ MN/m}^2)$$

$$MS \quad \frac{\sigma_{cr}\, t_s}{N_s} - 1$$

$$\frac{69,000\ (0.89)}{15,000} - 1$$

$$+0.30$$

Forward dome. - The maximum stresses in the forward dome occur at the region near the polar boss where the membrane component is predominant and at the tangent plane where the discontinuity bending stresses are at a maximum.

At a radius of 11.4 in. (290 mm), just outboard of the polar boss, the membrane stresses may be obtained by the "netting" approach because of the near equality of the strain levels in the two principal directions. The discontinuity bending stresses are small in this area and thus will be neglected. The predicted filament stress at 5,000 psig (34.5 MN/m^2g) is:

$$\sigma_{\alpha g} \quad \frac{N_\varphi}{t_{\alpha g} \cos^2 \alpha}$$

$$\frac{123,000}{0.74 \cos^2 46^\circ}$$

$$= 240,000 \text{ psi } (1.65 \text{ GN}/m^2)$$

The filament stress at the tangent plane is essentially a function of the meridional membrane loading and the bending moments (local in this area). From the skirt-dome-case discontinuity analysis, the local bending moment is around 4,000 in. lb/in. (18,000 Nm/m), and combined with the membrane loading, the polar filament stress is as follows (where the effect of the hoop strain is neglected).

Forward polar boss. - The forward polar boss was designed to be compatible with the Vessel 2 forward closure which was reworked to facilitate the installation of a 2 in. (50.8 mm) inlet pipe. The boss material was AISI type 4340 steel forging, similar to that of the closure, with an ultimate strength level of 160 to 180 ksi (1.1 to 1.2 GN/m^2) and an elongation of around 18 percent. The closure was joined to the boss by 30 bolts (5/8-18 UNF) with a minimum ultimate tensile strength of 180 ksi (1.2 GN/m^2).

The loads and deflections in the boss-closure assembly were determined by a discontinuity analysis similar to that shown for the Vessel 1 forward boss. The torsional stiffness of the fiberglass dome buildup over the boss was considered small as compared to that of the steel boss and therefore was neglected in this analysis. The configuration of the analyzed assembly, the boundary loads at an internal pressure of 5,000 psig (34.5 MN/m^2g), and the location of the high stress areas are shown in Figure 61. The two boundary loads N_R and Q_R, at the dome-polar boss interface were determined from equations (29) and (30), respectively.

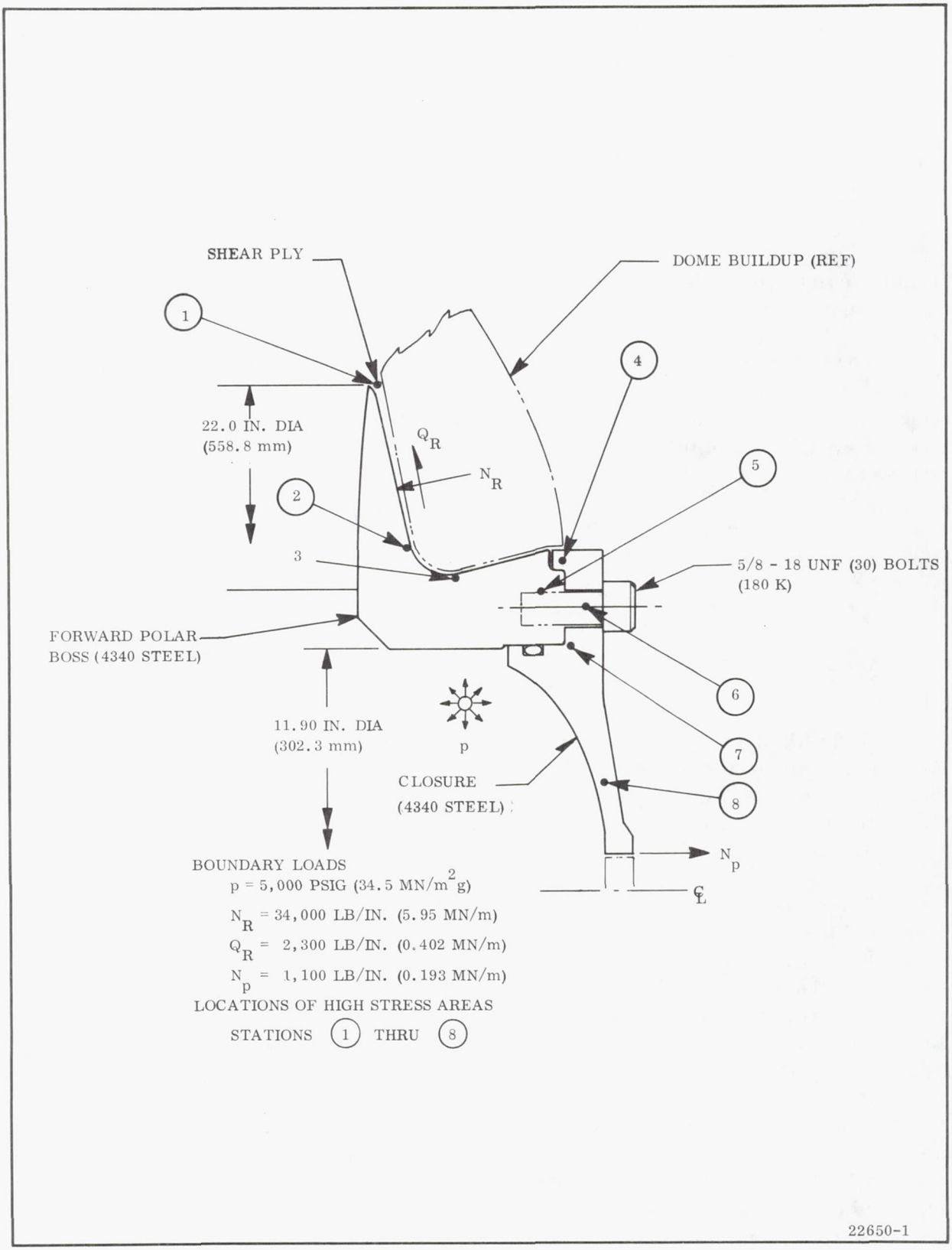

Figure 61. 54-In. Subscale Forward Polar Boss and Closure

The predicted loads and deflections from the discontinuity analysis at a pressure of 5,000 psig (34.5 MN/m^2g) are as follows:

$$\sigma_{\alpha g} = \frac{N\varphi}{t_{\alpha g}} + \frac{6M}{t^2}\left(\frac{E_g}{E_{\varphi\beta}}\right)\cos^2\alpha$$

$$= \frac{66,200}{0.24} + \frac{6\,(4,000)}{(0.95)^2}\left(\frac{12.4}{7.0}\right)\cos^2\alpha$$

$$= 327,000 \text{ psi } (2.25 \text{ GN/m}^2)$$

The indicated margin of safety at the tangent plane is +0.01, assuming that the bending moment does not decay out due to local resin crazing.

The contour of the forward dome was based on a hoop to meridional load ratio of -0.17 or a compressive membrane hoop bias of 27,000 psi (186 MN/m^2). This design parameter was identical to that used for the polar wrapped 18-in. diameter vessels.

Location	M (in.-lb/in.)	Q (lb/in.)	N_φ (lb/in.)	ΔR (in.)	$\Delta\theta$ (rad)
2	-24,900	1,920	19,200	0.00520	0.00191
3	-33,500	-13,200	13,500	0.00314	0.00191
4, 5, and 6	11,000	-24,200	13,400	-0.00097	0.00723[a]
7	11,900	-20,600	15,000	-0.00444	0.00723
	(Nm/m)	(MN/m)	(MN/m)	(mm)	(rad)
2	-110,000	0.336	3.36	0.1321	0.00191
3	-149,000	-2.31	2.36	0.0798	0.00191
4, 5, and 6	49,000	-4.24	2.35	-0.0246	0.00723
7	53,000	-3.61	2.63	-0.1128	0.00723

[a] The effects of bolt elongation included.

The predicted stresses in the critical areas shown in Figure 61 as a result of the loads and deflections shown above are in the following tabulation.

Location	Item	Stress Magnitude Type (psi)	(MN/m^2)	
1	Shear Ply	710	4.9	shear
2	Polar Boss	125,000	862	tensile
3	Polar Boss	120,000	827	tensile
4	Shear Lip	91,000	627	shear
5	Bolt	160,000	1.10	tensile
6	Bolt	85,000	586	thread shear
7	Flange	157,000	1.08	tensile
8	Closure	90,000	621	tensile

The critical area on the assembly was the closure flange with a local tensile stress of 157,000 psi (1.08 GN/m^2). Neglecting the effects of yield, the indicated margin of safety was +0.01.

Aft polar boss. - The aft polar boss was designed to react the discontinuity loadings at the hydrotest fixture attachment area and to be compatible with the deflections of the aft dome. The boss and fixture material was AISI type 4340 steel forging with an ultimate tensile strength of 160 to 180 ksi (1.1 to 1.2 GN/m^2). The strength was primarily needed in the shear lip area of both the boss and fixture in order to withstand the high transverse shear loading as induced by both the radial discontinuity shear and bending moment loads at the bolt. The piston housing was attached to the boss by 60 bolts (7/8-14 UNF) having a minimum tensile strength of 180 ksi (1.2 GN/m^2).

The assembly of the two components was analyzed with a discontinuity analysis similar to that used on the forward boss and closure. The influence of the aft dome shell and buildup was again neglected with only the two interface loads (N_R and Q_R) and the internal pressure considered as the primary influential boundary conditions.

Figure 62 shows the polar boss fixture assembly with the locations of the high stress areas and the pertinent boundary loads included. The loads and deflections, as obtained from discontinuity analysis at a pressure of 5,000 psig at these high stress areas, are as follows:

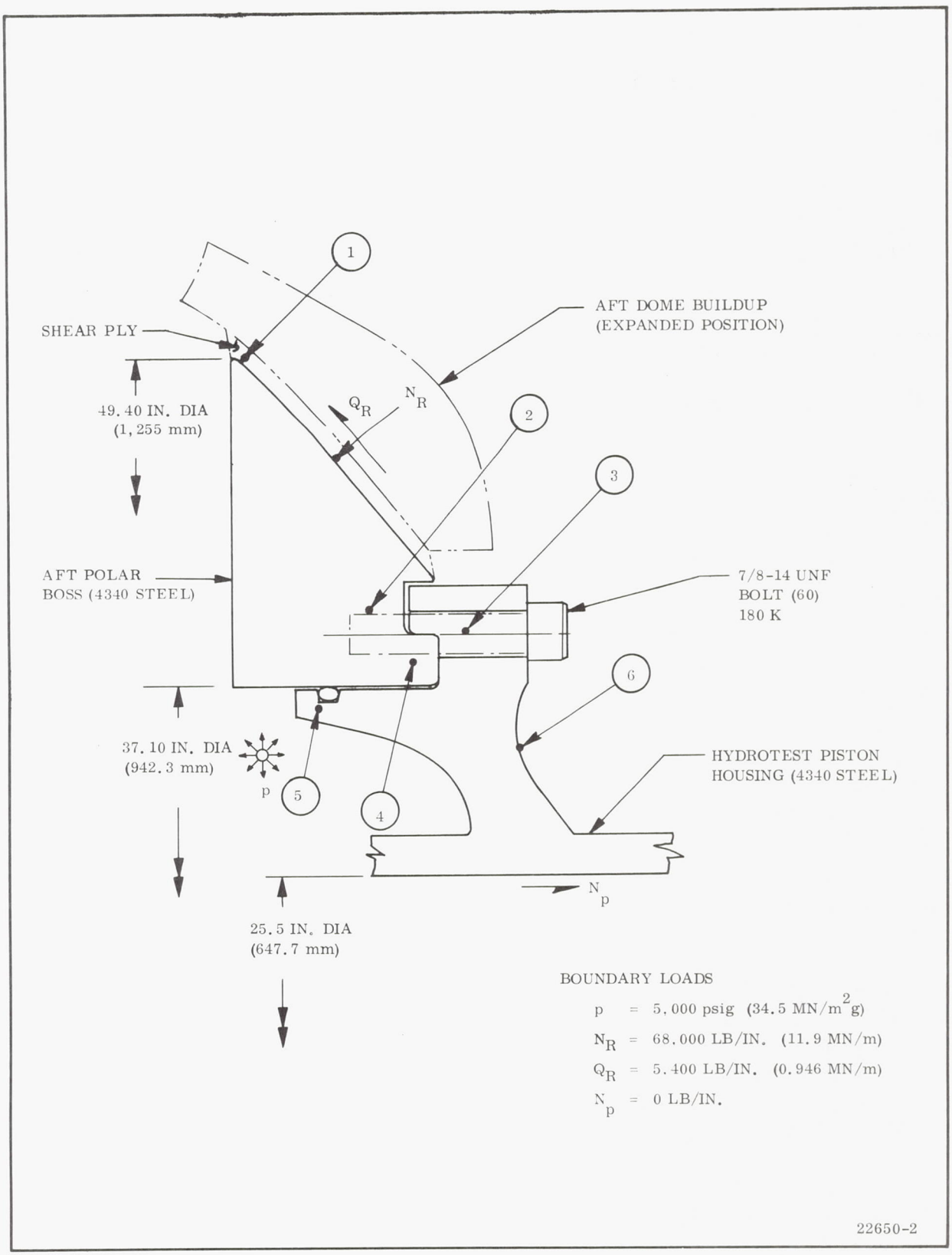

Figure 62. 54-In. Subscale Aft Polar Boss and Hydrotest Fixture

Location	M (in.-lb/in.)	Q (lb/in.)	N (lb/in.)	ΔR (in.)	$\Delta\theta$ (rad)
2 thru 5	-23,300	-11,100	23,000	+0.00612	0.0177
6	-36,000	+ 6,600	33,300	-0.00342	0.0127[a]
	(Nm/m)	(MN/m^2)	(MN/m^2)	(mm)	
2 thru 5	-104,000	-1.94	4.03	0.1554	
6	-160,000	1.16	5.83	0.0869	

[a]Includes rotation due to bolt elongation.

The predicted stresses at these locations are as tabulated:

Location	Item	Stress Magnitude Type (psi)	(MN/m^2)	
1	Shear Ply	890	6.14	shear
2	Bolt Thread	67,500	465	shear
3	Bolt	142,000	979	tensile
4	Shear Lip	33,000	228	shear
5	Flange	37,000	255	shear
6	Housing	118,000	814	tensile

The bolt was the critical component in the assembly with a predicted stress of 140,000 psi (965 MN/m^2) at ultimate pressure. The margin of safety was +0.28. The bolt was sized to react the basic blowout loading and to tolerate the boss rotation as limited by the gap between the boss and fixture flange. The radial load coupling between the fixture flange and shear lip reacted the bending moment at the bolt.

Aft dome. - The aft dome structure was designed to be compatible with the deflections of the polar boss to withstand the loads induced by the internal pressure. The shell was made up of interspersed polar layers and tape reinforcements, with the quantity of the latter established by the hoop loading at the polar boss. The quantity of polar wrap was essentially determined by the loads in the forward dome and by the discontinuity bending moment at the aft tangent plane.

The contour of the aft dome was determined by an iterative process using the "netting" and discontinuity analysis to balance out the stresses in the tape reinforcement and in the polar layers. Because of the low filament orientation of the polar layers, the tape reinforcements essentially were designed to carry all of the hoop loading, while the polar wrap carried the meridional membrane loading and reacted the discontinuity bending moments. The interface shear area between the

polar and tape laminates was critical at the termination of the tape layers near the aft tangent plane.

The strength of the total composite in the hoop direction around the polar boss area was really never established during the 18-in. diameter vessel task. However, the test results from Vessel 4 did indicate that the tape laminate could tolerate a 2.2 percent hoop strain level without any apparent indication of material fracture. Based on this data and the indicated tape filament strength level of 370 to 390 ksi (2.6 to 2.7 GN/m^2), a fracture criterion for the tape-polar composite was established at a hoop strain level of 2.5 percent. At this strain level it was estimated that the failure would be initiated by fracture occurring at the tape to tape interfaces and would be caused by crazing in the resin matrix.

The first contour estimate was obtained from the "netting" analysis and considered the filament orientation of only the reinforcements. The contour was then modified by reducing the rate of change in the meridional curvature until the bending stresses in the polar layers at the tangent plane were not overly excessive. The limiting factor was the stress in the tape reinforcements as a function of the hoop loading, which increases as the meridional curvature is decreased.

For the dome shell discontinuity analysis the two boundary loads N_R and Q_R at the dome-boss interface were again used in conjunction with the boss rotation as obtained from the boss fixture discontinuity analysis. The boss deflection was considered small compared to that of the dome and thus was neglected. Figure 63 shows the aft dome broken down into the respective free-bodies where the dome buildup over the boss was treated as a ring and the dome and cylindrical sections as short shell segments. The structural elastic properties, loads, and geometries that were entered into the digital computer are shown tabulated in Table XI. The final predicted loads and deflections from the discontinuity analysis which was made on the structure in the deflected position are shown in Table XII.

The dome buildup over the aft boss was critical with respect to the hoop strain in the composite structure. The predicted hoop strain is based on the deflections obtained from the discontinuity analysis and calculated from equation (33) using the radial distance to the ring centroid with the ring in the unexpanded position.

$$\epsilon_\theta = \frac{\Delta R_{1\text{-}2}}{R_c} = \frac{0.60}{24.7} = 0.024 \text{ in./in.} \qquad (33)$$

The resulting margin of safety is +0.04 for this area at a pressure of 5,000 psig (34.5 MN/m^2g). The predicted maximum strain in the outside polar layers of the ring at the intersection of the dome ring and shell is obtained from equation (32):

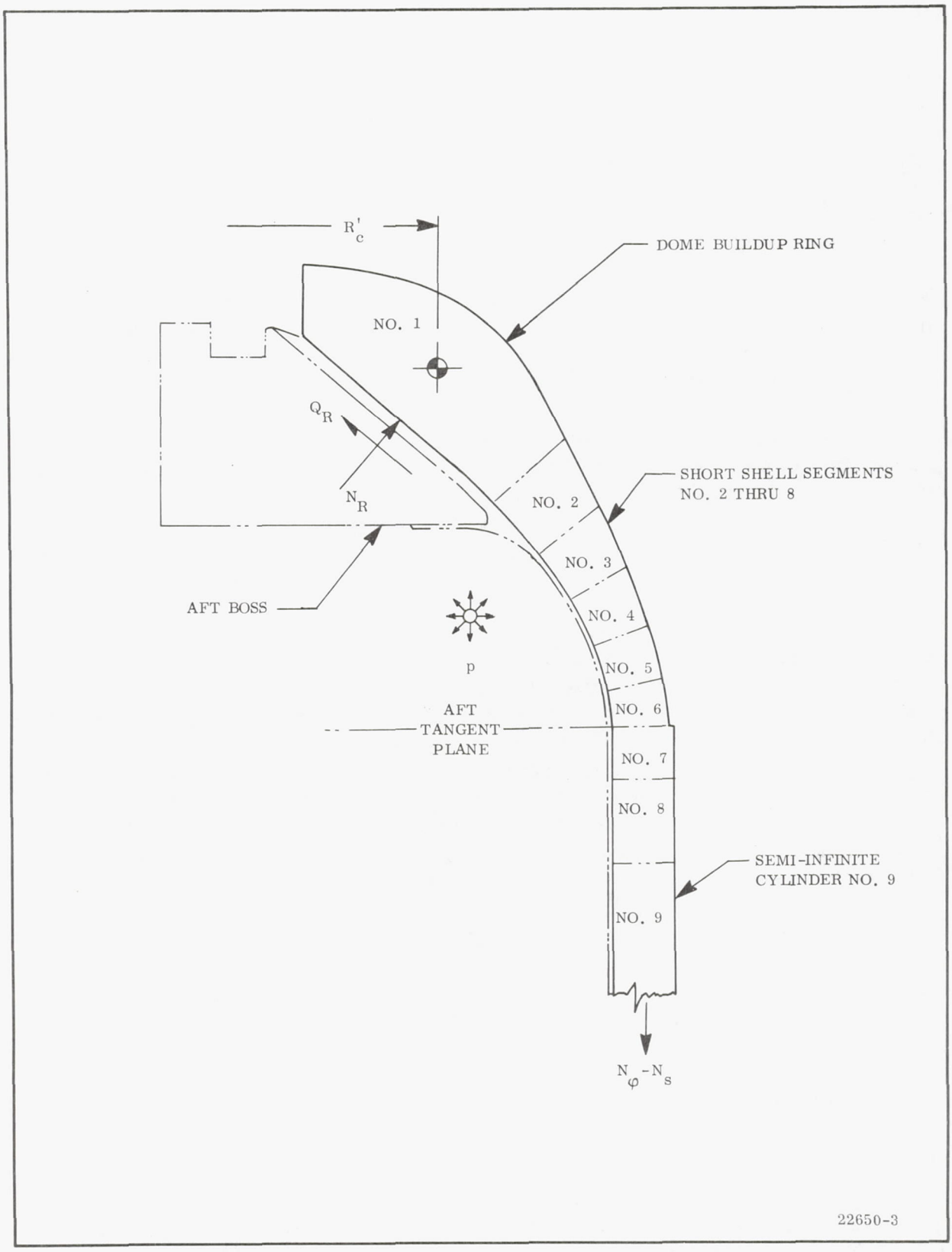

Figure 63. 54-In. Subscale Aft Dome Structure

TABLE XI

54-IN. SUBSCALE AFT DOME PROPERTIES FOR THE DISCONTINUITY ANALYSIS

Free Body No.	Free Body Data									Between Free Bodies (Expanded Position)					
	t_{ave}		E_{φ}		E_{θ}		$\mu_{\varphi\theta}$	Length		R_{ave}		N_{φ}		N_{θ}	
	(in.)	(mm)	(psi x 10^{-6})	(N/m^2)	(psi x 10^{-6})	(N/m^2)		(in.)	(mm)	(in.)	(mm)	(lb/in.)	(MN/m)	(lb/in.)	(MN/m)
1	2.70	(68.6)	2.3	(0.0159)	5.6	(0.0386)	0.14	5.0	(127)	25.6	(650)	61,000	(10.68)	162,000	(28.36)
2	2.00	(50.8)	2.6	(0.0179)	3.1	(0.0214)	0.31	1.5	(38)	26.4	(671)	58,000	(10.15)	7,000	(1.23)
3	1.75	(44.5)	2.9	(0.0200)	2.7	(0.0186)	0.34	1.5	(38)	27.1	(688)	57,000	(9.98)	-15,000	(-2.63)
4	1.48	(37.6)	3.1	(0.0214)	2.4	(0.0165)	0.34	1.2	(30)	27.6	(701)	56,000	(9.80)	-25,000	(-4.38)
5	1.25	(31.8)	3.3	(0.0228)	2.3	(0.0159)	0.34	1.0	(25)	27.8	(706)	55,000	(9.63)	-30,000	(-5.25)
6	1.13	(28.7)	3.4	(0.0234)	2.3	(0,0159)	0.34	1.0	(25)	27.8	(706)	55,000	(9.63)	-30,500	(-5.34)
7	1.06	(26.9)	2.8	(0.0193)	5.0	(0.0345)	0.049	1.5	(38)	27.8	(706)	55,000	(9.63)	140,000	(24.51)
8	1.06	(26.9)	2.8	(0.0193)	5.0	(0.0345)	0.049	3.0	(76)	27.8	(706)	55,000	(9.63)	140,000	(24.51)
9	1.06	(26.9)	2.8	(0.0193)	5.0	(0.0345)	0.049	--	--	--	--	--	--	--	--

TABLE XII

54-IN. SUBSCALE RESULTS FROM THE AFT DOME DISCONTINUITY ANALYSIS

Between Free Bodies (No.)	M		Q		ΔR		Δθ	
	(in.-lb/in.)	(Nm/m)	(lb/in.)	(MN/m)	(in.)	(mm)	(deg)	(rad)
1-2	-26,800	(-119,200)	-13,900	(-2.43)	-0.60	(-15.2)	-1.01	(-0.018)
2-3	-10,700	(-47,600)	-13,700	(-2.40)	-0.59	(-15.0)	-2.0	(-0.035)
3-4	+3,000	(13,300)	-6,700	(-1.17)	-0.56	(-14.2)	-2.1	(-0.037)
4-5	+8,600	(38,300)	-2,700	(-0.47)	-0.54	(-13.7)	-1.7	(-0.030)
5-6	+9,500	(42,300)	+900	(0.16)	-0.52	(-13.2)	-0.66	(-0.012)
6-7	+6,900	(30,700)	+4,200	(0.74)	-0.52	(-13.2)	+0.45	(+0.008)
7-8	+2,000	(8,800)	+2,400	(0.42)	-0.56	(-14.2)	+1.8	(+0.031)
8-9	-1,600	(7,100)	+280	(0.049)	-0.65	(-16.5)	+1.5	(0.026)
Midcylinder	--	--	--	--	-0.70	(-17.8)	--	--

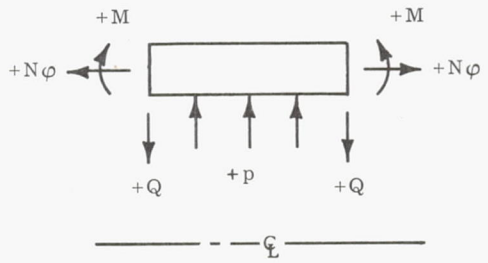

$$\epsilon_\varphi = \frac{1}{E_\varphi t}\left[N_\varphi + Q\cos\varphi + \frac{6M}{t}\right] - \mu_{\theta\varphi}\epsilon_\theta$$

$$= \frac{1}{2.5\ (2.0)}\left[61,000 - 13,900\cos 45° + \frac{6\ (26,800)}{1.87}\right] - 0.35\ (0.24) \qquad (32)$$

$$= 0.027 \text{ in./in.}$$

The stress in the polar and tape filaments in this area at the outside diameter of the polar boss is calculated from equation (34). The predicted stress in the polar filament is:

$$\sigma_{\alpha g} = \left[\frac{\sigma_\varphi \cos^2\alpha P}{E_\varphi} + \frac{\sigma_\varphi \sin^2\alpha P}{E_\theta}\right] E_g \qquad (34)$$

$$= \left[0.027\cos^2 25° + 0.024\sin^2 25°\right]\ 12.4 \times 10^6$$

$$= 328,000 \text{ psi } (2.26 \text{ GN/m}^2)$$

The predicted stress in the tape filament at this same location is also obtained from equation (34):

$$\sigma_{Tg} = \left[0.027\cos^2 63° + 0.024\sin^2 63°\right]\ 12.4 \times 10^6$$

$$= 310,000 \text{ psi } (2.14 \text{ GN/m}^2)$$

Based on a minimum design ultimate pressure of 330,000 psi (2.28 GN/m^2) for the polar and tape filaments, the dome buildup structure showed a positive margin of safety at ultimate pressure. The maximum transverse shear stress at the neutral axis of the shell locally in this area is a function of the shear load (Q) between bodies No. 1 and 2.

$$\tau_{12} = \left(\frac{3}{2}\right)\left(\frac{Q\sin\varphi}{t}\right)$$

$$= \frac{3\ (13,900)\sin 45°}{2\ (2.0)}$$

$$= 7,400 \text{ psi } (51.0 \text{ MN/m}^2)$$

The typical minimum interlaminar shear strength of an S-994 glass-epoxy laminate (as established from the ASTM test standard D2344) is about 9,000 psi (62 MN/m^2). Therefore, the aft dome structure was considered safe with respect to interlaminar shear.

The other critical area was around the tangent plane, where the influence of the cylindrical section on the dome shell induced fairly high discontinuity bending stresses.

The maximum axial stresses were predicted just aft of the tangent plane in the inside layers of the polar wrap. At this location between bodies No. 5 and 6, the hoop and meridional strains as obtained from equations (33) and (34), respectively, are:

$$\epsilon_\theta = 0.019 \text{ in./in.}$$

$$\epsilon_\varphi = 0.028 \text{ in./in.}$$

These strains result in a polar filament stress of 340,000 psi (2.34 GN/m^2) as calculated from equation (34) and based on a polar filament orientation of ± 8 deg (0.14 rad) at this location. While this value indicates a negative margin of safety of -0.03, the structure was still considered safe at 5,000 psig (34.5 MN/m^2g) due to the conservatism applied to the material properties prior to the design of Vessel 8. However, this stress value does indicate that this area will be the most probable area of rupture during the hydroburst test.

The load transfer between the tapes and the polar wrap is also at a maximum locally in this area due to the 2.8 percent meridional strain level. The maximum load that must be transmitted was assumed to be from the third tape laminate as sequenced from the inside diameter. The predicted load as obtained from equation (35) is:

$$N_{\alpha T} = \epsilon_\varphi \; E_{T\varphi} \; t_T$$

$$= 0.028 \; (1.5 \times 10^6) \; 0.04$$

$$= 1,700 \text{ lb/in. } (0.30 \text{ MN/m})$$

which is considered safe based on a strength level referenced in the analysis on the IR & D Vessel No. 4 aft dome structure. There it is shown that a glass-epoxy laminate is capable of safely transmitting a load of 2,000 lb per in. (0.35 MN/m) in single lap shear.

Fabrication

Mandrel tooling. - The 54-in. subscale was fabricated on a sand-PVA mandrel having a sand-PVA mixture identical to that established for the 18-in. vessels. The total mandrel was made up of four cast segments each having a sand bulkhead at one end, a reinforced plywood bulkhead at the other, and a steel hub running through the center.

The mandrel segments were cast in wooden molds having an interior surface of plaster which was swept to the desired diametral or dome surface contour. The center hub was fixtured relative to the swept surface prior to sand packing in order to get the desired concentricity and parallelism. The sand was hand packed starting

at the bottom to form the sand bulkhead and then worked up along the contour to form the wall. Five-in. diameter (127 mm) tubes were cast into the forward segment in order to give the segments additional radial strength to prevent collapsing during skirt installation. The remaining segments were hollow, with the inside diameter established by a single thin wall pipe with diameter slightly less than the bore in the aft polar boss.

Upon final assembly of the mandrel, the individual segments were slipped onto a master shaft as shown being done in Figure 64 where each hub was mechanically locked to the shaft and the sand castings bonded together.

The skirt mandrel was also a sand casting similar to a center segment of the case mandrel. However, the center hub of the casting was directly bolted to the wind axis adapter without the use of a center shaft.

The skirt fixture, which was used to install the skirt to hold it in place during the remainder of winding and cure, consisted of a large diameter plate and jacking screws.

The mandrels were removed from the finished parts by the addition of water internally in the mandrel. The water dissolved the PVA binder, thus reducing the sand casting to a loose composite which was readily washed out. The wooden bulkheads and metal tubes were removed as the sand was softened.

The case and skirt mandrels fully assembled for winding are shown in Appendix A, Drawing SK 42110.

Processing. - The 54-in. diameter vessel was filament wound with a 20-end S-994 glass roving identical to that used for the 18-in. vessels with Gen Gard V-45 rubber and again used for both the internal bladder and the shear ply. During the 18-in. diameter vessel effort the unidirectional reinforcement tapers were made at Wasatch Division, but for the 54-in. vessel the required quantity exceeded existing plant capability and therefore were purchased from 3M Co in 3- and 4-in. widths. The preimpregnated unidirectional tape material purchased from 3M Co, XP251S-S901, had essentially identical filament properties to that of the S-994 roving and had a resin system compatible with the E-717 prepreg material including an equivalent interlaminar shear strength.

The skirt and case were wound on the Accurate Machine & Tool Co winding machine, the same machine used to wind all of the polar wrapped 18-in. diameter vessels. The winding machine, which has both a planar and hoop delivery system, is compatible with a maximum case height of 160 in. (4.064 m), thus establishing the criterion for the length of the 54-in. diameter vessel.

The skirt was wound identically to the procedures established for the 18-in. vessels. The only difference was that the mandrel was made of sand-PVA and thus

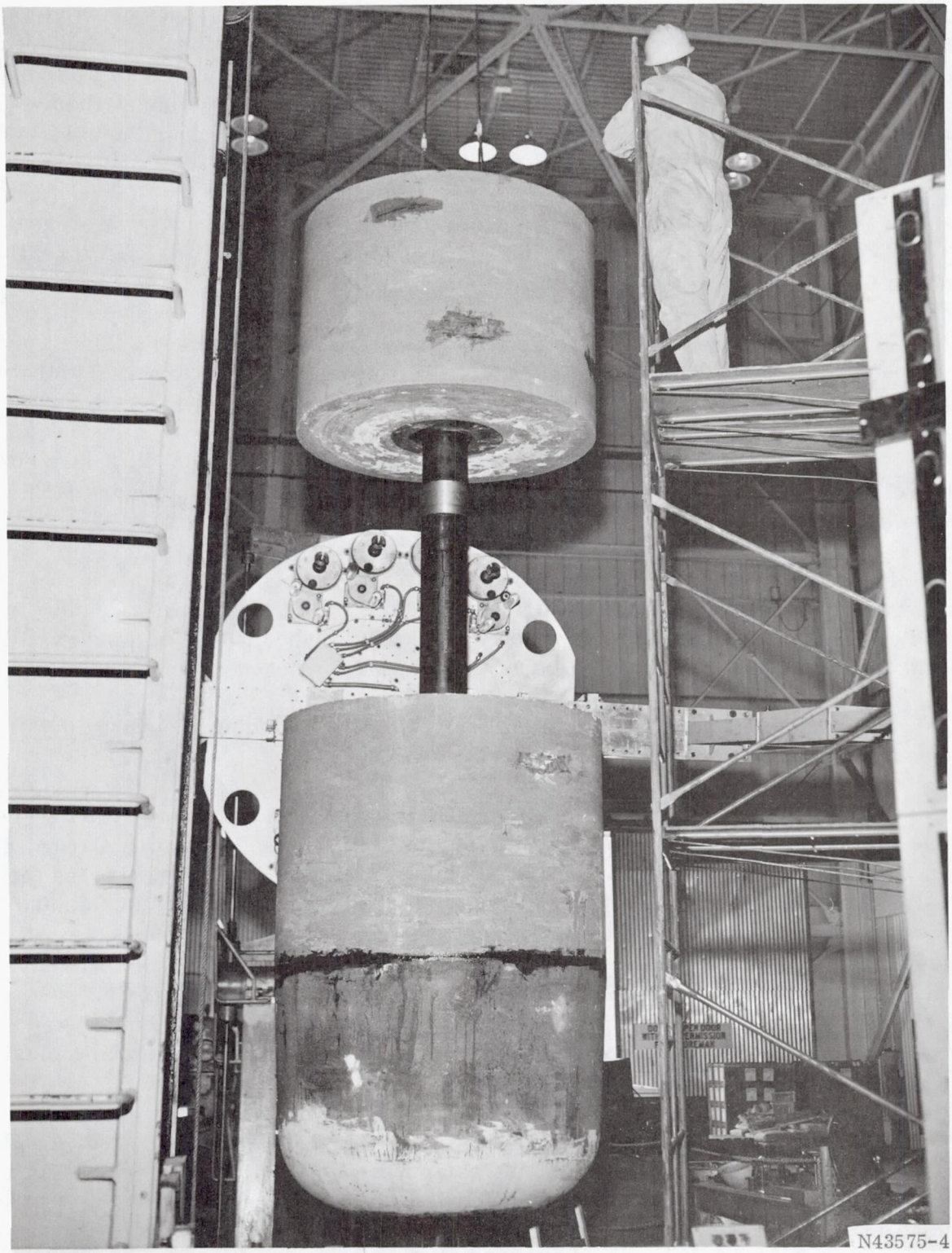

Figure 64. Installation of Segments on Center Shaft for 54-In. Subscale Case

was removed by the washout technique. Machining in the shear ply taper area was done on a vertical turret lathe prior to mandrel washout.

The case was also fabricated in accordance with procedures established during the 18-in. vessel task. The bladder and polar boss NBR shear ply were installed in the "green" condition, and the polar and hoop wrap were wound in an interspersed sequence. The two critical areas during case fabrication were the layup of the tape reinforcements and the installation of the skirt. The tapes were installed and debulked by hand between each winding of a complete polar layer (two ply). The polar wrap was originally set up in a one circuit pattern, but it was discovered that as the roving crossed over the tape layer it caused the tapes to further compress and move slightly. Near the closing of the single circuit pattern, the tapes formed a large wrinkle, which folded down and compacted upon completion of the layer. As a result of this wrinkling, the subsequent polar layers were wound in a three circuit pattern which required three revolutions of the mandrel to complete a single layer. The resulting advance of the roving minimized the extent of "walking" by the tapes and thus essentially eliminated the large wrinkle that formed at the close of the pattern. The three circuit polar pattern is shown being wound in Figure 65. Figure 66 shows how the three circuit pattern appeared as it covered a tape layer on the aft dome. The three circuit pattern did not create any undesirable buildups in the forward boss or skirt attachment areas.

At the completion of the final polar layer, the skirt was prepared for installation. The surface of the inner shear ply, which was cured along with the skirt structure, was mechanically cleaned with a high speed emery wheel and chemically cleaned with MEK. The shear ply surface was then coated with liquid epoxy resin (Union Carbide ERL-2774) in order to prewet the bonding surfaces and thus reduce the sliding friction incurred during installation. Figure 67 shows resin being applied over the cleaned surface of the inner shear ply.

The installation of the skirt was initiated by the removal of the case mandrel from the winding machine in the vertical position. The skirt and installation fixture were then placed on the winding axis and the case mandrel reinstalled, as is shown being done in Figure 68. The skirt was then forced in place on the case by four jack screws and was then retained by the fixture plate during the completion of fabrication.

The outer surface of the skirt taper was then cleaned with MEK, and "green" NBR for the outer shear and filler plies was installed using 30 mil (0.76 mm) sheet stock. The style S/34-901 glass fabric and hoop roving were alternately applied, as shown in Figures 69 and 70, respectively, until the total requirements of each were installed.

After completion of winding, the case-mandrel assembly was installed vertically in the oven, forward end down, and cured for 6 hr at 300° F (422° K). Upon cooldown, the mandrel was reinstalled in the winding machine, where the skirt was faced off and the aft dome opening cut with a high speed diamond wheel.

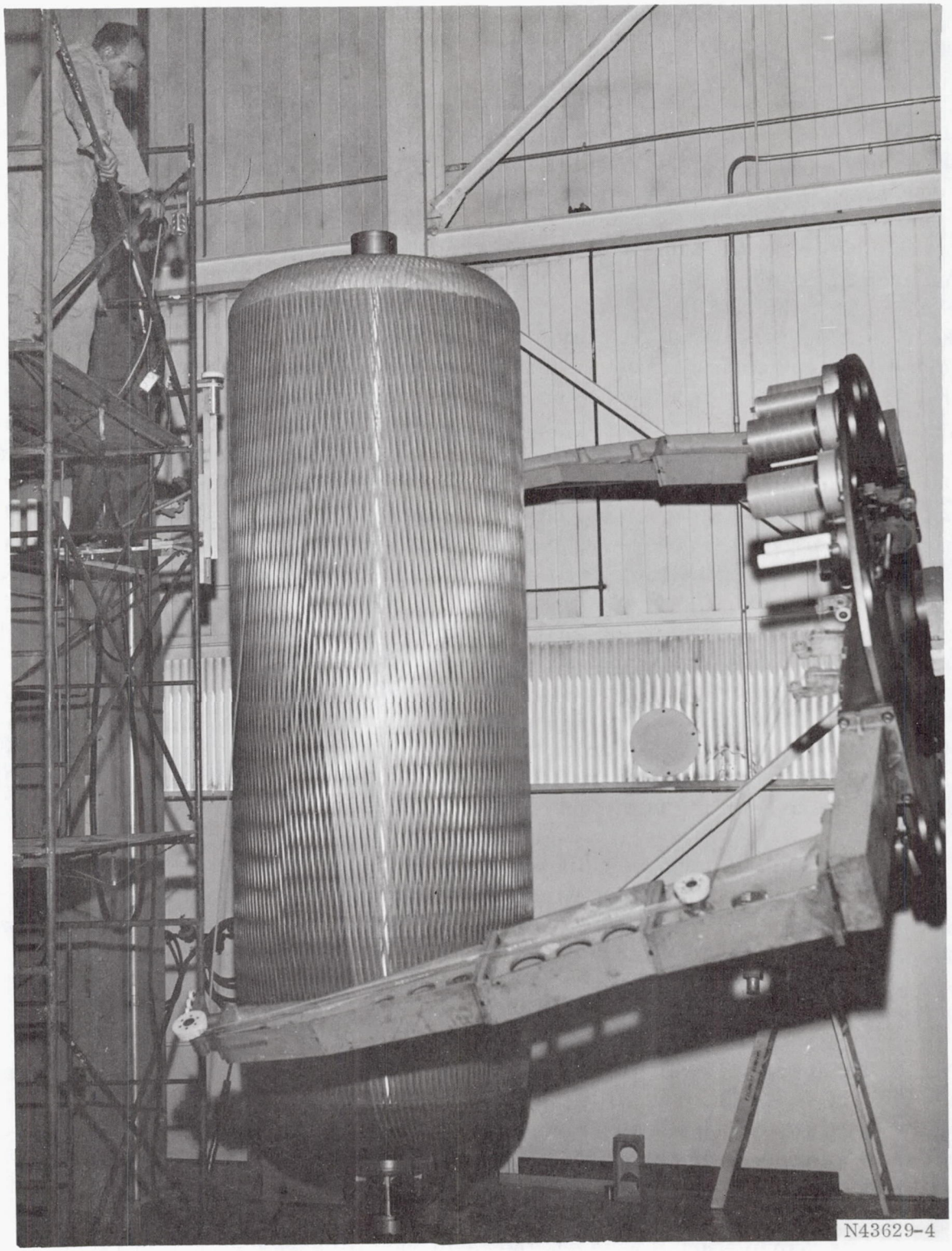

Figure 65. Winding of Three Circuit Polar Wrap Pattern for 54-In. Subscale Case

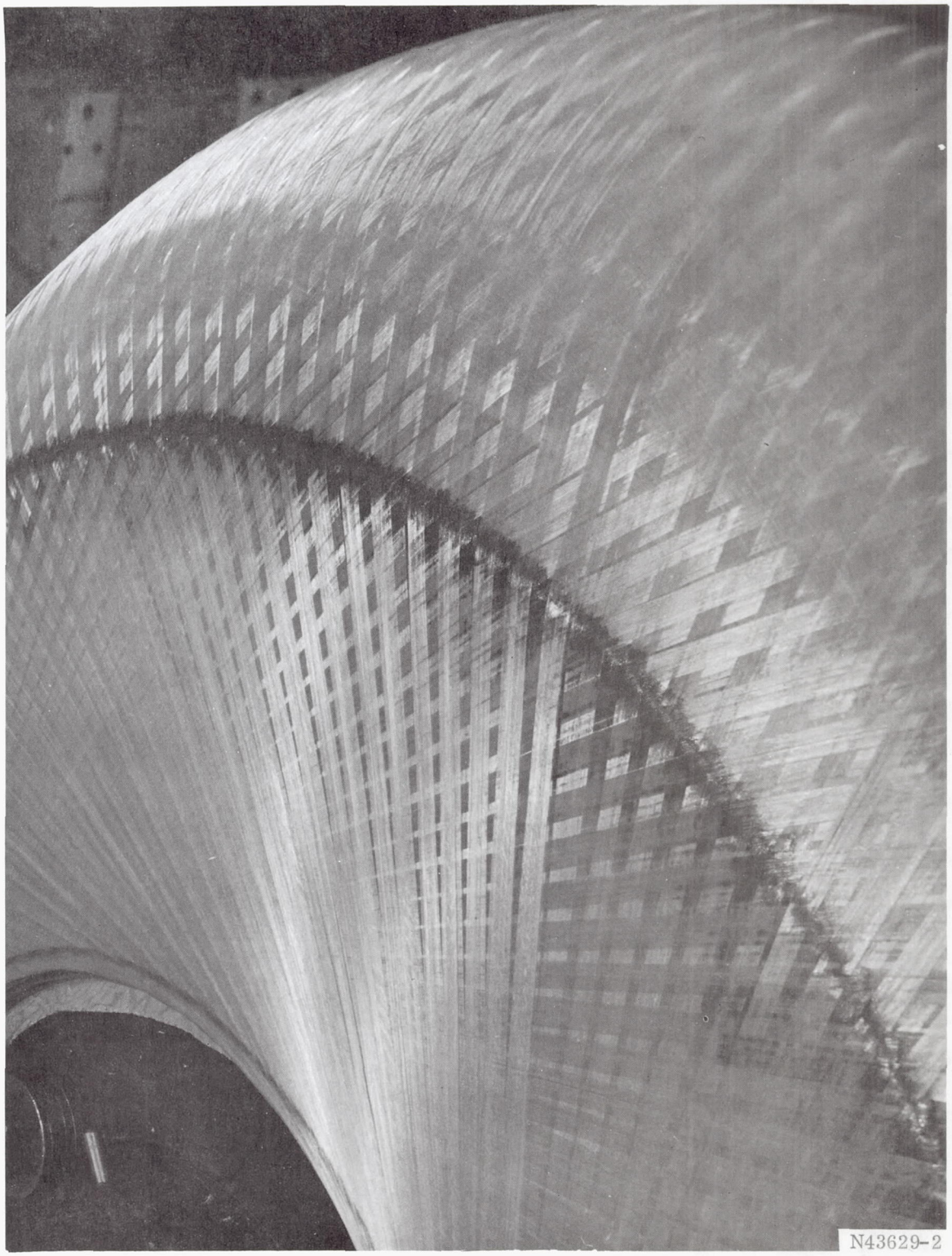

Figure 66. Three Circuit Polar Wrap Pattern and Aft Dome of 54-In. Subscale Case

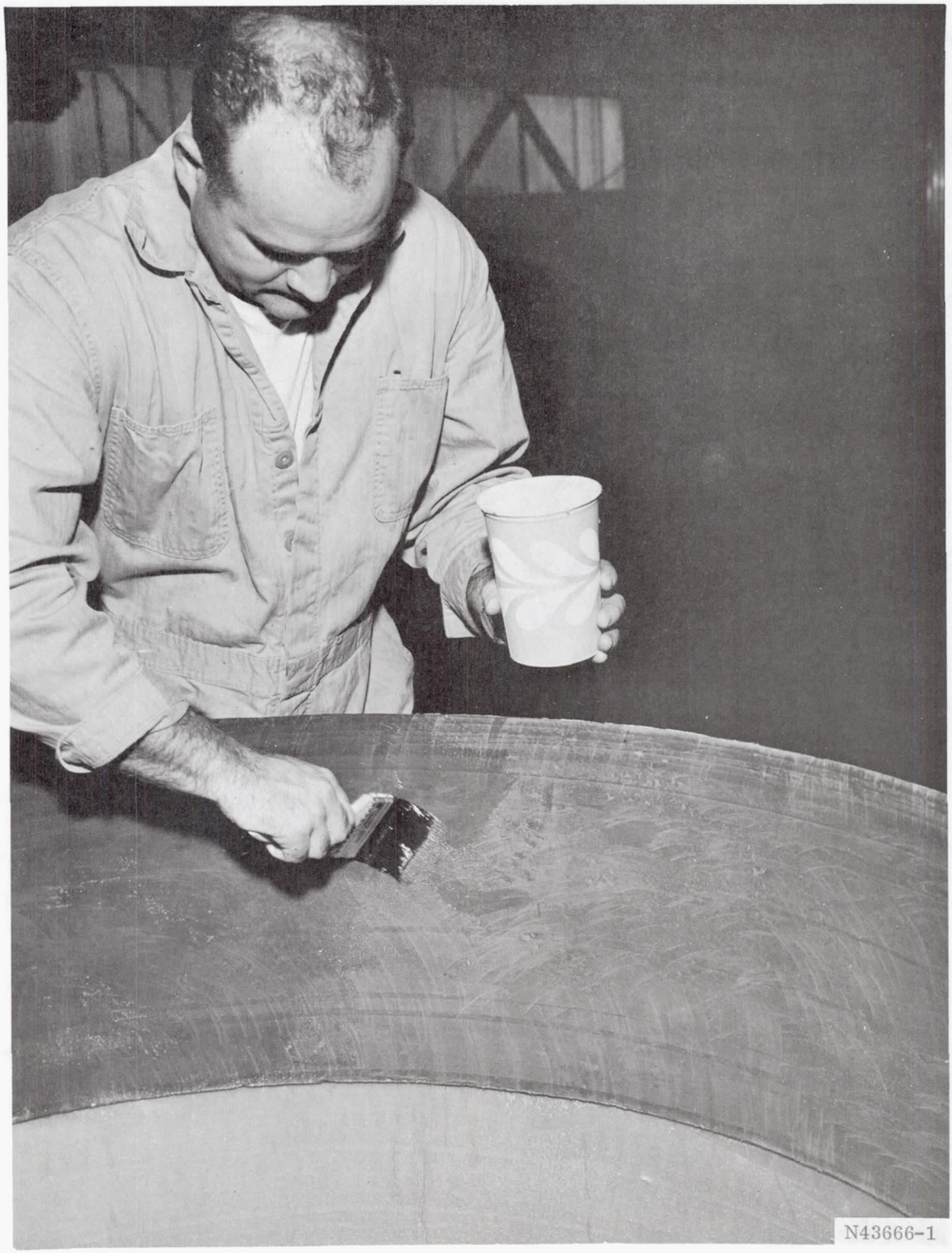

Figure 67. Application of Resin to Skirt Shear Ply Surface of 54-In. Subscale Case

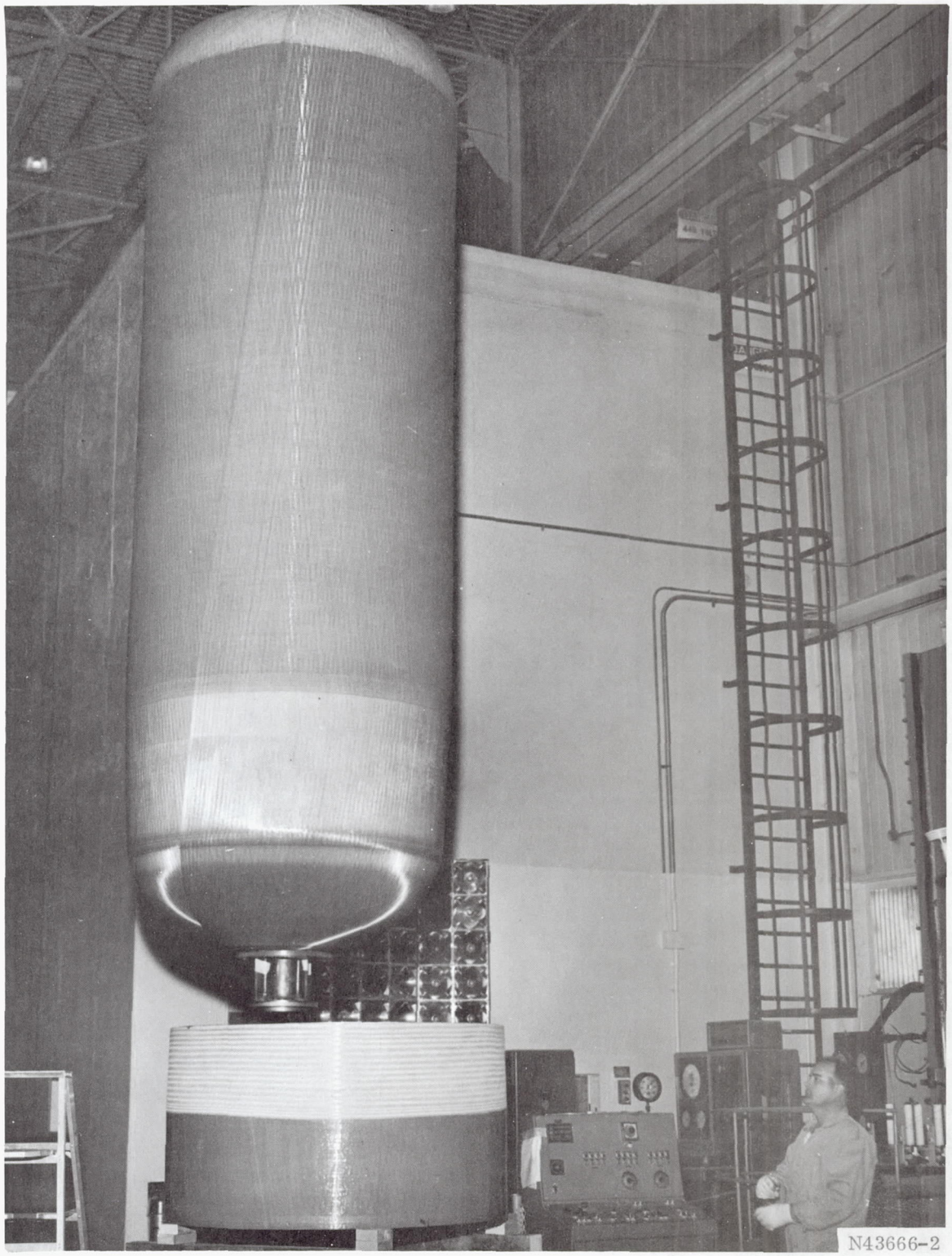

Figure 68. Installation of Skirt in 54-In. Subscale Case

Figure 69. Installation of Fabric Over Outer Shear Ply of 54-In. Subscale Case

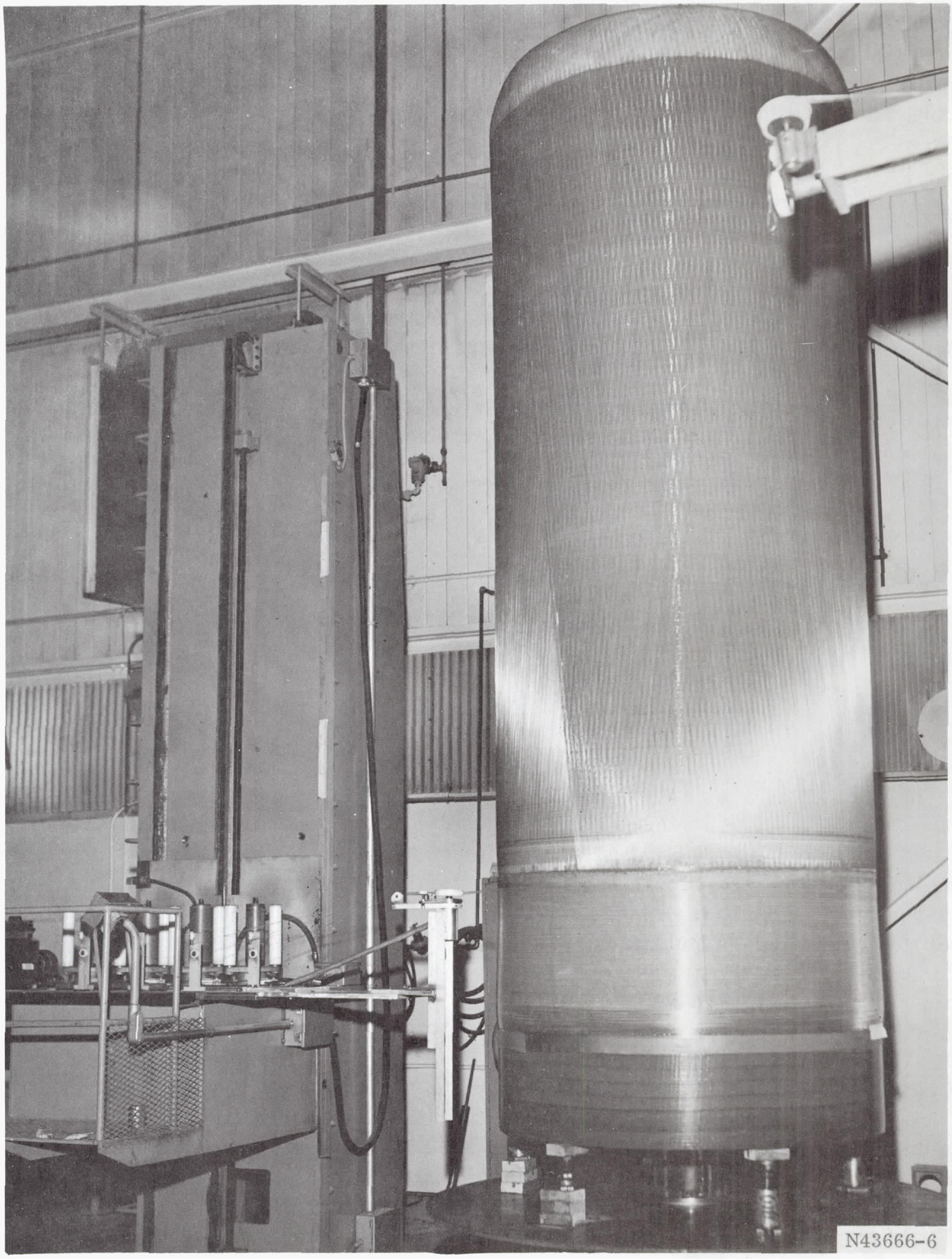

Figure 70. Winding of Hoop Roving Over Area of Outer Shear Ply

The mandrel was easily removed by the addition of water and the breaking up of the wooden bulkheads. The shaft, metal tubes, and sections of wooden bulkheads were removed through the aft port while the sand was washed out through the forward port. During mandrel removal the case was supported by the skirt in the vertical position, forward end down.

The completed case is shown in Figures 71 and 72. The slight discoloration in the area of the aft dome opening is from the application of ambient cure epoxy resin after the aft port machining operation in order to seal off the laminate and protect it from water during mandrel removal. The vessel had a total volume from the face of each boss of 322, 000 cu in. (5.28 m^3) and a total weight including the forward closure of 3, 580 lb (1623.9 Kg). The actual (or estimated) component weights are as follows:

Forward Closure and Bolts	56 lb	(25.4 Kg)	(actual)
Forward Polar Boss	107 lb	(48.5 Kg)	(actual)
Aft Polar Boss	580 lb	(263.1 Kg)	(actual)
Bladder and Shear Ply	117 lb	(53.1 Kg)	(estimated)
Skirt and Overwrap	350 lb	(158.8 Kg)	(estimated)
Pressure Vessel Structure	2, 370 lb	(1075.0 Kg)	(estimated)
Total	3, 580 lb	(1623.9 Kg)	(actual)

Hydrostatic Test

Testing. - The 54-in. (1.372 m) vessel was hydrostatically tested in an open air test bay where pressurization was performed by a portable Halliburton oil field pumping unit. The vessel was supported vertically in a test fixture having a skirt thrust platform, a thrust simulation piston, and eight 2 3/4-in. (69.9 mm) diameter steel tie rods to induce and transfer the thrust loading. The test arrangement with the wooden work platform around the area of the aft dome removed prior to pressurization is shown in Figure 73.

The vessel was pressurized during the proof cycle at an average rate of 639 psig per minute (0.0734 $MN/m^2g/sec$) to an average proof pressure of 3, 940 psig (27.17 MN/m^2g) which was held for a duration of 180 sec prior to pressure release. A visual inspection after the proof test revealed no abnormal crazing or structural degradation. The extensometers were then removed and the pressurization for the the burst cycle commenced. The vessel was pressurized at an average rate of 647 psig per minute (0.744 $MN/m^2g/sec$) until failure occurred at a pressure of 5, 860 psig (40.40 MN/m^2g). The actual pressure traces for both the proof and burst cycles are shown in Figure 74.

Failure occurred in the aft dome just aft of the tangent plane, where the polar wrap fractured completely around the circumference of the dome, driving the case and

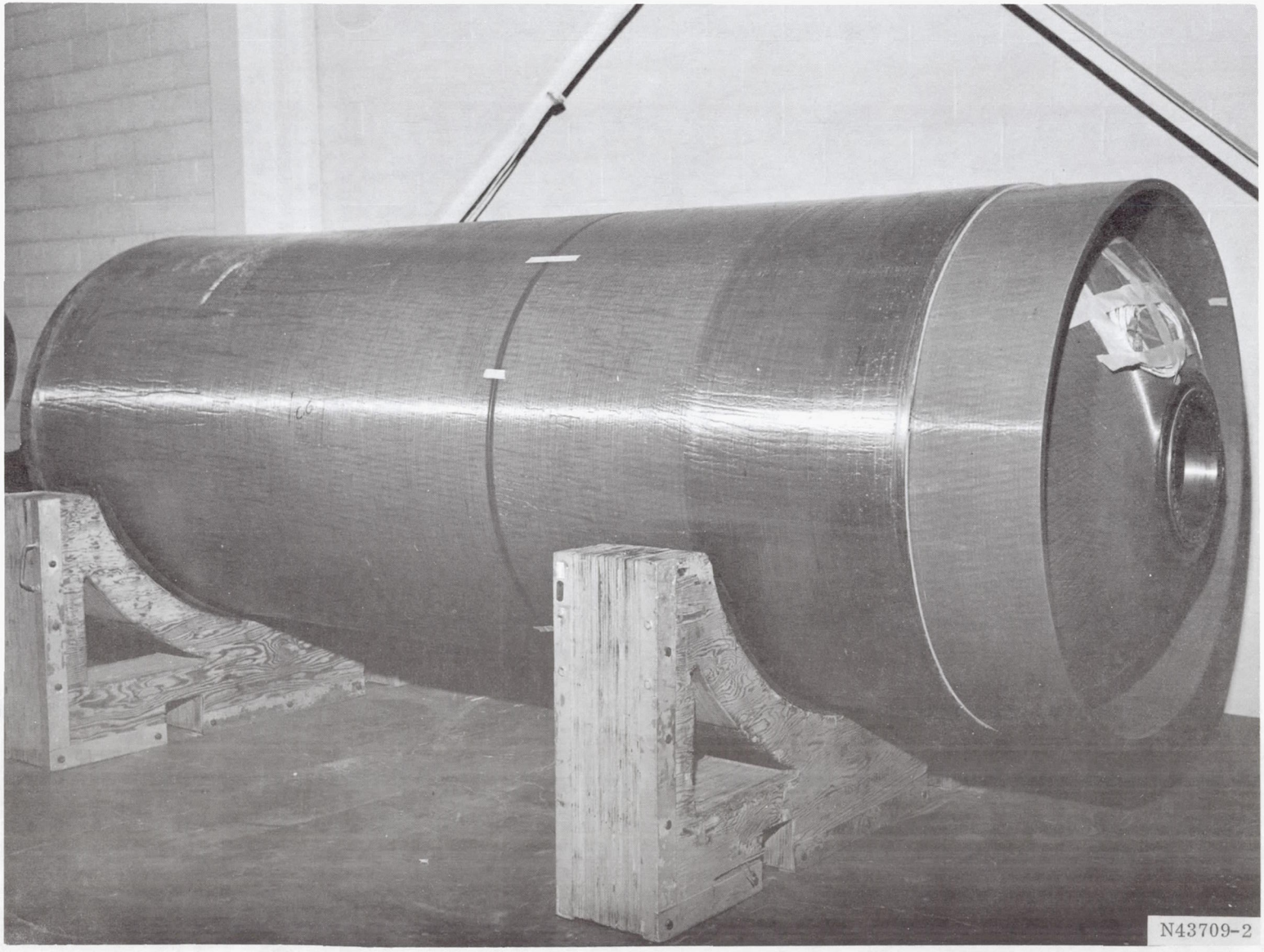

Figure 71. Forward End of 54-In. Subscale Case

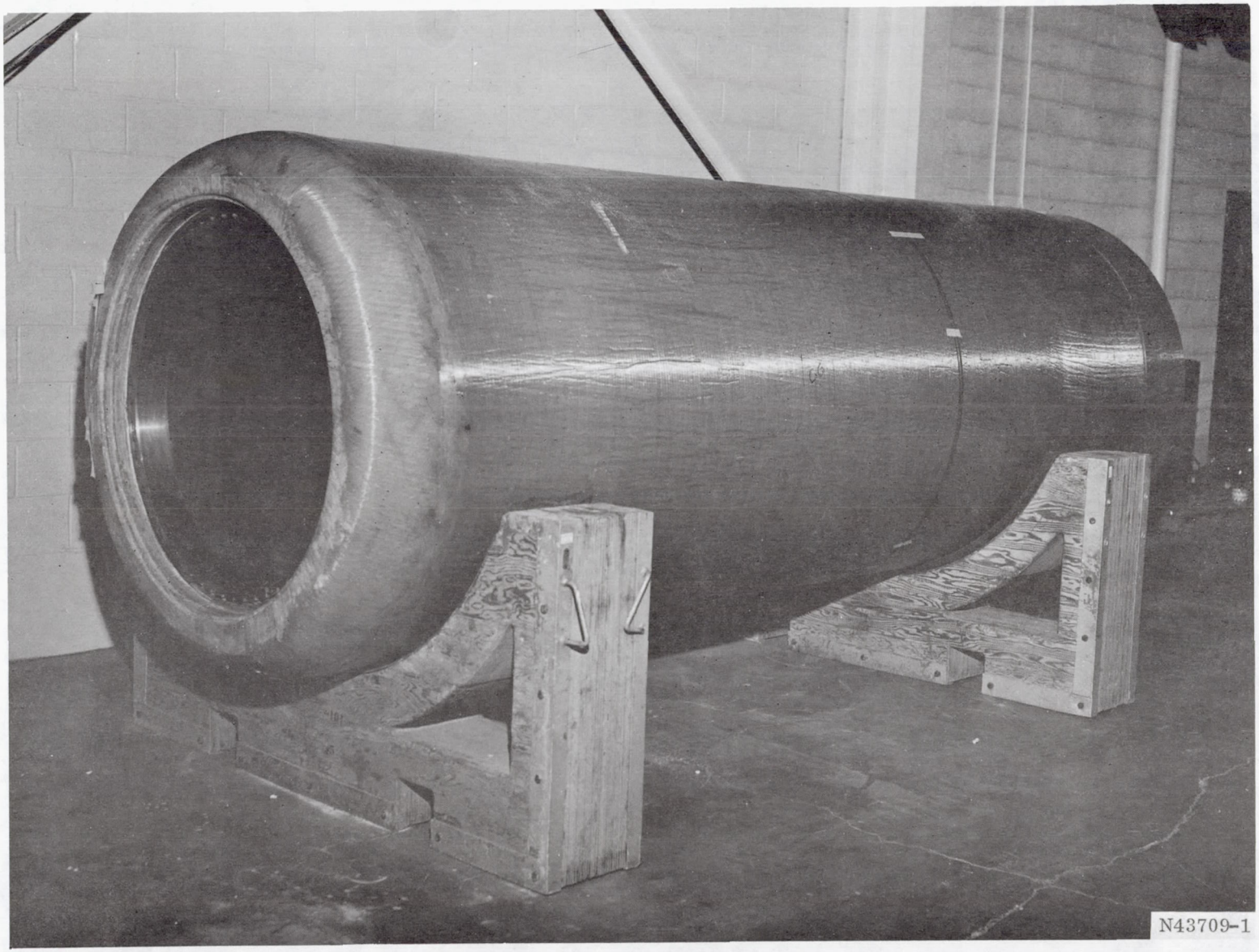

Figure 72. Aft End of 54-In. Subscale Case

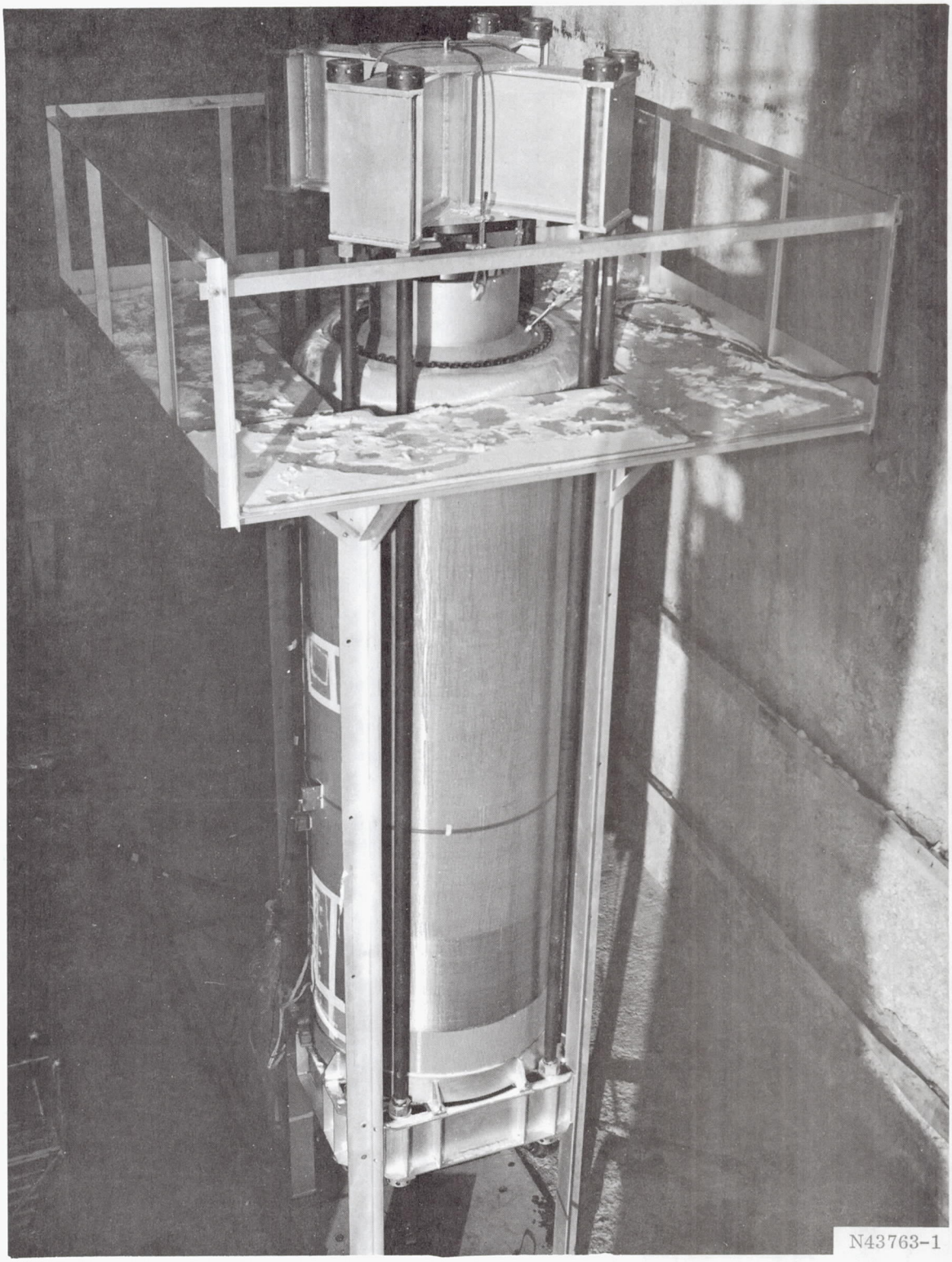

Figure 73. Hydrotest Arrangement for 54-In. Subscale Case

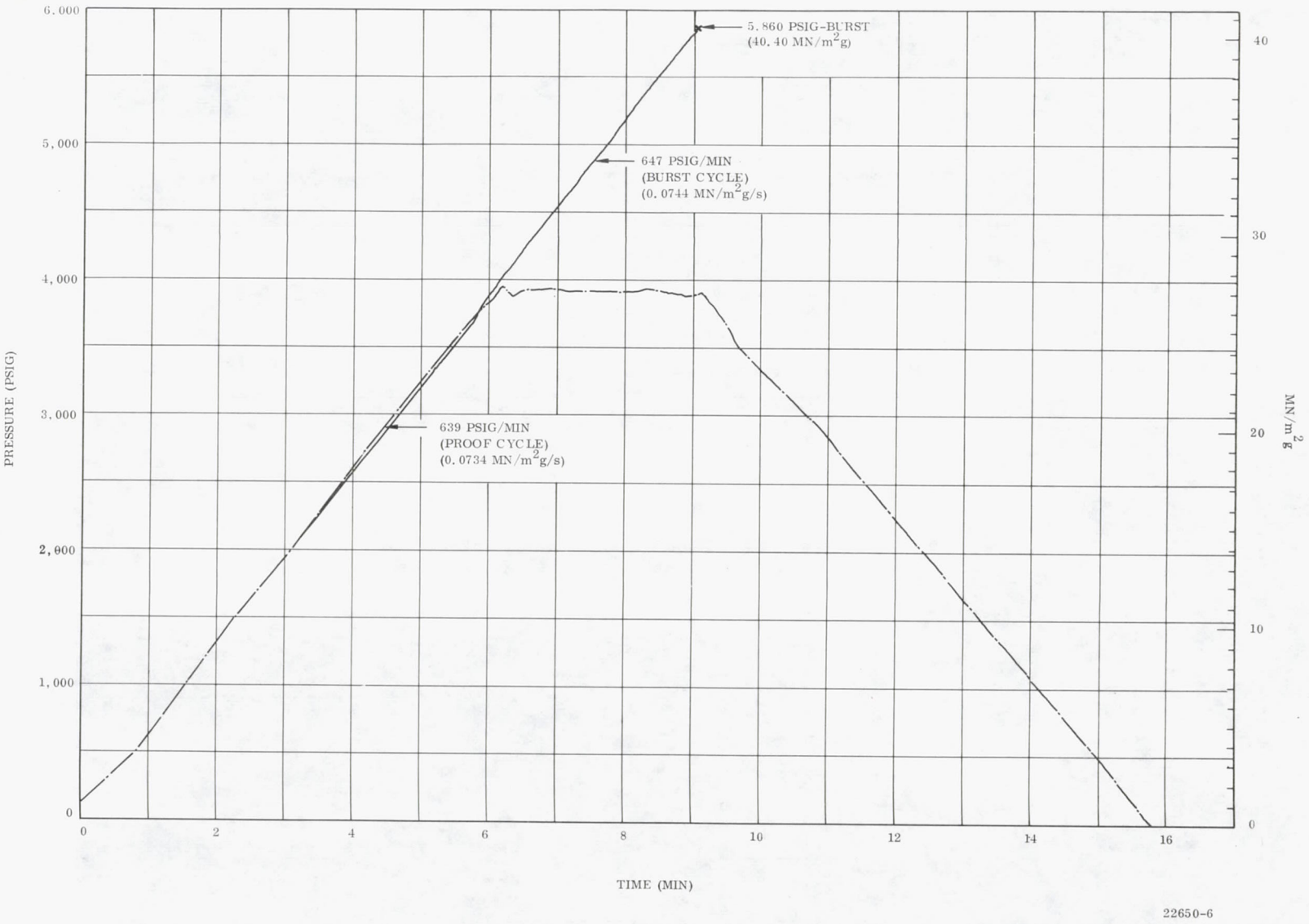

Figure 74. 54-In. Subscale Case Hydrotest Pressure vs Time Trace (Proof and Burst Cycles)

fixture into the floor of the test bay. A two frame photo sequence at failure is shown in Figure 75. The time interval between each frame was 0.0156 second. The vessel immediately after burst is shown in Figure 76. It appeared that the piston housing and aft polar boss broke completely away from case, struck the piston reaction structure, and fell back into the case. The aft dome also completely fractured away, but was restrained by the test fixture and fell back to its original position. A post-test inspection revealed that the instantaneous thrust load of 13,000,000 lb (57.82 MN), which was a result of the aft dome blowing off, caused the skirt inner shear ply to fail at the skirt interface, allowing the case to extrude itself through the skirt and skirt fixture until it hit the bay floor.

Test results. - At the burst pressure of 5,860 psig (40.40 MN/m^2g) the significant loads, stresses, and performance parameters were:

Total Thrust Load	3.02×10^6 lb	(13.43MN)
Skirt Compressive Loads	17,900 lb/in.	(3.134 MN/m)
Hoop Filament Stress	360,000 psi	(2.482 MN/m^2)
Hoop Composite Stress	153,000 psi	(1.055 MN/m^2)
Hoop Composite, σ/ρ	2.1×10^6 in.	(0.523 MNm/Kg)
Polar Filament Stress[a]	349,000 psi	(2.406 GN/m^2)
Polar Composite Stress[a]	176,000 psi	(1.213 GN/m^2)
Polar Composite Stress, σ/ρ [a][b]	2.4×10^6 psi	(16.55 GN/m^2)
Performance Factor, $\frac{pv}{W}$	0.53×10^6 in.	(0.132 MNm/Kg)

[a]At the midsection of the forward dome.
[b]Estimated value; an accurate density measurement could not be made after the test.

Actual measurements taken on the vessel before and after the test were:

Vessel OD (midcylinder)	55.0 in.	(1397. mm)
Cylindrical Wall Thickness	1.06 in.	(26.9 mm)
Cylindrical Wall Density	0.073 lb/cu in.	(2020.6 Kg/m^3)
Cylindrical Wall Resin Content, wt	21 percent	
Skirt OD	54.68 in.	(1388.9 mm)
Skirt Wall Thickness	0.97 in.	(24.6 mm)
Skirt Wall Density	0.073 lb/cu in.	(2020.6 Kg/m^3)
Skirt Wall Resin Content, wt	21 percent	

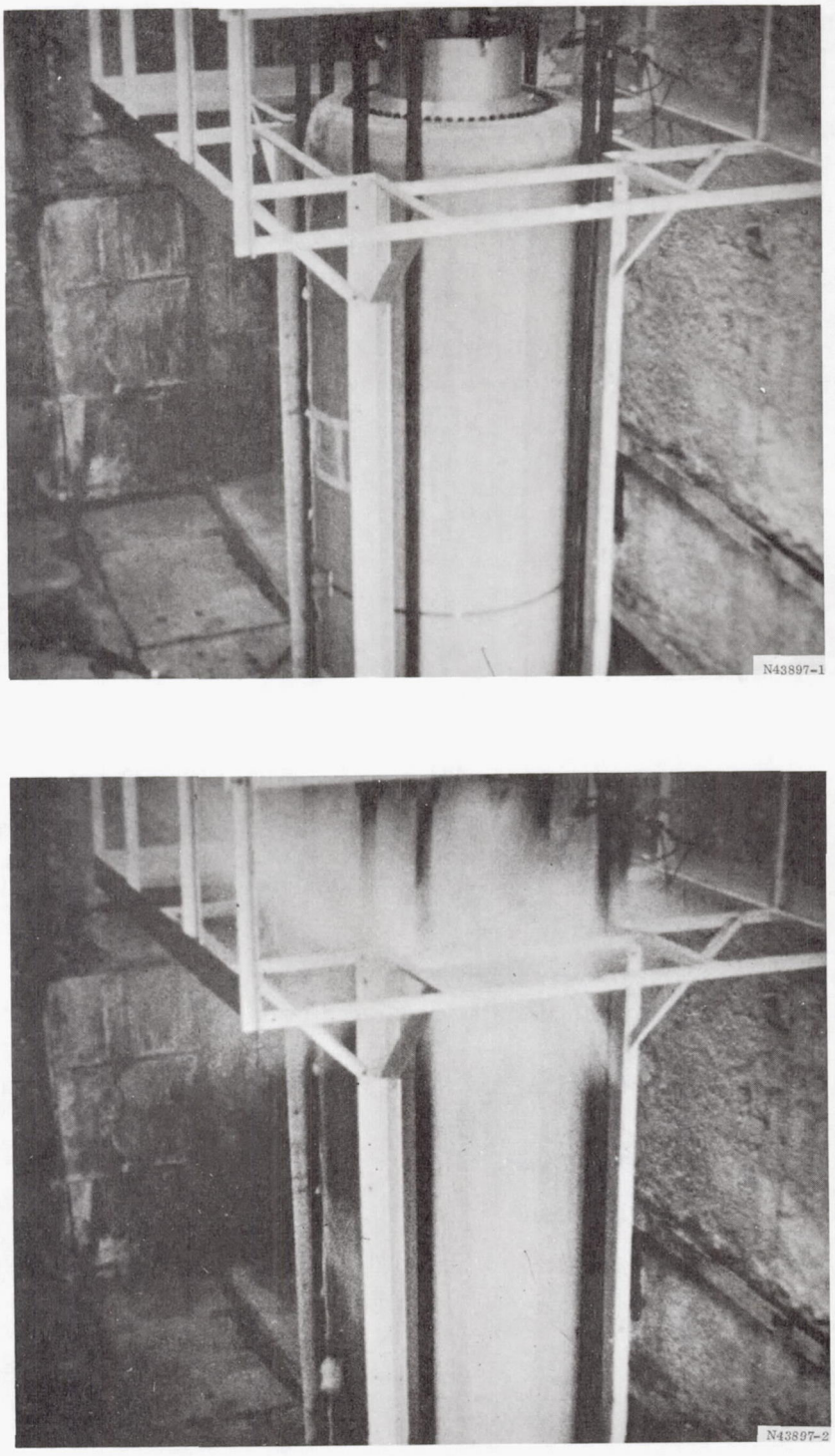

Figure 75. Photo Sequence of 54-In. Subscale Case Burst

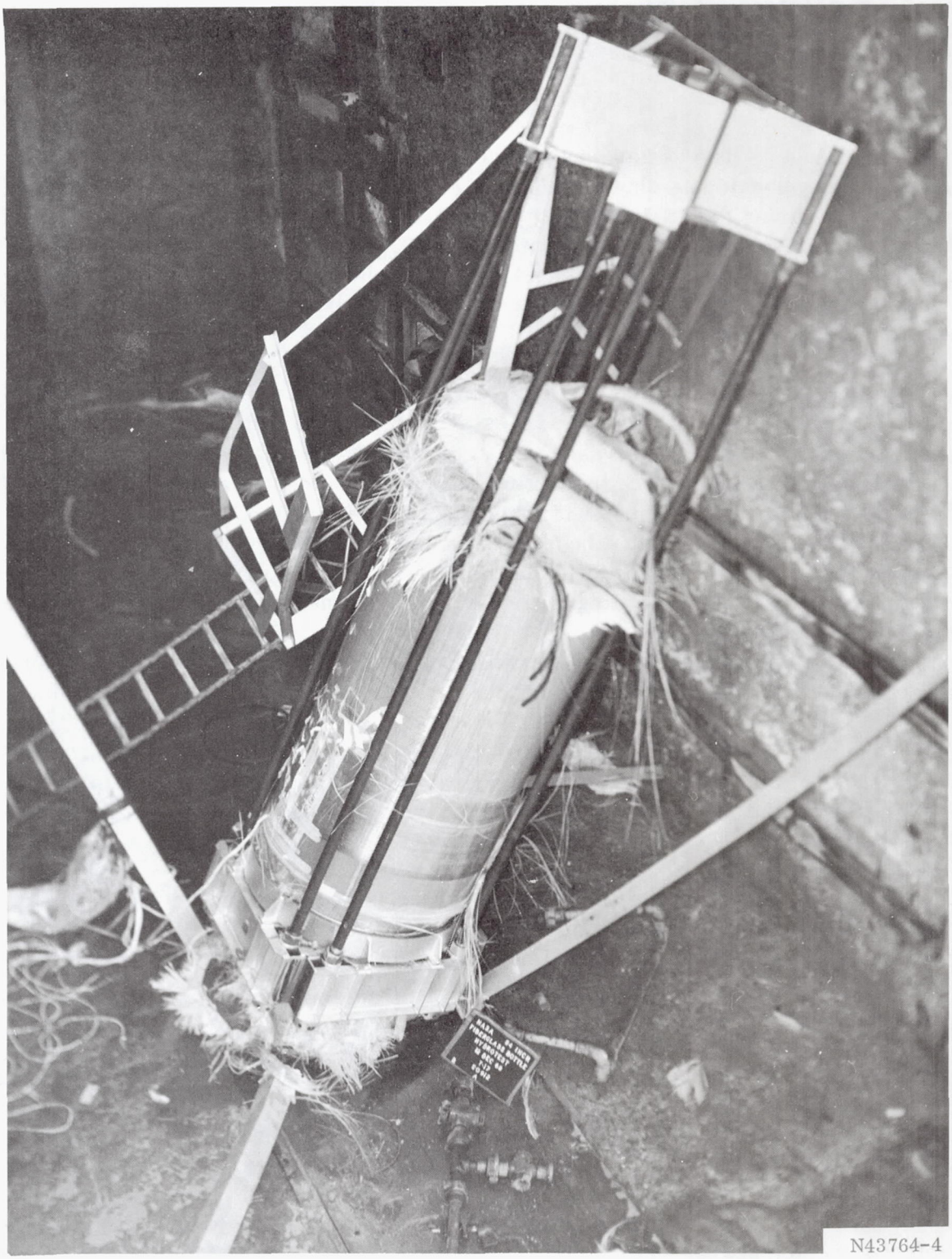

Figure 76. 54-In. Subscale Case After Hydroburst

Aft Dome Density	0.074 lb/cu in.	(2048.3 Kg/m^3)
Aft Dome Resin Content, wt	19 percent	
Case Length	159.7 in.	(4056 mm)

Test data. - The vessel was instrumented with 24 strain gages and four extensometers, located as shown in Figure 77. Both types of gages were identical to those used during the 18-in. vessel tests. The extensometers were again removed after the proof cycle. Only three strain gages (S001, S002, and S004) failed to operate through both cycles; therefore, the strains as measured by the operational gages will be shown for the burst cycle only. The deflections at burst were extrapolated from the extensometer data during proof.

The meridional strain at the external surface of the aft dome is shown in Figure 78. From study of this figure it is evident that the bending stresses were as significant as the membrane stresses. Gage S024 was in the area of failure, and the gage reading reflects the large discontinuity bending moment present in this area. The hoop strain in the aft dome, with gage S023 also in the location of fracture, is shown in Figure 79. The actual hoop strain was considerably lower than predicted due to conservatism in the prediction of the elastic properties and thicknesses of the tape laminates. The resulting increased tape thickness required additional hoop wrap between the polar layer locally at the tangent plane to prevent bridging of the polar wrap. This additional hoop restraint locally in this area also tended to reduce the magnitude of the hoop strain throughout the aft dome.

The axial and hoop strains at the outside surface of the skirt structure are shown in Figure 80. The actual magnitudes were less than predicted due to the conservatism in the prediction of the axial bending stiffness of shell wall in the area of the shear ply.

The axial strain in the shear ply overwrap is shown in Figure 81. The data shows the effects of crazing on the axial bending stiffness of the wall. As the pressure increased, it was noted that the axial bending stiffness decreased and the bending strain became predominant.

The hoop strains near the two tangent planes and at midcylinder are shown in Figure 82. During the burst cycle, gage S016 failed at around 4,300 psig (29.65 MN/m^2g) and thus the data had to be extrapolated to failure pressure. The data reduced from the D001 extensometer during the proof cycle is also shown. The data correlated exactly with the strain gage reading.

The only strain gage on the forward dome to survive the proof cycle was S003, which was located near the tangent plane and indicated a hoop strain of 0.0010 in./in. at burst. Extensometer D002 showed that the axial movement of the forward closure relative to the face of the skirt was 1.0 in. (25.4 mm) at proof pressure, which gives an extrapolated deflection value of 1.47 in. (37.3 mm) at burst. This deflection also

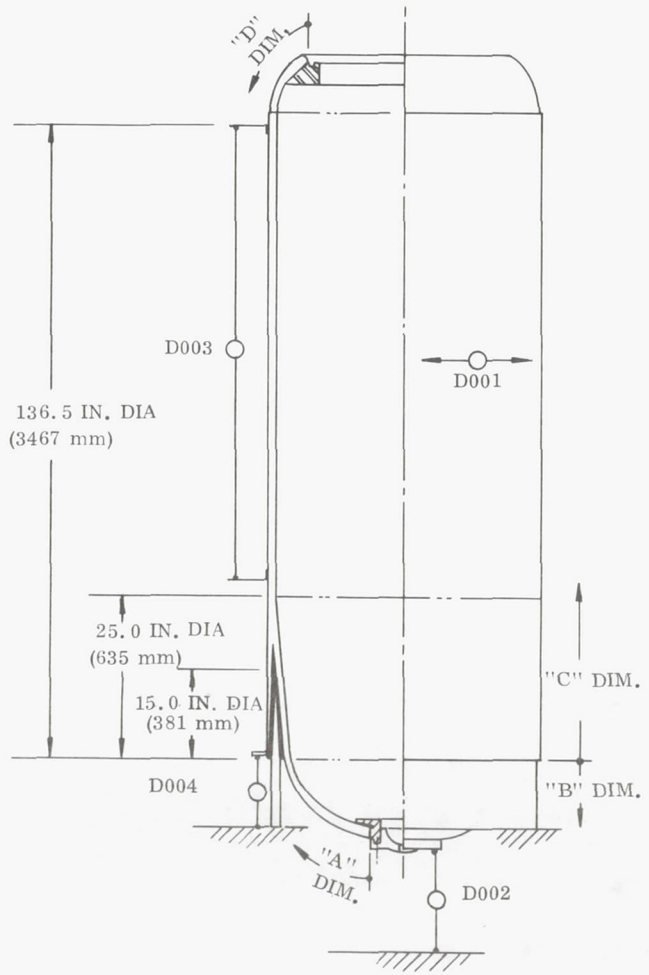

GAGE[a]	ORIENTATION	LOCATION	DIMENSION (IN.)		(mm)
D001	CIRCULAR	MIDCYLINDER	SHOWN		
D002	LONGITUDINAL	FORWARD DOME	SHOWN		
D003	LONGITUDINAL	CYLINDER	SHOWN		
D004	LONGITUDINAL	OVERWRAP	SHOWN		
S001	CIRCULAR	FORWARD DOME	A	6.00	(152.4)
S002	LONGITUDINAL	FORWARD DOME	A	6.00	(152.4)
S003	CIRCULAR	FORWARD DOME	A	18.50	(469.9)
S004	LONGITUDINAL	FORWARD DOME	A	18.50	(469.9)
S005	CIRCULAR	SKIRT	B	1.00	(25.4)
S006	CIRCULAR		B	2.50	(63.5)
S007	CIRCULAR		B	4.00	(101.6)
S008	LONGITUDINAL		B	2.50	(63.5)
S009	LONGITUDINAL	SKIRT	B	4.00	(101.6)
S010	LONGITUDINAL	OVERWRAP	C	4.00	(101.6)
S011	LONGITUDINAL		C	8.00	(203.2)
S012	LONGITUDINAL		C	12.00	(304.8)
S013	LONGITUDINAL		C	15.00	(381.0)
S014	LONGITUDINAL		C	19.00	(482.6)
S015	CIRCULAR	OVERWRAP	C	1.00	(25.4)
S016	CIRCULAR	CYLINDER	C	80.00	(2032.0)
S017	CIRCULAR	CYLINDER	C	136.00	(3454.4)
S018	CIRCULAR	AFT DOME	D	4.00	(101.6)
S019	CIRCULAR		D	7.00	(177.8)
S020	LONGITUDINAL		D	7.00	(177.8)
S021	CIRCULAR		D	9.00	(228.6)
S022	LONGITUDINAL		D	9.00	(228.6)
S023	CIRCULAR		D	11.50	(292.1)
S024	LONGITUDINAL	AFT DOME	D	11.50	(292.1)

[a] D00X - EXTENSOMETER
S00X - STRAIN GAGE

22650-19

Figure 77. 54-In. Subscale Case Instrumentation Location

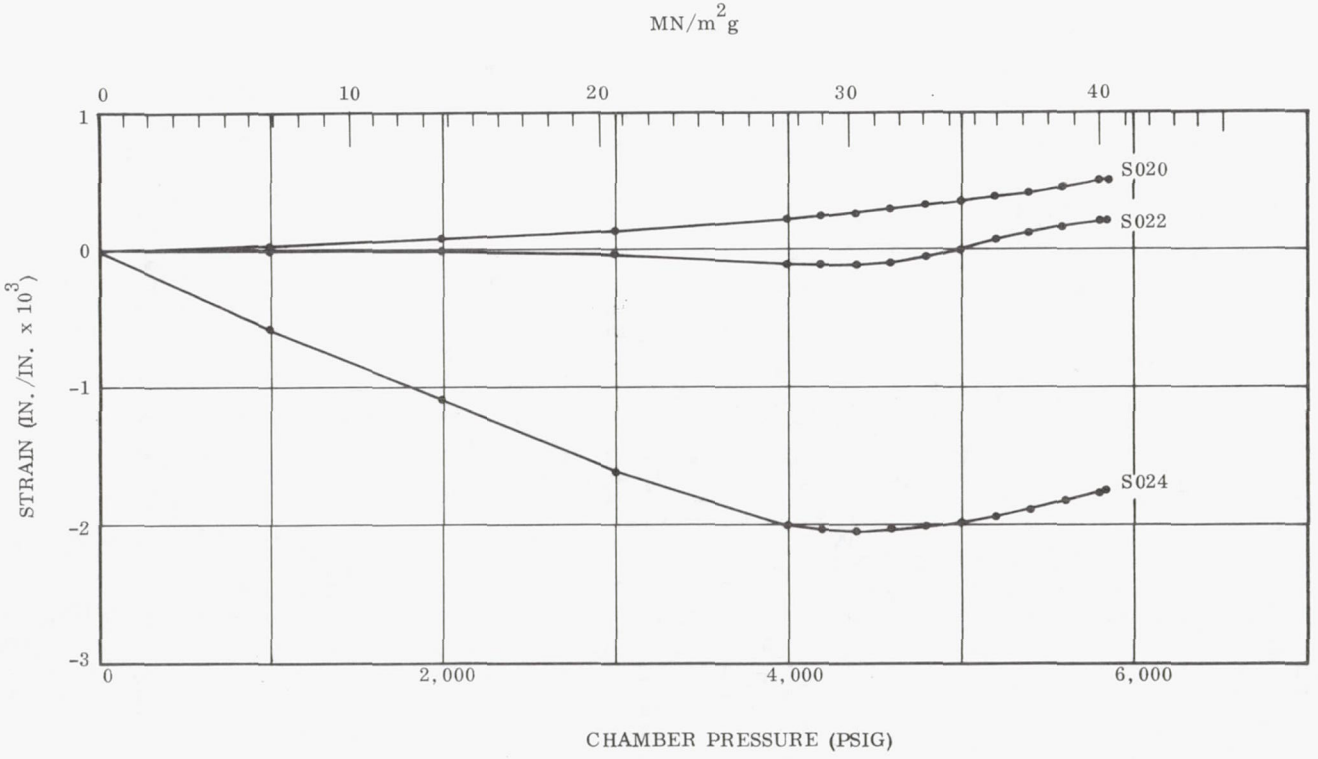

Figure 78. 54-In. Subscale Case Aft Dome Meridional Strain (Burst Cycle)

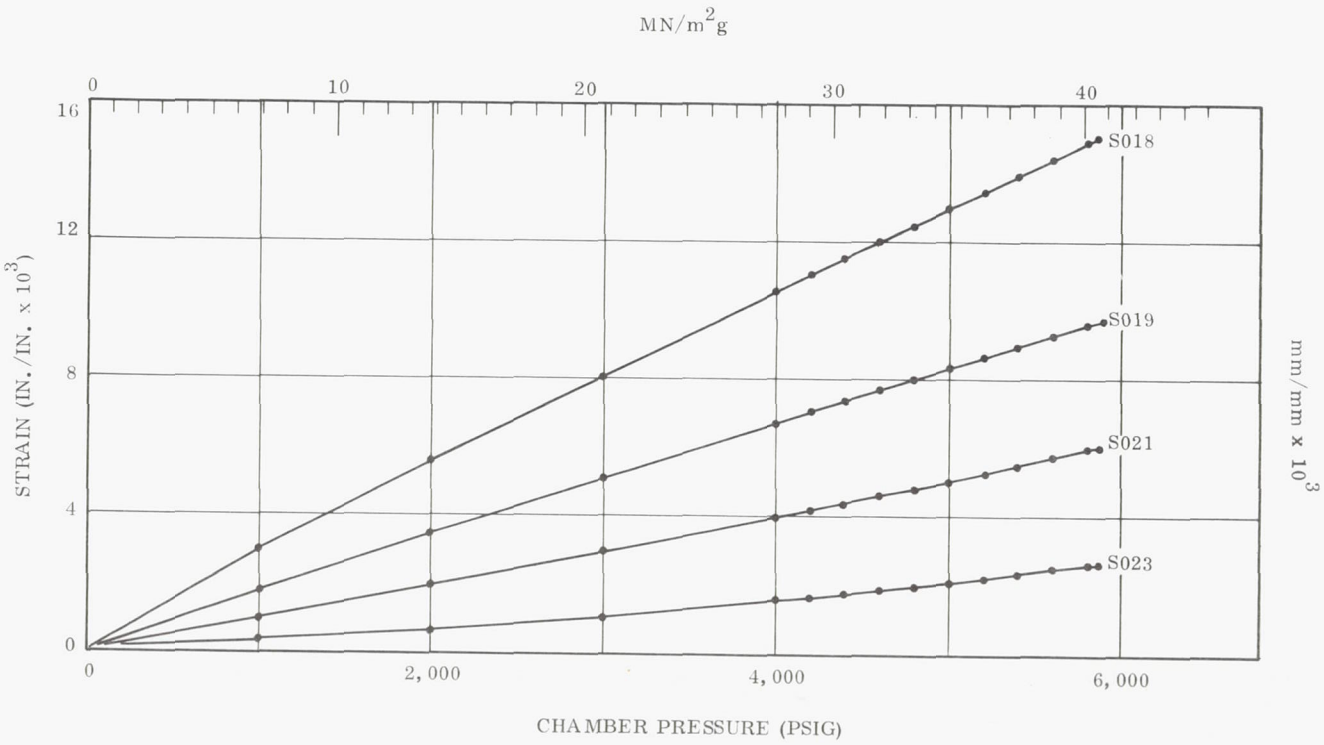

Figure 79. 54-In. Subscale Case Aft Dome Hoop Strain (Burst Cycle)

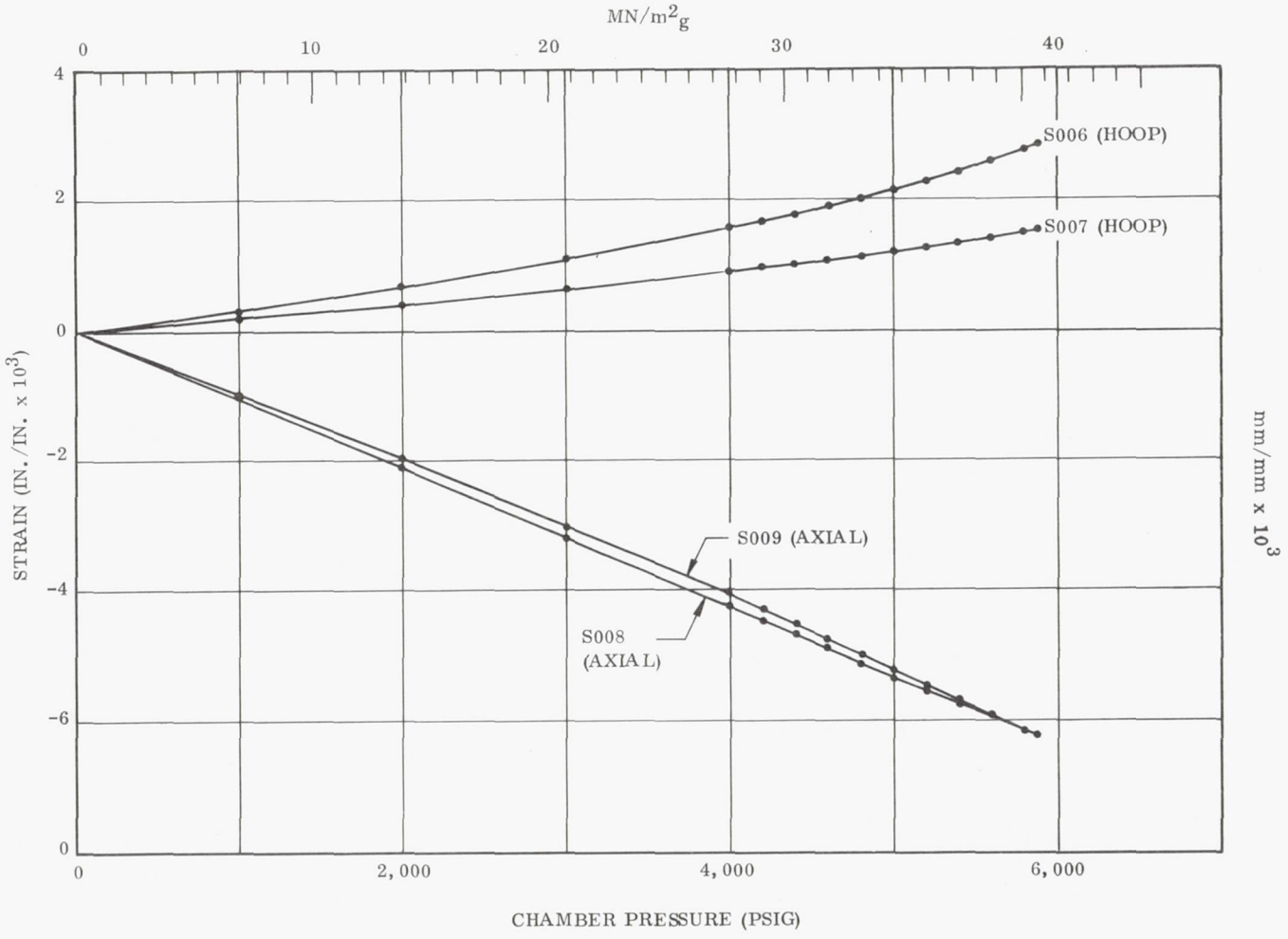

Figure 80. 54-In. Subscale Case Skirt Axial and Hoop Strain (Burst Cycle)

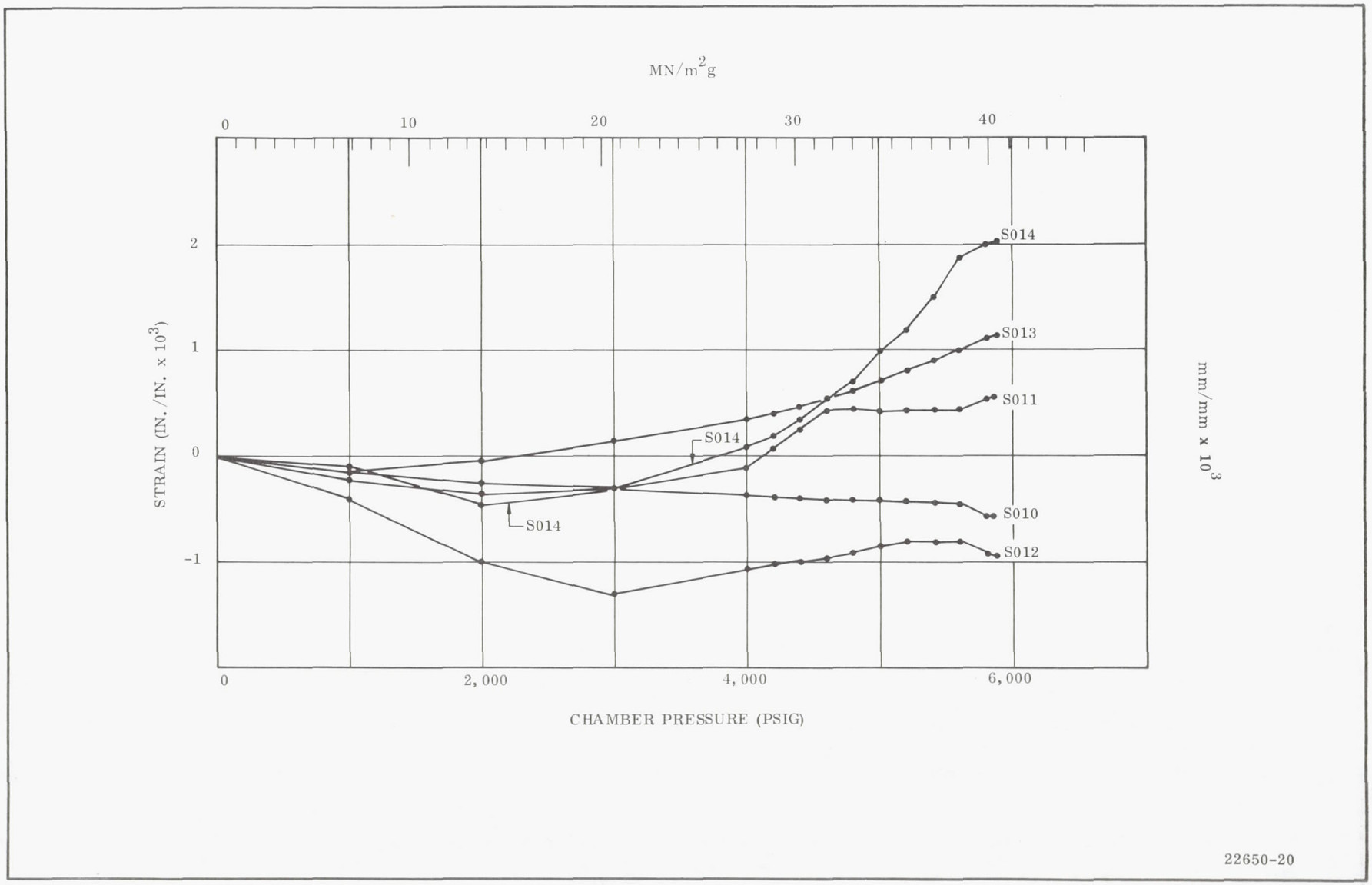

Figure 81. 54-In. Subscale Case Axial Strain in Shear Ply Overwrap (Burst Cycle)

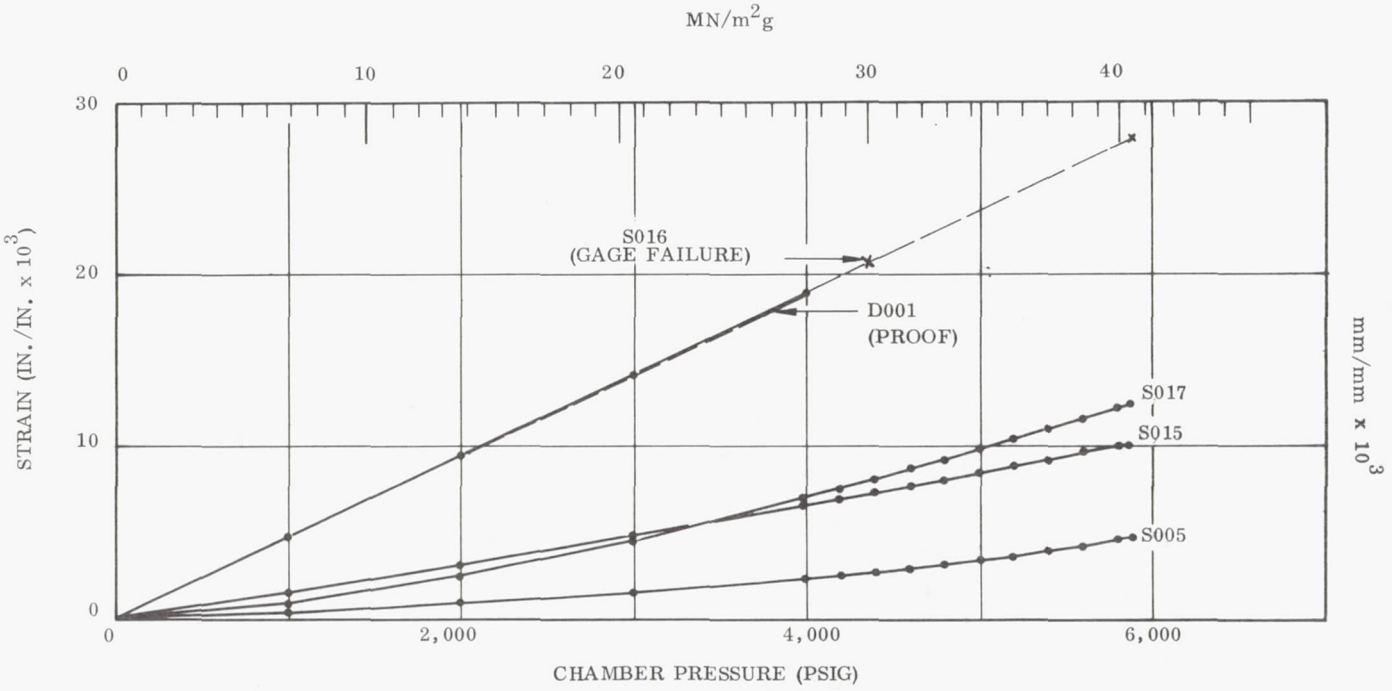

22650-12

Figure 82. 54-In. Subscale Case Hoop Strain in Cylindrical Section (Burst Cycle)

includes the axial movement of skirt relative to the case, which was measured by the D004 extensometer during the proof cycle. The axial displacement of the skirt relative to the forward face of the overwrap at burst as extrapolated from the D004 data was 0.19 in. (4.8 mm). This displacement was not linear with pressure, as is shown in Figure 83, due to the shear strain effects on the stiffness of the rubber.

The axial strain in the cylindrical section of the case, away from skirt attachment area, was recorded by extensometer D003 during the proof cycle. The deflection measurement was linear with pressure, and thus at burst, the extrapolated strain value was 0.022 in./in.

The test data, in general, showed that the 54-in. subscale design was a little conservative and could be made more efficient by utilizing the results of this test data. Based on a comparison of the actual and predicted stresses, it is estimated that an 8 percent reduction in the weight of the structure could be safely made.

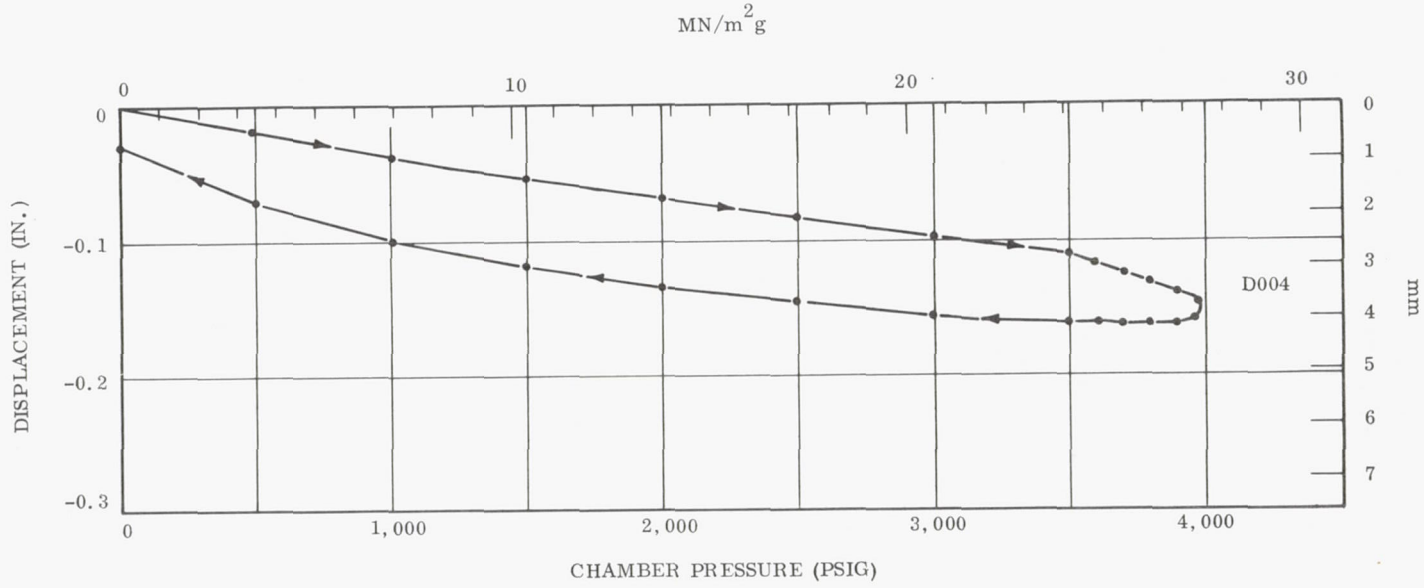

22650-21

Figure 83. 54-In. Subscale Case Axial Movement of Skirt (Proof Cycle)

260-INCH VESSEL DIAMETER DESIGN RECOMMENDATION

The results from the 54-in. (1.372 m) diameter subscale vessel test have demonstrated the basic design concepts, the employed analytical techniques, and the behavior of the structural materials relative to a 260-in. (6.6 m) motor case design. The only task that has not yet been fully demonstrated is the processing techniques involved in the fabrication of a case of this size in order to achieve the required high performance fiberglass structure.

The two critical areas on the 260-in. design were the skirt attachment concept and the structural integrity of the aft dome shell. The test results from the 54-in. subscale has now demonstrated that these two areas are structurally compatible with the loads and geometry associated with a 260-in. motor. The design approaches and methods of analyses were based on conventional shell theories, which are just as readily applicable to a 260-in. motor case as they are to a 18-in. subscale vessel. The only potential variables are the fiberglass composite material properties, which are directly a function of processing quality.

In addition to the two established requirements of a 70 percent aft port opening and a 15,000 lb/in. (2.63 MN/m) skirt loading, the 260-in. motor design will probably have a L/D ratio of 5. The cut dome-polar wrap design has proven to be compatible to the first two requirements by the 54-in. subscale test, and the winding feasibility relative to a L/D ratio of 5 was demonstrated during the fabrication of Vessel 3. The only foreseeable drawbacks to the cut dome-polar wrap design are the handling and installation problems associated with the tape reinforcements during fabrication. Fabricating a 260-in. case with an L/D ratio of 5 in the vertical position seems rather impractical; thus special fixturing would be required to install and hold the reinforcement tapes in place prior to and during the winding of a polar layer.

An alternate design approach would be a helically wound vessel with no dome reinforcements. This case design would be less efficient but would be readily compatible with winding in the horizontal position. However, the design of the helical delivery system would entail considerable technical effort.

Based on the 18- and 54-in. diameter vessel test results, a 260-in. fiberglass motor case would have a probable minimum Performance Factor $\frac{(pV)}{W}$ of 0.53×10^6 in. (0.132 MN.m/Kg) for a cut dome-polar wrap design and 0.45×10^6 in. (0.112 MN.m/Kg) for a helical design. Since the primary merit of a fiberglass motor case is its structural efficiency, it is recommended that a full scale case be of a cut dome-polar wrap design similar to that of the 54-in. subscale. It is foreseeable that the techniques and tooling required to properly install the tape reinforcements and properly wind the polar and hoop patterns could be developed.

The mandrel tooling and fixture designs, along with the case processing procedures, would all have to be developed and proven, just as the case design concept was developed and proven during this program.

Page Intentionally Left Blank

APPENDIX A

VESSEL DESIGNS

Page Intentionally Left Blank

REVISIONS				
ZONE	LTR	DESCRIPTION	DATE	APPROVED

TABLE # 5
SKIRT WRAP SCHEDULE (ITEM 6)

P - POLAR WRAP LAYER, 10°-12°, 201-205 ENDS/IN/PLY
H - HOOP WRAP PLY, 198-202 ENDS/IN/PLY - ITEM 7

LOCATION	SEQ. NO	TYP	QTY	THICKNESS REF
ID	1	P	1 LAYER	.0140 REF (TYP)
	2	H	2 PLY	.0134 REF (TYP)
	3	P	1 LAYER	
	4	H	2 PLY	
	5	P	1 LAYER	
	6	H	2 PLY	
	7	P	2 LAYER	
	8	H	4 PLY	
	9	P	2 LAYER	
	10	H	4 PLY	
	11	P	2 LAYER	
	12	H	4 PLY	
	13	P	2 LAYER	
	14	H	4 PLY	
	15	P	2 LAYER	
	16	H	5 PLY	
	17	P	2 LAYER	
	18	H	5 PLY	
	19	P	2 LAYER	
	20	H	5 PLY	
	21	P	2 LAYER	
	22	H	5 PLY	
	23	P	2 LAYER	
	24	H	5 PLY	
	25	P	2 LAYER	
	26	H	5 PLY	
	27	P	2 LAYER	
	28	H	4 PLY	
	29	P	2 LAYER	
	30	H	4 PLY	
	31	P	2 LAYER	
	32	H	4 PLY	
	33	P	2 LAYER	
	34	H	4 PLY	
	35	P	1 LAYER	
	36	H	2 PLY	
	37	P	1 LAYER	
	38	H	2 PLY	
	39	P	1 LAYER	
OD	40	H	2 PLY	

TABLE # 3 (CONTINUED)

LOCATION	SEQ. NO	TYPE	QTY	TERMINATION FWD	TERMINATION AFT
	35	P	1	—	—
	36	T1 T2 T3 H	1 1 1 4	— — — STA 2-45	STA 14 STA 14 Lt+1.50 STA 14
	37	P	1	—	—
	38	T1 T2 T3 H	1 1 1 4	— — — STA 2-45	STA 14 STA 14 Lt+2.00 STA 14
	39	P	1	—	—
	40	T1 T2 T3 H	1 1 1 4	— — — STA 2-45	STA 14 STA 14 Lt+2.50 Lt+5.50 STA 14
	41	P	1	—	—
	42	T1 T2 T3 H	1 1 1 4	— — — STA 2-45	STA 14 STA 14 Lt+3.00 STA 14
	43	P	1	—	—
	44	T1 T2 T3 H	1 1 1 4	— — — STA 2-45	STA 14 STA 14 Lt+3.50 STA 14
	45	P [5]	1	—	—
	46	T1 T2 T3 H [5]	1 1 1 4	— — — STA 2-45	STA 14 STA 14 Lt+4.0 STA 14
	47	P	1	—	—
	48	T1 T2 T3 H	1 1 1 4	— — — STA 1F (REF DETAIL)	STA 14 STA 1F Lt+4.50 STA 14
	49	P	1	—	—
	50	T1 T2 H	1 1 4	— — STA 1F (REF DETAIL)	STA 14 STA 14 STA 14
	51	P	1	—	—
	52	T1 H	1 8	— STA 1F (REF DETAIL)	STA 14 STA 14
OD	53	P	1	—	—

TABLE #4
CASE WRAP SCHEDULE AFTER SKIRT INSTALLATION

F - FABRIC PLY (.009 IN REF) - ITEM 9
H - HOOP PLY (.0045 IN REF) - ITEM 7
R - RUBBER PLY (.050 IN REF) - ITEM 4

SEQ NO	TYPE	QTY	TERMINATION FWD	POINTS AFT
54		INSTL OF	ITEM 1 (REF)	
55	R	3	SEE DETAIL A	SEE DETAIL A
56	F	2	SEE DETAIL A	SEE DETAIL A
57	H	4	Lo = 0	[8]
58	F	2	SEE DETAIL A	SEE DETAIL A
59	H	4	Lo = 0	[8]
60	F	2	SEE DETAIL A	SEE DETAIL A
61	H	4	Lo = 0	[5]
62	F	2	SE DETAIL A	SEE DETAIL A
63	H	4	Lo = .50	[8]
64	F	2	SEE DETAIL A	SEE DETAIL A
65	H	4	Lo = .50	[8]
66	F	2	SEE DETAIL A	SEE DETAIL A
67	H	4	Lo = .50	[5]
68	F	2	SEE DETAIL A	SEE DETAIL A
69	H	4	Lo = .50	[8]
70	F	2	SEE DETAIL A	SEE DETAIL A
71	H	4	Lo = 1.00	[8]
72	F	2	SEE DETAIL A	SEE DETAIL A
73	H	4	Lo = 1.00	[4]
74	F	2	SEE DETAIL A	SEE DETAIL A
75	H	4	Lo = 1.00	STA W 19 (END SEG) STA 8.18 (SEE DTL.)
76	H	3	Lo = 0	

TABLE # 3
CASE WRAP SCHEDULE PRIOR TO SKIRT INSTALLATION

P - POLAR WRAP LAYER, 6°-8°, 201, 205 ENDS/IN/PLY - ITEM 2
H - HOOP WRAP PLY, 198-202, ENDS/IN/PLY - ITEM 7
T1 - TAPE LAYER, TAPE WIDTH = 4.00, QTY = 60 TAPES - ITEM 19
T2 - TAPE LAYER, TAPE WIDTH = 5.00, QTY = 80 TAPES - ITEM 20
T3 - TAPE LAYER, TAPE WIDTH = 3.00, QTY = 60 TAPES - ITEM 21

LOCATION	SEQ NO	TYPE	QTY	TERMINATION FWD	POINTS AFT
I.D.	1	P	1	—	—
	2	T1 H	1 8	— STA 2-45	STA 1A STA 1A
	3	P	1	—	—
	4	T1 T2 H	1 1 4	— — STA 2-45	STA 1A STA 1A STA 1A
	5	P	1	—	—
	6	T1 T2 T3 H	1 1 1 4	— — — STA 2-45	STA 1A STA 1A Lt+4.50 STA 1A
	7	P	1	—	—
	8	T1 T2 T3 H	1 1 1 4	— — — STA 2-45	STA 1A STA 1A Lt+4.00 STA 1A
	9	P	1	—	—
	10	T1 T2 T3 H	1 1 1 4	— — — STA 2-47	STA 1A STA 1A Lt+3.50 STA 1A
	11	P	1	—	—
	12	T1 T2 T3 H	1 1 1 4	— — — STA 2-47	STA 1A STA 1A Lt+3.00 STA 1A
	13	P	1	—	—
	14	T1 T2 T3 T5 H	1 1 1 1 4	— — — — STA 2-47	STA 1A STA 1A Lt+2.50 Lt+5.50 STA 1A
	15	P	1	—	—
	16	T1 T2 T3 H	1 1 1 4	— — — STA 2-47	STA 1A STA 1A Lt+4.50 STA 1A
	17	P	1	—	—
	18	T1 T2 T3 H	1 1 1 4	— — — STA 2-47	STA 1A STA 1A Lt+4.00 STA 1A
	19	P	1	—	—
	20	T1 T2 T3 H	1 1 1 4	— — — STA 2-47	STA 1A STA 1A Lt+3.50 STA 1A
	21	P	1	—	—
	22	T1 T2 T3 H	1 1 1 4	— — — STA 2-47	STA 1A STA 1A Lt+3.0 STA 1A
	23	P	1	—	—
	24	T1 T2 T3 T5 H	1 1 1 1 4	— — — — STA 2-47	STA 1A STA 1A Lt+2.50 Lt+5.00 STA 1A
	25	P	1	—	—
	26	T1 T2 T3 H	1 1 1 4	— — — STA 2-47	STA 1A STA 1A Lt+2.00 STA 1A
	27	P	1	—	—
	28	T1 T2 T3 T5 H	1 1 1 1 4	— — — — STA 2-47	STA 1A STA 1A Lt+1.50 Lt+3.50 STA 1A
	29	P	1	—	—
	30	T1 T2 T3 H	1 1 1 4	— — — STA 2-47	STA 1A STA 1A Lt+1.00 STA 1A
	31	P	1	—	—
	32	T1 T2 T3 T5 H	1 1 1 1 4	— — — — STA 2-47	STA 1A STA 1A Lt+.50 Lt+3.00 STA 1A
	33	P	1	—	—
	34	T1 T2 T3 H	1 1 1 4	— — — STA 2-47	STA 1A STA 1A Lt+1.00 STA 1A

(CONT.)

TABLE #1
FWD CASE DOME

STATION	W ±.020 RADIUS	X ±.020 DIM	
1F	26.480	0	CONICAL SECTION
2F	25.034	24.985	
3F	24.940	25.947	
4F	24.758	26.917	
5F	24.495	27.857	
6F	24.154	28.774	
7F	23.741	29.658	
8F	23.257	30.508	
9F	22.708	31.317	
10F	22.100	32.083	
11F	21.457	32.803	
12F	20.725	33.476	
13F	19.969	34.095	
14F	19.175	34.667	
15F	18.346	35.189	
16F	17.488	35.661	
17F	16.605	36.085	
18F	15.700	36.461	
19F	14.774	36.790	
20F	13.835	37.071	
21F	12.881	37.335"	
22F	11.800	37.580	

TABLE #2
AFT CASE DOME

STATION	Y ±.020 RADIUS	Z ±.020 DIM
1A	26.480	0
2A	26.440	.494
3A	26.372	.989
4A	26.253	1.484
5A	26.085	1.970
6A	25.877	2.424
7A	25.629	2.860
8A	25.351	3.286
9A	25.053	3.694
10A	24.735	4.092

SHEET 2 7U42115

QTY REQD PER DASH NO.	ITEM NO.	CODE IDENT	PART OR IDENTIFYING NO.	NOMENCLATURE OR DESCRIPTION	MATERIAL	SPECIFICATION	ZONE

LIST OF MATERIAL OR PARTS LIST

UNLESS OTHERWISE SPECIFIED DIMENSIONS ARE IN INCHES
MACHINED SURFACES
ALL SHARP EDGES TO BE BROKEN
ALL WELDING PER MIL-STD-
DIMENSIONS PRE-WELD
TANK SHALL BE FREE FROM
ALL WELDING TO BE PERFORMED BY
TOLERANCES PER
SURFACES ROUGHNESS
ALL ASA 36.1
ALL FINISHED SURFACES

CONTR NO.
DRAWN 2-24-64
CHECKED

THIOKOL CHEMICAL CORPORATION
WASATCH DIVISION BRIGHAM CITY, UTAH

NASA 54 INCH DIA VESSEL

NEXT ASSEMBLY | USED ON | PART NO.
APPLICATION

SIZE E | CODE IDENT NO. 07703 | 7U42115
SCALE | SHEET 2 OF 3

Page Intentionally Left Blank

REVISIONS				
ZONE	LTR	DESCRIPTION	DATE	APPROVED

NOTES:

1. MARK PART NO PER TUS-59-33, METHOD G.
2. THE POLAR WRAP SHALL HAVE AN ORIENTATION OF 6°00'±0°30' IN THE CYLINDRICAL SECTION. EACH LAYER SHALL CONSIST OF 2 PLIES WITH AN END DENSITY OF 201-205 END/IN/ PLY. EACH PLY SHALL BE WOUND AT A NOMINAL BAND WIDTH OF .394 INCHES AND WITH A TENSION OF .6±.1 LBS/END.
3. THE HOOP WRAP SHALL CONSIST OF PLIES HAVING 198-202 END/IN/PLY WOUND AT A NOMINAL BAND WIDTH OF .400 INCHES AND WITH A TENSION OF .6±.1 LBS/END.
4. THE POLAR WRAP SHALL HAVE AN ORIENTATION OF 11°30' ±1°30' EACH LAYER SHALL CONSIST OF 2 PLIES WITH AND END DENSITY OF 201-205 END/IN/PLY. EACH PLY SHALL BE WOUND AT A NOMINAL BAND WIDTH OF .390 INCHES AND WITH A TENSION OF .6±.10 LBS/END.
5. GLASS FILAMENTS SHALL BE S-994 WITH HTS FINISH, STYLE XP7030 (U.S. POLYMERIC OR EQUIV). PREIMPREGNATED WITH E717 EPOXY RESIN (US. POLYMERIC OR EQUIV.) RESIN CONTENT SHALL BE 20-25% BY WEIGHT. PER SPECIFICATION TWS-RM-1028.
6. GLASS FABRIC SHALL BE STYLE S/34-901 MIL-C-9084, TYPE V PREIMPREGNATED WITH E717 EPOXY RESIN (U.S. POLYMERIC OR EQUIV.) RESIN CONTENT SHALL BE 27-33% BY WEIGHT.
7. PRIOR TO BONDING ITEM 4 TO ITEMS 2 & 3 WITH ITEM 12 CLEAN & SAND BLAST ITEMS 2 & 3 IN AREA OF BOND.
8. PARKER SEAL CO., CULVER CITY, CALIF. CODE IDENT 83259.
9. SILICA FILLED NBR, GEN-GARD V-45, .030 PLY THICKNESS, GENERAL TIRE & RUBBER CO, AKRON, OHIO.
10. SILICONE GREASE, DC11, DOW CORNING CORP, MIDLAND, MICH.
11. ALL MATERIAL LOT OR SERIALIZATION NUMBERS SHALL BE RECORDED IN THE APPROPRIATE PART QUALITY CONTROL RECORDS
12. CURE THE -01 & -02 ASSEMBLIES FOR 6 HOURS AT A GLASS-RESIN COMPOSITE TEMPERATURE OF 300°-320° F.

13. LIQUID EPOXY RESIN EQUIVALENT TO THE US POLYMERIC E-717 EPOXY RESIN SYSTEM.
14. ROUGHEN THE CONTACT SURFACE OF ITEM 1 & PAINT THE CONTACT SURFACES OF ITEMS 1 & 5 WITH ITEM 13
15. .25 APT OF PRIOR FABRIC LAYER.
16. 1.00 APT OF PRIOR FABRIC LAYER.
17. INSTRUMENTATION SHALL BE INSTALLED IN ACCORDANCE WITH DRAWING 7U41666.
18. UNIDIRECTIONAL PREPREG TAPE REINFORCED WITH S-901 GLASS FILAMENTS AND EPOXY RESIN (SCOTCHPLY XP-2515 OR EQUIV.) RESIN CONTENT SHALL BE 25±3% BY WEIGHT AND THE FILAMENT END DENSITY SHALL BE 198-205 ENDS/IN/TAPE.
19. THE T1 TAPE LAYER SHALL CONSIST OF 60 TAPES WITH A TAPE WIDTH OF 4.00 IN.
20. THE T2 TAPE LAYER SHALL CONSIST OF 80 TAPES WITH A TAPE WIDTH OF 3.00 IN.
21. THE T3 TAPE LAYER SHALL CONSIST OF 60 TAPES WITH A TAPE WIDTH OF 3.00 IN.
22. SILICA FILLED NBR RUBBER .030 PLY THICKNESS PER TUS-60-69, TYPE I.
23. ITEM 9 SHALL BE INSTALLED WITH THE "FILL" PARALLEL TO THE AXIS OF THE -01 ASSEMBLY.
24. THE FIRST LAYER OF TAPES (ITEM 19) SHALL BE LAYED UP TANGENT TO A 20.20-20.66 RADIUS. THE TANGENTIAL RADIUS FOR THE SUBSEQUENT TAPE LAYERS SHALL BE CONTINUALLY STAGGERED OUTBOARD APPROX. .02 INCHES PER EACH TAPE LAYER.
25. RECORD DIMENSIONS PRIOR TO MANDREL REMOVAL
26. RECORD DIMENSIONS AFTER MANDREL REMOVAL
27. APPLY SUFFICIENT AXIAL FORCE ON ITEM 1 DURING THE INSTALLATION OF ITEM 1 TO PRODUCE A POSITIVE INTERFACE PRESSURE ALONG THE ENTIRE CONTACT AREA.
28. AXIS [C] IS DEFINED AS A LINE PASSING THRU THE CENTERS OF DIAMETERS [A] & [B].
29. MOLYKOTE TYPE Z, THE ALPH-MOLYKOTE CORP., STAMFORD, CONN. OR EQUIV.
30. COAT ITEM 17 WITH ITEM 23 AND TORQUE TO 130-140 FT/LBS.
31. AFTER COMPLETION OF SEQUENCE NO. 80, ASSUME VERTICAL CUT AT STA 87. IT SHOULD CUT EXCESS SPOOL IN, TERMINATE IN WRAP AT STA 130. RE, 6.25-.100 IN. END OF STA 87.

ITEM NO.	CODE IDENT	PART OR IDENTIFYING NO.	NOMENCLATURE OR DESCRIPTION	MATERIAL	SPECIFICATION	ZONE
			QTY REQD PER DASH NO. -08 -02 -01			
25			8046	4TL	4840	
24			CLOSURE	MAKE FROM	7U41361-04	
23			LUBRICANT	29		
22			FILLED NBR	8		
21			T3 TAPE LAYER	31	18	
20			T2 TAPE LAYER	30	19	
19			T1 TAPE LAYER	19	18	
		7U41666-	INSTRUMENTATION	17		
18						
17		MS-20010-10	BOLT			
16			LUBRICANT	10		
15		S-452-N300-9	BACK-UP RING			
14			O RING	8		
13			EPOXY RESIN	5		
12			ADHESIVE	CHEMLOCK 220	TWS-MJ-210	
11						
10		-08	FWD CLOSURE			
9			FIBERGLASS, FABRIC	6		
8						
7	A/R		HOOP PLY	1 3		
6	A/R		POLAR LAYER	4 3		
5	A/R		POLAR LAYER	2 3		
4	A/R		FILLED NBR	12		
3	1	7U42048-02	AFT POLAR BOSS			
2	1	7U42042-01	FWD POLAR BOSS			
1	1	-02	SKIRT			

SHEET 2 OF 3 7U42115

LIST OF MATERIAL OR PARTS LIST

NEXT ASSEMBLY	USED ON	PART NO.
APPLICATION		

UNLESS OTHERWISE SPECIFIED DIMENSIONS ARE IN INCHES TOLERANCES .XX ±.01 .XXX ±.010 ANGLES ± 0°30' FRACTIONS ± 1/64 BREAK SHARP EDGES .005-.015 ALL SMALL FILLETS .020-.045 MACHINING PER MIL-STD-8 EMBRITTLING PER MIL-STD-8 WELD SYMBOLS PER AWS A2.4-67 NONDESTRUCTIVE TESTING SYMBOLS PER MIL-STD-22 SURFACE TEXTURE TO STD-11 APPLIES SURFACE ROUGHNESS SYMBOLS PER ASA B46.1 ALL FINISHED SURFACES 125 √

CONTR NO.
DRAWN Ann Hannah 6-18-68
CHECKED
APPROVED
RELEASED

THIOKOL CHEMICAL CORPORATION
WASATCH DIVISION BRIGHAM CITY, UTAH

NASA 54 INCH DIA VESSEL

SIZE E | CODE IDENT NO. 07703 | 7U42115

SCALE 1/8 SHEET 1 OF 3

Page intentionally left blank

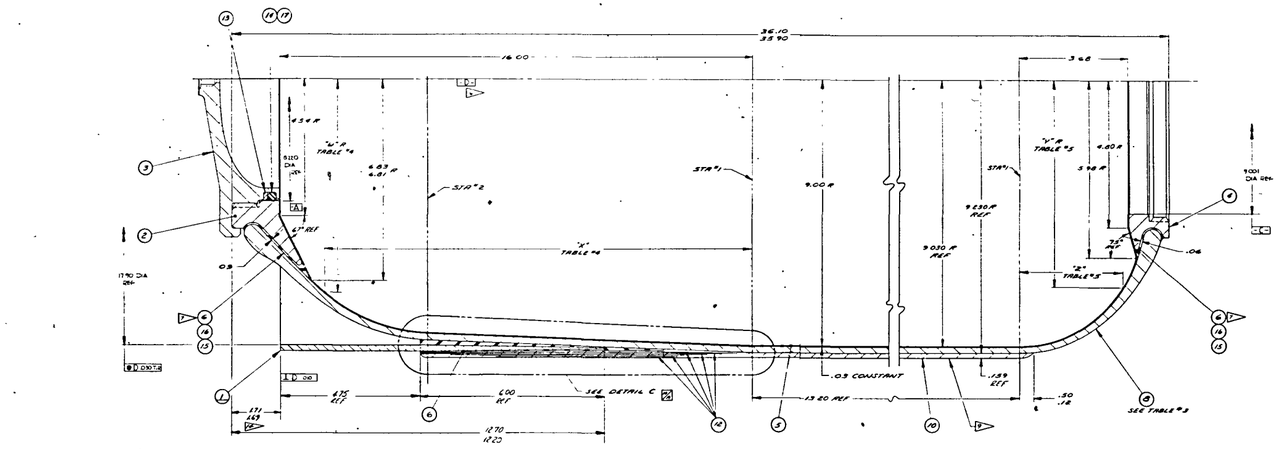

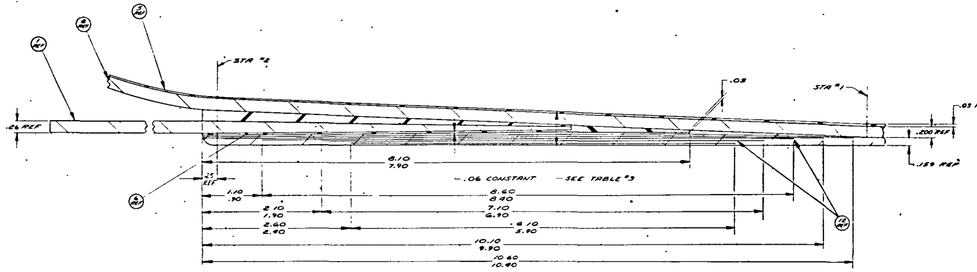

DETAIL C
SCALE 1

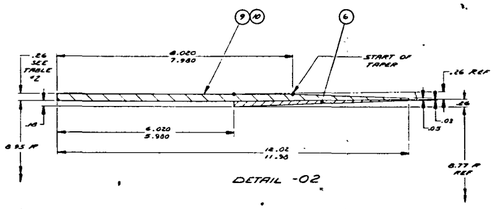

DETAIL -02

REVISIONS			
ZONE	LTR	DESCRIPTION	DATE
	A	SEE SHT 1	

9U41359 A

SPT DRWG TBE SHEET NO	ITEM NO	CODE IDENT	PART OR IDENTIFYING NO	NOMENCLATURE OR DESCRIPTION	MATERIAL	SPECIFICATION	SCRAP

LIST OF MATERIAL OR PARTS LIST

NEXT ASSEMBLY	USED ON	PART NO.
APPLICATION		

THIOKOL CHEMICAL CORPORATION
Wasatch Division — Brigham City, Utah

NASA 18 INCH DIA
VESSEL NO. 1

SIZE	CODE IDENT NO	DRAWING NO
J	07703	9U41359

SCALE 1/2 | SHEET 3

9U41359 | 3

Page intentionally left blank

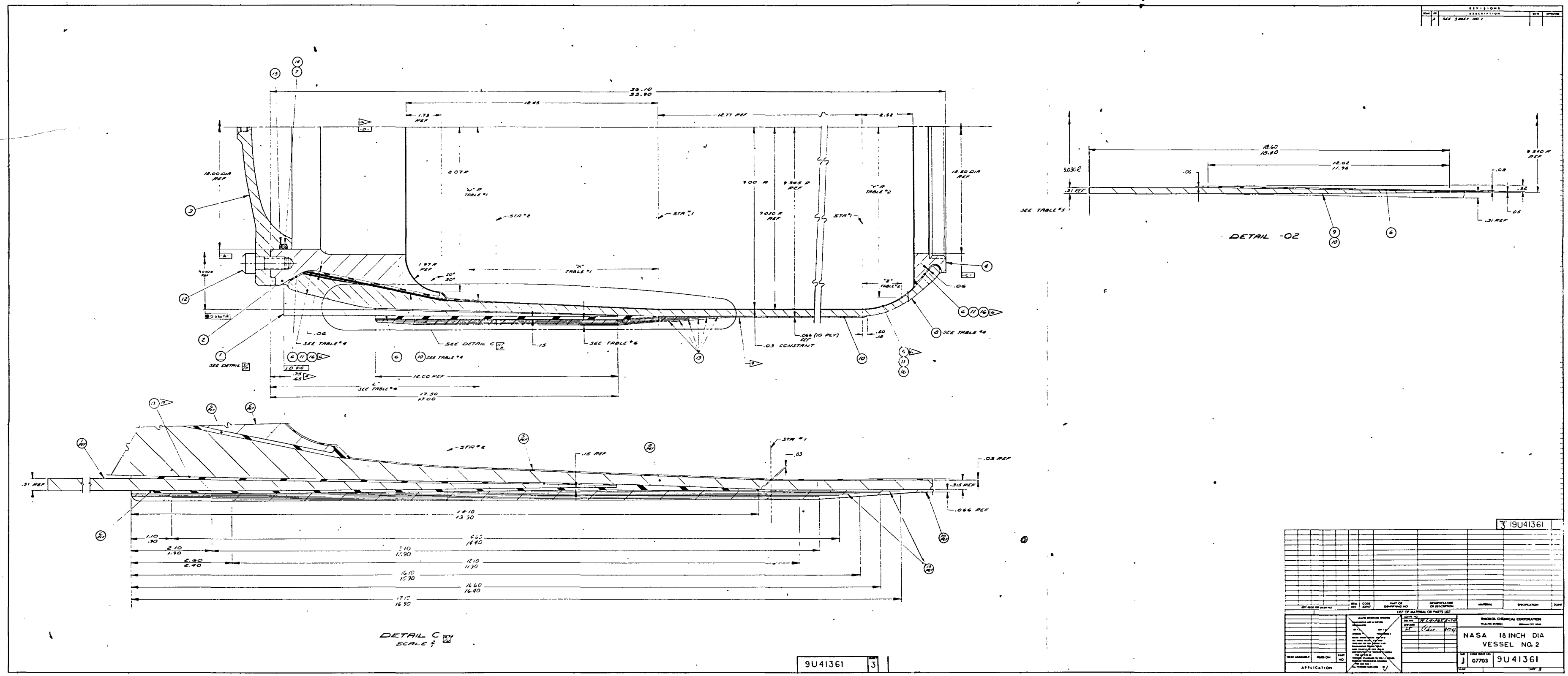
REVISIONS
SEE SHEET NO 1
DETAIL -02
DETAIL C
SCALE
9U41361
3
9U41361
THIOKOL CHEMICAL CORPORATION
NASA 18 INCH DIA
VESSEL NO. 2
07703
9U41361

Page intentionally left blank

SHEET	9U41363	A
3		

THIOKOL CHEMICAL CORPORATION

NASA 18INCH DIA
VESSEL NO. 3

CAGE CODE NO	DRAWING NO
J 07703	9U41363

DETAIL - PRIOR TO MACHINING

DETAIL OF THREE LAYUP CONSTRUCTION SUBSEQUENT LAYERS TO BE STAGGERED BY 3"

DETAIL -02

DETAIL 'C'
SCALE 2

9U41363	3

Page intentionally left blank

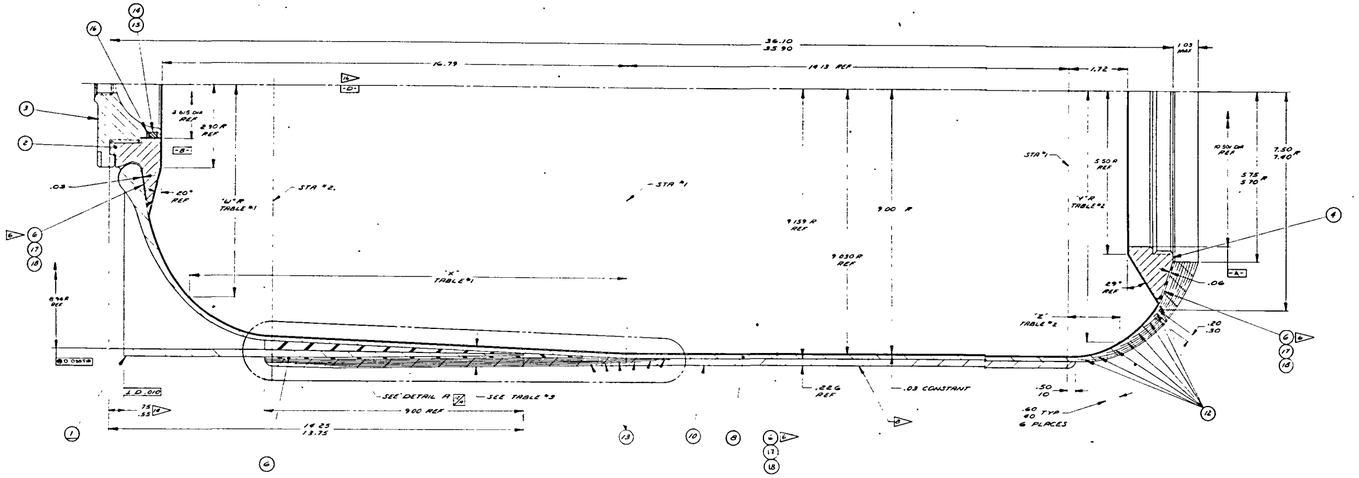

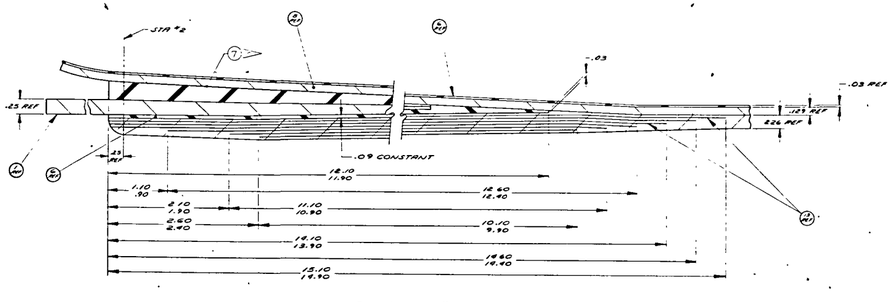

DETAIL A
SCALE 1/2

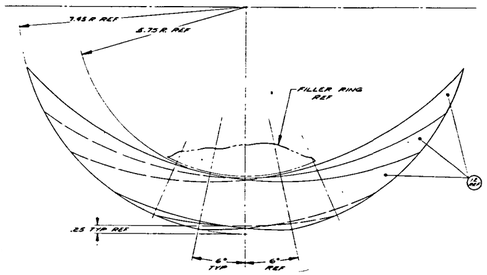

DETAIL OF TAPE LAYUP CONSTRUCTION,
SUBSEQUENT LAYERS TO BE STAGGERED @ 3°

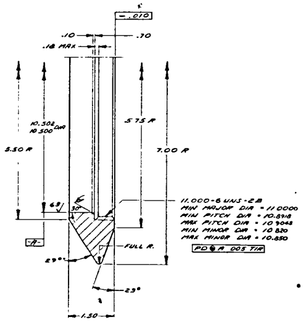

DETAIL -05

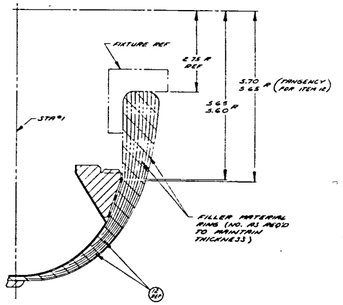

DETAIL - PRIOR TO MACHINING

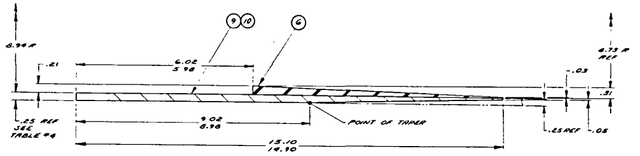

DETAIL -02

REVISIONS				
REVISION LTR	DESCRIPTION		DATE	APPROVED
	A	SEE SHEET NO. 1		
	B	SEE SHEET NO. 1		

SHEET 2	9U41364	B

QTY REQD PER DRAWN UNIT	ITEM NO.	CODE IDENT.	PART OR IDENTIFYING NO.	NOMENCLATURE OR DESCRIPTION	MATERIAL	SPECIFICATION	SIZE

LIST OF MATERIAL OR PARTS LIST

NEXT ASSEMBLY	MFR OR CODE	PART OR IDENTIFYING NO.
APPLICATION		

UNLESS OTHERWISE SPECIFIED
DIMENSIONS ARE IN INCHES
TOLERANCES
X ± .1
ANGLES ± 1°
DECIMALS
.XX ± .03
.XXX ± .010
MACHINED SURFACES 125 OR BETTER
ALL DIMENSIONS TO BE APPLIED AT 68°F
DRAWING TO BE INTERPRETED PER MIL-STD-100
MATERIAL AND PROCESS SPECIFICATIONS TO BE LATEST REVISION

	NAME	DATE
DRAWN	[illegible]	8-24-62
CHECKED		
APPD	C.CHAT	11-62

CONTR. NO.	
MODEL	
SERIAL NO.	

RHODES CHEMICAL CORPORATION
MOULTON DIVISION — BRISTOL, CONN. 06010

NASA 18 INCH DIA
VESSEL NO.4

SIZE	CODE IDENT NO.	DRAWING NO.
J	07703	9U41364

SCALE 1 | SHEET 1

9U41364 | 2

Page intentionally left blank

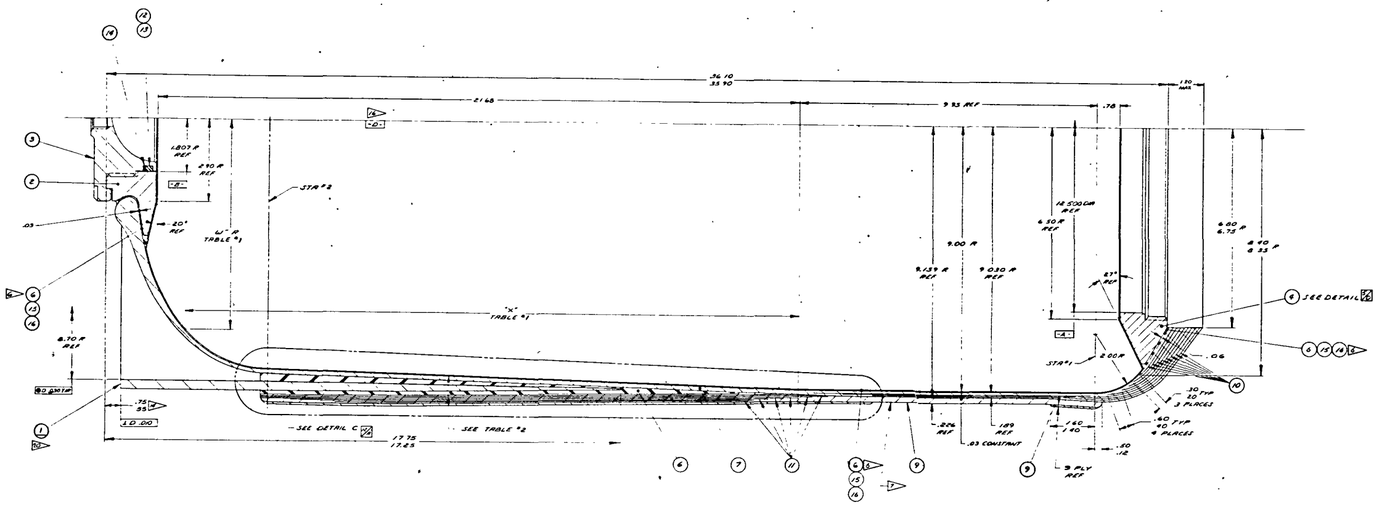

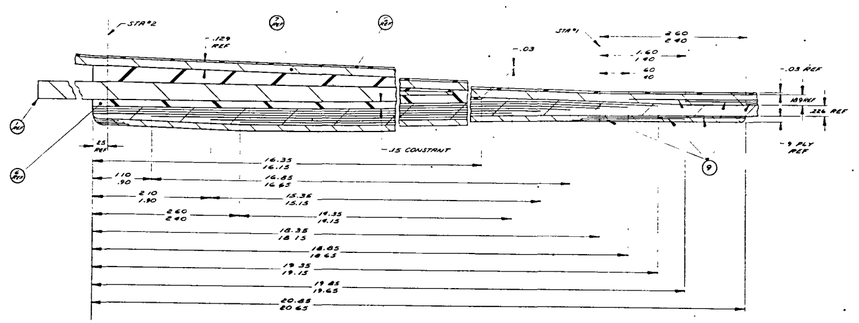

DETAIL C
SCALE f

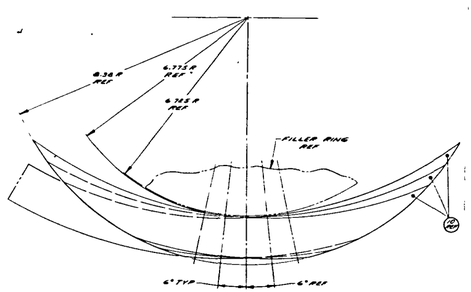

DETAIL OF TAPE LAYUP CONSTRUCTION
SUBSEQUENT LAYERS TO BE STAGGERED BY 3"

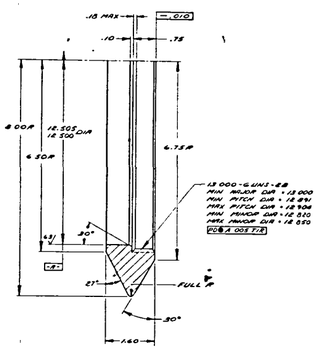

DETAIL -05

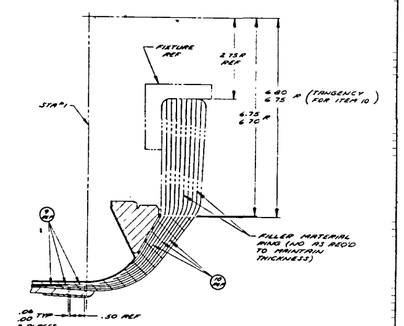

DETAIL - PRIOR TO MACHINING

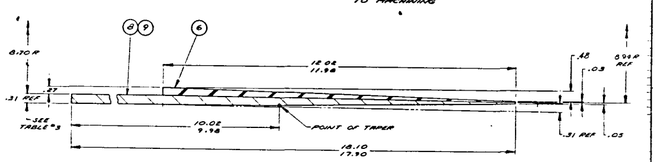

DETAIL -02

REVISIONS			
ZONE	LTR	DESCRIPTION	DATE	APPROVED
	A	SEE SHEET NO. 1		
	B	SEE SHEET NO. 1		

9U41365 B

ITEM NO.	CODE IDENT	PART OR IDENTIFYING NO.	NOMENCLATURE OR DESCRIPTION	MATERIAL	SPECIFICATION	ZONE

LIST OF MATERIAL OR PARTS LIST

NEXT ASSEMBLY	USED ON	PART NO.	APPLICATION

CONTR NO. NAS 8-11404 D.O. 3-3
CHK'D

THIOKOL CHEMICAL CORPORATION
WASATCH DIVISION BRIGHAM CITY, UTAH

NASA 16 INCH DIA
VESSEL NO. 5

J 07703 | 9U41365

SCALE | SHT 2

9U41365 2

Page intentionally left blank

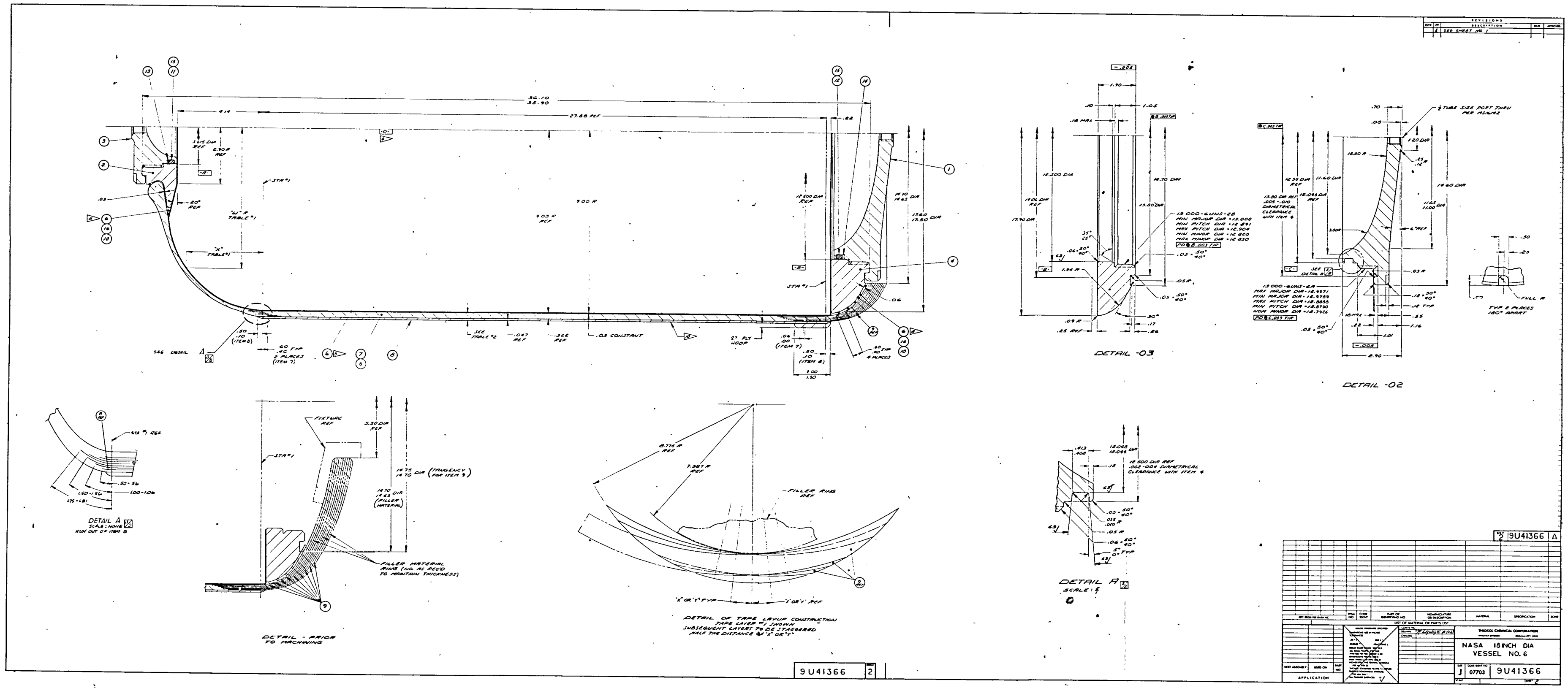
DETAIL -03
DETAIL -02
DETAIL A
SCALE: NONE
RUN OUT OF ITEM 9
DETAIL - PRIOR TO MACHINING
DETAIL OF TAPE LAYUP CONSTRUCTION
TAPE LAYER #1 SHOWN
SUBSEQUENT LAYERS TO BE STAGGERED
HALF THE DISTANCE OF 'E' OR 'F'
DETAIL A
SCALE: 1/2
TYP 6 PLACES
180° APART
NASA 18 INCH DIA
VESSEL NO. 6
9U41366
APPLICATION

Page intentionally left blank

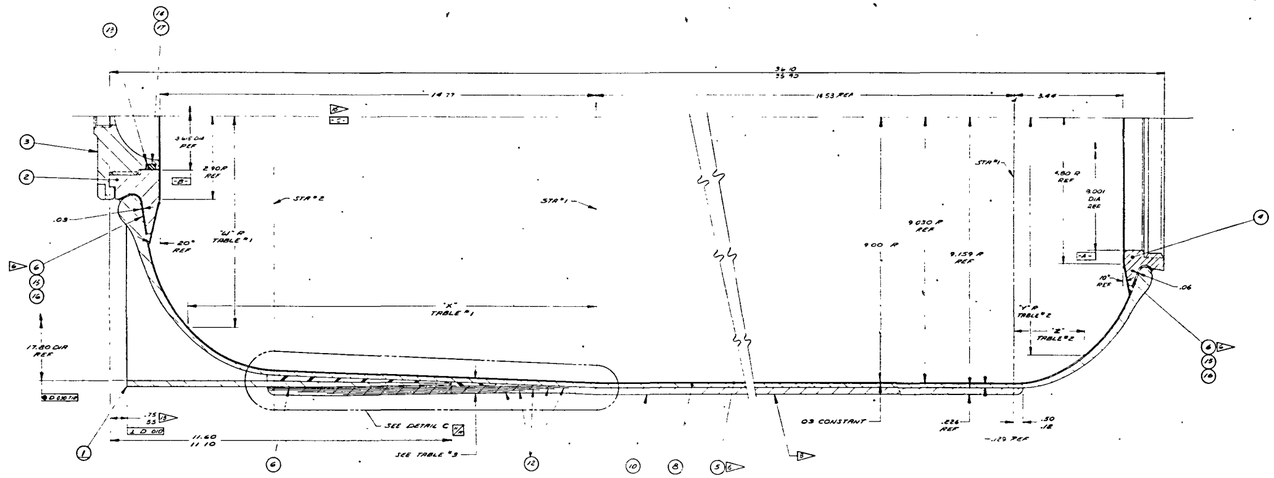

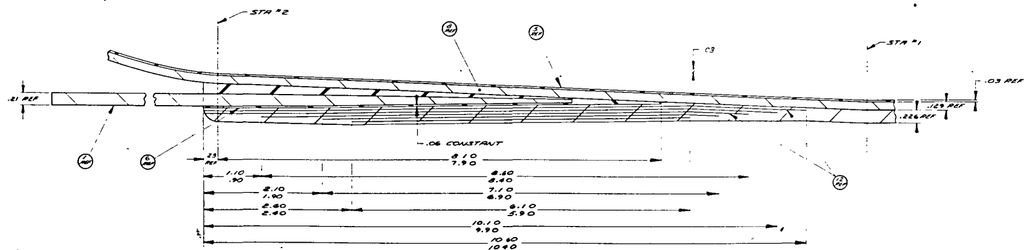

DETAIL C
SCALE 1

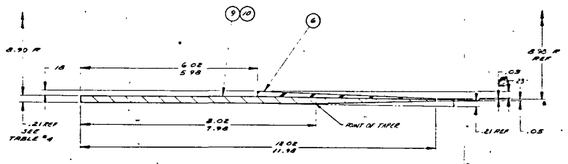

DETAIL -02

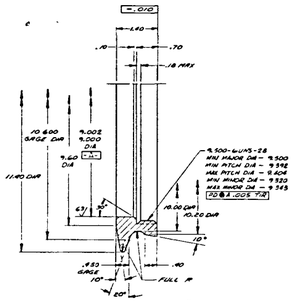

-03 DETAIL

REVISIONS			
REV	NO	DESCRIPTION	DATE	APPROVED

QPL NSNS PIN THDR NO	MFGR CODE	PART OR IDENTIFYING NO	NOMENCLATURE OR DESCRIPTION	MATERIAL	SPECIFICATION	ITEM
LIST OF MATERIAL OR PARTS LIST						

NEXT ASSEMBLY	USED ON	QUANTITY PER	APPLICATION

THIOKOL CHEMICAL CORPORATION
Wasatch Division, Brigham City, Utah

NASA 18 INCH DIA
VESSEL NO. 7

SIZE	CAGE IDENT NO	DRAWING NO
J	07703	9U41367

SCALE | SHEET 2

DRAWING NO	SHEET
9U41367	2

Page intentionally left blank

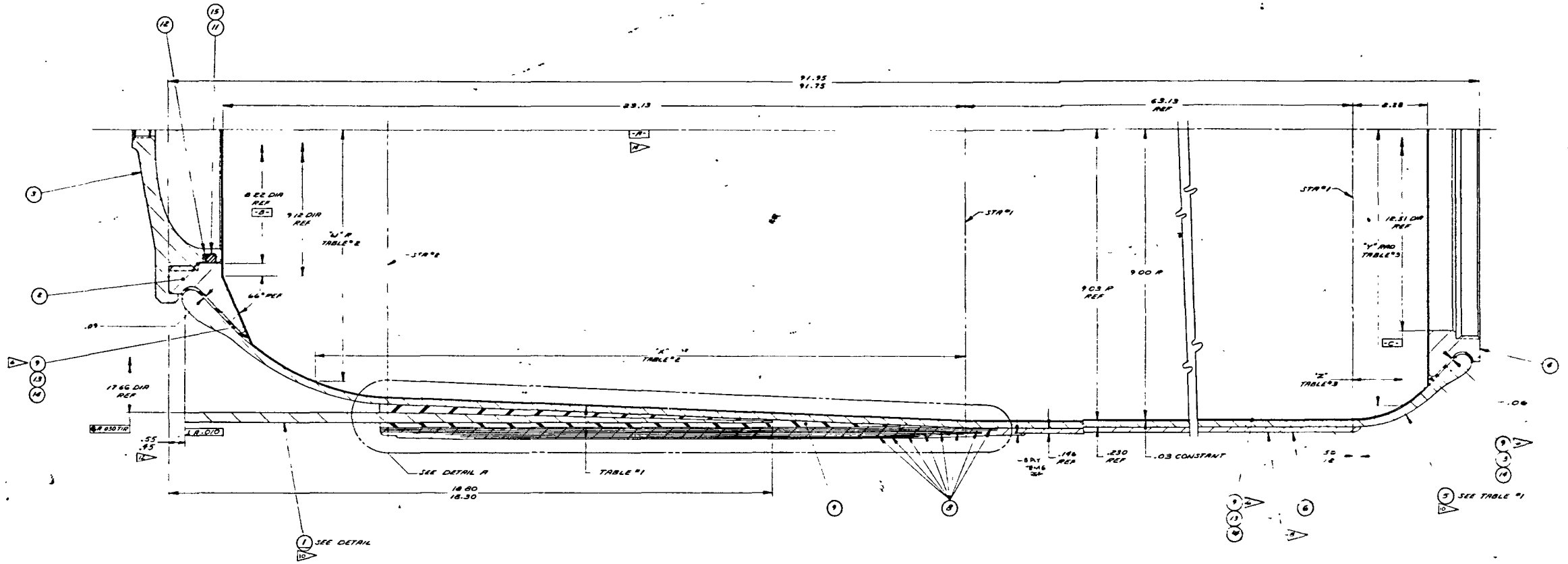

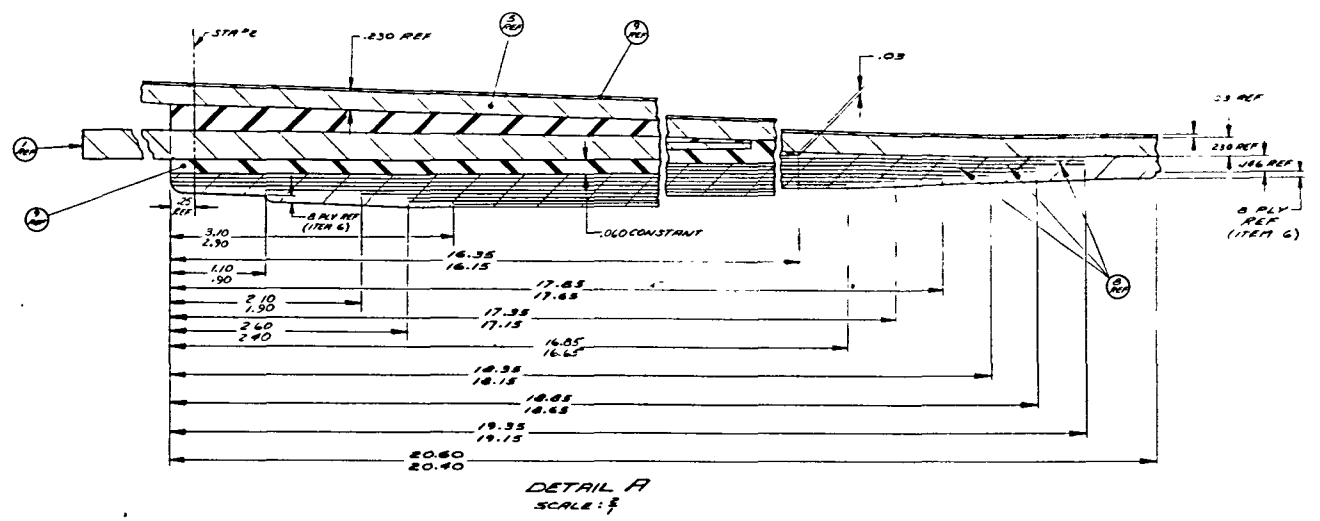

DETAIL A
SCALE: 1

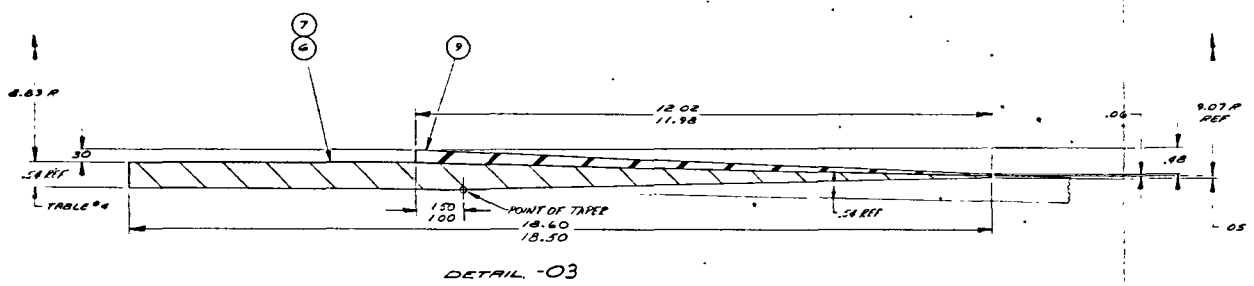

DETAIL -03

TABLE #1
CASE LUGS SCHEDULE

LOCATION	NO. REQD	ITEM NUMBER #	THK
FWD	16	4	.250
	1	5	—
	1	6	.040
	1	6	.060
	1	6	.0730
	1	6	.0890
	1	6	.1050
	1	6	.0970
	1	6	.0750
	1	6	.0590
	1	6	.0430
	1	6	.0270
	1	6	.0110
	1	6	.0250
	1	6	.0090
	1	6	.0390
	1	6	.0230
	1	6	.0070
AFT	16	6	.0250

TABLE #2
SHIRT MARKER SCHEDULE

LOCATION	NO. REQD	ITEM NUMBER #	THK
FWD	1	3	
	1	4	
	1	5	
	2	6	
	2	7	16 TOTAL
	2	6	
	2	7	
	2	6	
	2	7	
	2	6	
	2	7	
	2	6	
	2	7	
	2	6A	
	2	7	
	2	6	
	2	7	
	1	6	
	1	7	
AFT	2	6	

TABLE #3
AFT DOME

STATION	"Y"	"Z"
1	9.000	.000
2	8.969	.375
3	8.869	.744
4	8.703	1.107
5	8.472	1.461
6	8.182	1.800
7	7.825	2.117

TABLE #4
FWD DOME

STATION	"Y"	"X"
1	9.000	.000
2	8.974	17.398
3	8.881	18.483
4	8.748	18.747
5	8.558	19.198
6	7.917	19.918
7	7.748	20.371
8	7.537	20.823
9	7.304	21.274
10	7.047	21.681
11	6.736	22.087
12	6.499	22.498

NOTES:

1. THE NELON LINER SHALL HAVE AN ORIENTATION OF ±5°00'±0°30' IN THE CYLINDRICAL SECTION. EACH LINER SHALL CONSIST OF 8 PLIES WITH AN END DENSITY OF 201-205 END/IN/PLY. EACH PLY SHALL BE WOUND AT A NOMINAL BAND WIDTH OF .394 INCHES AND WITH A TENSION OF .35±.1 LBS/END.
2. THE POLAR LINER SHALL HAVE AN ORIENTATION OF ±90°±1° IN THE EQUATOR. EACH LAYER SHALL CONSIST OF 2 PLIES WITH AN END DENSITY OF 201-205 END/IN/PLY. EACH PLY SHALL BE WOUND AT A NOMINAL BAND WIDTH OF .390 INCHES AND WITH A TENSION OF .35±.1 LBS/END.
3. THE HOOP WIND SHALL CONSIST OF PLIES HAVING 138-208 END/IN/PLY. WOUND AT A NOMINAL BAND WIDTH OF .400 INCHES AND WITH A TENSION OF 5.5±1 LBS/END.
4. GLASS FILAMENTS SHALL BE S-994 WITH HTS FINISH, STYLE XP7030 (U.S. POLYMERIC OP 6004-1), PREIMPREGNATED WITH EPOXY RESIN (U.S. POLYMERIC OF 6004). RESIN CONTENT SHALL BE 20-25% BY WEIGHT. PER SPECIFICATION TUS-MH-6008.
5. GLASS FABRIC SHALL BE S-994HS, STYLE PER MIL-C-9084, TYPE II, PREIMPREGNATED WITH EPOXY RESIN (U.S. POLYMERIC OF 6004). RESIN CONTENT SHALL BE 27-33% BY WEIGHT. INSTALL WITH WARP PARALLEL TO Z OF CASE.
6. PRIOR TO BONDING ITEMS #6 & 7 TO ITEM 5 WITH ITEM 16, CLEAN AND PRIME ITEMS #6A IN AREA OF BOND WITH ITEM 13.
7. PARKER SEAL CO., CULVER CITY, CALIF. CODE IDENT #3859
8. MARK PART NUMBER PER TUS-59-33, METHOD G.
9. SILICA FILLED NBR, GEN-GARD V-45, GENERAL TIRE AND RUBBER CO, AKRON, OHIO. CODE IDENT 13808
10. ROUGHEN THE CONTACT SURFACE OF ITEM 1 PRIOR TO CONTACT SURFACE OF ITEM 16 WITH ITEM 16 PRIOR TO THE INSTALLATION OF ITEM 1.
11. SILICONE GREASE (DC-11 COOK CHEMICAL CORP., MIDLAND, MICHIGAN
12. TRIM ITEM 1 AFTER ASSEMBLY AND CURE.
13. CURE THE DIE-03 ASSEMBLIES FOR 8 HRS AT A GLASS-RESIN COMPOSITE TEMPERATURE OF 300°±10°F.
14. AXIS (A) IS DEFINED AS A LINE PASSING THRU THE CENTERS OF DIAMETERS (P) & (C).
15. ANL MATERIAL LOT OR SERIALIZATION NUMBERS SHALL BE RECORDED IN THE RADIOGRAPH'S PART QUALITY CONTROL RECORDS.
16. INSTRUMENTATION SHALL BE IN ACCORDANCE WITH DRAWING TUR1666.
17. LIQUID EPOXY RESIN EQUIVALENT TO THE U.S. POLYMERIC E317 EPOXY RESIN SYSTEM.

REVISIONS			
REV	LTR	DESCRIPTION	DATE
	A	(1-47) SEE ECO #1	1/64

	AR 16		EPOXY RESIN		
	AR 15		LUBRICANT		
				SIZE	9U41369 A
	AR 14		ADHESIVE	CHEMLOK 220 TWJ-MH-210	
	AR 13		PRIMER	CHEMLOK 205 TWJ-MH-2005	
	1 12	8-999-N3100-9	BOSS-UP RING	MATERIAL 7075	
	1 11	MS28775-496	O-RING		
	1 10	TUR1666-01	INSTRUMENTATION		
	AR 9		FILLED JOINT		
	AR 8		FIBERGLASS LAMINATE		
	1 7		POLAR LINER		
	AR 6		HOOP PLY		
	AR 5		HELICAL LINER		
	1 4	9U41341-05	AFT POLAR BOSS		
	1 3	9U41339-09	FWD CLOSURE		
	1 2	9U41331-03	FWD POLAR BOSS		
	1 1	-03	SHIRT		
-03	-01	PART OR IDENTIFYING NO.	NOMENCLATURE OR DESCRIPTION	MATERIAL	SPECIFICATION

LIST OF MATERIAL OR PARTS LIST

NEXT ASSEMBLY	USED ON	FAIR NO.
APPLICATION		

DRAWN	J. F. Hughes	11-15-63
TRACED	J. F. Hughes	11-15-63
DESIGN	R. A. Smith	11-15-63
STRESS	R. A. Smith	11-15-63
APPD		

INDIVIDUAL CHEMICAL CORPORATION

NASA 18INCH DIA VESSEL NO.9

CAGE	SIZE	DRAWING NO.
J	07703	9U41369

SCALE 1 SHEET 1 OF 1 SHEETS

9U41369

Page intentionally left blank

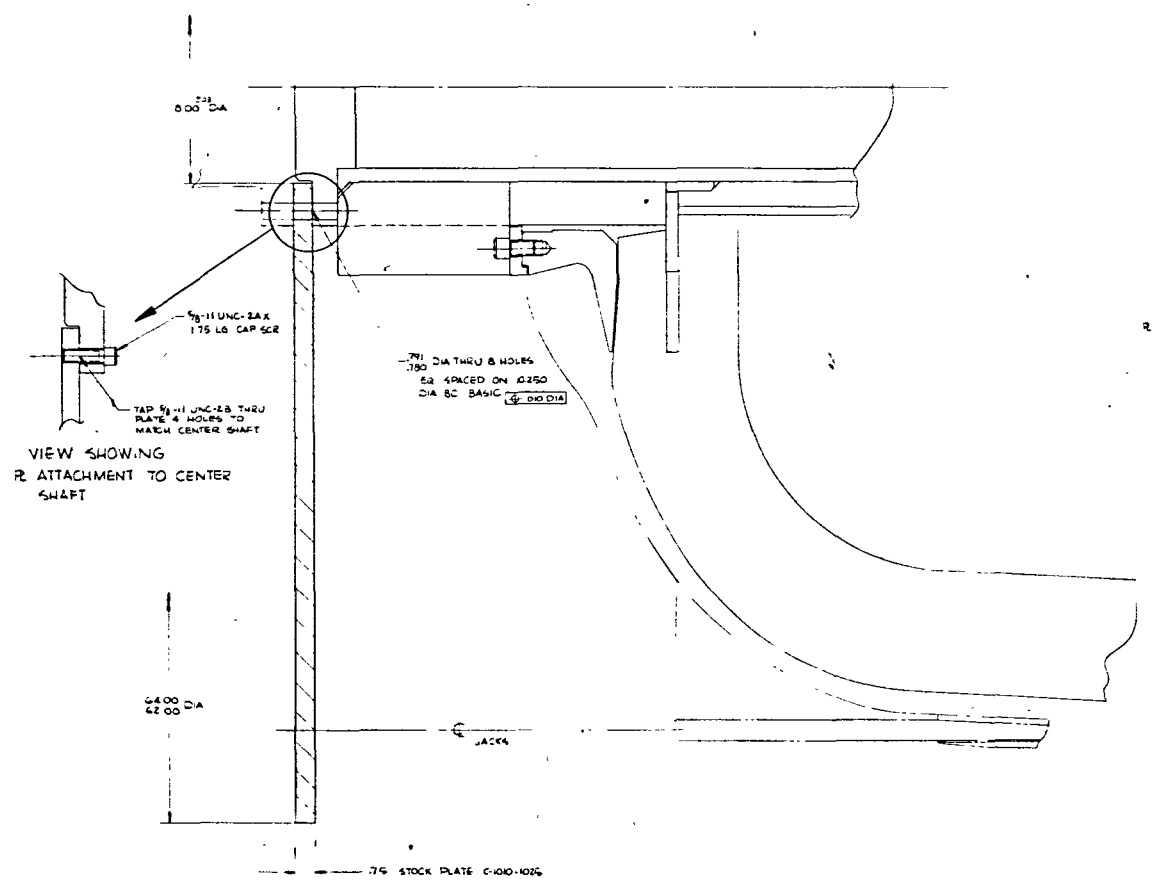

SKIRT INSTALLATION CONFIG.

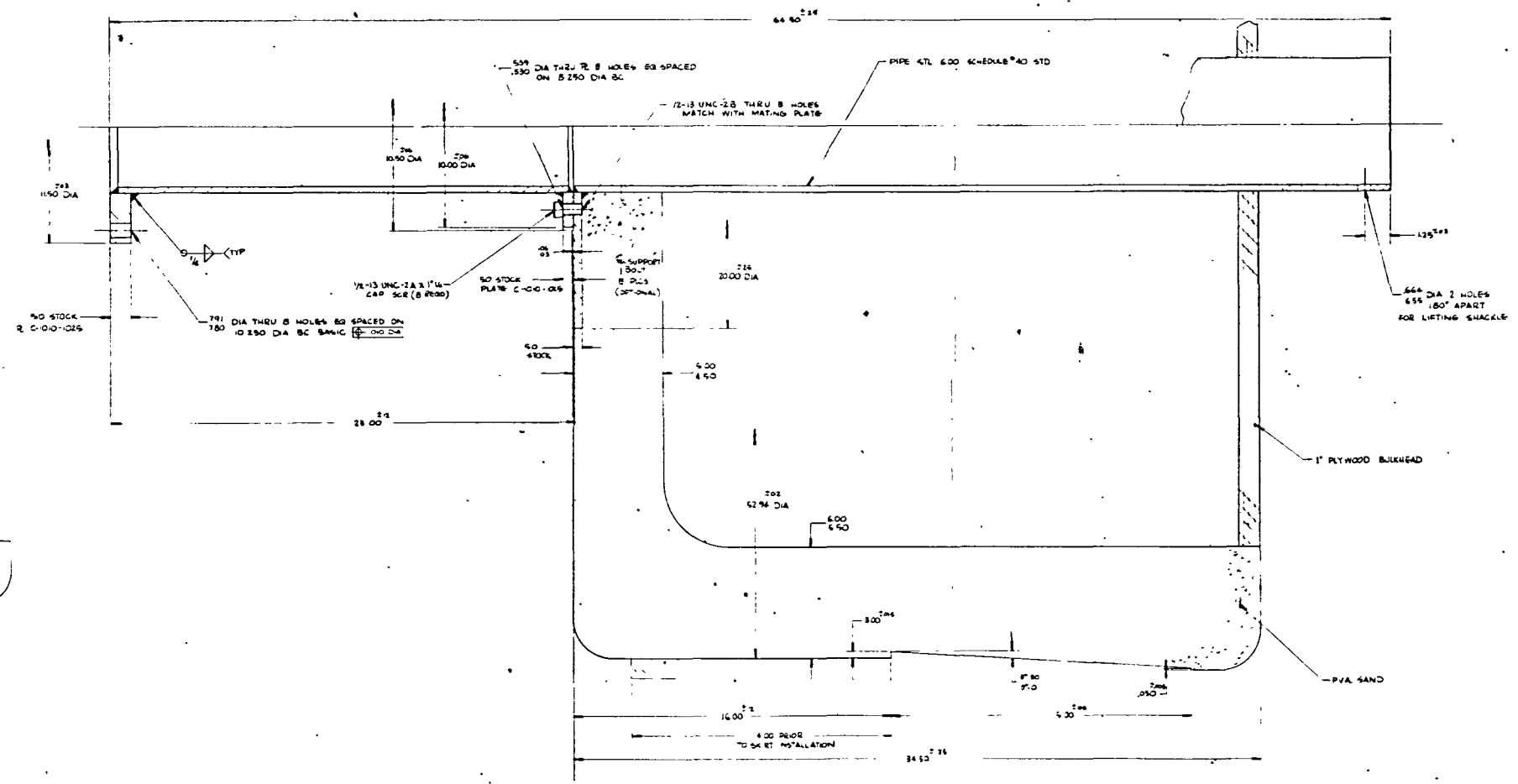

SKIRT MANDREL

ITEM NO	QUAN	PART OR IDENTIFYING NO	NOMENCLATURE OR DESCRIPTION	MATERIAL	SPECIFICATION	ZONE

LIST OF MATERIAL OR PARTS LIST

NEXT ASSEMBLY	USED ON
APPLICATION	

MORTON CHEMICAL COMPANY

NASA 54" MANDREL

SIZE	CODE IDENT NO	SK42110
J	07703	

SCALE 1/8 SHEET 2 OF 2

Page intentionally left blank

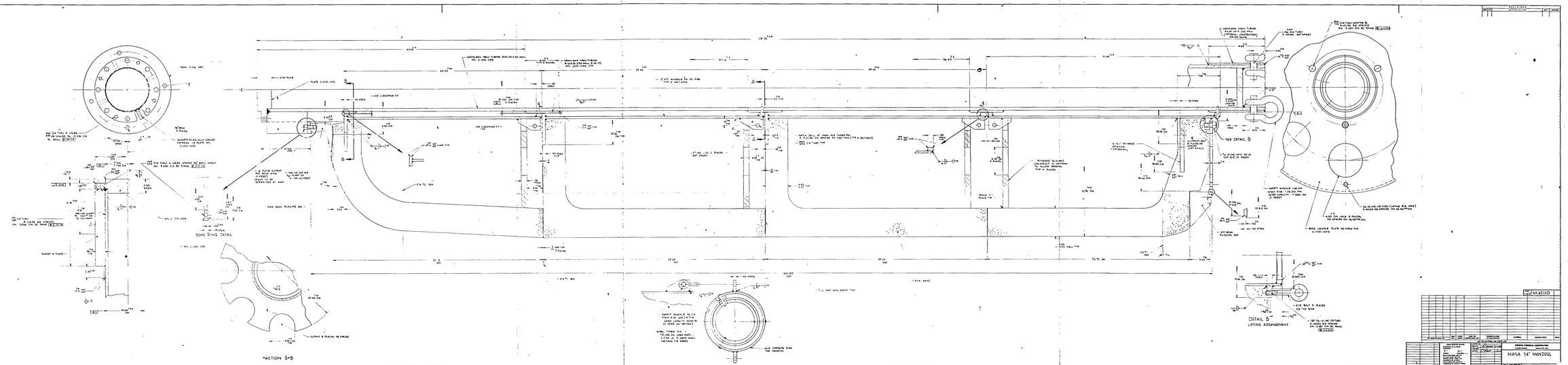
SEE DETAIL B
SEAL RING DETAIL
SECTION B-B
SECTION A-A
DETAIL B
LIFTING ARRANGEMENT
NASA 54" MANDREL
SK 42110

Page intentionally left blank

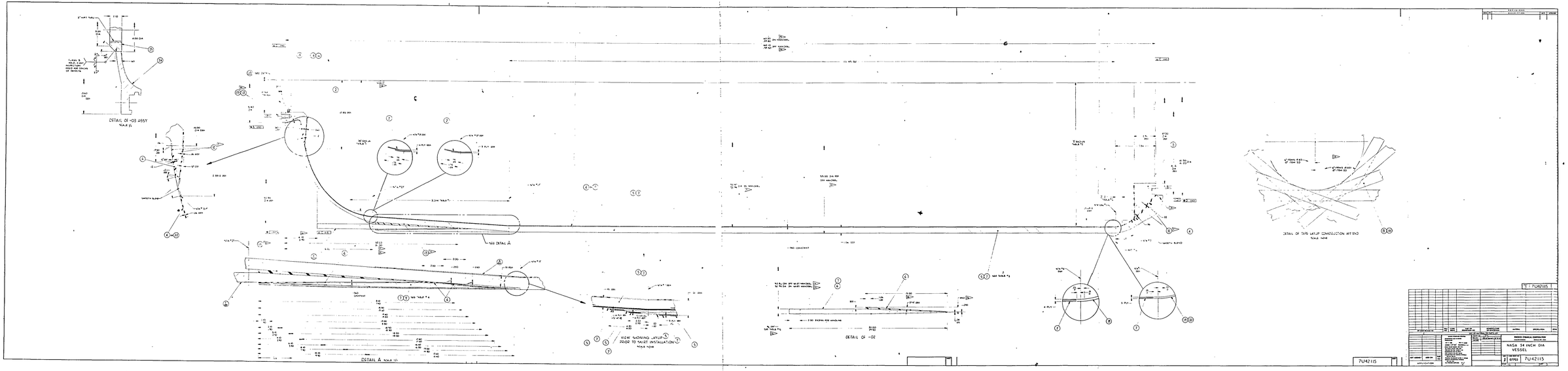
DETAIL OF HDS ASSY
SCALE 1/1
DETAIL A
SCALE 1/1
VIEW SHOWING LAYUP PRIOR TO MAT INSTALLATION
DETAIL OF -102
DETAIL OF TAPE LAYUP CONSTRUCTION AFT END
NASA 54 INCH DIA VESSEL
7U42115

Page intentionally left blank

GLOSSARY OF SYMBOLS

A	Fracture indicator in equation (18).
C	Axial compressive buckling coefficient - reference Figure 9.
D	Diameter of case (in., mm).
E_A, E_B, E_φ, E_θ	Composite extensional modulus of elasticity (psi, MN/m^2).
Eg	Elastic modulus of a glass filament (psi, MN/m^2).
F_x, F_y, F_z, F_s	Composite material strength (psi, MN/m^2).
F_g	Glass filament strength (psi, MN/m^2).
G	Shear modulus (psi, MN/m^2).
L	Length (in., mm)
M	Unit discontinuity bending moment (in.-lb/in., MN/m)
N_φ, N_θ	Unit membrane load in shell (lb/in., MN/m)
N_s	Skirt thrust loading (lb/in., MN/m)
P_{o1}, P_{o2}	Unit axial load in skirt overwrap (lb/in., MN/m)
P_T	Polar boss blowout load (lb, N)
p	Pressure (psi, MN/m^2)
Q	Unit discontinuity shear load (lb/in., MN/m)
Q_R	Unit load along shear ply (lb/in., MN/m)
$\bar{R}$, R_o, R_{CYL}	Radius of shell (in., mm)
R_E	Radius of dome opening (in., mm)
t_s, t_c	Shell thickness (in., mm)

V	Volume (in.^{3}, cm^3)
W	Weight (lb, kg)
x	Axial distance (in., mm)
ΔR	Radial deflection of the shell structure (in., mm)
α, α_o	Filament orientation (deg, rad)
$\bar{\alpha}$	Polar wrap wind angle (deg, rad)
α	Slope of the skirt shear ply (deg, rad)
β	Slope of skirt wall in the area of the shear ply (deg, rad)
γ	Shear strain (in./in., mm/mm)
$\epsilon_\varphi, \epsilon_\theta$	Extensional strain (in./in., mm/mm)
$\mu_{\varphi\theta}, \mu_{\theta\varphi}$	Poisson's ratio
ρ	Density (lb/in.^{3}, kg/cm^3)
σ_A, σ_B	Extensional stress in area of shear ply (psi, MN/m^2)
$\sigma_{g\alpha}, \sigma_{g\theta}, \sigma_{g\tau}$	Glass filament stress (psi, MN/m^2)
σ_{cr}	Critical buckling strength (psi, MN/m^2)
τ_{xy}	Inplane shear stress (psi, MN/m^2)
τ_R	Lap shear stress in shear ply (psi, MN/m^2)
τ	Interlaminar shear stress (psi, MN/m^2)
φ	Slope of the shell relative to the centerline (deg, rad)
ψ	Slope of the shell relative to the tangent plane (deg, rad)
ω	Radial deflection of the shell wall (in., mm)
$\Delta\theta$	Rotation of shell wall (deg, rad)

Subscripts

A	Aft
C	Resin-glass composite
F	Forward
g	Glass filament
S	Skirt
T	Total, tape
x	Direction of filament
y	Direction transverse to the filament
α	Polar or helical wrap
θ	Hoop direction
φ	Axial or meridional direction

REFERENCES

1. Shaffer, B. W.: The Influence of Filament Orientation on the Material Properties of Reinforced Plastics. Technical paper presented at 18th Annual SPI Conference, Reinforced Plastics Division, Chicago, Illinois: 5-7 February 1963.

2. Ekvall, J. C.: Elastic Properties of Orthotropic Monofilament Laminates, ASME Paper 61-AV-56. Presented at Aviation Conference, Los Angeles, California: 12-16 March 1961.

3. Kuhn, P.: Stresses in Aircraft and Shell Structure. New York: McGraw-Hill Book Company, Inc, 1956.

4. Azzi, V. D. and Tsai, S. W.: "Anisotropic Strength of Composites," Experimental Mechanics. September 1965.

5. Strickler, C. T., Voce, S. J., and Zophres, W.: Design Buckling Criteria for Cylinders and Truncated Cones of Small Semivertex Angles of Low R/t and Z Parameter Ranges, Technical Paper No. 6120-J280-RU000. Presented at TRW Space Technology Laboratory, Redondo Beach, California: 29 November 1963.

DISTRIBUTION LIST

No. of Copies	Recipient
	NASA Lewis Research Center 21000 Brookpark Road Cleveland, Ohio 44135 Attn:
	Contracting Officer
1	Mail Stop 500-313 Solid Rocket Technology Br.
8	Mail Stop 500-205 Technical Library
2	Mail Stop 60-3 Tech. Report Control Office
1	Mail Stop 5-5 J. Kennard
1	Mail Stop 3-17 Tech. Utilization Office
1	Mail Stop 3-19 Patent Counsel
1	Mail Stop 500-311
	National Aeronautics and Space Administration Washington, D. C. 20546 Attn:
3	RPM/William Cohen
1	RPS/Robert W. Ziem
2	ATSS-AL/Technical Library
	NASA Ames Research Center Moffett Field, California 94035
1	Attn: Technical Library
	NASA Langeley Research Center Langley Station Hampton, Virginia 23365 Attn:
1	Robert L. Swain
1	Technical Library

DISTRIBUTION LIST (Cont)

No. of Copies	Recipient
	NASA Goddard Space Flight Center Greenbelt, Maryland 20771
1	Attn: Technical Library
	NASA Manned Spacecraft Center 2101 Webster Seabrook Road Houston, Texas 77058
1	Attn: Technical Library
	NASA George C. Marshall Space Flight Center Redstone Arsenal Huntsville, Alabama 35812 Attn:
1	Technical Library
1	R-P & VE-PA/K., Chandler
	Jet Propulsion Laboratory Calif. Institute of Technology 4800 Oak Grove Drive Pasadena, California 91003 Attn:
	Richard Bailey
1	Technical Library
	Scientific & Technical Information Facility NASA Representative P.O. Box 33 College Park, Maryland 20740
6	Attn: CRT
	Government Installations
	AF Space Systems Division Air Force Unit Post Office Los Angeles, California 90045
1	Attn: Col. E. Fink
	AF Research & Technology Division Bolling AFB, D. C. 20332
1	Attn: Dr. Leon Green, Jr.

DISTRIBUTION LIST (Cont)

No. of Copies	Recipient
	AF Rocket Propulsion Laboratory Edwards AFB, California 93523
2	Attn: RPM/Mr. C. Cook
	AF Materials Laboratory Wright-Patterson AFB, Ohio 45433 Attn:
1	MANC/D. Schmidt
1	MAAE
	AF Ballistic Missile Division P.O. Box 262 San Bernadino, California
1	Attn: WDSOT
	Structures Division Wright-Patterson AFB, Ohio 45433
1	Attn: FDT/R. F. Hoener
	Army Missile Command Redstone Scientific Information Center Redstone Arsenal, Alabama 35809
1	Attn: Chief, Document Section
	Ballistic Research Laboratory Aberdeen Proving Ground, Maryland 21005
1	Attn: Technical Library
	Picatinny Arsenal Dover, New Jersey 07801
1	Attn: Technical Library
	Navy Special Projects Office Washington, D. C. 20360
1	Attn: H. Bernstein
	Naval Air Systems Command Washington, D. C. 20360
1	Attn: AIR-330/Dr. O. H. Johnson

DISTRIBUTION LIST (Cont)

No. of Copies	Recipient
	Naval Propellant Plant Indian Head, Maryland 20640
1	Attn: Technical Library
	Naval Ordnance Laboratory White Oak Silver Spring, Maryland 20910
1	Attn: Technical Library
	Naval Ordnance Test Station China Lake, California 93557 Attn:
1	Technical Library
1	C. J. Thelen
	Naval Research Laboratory Washington, D. C. 20390
1	Attn: Technical Library
	Chemical Propulsion Information Agency Applied Physics Laboratory 8621 Georgia Avenue
1	Silver Spring, Maryland 20910
	Defense Documentation Center Cameron Station 5010 Duke Street
1	Alexandria, Virginia 22314
	Defense Materials Information Center Battelle Memorial Institute 505 King Avenue
1	Columbus, Ohio 43201
	Materials Advisory Board National Academy of Science 2101 Constitution Ave., N.W. Washington, D. C. 20418
1	Attn: Capt. A. M. Blamphin

DISTRIBUTION LIST (Cont)

No. of Copies	Recipient
	Institute of Defense Analyses 1666 Connecticut Ave., N.W. Washington, D. C.
1	Attn: Technical Library
	Advanced Research Projects Agency Pentagon, Room 3D154 Washington, D. C. 20301
1	Attn: Technical Information Office
	Industry Contractors
	Aerojet-General Corporation P.O. Box 1168 Solid Rocket Plant Sacramento, California 94086 Attn:
1	Dr. B. Simmons
1	Technical Information Center
	Aerojet-General Corporation P.O. Box 296 Azusa, California 91702
1	Attn: Technical Library
	Lockheed Missiles & Space Company P.O. Box 504 Sunnyvale, California
1	Attn: Technical Library
	Aerospace Corporation 2400 East El Segundo Boulevard El Segundo, California 90245 Attn:
1	Technical Library
1	Solid Motor Dev. Office
	Aerospace Corporation P.O. Box 95085 Los Angeles, California 90045
1	Attn: Technical Library

DISTRIBUTION LIST (Cont)

No. of Copies	Recipient
	Atlantic Research Corporation Shirley Highway at Edsall Road Alexandria, Virginia 22314
1	Attn: Technical Library
	Battelle Memorial Library 505 King Avenue Columbus, Ohio 43201
1	Attn: Edward Unger
	Boeing Company P.O. Box 3999 Seattle, Washington 98124
1	Attn: Technical Library
	Chrysler Corporation Space Division Michoud Operations New Orleans, Louisiana
1	Attn: Technical Library
	Douglas Missiles & Space Systems Huntington Beach, California
1	Attn: T. J. Gordon
	Hercules Company Allegany Ballistics Laboratory P.O. Box 210 Cumberland, Maryland 21502
1	Attn: Technical Library
	Hercules Company Bacchus Works P.O. Box 98 Magna, Utah 84044
1	Attn: Technical Library

DISTRIBUTION LIST (Cont)

No. of Copies	Recipient
	Lockheed Propulsion Company P.O. Box 111 Redland, California 93273
1	Attn: Bud White
	Martin Marietta Corporation Baltimore Division Baltimore, Maryland 21203
1	Attn: Technical Library
	Mathematical Sciences Corporation 278 Renook Way Arcadia, California 91107
1	Attn: M. Fourney
	Philco Corporation Aeronutronics Division Ford Road Newport Beach, California 92660
1	Attn: Technical Library
	Rocketdyne Solid Propulsion Operations P.O. Box 548 McGregor, Texas
1	Attn: Technical Library
	Rocketdyne 6633 Canoga Avenue Canoga Park, California 91304
1	Attn: Technical Library
	Rohm and Haas Redstone Arsenal Research Division Huntsville, Alabama 35807
1	Attn: Technical Library

DISTRIBUTION LIST (Cont)

No. of Copies	Recipeint
1	Rohr Corporation Space Products Division 8200 Arlington Boulevard Riverside, California
20	Thiokol Chemical Corporation Wasatch Division Brigham City, Utah 84302
1	Thiokol Chemical Corporation Elkton Division Elkton, Maryland 21921 Attn: Technical Library
1	Thiokol Chemical Corporation Huntsville Division Huntsville, Alabama 35807 Attn: Technical Library
1	TRW, Inc. Structures Division 23444 Euclid Avenue Cleveland, Ohio 44117 Attn: L. Russell
1	United Technology Center P.O. Box 358 Sunnyvale, California 94088 Attn: Technical Library